

PERIPHERAL NERVE INJURIES: PLEIOTROPHIN-MEDIATED
REGENERATION ACROSS LONG-GAP INJURIES AND
INVESTIGATIONS INTO AMPUTATION NEUROMA PAIN

By

BENJAMIN JOHNSTON

Presented to the Faculty of the Graduate School of
The University of Texas at Arlington in Partial Fulfillment
of the Requirements
for the Degree of

DOCTOR OF PHILOSOPHY

THE UNIVERSITY OF TEXAS AT ARLINGTON

MAY 2014

Copyright © by BENJAMIN JOHNSTON 2014

All Rights Reserved

Acknowledgements

I would first and foremost like to thank my family for their support throughout my education. I am one of the luckiest people to have grown up in the family I did. I deeply thank my research advisor and mentor Dr. Mario Romero-Ortega, PhD. This work is the direct result of his guidance and support. I would also like to thank my research partner Dr. Rafael Granja-Vazquez, MD - I am grateful to have such a great friend to work through the challenges of this research. There are so many others to thank from the Regenerative Neurobiology Lab, but I would like to especially thank Swarup Dash, PhD, Collins Watson, PhD, Jeff Compton, Shannon Trinh, Matthew Le, Colten Philpott, Nesreen Alsmadi, and Aswini Kanneganti.

I would like to thank my dissertation committee for their guidance: Dr. Young-tae Kim, PhD; Dr. Yi Hong, PhD; Dr. Scott Oishi, MD; Dr. Samarendra Mohanty, PhD.

I would like to thank the collaborators from the Mohanty lab: Bryan Black and Kamal Dhakal. I thank the Yawo Lab from Sendai, Japan for graciously providing some of the animals used for these experiments. I thank Guenter Gross from the CNNS Lab at UNT. I would also like to thank Dr. Erick Jones, PhD and the collaborators from the RAID lab. I

also thank Dr. Shan Sun-Mitchell, PhD for assisting with statistical analysis.

Lastly, I would like to thank the patients that inspired this work, chiefly Major David Underwood. Meeting Major Underwood changed the direction of my life. As I transition into medical school, I am eager to work for patients directly and dedicate my life to their health.

APRIL 21ST, 2014

Abstract

PERIPHERAL NERVE INJURIES: PLEIOTROPHIN-MEDIATED REGENERATION ACROSS LONG-GAP INJURIES AND INVESTIGATIONS INTO AMPUTATION NEUROMA PAIN

Benjamin Johnston

The University of Texas at Arlington, 2014

Supervising Professor: Mario I. Romero-Ortega

Peripheral nerve injuries can be a chronic clinical challenge for patients. Long recovery periods, functional deficits, and neuropathic pain all complicate healing. Although peripheral nerves are able to regenerate, most gap nerve injuries are repaired by autograft, which induces a secondary injury and provides suboptimal recovery of function. This work provides insights into the use of Pleiotrophin (PTN) to bridge long-gap injuries and assess the functional recovery of the common peroneal nerve (CPN) injury model. In addition to regeneration strategies, a painful neuroma-blocking conduit was developed to help patients with amputation neuromas. Lastly, this work addresses the unusual phenomenon of radio frequency (RF) wave elicited neuroma pain. *In vivo* and *in vitro* testing indicates a mechanism by which RF-stimulus elicits pain.

Table of Contents	
Acknowledgements.....	iii
Abstract.....	v
List of Illustrations	xi
List of Tables.....	xviii
Chapter 1 Pleiotrophin Mediated Regeneration Across Long-	
Gap Injuries.....	1
Introduction	1
Peripheral Nerve Regeneration	1
Growth Factors	5
Neurotrophins.....	5
Pleiotrophins	6
Conduits.....	6
Preliminary Work (3-cm Gap Injury)	7
5-Cm Gap Injury Experiment.....	10
Experimental Design.....	10
Materials & Methods	11
BNI Fabrication	11
Surgery.....	19
Behavioral Assays.....	20
Tissue Fixation	23

Results	24
BNI Fabrication	24
Behavior Assays	25
Discussion	29
4-Cm Gap Injury Experiment.....	30
Experimental Design.....	30
Materials & Methods	31
BNI Fabrication	31
Behavioral Assays.....	33
Tissue Processing & Immunohistochemistry	35
Results	37
BNI Fabrication	37
Tissue Regeneration	38
Behavioral Assays.....	40
Discussion	48
Conclusion	50
Chapter 2 Multi-Luminal Conduit To Impede Neuroma	
Development And Peripheral Nerve Pain	52
Introduction	52
Neuroma	52
Multi-Luminal Neuroma Conduit Experiment	53

Experimental Design.....	53
Materials & Methods	55
Animal Model	55
Multi-Luminal Gel-Gradient Conduit Construction.....	55
TNT Surgery.....	58
Behavioral Assays.....	59
Tissue Fixation	60
Statistics.....	60
Results.....	62
Discussion	64
Conclusion	65
Chapter 3 Investigations Into Radio-Frequency Induced	
Neuropathic Pain	66
Introduction	66
Neuropathic Pain	66
Clinical Presentation	67
Electromagnetic Field (EMF) Effects	68
Pilot Experiments.....	69
In Vivo Experiments	70
Experimental Design.....	70
Materials & Methods	72

Radio Frequency Environmental Characterization.....	72
RF Skin Temperature Testing	73
Laser & Optogenetic Animals.....	73
Surgery.....	74
RF Assay.....	74
Thermal Nociception Assay	75
Von Frey Assay.....	75
OLVF	76
RF Anxiety Chamber.....	76
Results.....	77
Radio Frequency Environmental Characterization.....	77
RF Skin Temperature Testing	78
RF Assay.....	81
Thermal Nociception Assay	86
Von Frey Assay.....	91
OLVF	96
RF Anxiety Chamber.....	97
Discussion	98
In Vitro Experiments.....	106
Experimental Design.....	106
Materials & Methods	107

MEA Experiments	107
Calcium Imaging	108
Radio Frequency.....	110
Field Modeling.....	110
Results.....	113
MEA Experiments	113
Calcium Imaging	115
Field Modeling.....	121
Discussion	123
Conclusion	126
Dissertation Summary Statement	130
Appendix A International Patent Application PCT/US14/16905	131
Appendix B International Patent Application PCT/US14/16801	201
References.....	236
Biographical Information	244

List of Illustrations

Figure 1-1 : Absolute toe-spread of the injured and uninjured feet of all animals post-surgery (mean with SD) (two-tailed paired t-test $p < 0.001$) ³⁶	26
Figure 1-2: Average number of licks per 10 minutes following formalin injection for both uninjured and injured animals (adapted from Prasad, P., 2012)(mean with SD) (two-tailed paired t-test $p < 0.001$) ³⁶	27
Figure 1-3: Muscle force of the tibialis anterior muscle during CPN electrical stimulation (adapted from Prasad, P., 2012)(mean with SD) (two-tailed paired t-test $p < 0.001$) ³⁶	28
Figure 1-4: The mid-swing ankle angle for all animals for the injured and uninjured CPN state (adapted from Prasad, P., 2012)(mean with SD) (two-tailed paired t-test $p < 0.01$) ³⁶	29
Figure 1-5: Cumulative PTN release into simulated body environment from PLGA micro-particles.....	37
Figure 1-6: Maximum GF concentration for each day of the regeneration time frame. A maximum concentration is reached on day 4 (100 ng/ml).38	
Figure 1-7: Image of explanted BNI with BSA micro-particles (N13) (Proximal End). Direction of outgrowth is from right to left.....	39
Figure 1-8: Image of explanted BNI with PTN micro-particles (N19) (Proximal End). Direction of outgrowth is from right to left.....	39

Figure 1-9: Formalin test results. No significant differences between experimental treatments in recovery of sensory function (one-way ANOVA).41

Figure 1-10: Mid-swing ankle angle recovered after injury. Positive values represent the treatment group had greater recovery of function. No significant difference was observed between experimental groups (one-way ANOVA; $p=0.055$).42

Figure 1-11: The percent of TSI recovery is plotted. One-way ANOVA of the groups yielded a significant difference between the Autograft and BSA experimental groups ($p=0.0297$).44

Figure 1-12: The calculated M-Peak values. The Autograft group had the highest M-Peak wave amplitude, and the difference between the BNI w/ BSA and BNI w/ PTN was highly significant ($p<0.0001$). No significant difference was observed between the two BNI groups.45

Figure 1-13: Top, Animal N13 (BNI w/ BSA); Middle, Animal N19 (BNI w/ PTN); Bottom, Animal N11 (Autograft). B-Tubulin (red) and P0 staining (green) shows clear indication of myelination around most axons in the autograft sample with little to no indication in the BSA or PTN animals. ..46

Figure 1-14: # of B-Tubulin positive axons in the same cross-sectional area (1388x1040 pixels). The Autograft group has a significantly higher axonal density.47

Figure 2-1: Multi-luminal gel-gradient conduit design.	56
Figure 2-2: Stitched image of multi-luminal neuroma conduit before implantation.....	57
Figure 2-3: Stages of Von Frey stimulation withdrawal. Frame A: Von Frey filament contact, Frame B: withdrawal initiation, Frame C: maximum withdrawal. Withdrawal occurs after filament contact. Total withdrawal time: <0.5 seconds.....	62
Figure 2-4: Mechanical pain assessment for three experimental groups. Groups are plotted as means with SD, but significance is indicated based on the non-parametric Wilcoxon Rank-Sum testing ($p < 0.05$).	63
Figure 2-5: An explanted multi-luminal gel-gradient conduit. Nervous tissue is confined to tracks within the conduit (yellow arrows).....	64
Figure 3-1: Cell phone tower used for RF environmental characterization.	77
Figure 3-2: RF power output as it relates to distance from the antenna. ..	78
Figure 3-3: Skin temperatures during RF stimulus. Each experimental period is 90 recordings (one-way ANOVA with multiple comparison Tukey's test; $p < 0.0001$).	80
Figure 3-4: Skin temperature values for each minute of baseline, RF- stimulus, and recovery periods. Each point represents the average of 9 values and the standard error of the mean is added for each point.	81

Figure 3-5: Top: Stages of RF stimulation withdrawal. Frame A: relaxed, Frame B: withdrawal initiated, Frame C: withdrawal maximum. Withdrawal occurs less than 10 seconds after initiating RF stimulation, only in limb with neuroma. Total withdrawal time: <0.20 seconds. Middle: Stages of RF stimulation stretching. Frame A: relaxed state, Frame B: stretch initiation, Frame C: stretching maximum. Stretching occurs while stimulation is on, only in limb with neuroma. Total stretching time: approximately 5 seconds. Bottom: Stages of RF stimulation licking. Frame A: relaxed state, Frame B: licking initiation, Frame C: licking. Licking occurs while stimulation is on, only in limb with neuroma. Total licking time: approximately 15 seconds.82

Figure 3-6: RF stimulus pain responses. Each animal is plotted with group means. TNT-Neuroma responses significantly different from sham animal responses ($p < 0.05$).83

Figure 3-7: A comparison of pain responses of TNT-neuroma animals undergoing RF-stimulus with and without Lidocaine (Mann-Whitney; $p = 0.0026$; significant difference).84

Figure 3-8: RF-stimulus pain responses. Significantly different responses were recorded for animals with and without nerve injury (SHAM-SHAM vs. TNT-SHAM + TNT-BD), but no significant was observed between groups with nerve injury (TNT-SHAM vs. TNT-BD)85

Figure 3-9: All RF-stimulus pain responses from animals across 9 trials. 86

Figure 3-10: The changes in skin temperature when the heating bulb was on or off (one-way ANOVA with multiple comparisons Tukey's test; $p < 0.0001$).....87

Figure 3-11: Pain responses of Sham and TNT-Neuroma animals were significantly different ($p = 0.0079$).....88

Figure 3-12: A comparison of pain responses of TNT-neuroma animals undergoing thermal-stimulus with and without Lidocaine (Mann-Whitney; $p = 0.4958$; non-significant difference).....89

Figure 3-13: Thermal pain responses post bulb disconnection. Significantly different responses were recorded for animals with and without nerve injury (SHAM-SHAM vs. TNT-SHAM + TNT-BD), but no significant was observed between groups with nerve injury (TNT-SHAM vs. TNT-BD).....90

Figure 3-14: All responses to thermal stimulus across 9 trials.....91

Figure 3-15: Pain responses to mechanical palpation by week for the sham and TNT-neuroma groups.....92

Figure 3-16: A comparison of pain responses of TNT-neuroma animals undergoing VF stimulus with and without Lidocaine (Mann-Whitney; $p = 0.0041$; significant difference).....93

Figure 3-17: The pain responses for Von Frey palpation post bulb disconnection surgery. See above results for statistical analysis.95

Figure 3-18: All pain responses to mechanical palpation by Von Frey filament across 9 trials (hyper-reactive animals are not plotted).....96

Figure 3-19: TNT-neuroma animals show an enhanced selection preference for the RF-shielded chamber ($p=0.0358$).....98

Figure 3-20: Thermal nociception (doubled) and RF nociception mean scores for all animals each recording session (9 trials each assay)..... 100

Figure 3-21: Mean RF nociception and thermal nociception (doubled) plotted trial by trial..... 101

Figure 3-22: Linear regression of thermal nociception (doubled) vs. RF nociception trial means. 95% confidence interval lines calculated and simultaneously plotted. 102

Figure 3-23: Annotated screenshot of MEA activity (firing rate & active channels). Recording sequence is 3 hours..... 114

Figure 3-24: Two experimental ROIs are added to a 12-minute recording sequence. 2 minutes of baseline, then 6 minutes of RF-stimulus, then 4 minutes of recovery (Each frame is 10 seconds apart). A horizontal regression line was plotted to analyze the intensity of each recording sequence. Above each recording sequence is a screenshot with the ROIs

analyzed (exposure of the image does not reflect or effect ROI intensity measurements).....	116
Figure 3-25: A corresponding nonlinear residuals plot of Figure 3-24. The first 12 frames (baseline sequence – RF OFF) have low signal intensity change fro the Reference ROI. Frames 13-48 (RF ON) show large residuals above the mean intensity. Frames 49-72 (recovery) show residuals increasing in the negative direction rapidly following RF stimulus.	118
Figure 3-26: Annotated ROI analysis of rat cortical neurons with RF-stimulus using Nikon A1R+/A1+ confocal microscope system (30 seconds of baseline, 4.5 minutes of stimulus, 4 minutes of recovery).....	120
Figure 3-27: The velocity vs. time plot of a Ca ⁺⁺ ion in 37 C H ₂ O in a 915 MHz, 18 V/m field, with a power of 750 mW/m ²	122

List of Tables

Table 1: The RUNS Test results for ROI1 and ROI 2 from the nonlinear regression residuals.....	118
--	-----

Chapter 1

Pleiotrophin Mediated Regeneration Across Long-Gap Injuries

Introduction

In an effort to provide patients an off-the-shelf surgical repair product for peripheral nerve injury, scientists and clinicians have been encouraged by the inherent regenerative capability of peripheral nerves and the many factors that enhance neurite outgrowth. The challenge remains to execute on a strategy that addresses the various injury presentations and is a convincing alternative to the autograft procedure.

Peripheral Nerve Regeneration

Peripheral nerves are the nerves that emanate out from the central nervous system and either elicit an action (efferent), or respond to a stimulus (afferent)¹. The main cell body (soma) is located closer to the central nervous system and long extensions (axons) connect to muscles, organs, or skin¹. The axon may be myelinated or unmyelinated – referring to the lipid-based insulating material around an axon that is produced and maintained by peripheral glia (Schwann cells)¹. To clean up the myelin debris or other molecules that interrupt axon function, macrophages are recruited after an injury^{2, 3}. To create and maintain the structure of the nerve, fibroblasts produce both extra-cellular matrix (ECM) components that sheath the axons^{2, 3}. The complex interaction between these main

cell types largely determines the extent of peripheral nervous system repair and regeneration²⁻⁴.

The nerve has a complex substructure that insulates the axons from the environment¹⁻³. This barrier is made up of an outer layer of connective tissue – the epineurium^{2,3}. Within the epineurium, the perineurium divides axons into large parallel tracts^{2,3}. Within the perineurium is the endoneurium that provides a final layer of connective and supportive tissue to maintain the “blood-nerve barrier” analogous to the “blood-brain barrier”^{3,5}. Within the endoneurial tubes are the axons that require sustained electrolyte regulation to function properly¹. Neurons are poised at a sub-equilibrium potential by active transport of key ions (potassium, sodium, calcium, and others to lower degrees)¹. The communication of the nervous system occurs in pulses of potential changes¹. The regeneration process ideally restores the fidelity of these pulses in both the retrograde and anterograde directions^{2,3}.

Clinicians in two different scales have classified the degree of nerve injury: the Seddon and Sunderland scales⁶⁻⁸. The Sunderland scale is as follows: 1st degree – the myelin sheath is damaged; 2nd degree – the axon is severed; 3rd degree – the endoneurium is disrupted; 4th degree the perineurium is disrupted; 5th degree – the epineurium is disrupted^{2,3,7}. For every injury described in this work the extent of damage is 5th degree.

Further, the distance between the severed ends of the nerve greatly determines the chances function is restored^{2, 3}.

Surgeons must accurately assess the chances of recovery based on the injury presented. Nerves transected with little damage to the surrounding tissue can be connected by sealing the epineurium of the two stumps together^{2, 3}. Nerves that are more severely damaged and have gaps between the two nerve stumps are repaired with either tissue or synthetic bridges^{2, 3}. The synthetic bridges are made of common polymers or biopolymers^{2, 3, 9-12}. The harvested bridges are collected from mammalian sources: pigs (xenograft), cadaver (allograft), or the patient (autograft)^{13, 14}. The autograft is the preferred surgical repair option when the nerve ends cannot be connected easily³. This preference is largely justified by superior repair of damaged nerves, but is in spite of significant negative effects of the procedure³. Patients are forced to sacrifice the function of the appendage from which the donor nerve is harvested³. In addition, the donor nerve may become a painful neuroma³. Lastly, the donor nerve may be mismatched for the repair section in either fiber type (sensory or motor) or diameter³.

No matter the repair strategy, the nerve must essentially repair itself by regenerating from the point of injury to its original distal target^{2, 3}. Once the nerve is damaged, cytokines released by damaged Schwann

cells attract macrophages that further release inflammatory compounds^{2, 3, 15}. This reactive environment promotes the phagocytosis of cellular waste and the over-proliferation of Schwann cells¹⁵. Even if large sections of distal nerve, connective tissue, and muscle remain intact, this does not prevent Wallerian degeneration from occurring in distal nerve sections and atrophy of deinnervated muscles^{16, 17}. Wallerian degeneration is characterized by myelin and axon degradation and then overproduction of collagen by fibroblasts^{16, 17}. This establishes a haptotactic gradient of ECM that allows for enhanced growth cone motility¹⁸. Growth cones are the axon structures that form at the end of each neuron during regeneration¹⁹. They are among the most functionally ornate structures in biology possessing a fan-like lamellipodia and many finger-like filopodia that respectively pull the axon forward and sense the environment to guide growth¹⁹. The regeneration rate of the growth cone varies between mammalian species, but is generally thought to be a 1-2 mm per day progression^{2, 3}. Therefore, even with optimal regeneration conditions, if a nerve is injured 10 cm from the distal innervation site, it may take 100 days for a growth cone to reestablish a connection. Fibrin cables that emanate from the proximal nerve guide the growth cone to the distal nerve stump². These cables also facilitate Schwann cell migration and form a structure known as the “bands of Bungner”². In summary, within a few

days after injury, the neurons have sealed themselves and prepare to regenerate to their original distal target while Schwann cells provide trophic cues, fibroblasts provide support structures and ECM, and macrophages clear the route for regeneration.

Growth Factors

In addition to the haptotactic cues provided by fibroblasts in the regenerating nerve segment, there are also many chemotactic cues. For many generations of scientists, the most important class of chemotactic cues has been growth factors (GF)^{20, 21}. Growth factors are proteins secreted by support cells that have trophic effects on cells²¹. These are often called neurotrophins when their effect has been studied with neurons, but often there is a broad range of cells affected²⁰.

Neurotrophins

The quintessential neurotrophin is Nerve Growth Factor (NGF). NGF has been shown to attract neurons, and remains one of the most studied proteins in neuroscience²⁰. In addition to NGF, the following neurotrophins are highly tested: glial cell line-derived neurotrophic factor (GDNF), brain-derived neurotrophic factor (BDNF), neurotrophin-3 (NT-3)

²⁰.

Pleiotrophins

Pleiotrophins are growth factors that affect a wide range of cell types^{4, 22-24}. They are of particular interest for peripheral nerve repair because scientists have realized that a broad range of cells are essential for proper nerve function – not just neurons^{4, 22-24}. Pleiotrophin (PTN) is a less studied growth factor. A recent study looked at PTN mRNA expression levels in nerve segments following injury, and found that PTN was the most highly up-regulated growth factor⁴. This suggests that PTN is an important protein when peripheral nerves are regenerating to a distal target.

Conduits

Conduits are fabricated support structures that aid peripheral nerve repair¹⁰. They were adapted from synthetic vascular grafts¹⁰. Because of the inherent regenerative capabilities of peripheral nerves many conduit designs have been shown to work¹⁰. Initially, conduits were hollow and all FDA-approved conduits are hollow^{10, 25}. The materials used in FDA-approved conduits are: collagen, poly lactic co-glycolic acid (PLGA), poly DL-lactic-co-1-caprolactone (PCLC), polyvinyl alcohol (PVA), and harvested pig intestine^{10, 25}. None of the hollow conduits augment their effectiveness with growth factors or other soluble agents^{10, 25}. In addition

to these conduits, there is a recently approved FDA allograft from human cadaver tissue that has shown promising results^{14, 26, 27}.

In the laboratory setting, many more approaches have been tried to move away from hollow tube geometry: guidance fibers, grooves, extra-porous walls, multi-luminal channels, and combination approaches^{10, 28}. To augment these fabrication changes, researchers have used biological cues to promote regeneration – most commonly: growth factors, Schwann cells, or stem cells^{10, 28}. The critical conclusion to reach from this discussion on laboratory-grade nerve conduits is that the ability to vary designs is nearly endless, and success is highly-likely across short-gap injuries^{3, 29}. Attempts at long-gap injuries are the bar that must be cleared by conduits to gain clinical relevance²⁸. The size of the animal model influences what is considered a long-gap, but for humans it is generally a gap of longer than 3 cm^{28, 29}. All the conduits presented in this work are longer than 3 cm.

Preliminary Work (3-cm Gap Injury)

In 2009, an experiment in New Zealand White Rabbits (NZWR) laid out the framework for future nerve conduit work. The common peroneal nerve (CPN) was transected and a 3 cm gap was made between the two transected ends. To repair this gap, a biosynthetic nerve implant (BNI) was used³⁰. The BNI is a multi-channeled agarose filled tube. The outer

tube is 1.7 mm diameter polyurethane tubing that is cut to length and perforated. This outer tube is positioned on a casting device that allows narrow (250-350 micrometer) needles to be arranged and cast a negative in gelled agarose. In the negative void of the needles, gel collagen is used. This laboratory grade platform was validated in multiple animal trials before using in NZWR³⁰. The number of channels, the size of each channel, and a number of other design parameters were optimized at shorter repair lengths³⁰.

With the BNI design optimized for the CPN, work was undertaken to test the effectiveness of non-neurotrophic growth factors. *In vitro* work had shown the promise of PTN to entice neurite outgrowth, and another pleiotrophic growth factor vascular endothelial growth factor (VEGF) was used for comparison (*Dash, S., 2013 UT Arlington & UTSW Dissertation*). The following experimental groups were used to test the effectiveness of the BNI and the BNI with embedded growth factors:

1. Hollow Tube (Polyurethane) (3.2 cm long)
2. BNI (3.2 cm long / 3.0 cm of internal agarose)
3. BNI with VEGF micro-particles (3.2 cm long / 3.0 cm of internal agarose)
4. BNI with PTN micro-particles (3.2 cm long / 3.0 cm of internal agarose)

5. BNI with both PTN and VEGF micro-particles (1:1 PTN:VEGF and the same total micro-particle weight added of other experimental groups) (3.2 cm long / 3.0 cm of internal agarose)

The animals were all tested with the following functional assays:

1. Toe-Spread Index (TSI): a ratio of the dorsiflexion response between the injured and uninjured foot
2. Formalin Test: a formalin solution is injected into the dermatome of the CPN in the injured and uninjured foot

After weeks of evaluating the functional recovery of the CPN, gross morphology, and later axon counts the following could be concluded:

1. BNI-treated animals all showed nerve regeneration
2. No hollow tube-treated animals showed regeneration
3. PTN and VEGF increased axon counts (statistically significant)
4. PTN showed the highest motor recovery (statistically significant)

This work was awarded an R-21 from the National Institutes of Health (NIH) to continue evaluation of synergistic effects of Pleiotrophins and neurotrophins. The subsequent two studies in NZWR were to respectively test experimental growth factor delivery strategies of PTN and then the effect of PTN with GDNF.

5-Cm Gap Injury Experiment

Growth factors are susceptible to degradation in normal physiological environments³¹. During even the most mild fabrication processes, temperature and pH changes can compromise growth factor integrity³¹. A number of strategies have been employed to protect proteins to preserve to amount of growth factors that remain bioactive³¹. The secondary beneficial effect of these strategies is that they typically extend the residence time of the active compound³¹. A longer residence time means that sustained drug-delivery is achievable. Our team set out to bridge a 5 cm CPN gap with a BNI augmented with various PTN delivery strategies.

Experimental Design

NZWR were selected because of their long peripheral nerve tracts. The CPN was selected due to previous experiments with this nerve-injury model. Two methods of PTN delivery were employed. The first involved extruded PLGA fibers that contained unprotected PTN³². These fibers were wrapped into coils that surrounded the needles of the BNI casting device. This provided PTN from the edge of each channel into the collagen lumen. In addition to this fiber delivery technique PLGA micro-particles were used from the previous 3 cm work. The experimental groups were as follows:

1. BNI without growth factors (5.2 cm long / 5.0 cm of internal agarose) (negative control – hypothesized to not achieve functional recovery) (n=3)
2. BNI with coiled PLGA PTN fibers (5.2 cm long / 5.0 cm of internal agarose) (n=3)
3. BNI with PLGA PTN micro-particles (5.2 cm long / 5.0 cm of internal agarose) (n=3)

We were unsure of the effect of a CPN injury on gait, so in addition to previously used behavioral assays, we examined the gait patterns of NZWR while hopping on a treadmill. We hoped to find an optimal fabrication method for a long-gap BNI supplemented with PTN.

Materials & Methods

BNI Fabrication

Micro-particles. The PTN micro-particles used in this study were previously prepared and characterized for the 3 cm BNI trials, but the double emulsion technique was used. All steps were done using sterile techniques, and when possible in a bio-safety level 2 (BSL-2) hood. The PTN solution was made at a 10 µg/ml PTN (Peprtech, Inc) concentration in deionized (DI) ultrapure (UP) water. The hydrophobic phase of the process was made with 50:50 PLGA (Lakeshore Biomaterials) 200 mg/ml in dichloromethane (DCM) (Sigma). The final aqueous phase was made

with 200 mg of PVA (Sigma) in 20 ml of DI-UP water. The PTN solution was mixed into hydrophobic phase and vortexed for 30 seconds (technique note: sonication may be helpful if the process does not make micro-particles of the desired small size). This mixed solution is then added to the final aqueous solution and then is vortexed for 2 minutes (technique note: sonication may be helpful if the process does not make micro-particles of the desired small size). Gentle stirring for about 1 hour at room temperature then evaporates the remaining DCM. To collect the micro-particles, the solution can be spun at 4000 RPM for 15 minutes on a centrifuge. The particles should be re-suspended in 10 ml 1xPBS (phosphate buffer solution) and should be immediately freeze-dried (technique note: any delay in the freeze-drying process will allow the PTN to leech out of the micro-particles). After freeze-drying, the particles should be visually examined for size and shape abnormalities. This is best done by taking a very small sample, sputtering with silver (Ag) and then imaging with a scanning electron microscope (SEM). A Hitachi S-3000N was used for these experiments.

Coils. PLGA coils were made using an adapted wet-spinning technique³². An approximately 20% by weight solution of PLGA was dissolved into DCM. To this stock solution various proteins were added:

1. PTN (4µg/ml)(Peprotech, Inc.)

2. BSA (20 μ g/ml)(Sigma)

After completely dissolved, the solution was poured into a glass syringe of approximately 5 ml volume (Hamilton, Inc). A syringe pump was used to inject the solution through a bent cannula/needle into a coagulation bath that is maintained in a glass coagulation column (technique note: this part of the methodology is highly variable, and it is important to experiment with the flow rate to maintain even fibers). The fibers are allowed to dry at room temperature and then stored by wrapping on slides in the freezer.

PTN release. To assess the amount of PTN released, a substitute protein, bovine serum albumin (BSA) was used as a model from release from the same formulation of PLGA micro-particles and PLGA fibers. 1 mg of BSA particles (and 5, 10, and 20 cm sections of BSA fibers) were placed in 1 ml of 1xPBS and kept on a shaker-incubator at 37 C for 28 days. At 0, 2, 6, and 12 hours samples were taken with care to not remove the micro-particles from the 1.5 ml vial. In addition, at 1, 2, 3, 7, 14, 21, and 28 days samples were taken. These samples were the loaded into an enzyme-linked immunosorbent assay (ELISA) for BSA (ThermoScientific). The absorbance of these samples was measured at the immunosorbent frequency of 562 nm on a plate-reading spectrophotometer.

Other BNI components. The outer tubing of our conduits was either made of cross-linked urethane-doped polyester (CUPE; Synthesized at UTA) or microrenathane (Braintree Scientific, Inc.). Either tubing had an internal diameter of 1.7 mm and an outer diameter of 2.4mm. They were cut to length (52 mm) and then perforated by steel 250 μm needle attached to a Dremel rotary drill. Perforations were made lengthwise on the tube every 2-3 mm and in 4 evenly spaced tracts on the tube. The tubes are then individually inspected for defects and any burrs that remain from perforating are removed. The casting chamber was custom built by Zyvex, Inc. for this application out of biocompatible injection plastic. Each casting chamber requires 8 needles (7-250 μm , 1-350 μm ; Smallparts, Inc.) that are cut by wire cutter to approximately 100 mm long (350 μm should be longer) and filed by rotary sanding drill bit with the Dremel rotary drill. (Technique note: the point should be shaped like a rounded bullet rather than an icicle). The two remaining components are essential, and their care will be explained in the following section: Analytical-Grade Agarose (Promega; Gelling Point (1.5%): 24-28 C; Melting Point (1.5%): 65.5 C; Gel Strength (1%) $\sim 300 \text{ g/cm}^2$)³³ and Avian Collagen Kit ECM675 (EMD Millipore). After all components are built, there is a long disinfection process: wash in DI-UP water (3x), then 70% ethanol solution (3x), and finally leave under UV light overnight to dry.

Stepwise construction. A BNI is defective if the following are found after completing construction: large agarose bubbles, any collagen bubbles, or disrupted channels. Many of these defects are only observable under 20x magnification or after sufficient practice. Here are the steps (with many technique notes):

1. Assemble all necessary parts in BSL-2 hood after properly cleaning and disinfecting:
 - a. Perforated, disinfected tubing (in sealed petri dish)
 - b. 7-250 μm needles
 - c. 1-350 μm needles
 - d. 1.5% by weight agarose solution (approximately 40 ml)
(make sure it is pH balanced before gelling) (use filtered DI-UP water)(never boil solution)
 - e. Heating plate with 250 ml beaker filled with 100 ml water and accurate mercury thermometer \rightarrow heat water to 85 C
 - f. Dumont Tweezers #5 (2)
 - g. Frozen 1.5 ml Eppendorf tube holder
 - h. Collagen kit
 - i. Mix the first two components and the micro-particles and keep this solution on ice

- ii. Only add the cross-linker when the procedure calls for it
 - i. 25 or 30 gauge needles
 - j. Luer-Lok syringes (1 or 3 ml)
 - k. Kim wipes
- 2. Temperature regulation of all components is essential, here are some guidelines:
 - a. Collagen should never be thawed except when mixing in micro-particles and when loading into the well of the casting device.
 - b. The agarose should never be boiled, and once liquid should be maintained at 45 C. Avoid gelling and melting the agarose repeatedly.
- 3. Select the outer tubing with great care. Examine each tube to look for excessively large perforations, and excessive curvature.
- 4. Align the tube on the on the two end components of the casting chamber.
- 5. Insert the 350 μm needle into the central channel.
- 6. Carefully insert the next seven 250 μm needles in a circular fashion around the central needle. Make sure the top insertion is perfectly aligned with the bottom insertion.

7. Set the casting device down and look for any defects before injecting agarose.
8. If no defects are found, draw up over 1 ml of liquid agarose (45 C). Wipe off the tip of the syringe with a Kim wipe and lock the needle onto the syringe.
9. Insert the need through the outer tubing so the needle is barely touching the inner needles of the casting device.
10. Slowly, but smoothly, inject agarose with sufficient pressure that some agarose leaks out of the perforations.
11. Look to see if there are any bubbles along the entire BNI length. Discard if bubbles appear, and start the process over again.
12. Very gently wipe off any excess agarose.
13. Begin to thaw the collagen solution in your hand. This is quite variable based on the volume of collagen used (try to use about 200 μ l). Check every 10 seconds with a sterile pipette tip to see if it is thawed.
14. Once thawed, add the cross-linking agent. Mix very gently with the pipette tip. Do not add any bubbles to the solution. If bubbles form and do not vanish, discard the collagen, and start again.

15. If the collagen solution is without bubbles, after a gentle, quick mix, then immediately add to loading well. Do not waste any time with this step. Add at least 150 μ l to the loading well. Make sure the collagen bulges well above the loading well. This column height is helpful to ensure a successful BNI.
16. As soon as the collagen is in the loading well, you must be ready to pull the needles from the casting device. The needle entering the loading well highest should be pulled first, and then each needle should be pulled afterwards in a descending fashion.
 - a. Grab the loading well with one set of tweezers and grab the needle to be pulled with the other set. There is a small amount of resistance to get the needle moving, but then very little afterwards. Pull the needles very slowly (10 seconds/needle), but be mindful of the necessity to complete this step quickly (the collagen is polymerizing and will be too viscous to pulled through by the last needle if you move too slowly).
17. Observe each channel for bubble formation. The BNI is a failure if air bubbles occlude any channels.

18. With all needles pulled, removed the end caps of the casting device gently. Take care not to disrupt any of the now formed collagen channels.
19. Place the BNI in a bath of cold 1xPBS.
20. Visually inspect the BNI under a microscope and ensure no manufacturing defects.

Surgery

NZWR were fitted with an isoflurane breathing mask and provided 3% isoflurane in the oxygen supply during all surgical procedures or injections. Animals were anesthetized with intramuscular injection of a ketamine-xylazine solution (35 mg/kg ketamine; 5 mg/kg xylazine). The left thigh from knee to spine was shaved and cleaned with 70% ethanol and povidone-iodine. An incision line was traced from just caudal to the femur head to the head of the knee. A scalpel was used to cut the skin and expose the underlying muscle. Cutting the fascia overlying the sciatic nerve split the muscles and they were held open by retractor. The sciatic nerve was exposed from the sciatic notch to the top of the knee. This long exposure is essential to separate the peroneal (smaller) from the tibial nerve (larger) in the sciatic bundle. The peroneal nerve must be separated from the tibial by cutting the fascia with micro-scissors and then gently spreading apart with #5 Dumont tweezers. After complete

exposure and separation, the peroneal was transected with micro-scissors twice to remove a 5 cm segment. The BNI was gently placed in the surgical area and then moved into place with tweezers. The proximal end of the peroneal nerve is gently placed into the BNI and sutured in place with 10-0 nylon sutures. The epineurium is sutured to the BNI tubing with minimal damage to the underlying nerve structure. The distal end is then fixed in the same manner. The muscles are closed with 3-0 chromic sutures and the skin is stapled and coated with antibiotic ointment. The wound is then bandaged and the animal is removed from the isoflurane.

Post-operative care. Each animal was administered approximately 2 ml of trimethoprim sulfamethoxazole orally by cannula syringe. In addition, the animals received buprenorphine (1 mg/kg) once a day subcutaneously. After one week, the bandages were removed if the animal had healed properly.

Behavioral Assays

Toe-spread index. The peroneal nerve innervates the tibialis anterior muscle responsible for dorsiflexion. This motor function can be tested by the toe-spread index, which is the ratio of the injured foot width divided by the uninjured foot when the animal is in a startled state. A simulated drop initiates the startled state and the animal readies itself to land on the ground by spreading its feet. Toe-spread width was measured

by ruler and calculated in Excel. Toe-spread testing was compared between the experimental groups at multiple time-points.

Formalin test. To assess sensory function of the peroneal nerve, a nociceptive formalin assay was used. The animal is briefly anesthetized with isoflurane and then formalin is injected into the dorsal side of the foot. This region is part of the dermatome of the peroneal nerve. 200 μ l of 10 % (by weight) formalin (Sigma) is used in a 1xPBS solution. The animal will immediately be awoken from the isoflurane-induced stupor, and then will lick the dorsal section of the foot. The animal is recorded by video for 10 minutes (technique note: avoid entering the room after injecting the animal – any human interaction will interrupt normal pain behavior).

Isometric muscle force testing. Exposing the tibialis anterior muscle and attaching the distal end to a custom-built force-plate transducer that then was fixed to a rigid testing apparatus measured muscle force during contraction. This test was done for both the injured side and the uninjured side. This terminal procedure was performed with the animal under ketamine/xylazine, but not isoflurane. The peroneal nerve was exposed at the sciatic notch. The tibialis anterior muscle was exposed, and the distal tendon was severed to allow insertion into the load sensor. The load sensor was a Load Star force transducer (MFM-010-050-A) that was connected to a Load Star USB hub (DQ 1000U) and then

finally a PC laptop with the Load Star LoadVUE software installed. After the distal end of the muscle was inserted into a modified alligator clip, the load sensor was zeroed to eliminate any pre-stimulus force. The peroneal nerve was then stimulated proximal to the conduit (Model 2100 AM Systems) with increasing voltage until a maximum twitch force was achieved. The entire stimulus period was recorded for review in EXCEL.

Gait analysis. This experiment piloted a new analysis method for functional recover of the CPN. Animals were initiated to walking on a treadmill before surgery. Permanent colored markers (Sharpie, Inc) were used to make circular colored patches on shaved skin at the knee, ankle, and the head of the 4th metatarsal. The animal was then placed on a treadmill (Dogpacer, Inc) designed for small dogs. The animal was given a few moments to become comfortable with the treadmill before it was turned on and set to the lowest speed (<3 miles per hour; MPH). The hopping pattern is quite variable, so an absolute speed is difficult to report. Two digital cameras connected to the OmiPlex (Plexon, Inc) system are activated to record at 80 fps (frames per second). With the color-marked animal hopping on the treadmill at a reasonable frequency, the CinePlex recoding system is turned on (Plexon, Inc). The colored marks are entered into the system by activating the color-tracking ROI (region of interest) mode. Some adjustment will need to be made to ensure the

colored mark is recognized properly. The animals are recorded for a minimum of 10 hops and two files – an .AVI file and a .DVT file are saved for further analysis. To analyze the kinematics of the gait, there are two main methods. CinePlex can be used to calculate the angle between three ROIs (knee, ankle, and 4th metatarsal). ImageJ (NIH) can also be used with screenshots of the images of interest. The angle tool in ImageJ was used to calculate the angle of the ankle joint throughout the hop. This calculation was used to compare the re-innervation of the CPN to the tibialis anterior muscle. The mid-swing ankle angle was the main parameter analyzed.

Tissue Fixation

Animals were euthanized with Euthosol (87 mg/kg) through a peritoneal injection. Once the animal was non-responsive, the animal was opened just below the sternum, and then the diaphragm was separated from the rib cage. This exposed the heart, to insert a large diameter cannula into to left ventricle all the way to the aorta. A 0.9% NaCl (Sigma) solution was pumped by peristaltic pump. The right atrium is cut to allow sufficient blood drainage. After 500 ml of the salt solution has perfused through the animal, a 4% paraformaldehyde (Sigma) was injected through the same system. Once the animal was fixed, the tibialis anterior muscle was removed for weighing and the BNI with proximal and distal segments

intact was removed. The samples were placed in a cold 4% PFA solution overnight, and then transferred to a 1xPBS solution and stored at 4 C.

Statistical Analysis

Analyses were performed in GraphPad Prism 5 or in Microsoft Excel 2010. Graphical results reflect an average with error bars representing the +/- of one standard deviation (SD). Paired groups were analyzed with a two-tailed T-Test and multiple groups were analyzed with a one-way ANOVA (analysis of variance). The post-hoc test was selected based on the recommendations of the statistical software and statistical textbooks^{34, 35}. Designations of each p-value are represented in graphs as follows: $p < 0.05$ *, $p < 0.01$ **, $p < 0.001$ ***.

Results

The main and most important result from this experiment is that none of the animals had nerve tissue recovery. Even the animals that received PTN augmented BNI conduits were unable to regenerate the CPN across a 5 cm gap. This means that all results presented reflect the chronic injury state of CPN de-innervation, and serve as a reference for the 4 cm gap experiment.

BNI Fabrication

BNI fabrication from this experiment had a very high failure rate due to the number of complexities of design. Including PLGA coils to 250 μm

metal needle proved to dramatically increase the error rate. For 9 successful BNIs approximately 40 conduits were attempted.

Explanted BNIs showed little fabrication defects, and none showed full tissue regeneration. Some conduits had regenerated tissue separated into the micro-channels, which indicated that the environment was suitable for regeneration, but there was likely not enough trophic support to entire the CPN.

Behavior Assays

TSI. None of the animals had functional recovery and none showed significant recovery of their ability to spread their toes. The first post-operative assay and the final assay showed little to no difference. As a reference for the subsequent experiments, the final toe-spread values were calculated at week 12 (just before sacking). As would be expected the animals are able to spread their uninjured foot nearly double the width of the injured foot (Figure 1-1).

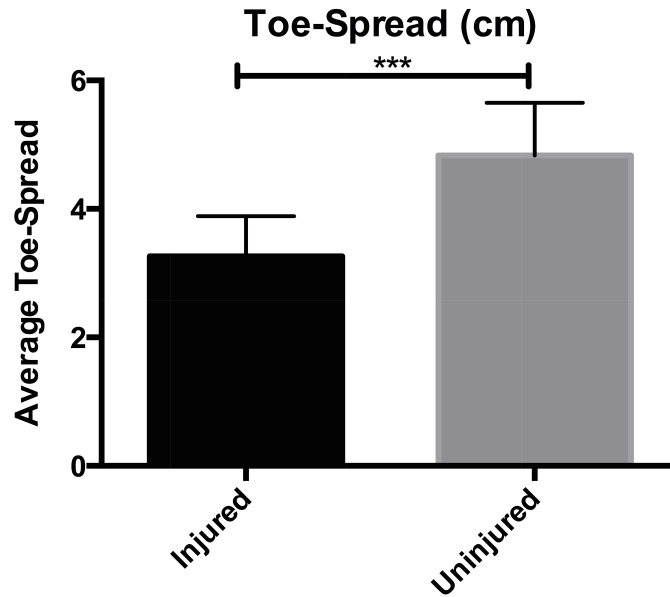


Figure 1-1 : Absolute toe-spread of the injured and uninjured feet of all animals post-surgery (mean with SD) (two-tailed paired t-test $p < 0.001$)³⁶

Formalin. No animals showed significant sensation recovery following the BNI implantation. There was a large amount of variability in the formalin response of the animals, but a significant decline in licks to the de-innervated area was observed (Figure 1-2; adapted from Prasad, P., 2012).

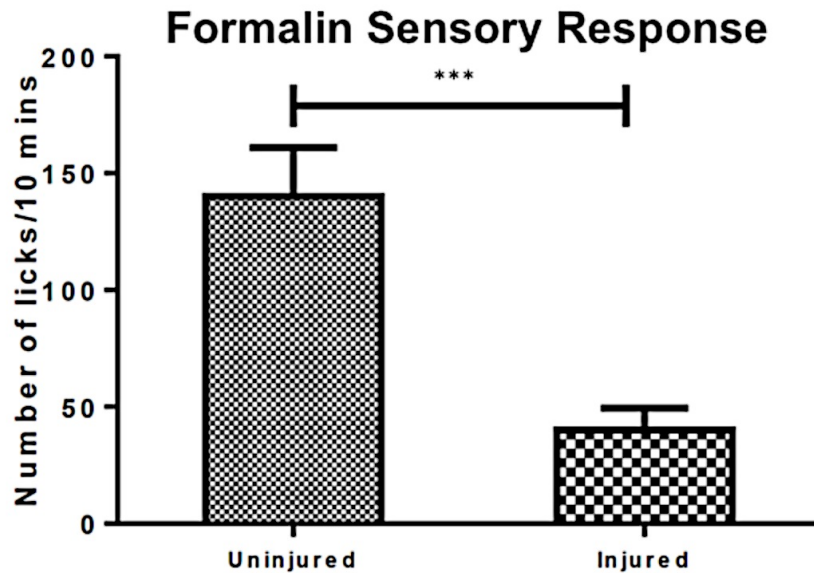


Figure 1-2: Average number of licks per 10 minutes following formalin injection for both uninjured and injured animals (adapted from Prasad, P., 2012)(mean with SD) (two-tailed paired t-test $p < 0.001$)³⁶

Isometric muscle force testing. As expected, very little muscle force of the tibialis anterior could be evoked by bi-polar electrode stimulation of the injured CPN. The uninjured side exhibited forceful contractions (Figure 1-3)³⁶.

Tibialis Anterior Muscle Force

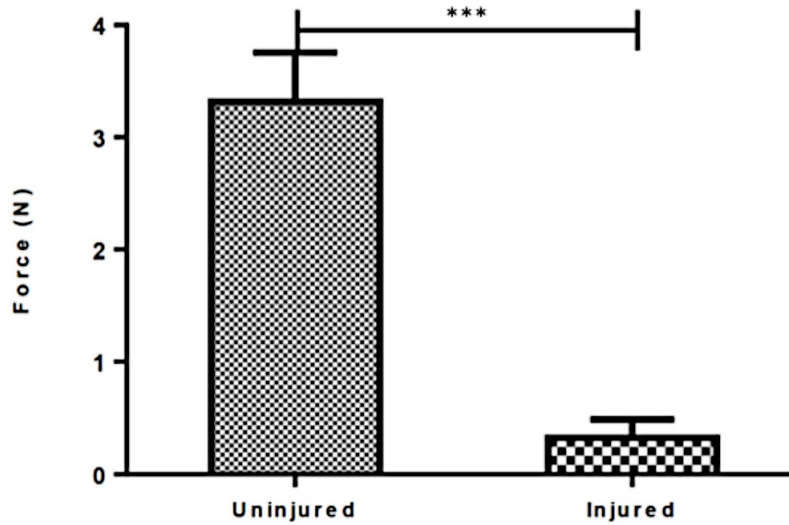


Figure 1-3: Muscle force of the tibialis anterior muscle during CPN electrical stimulation (adapted from Prasad, P., 2012)(mean with SD) (two-tailed paired t-test $p < 0.001$)³⁶

Gait analysis. Many parameters of the NZWR were analyzed, but the main finding was that post-injury the mid-swing ankle angle doubles when the injury to the CPN is chronic. The injury state of all animals is graphed below (Figure 1-4):

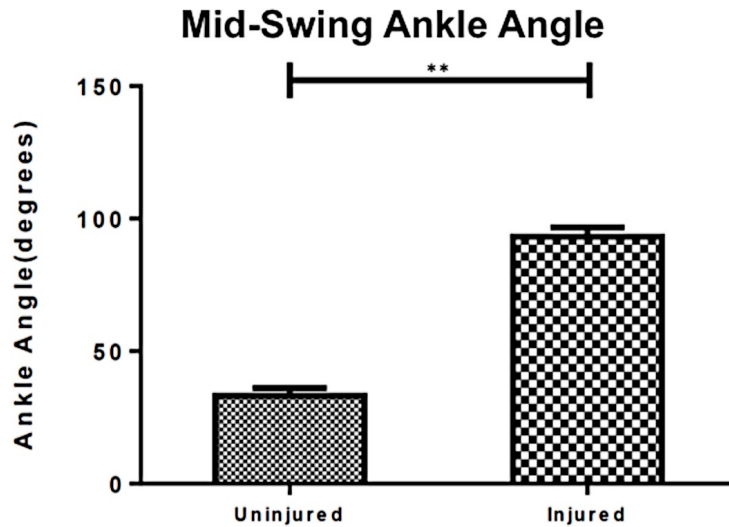


Figure 1-4: The mid-swing ankle angle for all animals for the injured and uninjured CPN state (adapted from Prasad, P., 2012)(mean with SD) (two-tailed paired t-test $p < 0.01$)³⁶

Discussion

From these preliminary experiments, we can conclude that CPN de-innervation leaves lasting functional deficits in NZWR. It appears that our delivery strategies for PTN proved to be inadequate to sustain peripheral nerve regeneration. The BNI does not seem to be the limiting element. It appears that sustained delivery of PTN across the full regeneration timeframe was a design limitation. The next experiment took a year to plan to ensure that PTN release was sufficient for the entire regeneration process.

4-Cm Gap Injury Experiment

After failing to regenerate the CPN across a 5 cm gap, we attempted to regenerate the CPN across a 4 cm gap with the most consistently reproducible growth factor delivery method. Initial work to accurately characterize growth factor release, was followed by a full NZWR experiment.

Experimental Design

24 NZWR were used to test the regeneration potential of BNIs at 4 cm gaps with pleiotrophic support. Other animals in the study were used to test hypotheses not included in this work. The experimental groups were as follows:

1. BNI without growth factors (BSA micro-particles) (4.4 cm long / 4.0 cm of internal agarose) (negative control – hypothesized to not achieve functional recovery) (n=5)
2. BNI with PLGA PTN micro-particles (4.4 cm long / 4.0 cm of internal agarose) (n=6)
3. Autograft (a 4 cm CPN segment was reversed and sutured in place) (n=4)

Functional recovery was assessed by toe-spread index (TSI), formalin nociceptive assay, and gait analysis.

Materials & Methods

Only differences from the previous BNI experiments will be explained.

BNI Fabrication

Growth factor release. To determine the quantity of growth factor released each day by PLGA micro-particles, an ELISA was run for each growth factor rather than a suitable alternative (previously, only BSA release was quantified by ELISA. The same time increments were measured as before, but the experiment was repeated to avoid an erroneous concentration. A daily concentration was calculated by the following method:

1. Calculation assumptions:
 - a. Growth factors were largely contained within the collagen matrix (two additional barriers: agarose and polyurethane tubing likely quarantined any escaped growth factors).
 - b. Growth factors were assumed to have a 4-day $\frac{1}{2}$ life in the area of implantation once eluted from the PLGA particle^{31, 37}. Little to no degradation was assumed while embedded³¹.
2. The release for day 1 was calculated by summing the growth factor released at 0, 2, 6, 12, and 24 hours.

3. Day 2 GF release was measured
4. Day 3 GF release was measured
5. Day 4 GF was assumed based on the amount of growth factor released on day 7. The cumulative amount of day 7 was divided for the calculation between days 4, 5, 6, and 7. This method likely underestimates the amount of GF actually released on day 4, but likely overestimates the amount released on day 7.
6. The remaining days up until day 28 were calculated individually by the method described above.
7. Once the daily release amounts were calculated, a $\frac{1}{2}$ life dependent factor was incorporated to find the true concentration of GF for each day.
 - a. Example of true GF concentration calculation (day 4) =
 - i. Amount released by particles on day 4
 - ii. +amount released on day 3 remaining:
 1. $(X_{\text{day3}})(1/2)^{(1/4)}$
 - iii. +amount released on day 2 remaining:
 1. $(X_{\text{day2}})(1/2)^{(2/4)}$
 - iv. +amount released on day 1 remaining:
 1. $(X_{\text{day1}})(1/2)^{(3/4)}$

- v. The sum was calculated for each day in this manner.

The daily amount of GF released was then converted into an absolute concentration by dividing by the volume of the BNI collagen. The amount of micro-particles was measured so as to never exceed the reported inhibitory concentrations in the literature (100 ng/ml)²²⁻²⁴. The exact same amount (weight) of PLGA micro-particles was added to the collagen. This was done to control for the effect of PLGA in the BNI channels. The correct amount of the GF PLGA particles was added, and then the necessary amount of BSA PLGA particles was added to account for the necessary mass.

Behavioral Assays

All behavioral assays were largely conducted in the same manner as the previous 5 cm experiment. However, each assay was systemically reviewed and optimized.

Toe-spread index. Previously, NZWR were given a simulated drop that was done by hand. To ensure a more consistent drop, a large sturdy vertical platform was constructed to support a moving track. The track supported a harness in which the NZWR was placed. The animal could be dropped repeatedly and consistently for each trial. Furthermore, rather than measuring the TSI by hand, a high-speed video camera was used to

track the animal, and the width of the feet was measured with ImageJ (NIH) and converted to centimeters.

Compound muscle action potential. In substitute of the muscle force testing, the evoked compound muscle action potentials (CMAP) were recorded for each animal. Immediately prior to sacking the animals, the BNI was exposed. A bipolar stimulating electrode was held proximal to the BNI and a stimulation pulse of up to 4.5 V was applied. The signal was recorded in the tibialis anterior and peroneal muscle (the muscles are in close proximity, but only one needle electrode was used). The stimulation and response waves were recorded on the Plexon OmniPlex System (Plexon, Inc.) at 40,000 Hz analog to digital conversion. Spikes were sorted to only look for amplitude changes consistent with the high voltage stimulation peak. Each peak identified served as a reference to save the signal 10 ms prior and 50 ms post-peak. The amplitudes of the response wave (action potential generated in the muscle; M-Peak) were calculated for each animal. If an animal showed an M-Peak, 1-2 drops of Lidocaine were applied to confirm that no peak remained. In addition, the compound action potential was measured in the anterograde and retrograde directions to examine the nerve conductivity.

Tissue Processing & Immunohistochemistry

After sacrificing the animals, tissue processing was performed on each conduit and autograft in the same manner. Each BNI was gently cleaned in a 1xPBS solution with careful attention to not disturb micro-channel architecture (note: it is difficult to prevent any damage to the very soft agarose, and pictures were taken on a Leica MZ75 of the BNIs before removing the outer tubing). The outer tubing of the BNI was removed to expose the agarose micro-channels. All nerve samples were split into proximal, middle, and distal sections for cross sectional axon comparison. These samples were sent to UT Southwestern Medical Center to be embedded in paraffin wax. The returned paraffin blocks were sectioned on a Leica microtome to approximately 10 μm in thickness and each slice was placed on a glass slide (Fisherbrand Superfrost Plus, FisherScientific, Inc.). The sections were further processed - dissolving the paraffin by heating the slides to 60 C for 15 minutes, and then immersing in xylene. The samples were then immersed in a series of decreasing concentration (diluted with deionized water) alcohol baths (100%, 90%, 70%, 0%) – concluding with a citric acid bath for 15 minutes at 80 C. The slides were then cooled for approximately 10 minutes. The slides were washed twice with 1xPBS and then incubated with a blocking solution (250 μL per slide; 4% Goat Serum) for one hour. Blocking solution is removed and primary

antibodies are added in the blocking solution (1:400 Mouse Anti-Beta-Tubulin; 1:325 Chicken Anti-P0; Invitrogen, Inc.) for one hour. B-Tubulin was used to stain for axons, and P0 was used to stain for myelination. The slides were washed three times for 10 minutes on a slow shaker. Secondary antibodies were added (1:400 Goat Anti-Chicken 488; 1:400 Goat Anti-Mouse Cy3) for one hour with no shaking. Samples were washed four times. The slides were then finished with mounting media and coverslip. They were maintained at 4 C until imaging. All imaging was performed on distal sections of the BNI or Autograft samples at 20X objective (1X OptoVar) using a Zeiss Observer Z1. Zeiss AxioVision software was used to perform a multidimensional image acquisition (Cy3 and GFP). Samples were chosen that had the highest density of B-Tubulin positive staining. Exposure was set by the measure function in AxioVision. Images were exported in TIF format for analysis in FIJI. The Cell Counter plugin was used in FIJI to count the number of B-Tubulin positive axons. The entire field of view was analyzed of intact samples. Some samples were excluded if there was indication of unspecific staining or high auto-fluorescence.

Results

BNI Fabrication

The BNI fabrication success rate improved substantially thanks to the improved temperature regulation of the agarose and collagen along with a more controlled introduction of the PLGA micro-particles to the collagen matrix. To successfully make 20 4.4 cm BNIs 28 were attempted. This is a success rate of 71%.

For PTN the cumulative release can be characterized as a burst within the first 48-hour period of implantation (Figure 1-5)³⁸:

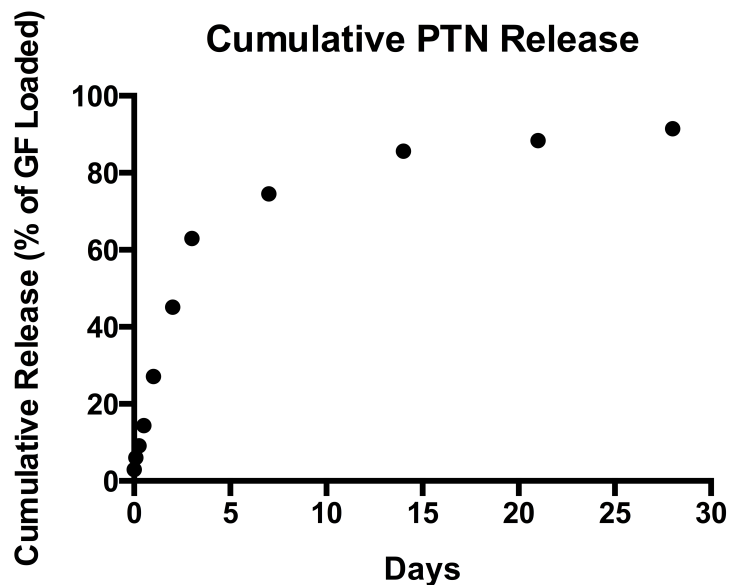


Figure 1-5: Cumulative PTN release into simulated body environment from PLGA micro-particles.

As was described in the methods section, a more analytical method was developed to report actual GF concentration within a BNI with the assumption that released GF does not immediately degrade, but rather has a 1/2 life. Additionally, this model provides the maximum concentration reached throughout the regeneration time frame so as to avoid inhibitory levels of GF (Figure 1-6):

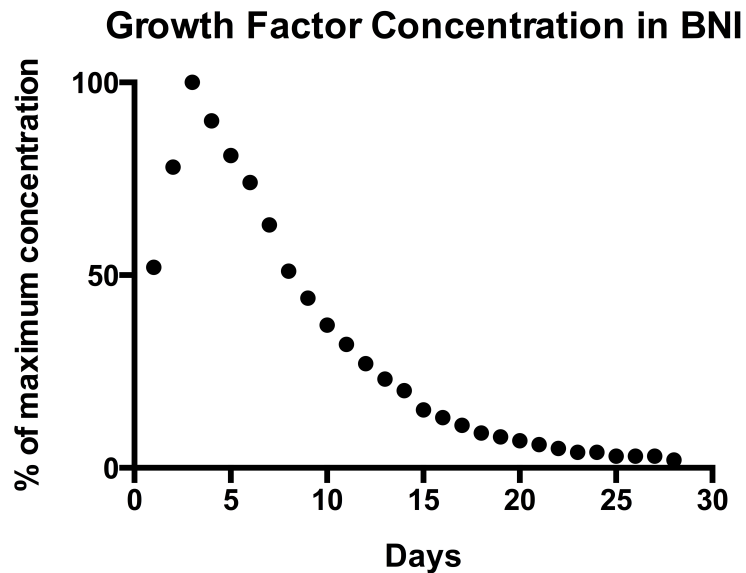


Figure 1-6: Maximum GF concentration for each day of the regeneration time frame. A maximum concentration is reached on day 4 (100 ng/ml).

Tissue Regeneration

The explanted BNIs were intact and showed no sign of infection or rejection. The regeneration of tissue across the 4 cm gap was very limited

in the BSA and PTN BNI groups. However, some animals showed clear regeneration tissue emanating from the proximal stump into the BNI.

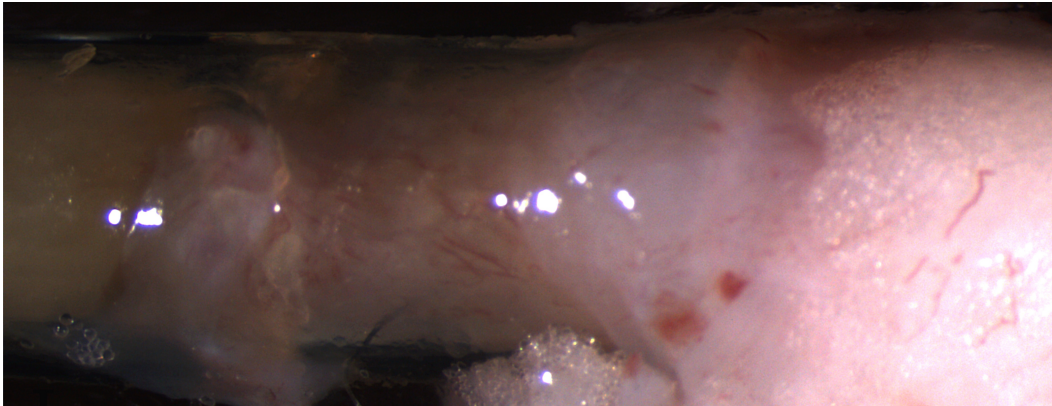


Figure 1-7: Image of explanted BNI with BSA micro-particles (N13) (Proximal End). Direction of outgrowth is from right to left.

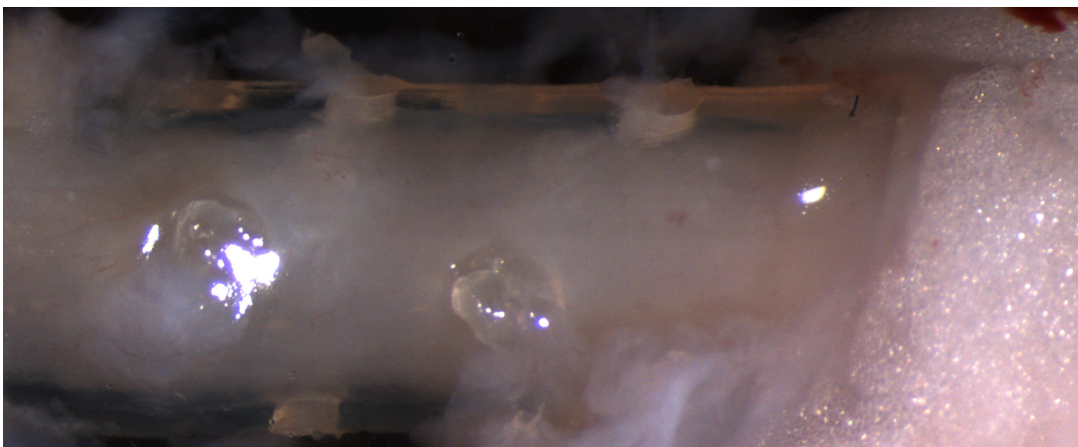


Figure 1-8: Image of explanted BNI with PTN micro-particles (N19) (Proximal End). Direction of outgrowth is from right to left.

Regeneration beginning at the proximal end appeared to be interrupted in a number of samples by either a cessation of regeneration,

or damage to the agarose channels during tissue processing (note: likely due to the connective tissue that surrounds the BNI and infiltrates through the outer pores).

Behavioral Assays

Animal behavior can be a highly variable and as such it was important to look at as many indications of functional recovery.

Furthermore, all animals were coded so the researchers were blind as to which animals had received which treatment.

Formalin test. The formalin test relies on functional re-innervation of the dermatome of the dorsal section of the foot. If the CPN does not re-innervate this area it is assumed that there will be no reaction to the painful injection. However, if the foot is re-innervated then the animal will begin licking the foot (it is assumed that number of licks corresponds to pain). The formalin assay was performed twice for each animal giving a cumulative n of 48. The number of licks was compared between groups in a one-way ANOVA with a multiple comparisons Tukey's post-hoc test, and no significant difference between groups was observed ($p=0.28$) (Figure 1-9).

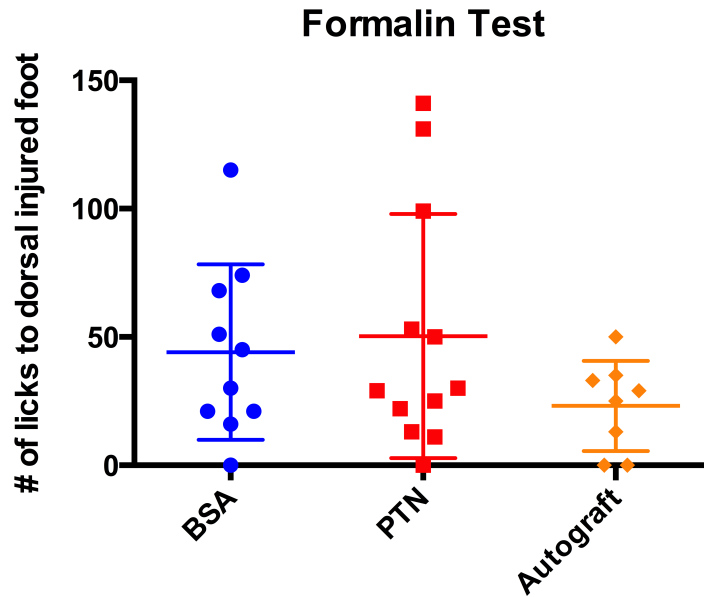


Figure 1-9: Formalin test results. No significant differences between experimental treatments in recovery of sensory function (one-way ANOVA).

Gait analysis. The gait was recorded for each animal once before surgery and then 5 times after surgery. Each animal had 10 hops analyzed for mid-swing ankle angle (MSAA; minimum angle achieved while hopping). The cumulative number of hops analyzed was approximately 1,400. The first two post-operative trials were combined to serve as a post-injury baseline, and compared to the final gait analysis. This served as a measure of the MSAA recovered for normal locomotion. The groups were analyzed by one-way ANOVA with a multiple comparisons Tukey's test. No significant difference between groups was

observed ($p=0.055$), but clearly the autograft had the largest functional recovery. In an unpaired two-tailed t test with Welch's correction, a significant difference was observed between the Autograft and PTN group ($p=0.028$). (Figure 1-10).

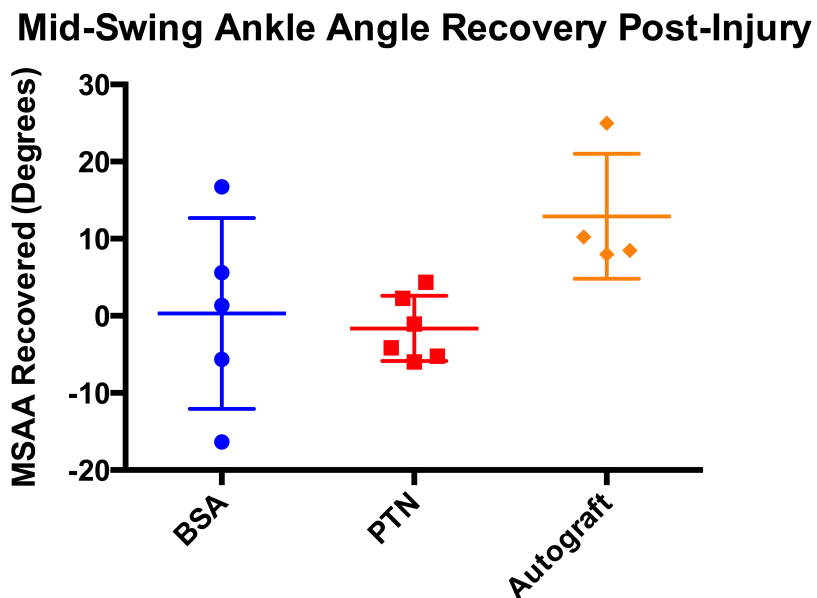


Figure 1-10: Mid-swing ankle angle recovered after injury. Positive values represent the treatment group had greater recovery of function. No significant difference was observed between experimental groups (one-way ANOVA; $p=0.055$).

Toe-spread index. The toe-spread index(TSI) is a ratio of the injured foot to the uninjured foot when the animal is startled into spreading its feet. A TSI value of 1.0 indicates that the animal spreads its feet equally. For the TSI assay the animal was recorded for each animal once

before surgery and 5 times after surgery. Each trial includes 5 repeated measures. This gives a total number of trials analyzed of approximately 700. To calculate the recovery of function, the final TSI was compared to the baseline TSI. This ratio was reported as the percent recovery of TSI. When groups were compared, there was a significant difference between groups by one-way ANOVA ($p=0.0297$). The significant difference was further analyzed by Tukey's multiple comparisons test, and only the Autograft and BNI with BSA groups were significantly different ($p=0.0324$). Autograft and PTN were not significantly different ($p=0.0634$), but had less range overlap than did the PTN and BSA comparison ($p=0.8598$) (Figure 1-11).

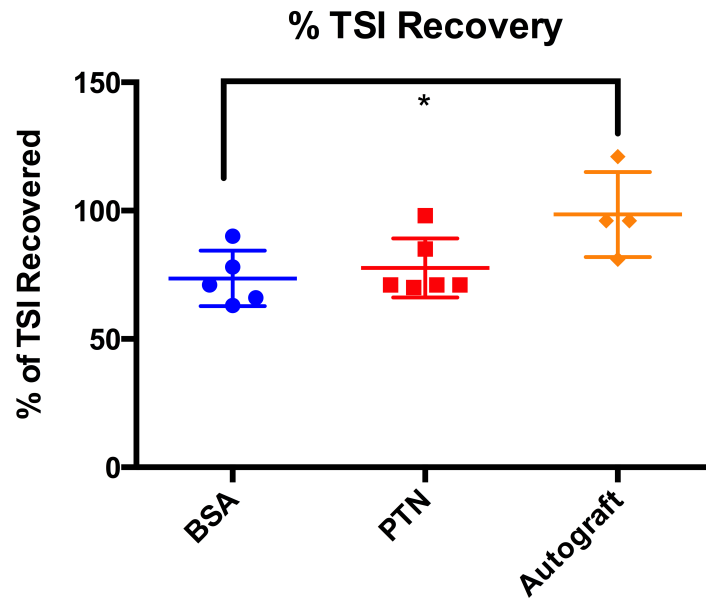


Figure 1-11: The percent of TSI recovery is plotted. One-way ANOVA of the groups yielded a significant difference between the Autograft and BSA experimental groups ($p=0.0297$).

CMAP. The CMAP of each animal was plotted and then the maximum M-Peak amplitude was calculated. A one-way ANOVA with Tukey's post-hoc multiple comparisons test showed a highly significant difference ($p<0.0001$) between the experimental groups and the positive control Autograft group (Figure 1-12).

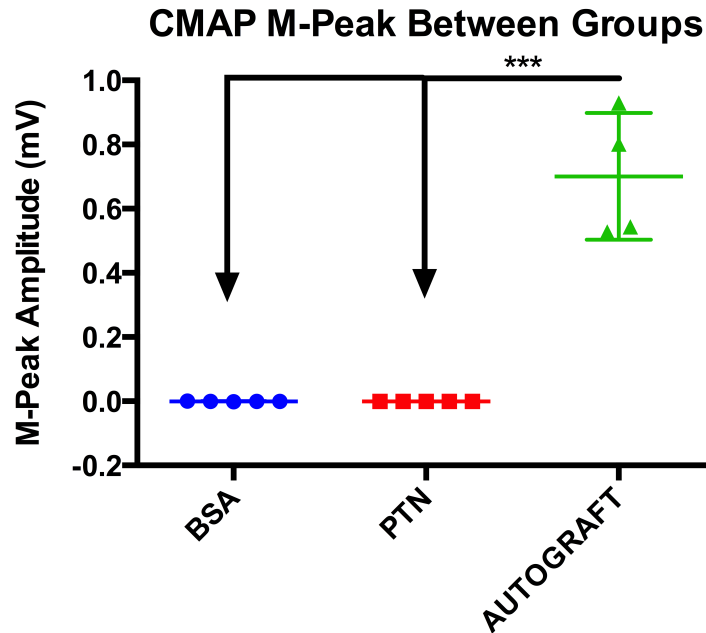


Figure 1-12: The calculated M-Peak values. The Autograft group had the highest M-Peak wave amplitude, and the difference between the BNI w/ BSA and BNI w/ PTN was highly significant ($p < 0.0001$). No significant difference was observed between the two BNI groups.

Immunohistochemistry. The BSA and PTN groups showed some evidence of B-tubulin positive axons distal to the BNI implant whereas the Autograft group showed a dramatically higher number of axons. There were very few myelinated axons in any sample analyzed for the BSA and PTN groups, whereas significant myelination was observed for the Autograft group.

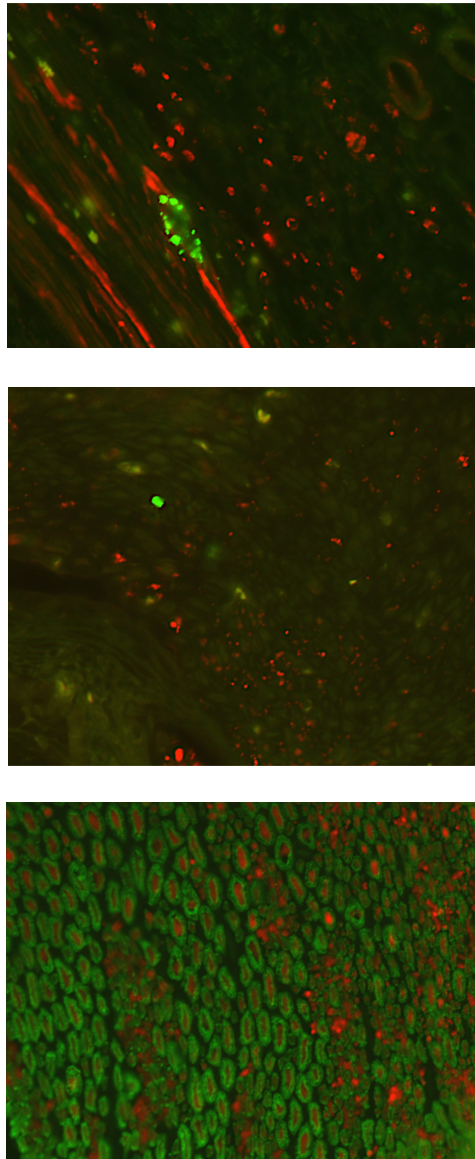


Figure 1-13: Top, Animal N13 (BNI w/ BSA); Middle, Animal N19 (BNI w/ PTN); Bottom, Animal N11 (Autograft). B-Tubulin (red) and P0 staining (green) shows clear indication of myelination around most axons in the autograft sample with little to no indication in the BSA or PTN animals.

The same cross sectional area (1388 by 1040 pixels at 20X objective and 1X OptoVar), was analyzed for the total number of axons. A one-way ANOVA showed a significant difference between the Autograft and the BNI groups ($p < 0.0001$). Autograft samples had significantly higher axonal density. There was no significant difference between the BNIs with BSA or PTN.

B-Tubulin+ Axons (Same Cross-Sectional Area)

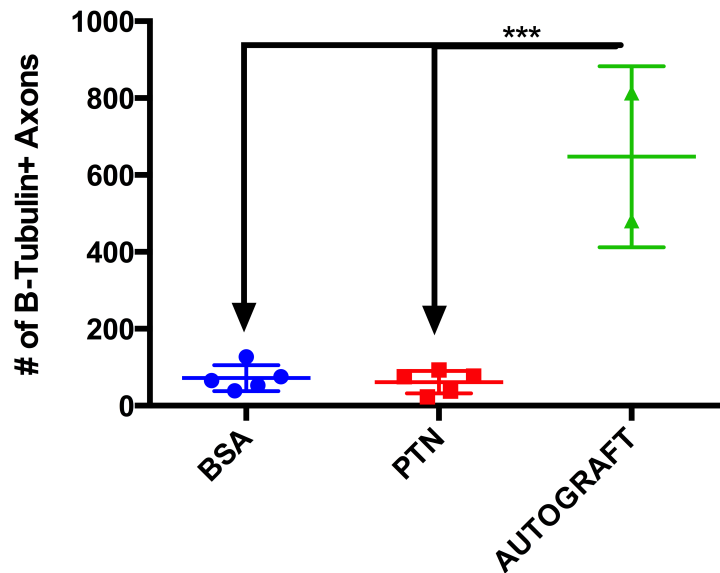


Figure 1-14: # of B-Tubulin positive axons in the same cross-sectional area (1388x1040 pixels). The Autograft group has a significantly higher axonal density.

Discussion

This study is one of the largest, most thorough investigations into trophic support of peripheral nerve regeneration. The 4 cm gap trials allow us to conclude the following: to regenerate functional nervous tissue beyond 3 cm sustained sub-inhibitory concentration PTN (100 ng/ml) delivery is not sufficient. The PTN augmented BNIs showed signs of regenerated tissue, but gaps in the tissue indicate incomplete recovery. The same is true for the BSA BNI group.

During this same experiment, a trial of synergistic growth factors (PTN and GDNF) was attempted and showed regeneration in 2 out of 5 animals. This indicates that our step-by-step approach to adding all the components necessary will likely be successful.

This study also demonstrated the importance of accurate modeling of growth factor support. Without accurate drug delivery, a researcher has only increased the variables in a controlled experiment. Our work at 5 cm did not control adequately for the amount of GF released and maintained in the lumen of the BNI. The modeling presented here serves as an important addition to the field for implants that maintain an isolated environment from the body.

Behavioral assays remain a troublesome aspect of animal work. The lack of clear results between the experimental groups indicates that

likely many factors need to be combined to yield an accurate picture of functional recovery (i.e. the sciatic functional index)^{6, 39-41}. It was very useful to have multiple assays to fully characterize functional difference between groups. Ultimately, CMAP analysis proved to provide the most clarity, confirming that the tissue regenerated in each BNI was highly unlikely to be functional.

From the immunohistochemistry samples there is little evidence of axons in the BSA or PTN BNI groups becoming re-myelinated. This result, coupled with the CMAP analysis, indicates that although some axons were able to bridge a 4 cm gap it is likely that these axons were not mature or functional at the time of sacking.

Differences between the pre-injury and post-injury state (as seen in the 5 cm work), are interesting, but do not give a clear picture as to which treatment is working better. Although many of the behavioral differences between experimental groups are not significant in this 4 cm work, it should be recognized that this analysis was done to isolate one variable over a 4-month recovery period. This experimental design both increases the importance of the work, and decreases the chances of large effect sizes.

Conclusion

In conclusion, peripheral nerve regeneration across long-gap defects remains a significant problem for both surgeons and patients. Although our research group has been able to show functional regeneration across 3 cm gaps, consistent 4 cm gap recovery did not occur. Axons that did bridge the gap at 4 cm do not show evidence of mature myelination or functionality. This indicates that the BNI approach is very much a viable model for peripheral nerve repair at 4 cm, but the growth factor delivery system employed in this work was not sufficient to provide functional recovery even with axons that spanned 4 cm deficits. Work undertaken to improve the growth factor delivery not presented here was submitted for an international patent in Appendix A (PCT/US14/16905).

In addition, working with large animals was an important challenge for our research group. Many experimental treatments for peripheral nerve repair focus on short gaps in small animal models. The added complexities of long-gaps and large animals make this work more relevant for patients.

It remains that the gold standard in peripheral nerve repair is the harvested autograft, but with the advent of more precise additive

manufacturing, and advanced drug-delivery methods, it is possible that a synthetic peripheral nerve conduit could perform as well as an autograft.

Chapter 2

Multi-Luminal Conduit To Impede Neuroma Development And Peripheral Nerve Pain

Introduction

Neuroma

Following axotomy in an intact appendage, the regeneration program of the nerve begins. With a distal target found, the nerve will mature and arrest regeneration⁴². There is no such signaling for nerve regeneration in an amputated limb. With no intact distal target the nerve will continue to regenerate leading to a mass of intertwined axons, connective tissue, and inflammatory cells⁴²⁻⁴⁸. This benign tumor known as a neuroma will generate debilitating pain signals in many patients⁴⁸. Any successful neuroma therapy must successfully inhibit the neuroma-associated pain that for many patients is intractable⁴⁸.

Each year over 185,000 patients in the United States undergo an amputation procedure^{49, 50}. In addition over 2 million patients live with an amputation^{49, 50}. Patients will develop a neuroma at the distal stump of their amputated appendage, but the incidence of neuropathic pain is variable⁴⁸. The neuropathic pain is often treated surgically by removing the neuroma bulb, and then ablating the tissue proximal to the neuroma⁴⁴. Other surgical techniques include burying the nerve ending in skeletal

bone or suturing the epineurium^{44, 45}. The bulb serves as a focal point of peripheral nerve pain, and has been shown to respond to mechanical, thermal, and chemical nociception⁵¹. C-fibers have been implicated as the main determinant of neuroma bulb pain, but other fiber sub-types may play a role in neuroma pain^{42, 43, 52}.

Conduits approved for peripheral nerve repair are also approved for peripheral neuroma treatment, but adoption of this technique is not widespread^{25, 53}. Originally, conduits were proposed as a method to mechanically isolate the neuroma bulb^{25, 53}.

Multi-Luminal Neuroma Conduit Experiment

Experimental Design

This experiment was designed to test if a multi-luminal conduit would keep regenerating nervous tissue in separate channels and limit intertwining of nerve endings. Intertwining nerve endings may increase the potential of co-activation (an action potential is induced by an action potential in an adjacent axon)^{51, 52}. Our hypothesis that the combination of mechanical isolation in a conduit with multi-channels would provide significant pain attenuation of mechanically induced neuroma pain. In addition to the multi-luminal approach, we hypothesized that introducing different concentration agarose gels into the ends of each

lumen would provide a soft zone for the nerves to complete their regeneration attempt.

To create an amputation model in animals, we chose the Tibial Nerve Transition (TNT) model⁵¹. This is a well-categorized model that was developed at Johns Hopkins Hospital for studying amputation neuromas without creating an amputation⁵¹. The experimental groups are as follows:

1. Exposed TNT Neuroma (negative control) (n=5)
(hypothesized to exhibit the most pain)
2. TNT neuroma in hollow conduit (n=6) (hypothesized to have less pain than the exposed neuroma group)
3. TNT neuroma in a multi-luminal gel-gradient conduit (n=6)
(hypothesized to have the least pain of the experimental groups)

The main parameter this experiment tested was mechanically induced neuroma pain. Using well-studied Von Frey filaments and the pain scale developed at Johns Hopkins Hospital we conducted our experiments on Lewis rats.

Materials & Methods

Animal Model

17 Lewis rats were used to begin this experiment. They were the same sex (female), weight, and age. Animals received no noxious stimulus before their surgery.

Multi-Luminal Gel-Gradient Conduit Construction

All of the same materials used to make the BNI conduits were used to make the conduits for this experiment; with the sole exception that super-glue (Fisher Scientific, Inc.) was included to cap the distal end of the conduit. All of the temperature and cleaning preparations taken for BNI fabrication were repeated for neuroma conduits. The order of fabrication is as follows:

1. All materials were assembled and disinfected in a BSL-2 hood.
2. Polyurethane tubing (MRE-095; Braintree Scientific, Inc.) was cut to length (1.5 cm) and not perforated like in the BNI fabrication.
3. Two agarose solutions were prepared (1.5% and 3.0%).
4. The distal end of the conduit was filled with 3.0% agarose until approximately 1/3 of the volume was occupied.
5. The agarose was allowed to gel and become solid.

6. The 1.5% agarose solution was injected proximally to the 3.0% agarose and 250 μm needles (n=3) were positioned in the cooling agarose. A 3 mm void was left in the proximal end of the conduit for tibial nerve insertion.
7. The needles were removed once the agarose gelled.
8. The distal end of the conduit was sealed with a thin layer of super glue.
9. The completed conduit was placed in 1x PBS. The full design can be seen in Figure 2-1:

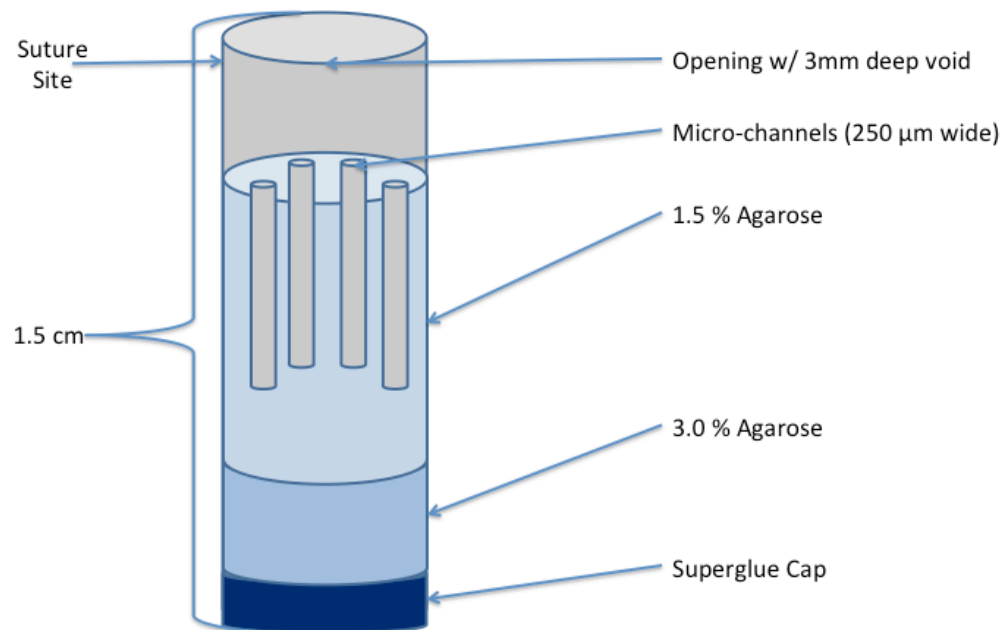


Figure 2-1: Multi-luminal gel-gradient conduit design.

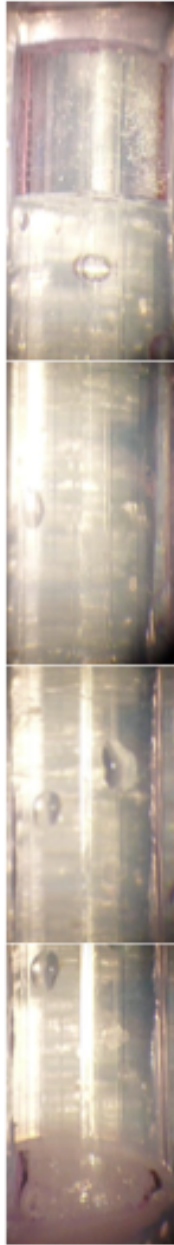


Figure 2-2: Stitched image of multi-luminal neuroma conduit before implantation.

TNT Surgery

Lewis rats (LR) were fitted with an isoflurane breathing mask and provided 1.5% isoflurane in the oxygen supply during all surgical procedures or injections. The left thigh from knee to spine was shaved and cleaned with 70% ethanol and povidone-iodine. An incision line was traced from just caudal to the femur head to the head of the knee. A scalpel was used to cut the skin and expose the underlying muscle. Cutting the fascia overlying the sciatic nerve split the muscles and they were held open by retractor. The sciatic nerve was exposed from the sciatic notch to the middle of the femur. This long exposure is essential to separate the peroneal (smaller) from the tibial nerve (larger) in the sciatic bundle. The tibial nerve must be separated from the peroneal by cutting the fascia with micro-scissors and then gently spreading apart with #5 Dumont tweezers. After complete exposure and separation, the tibial was transected with micro-scissors to create an approximately 2 cm segment. This section of tibial nerve was brought to the top of the quadriceps muscle and fixed in place by suture. This completes the surgery for the TNT neuroma, but additional steps were necessary to fix the hollow, and multi-luminal conduits. The conduits gently placed in the surgical area and then moved into place with tweezers. The proximal end (approximately 3 mm of nervous tissue) of the tibial nerve is gently placed

into the conduit and sutured in place with 10-0 nylon sutures. The epineurium is sutured to the BNI tubing with minimal damage to the underlying nerve structure. The distal ends of the conduits were then fixed to the muscle to prevent movement. The location of the neuroma or conduit was demarcated on the skin by permanent marker and surgical staple. The muscles are closed with 3-0 chromic sutures (the tibial nerve projects through the suture line) and the skin is stapled and coated with antibiotic ointment. The animal is removed from the isoflurane.

Post-operative care. The animals received sustained-release buprenorphine (1 mg/kg) every 3 days subcutaneously for one week.

Behavioral Assays

Von frey filament mechanical assay. Von Frey filaments are flexible needles designed to deliver a certain force to the skin before bending. In this experiment 300 g filaments were used (Ugo Basile, Inc.). Each animal had the neuroma site marked from surgery, and a brief shave revealed the area quickly. Each animal was coded by a research assistant, and then given to the research tester (tester was blind to the experimental group of the animal). The tester would apply the Von Frey filament to the neuroma site 10 times and score each application: 0-no response, 1-withdrawal, 2-quick withdrawal, shaking, licking, or audible squeal. The same process was completed on the contralateral side.

Tissue Fixation

Animals were euthanized with Euthosol (87 mg/kg) through a peritoneal injection. Once the animal was non-responsive, the animal was opened just below the sternum, and then the diaphragm was separated from the rib cage. This exposed the heart, to insert a large diameter cannula into to left ventricle all the way to the aorta. A 0.9% NaCl (Sigma) solution was pumped by peristaltic pump. The right atrium is cut to allow sufficient blood drainage. After 100 ml of the salt solution has perfused through the animal, a 4% paraformaldehyde (Sigma) was injected through the same system. Once the animal was fixed, the neuroma bulb, hollow conduit, or multi-luminal conduit was removed. In addition to the neuroma bulb, spinal cord sections (L 3-5) were taken. The samples were placed in a cold 4% PFA solution overnight, and then transferred to a 1xPBS solution and stored at 4 C.

Statistics

In addition to the previously used statistical methods, an additional set of methods was used specifically for this experiment. The scoring system for animal behavior necessitated a more advanced statistical method. Dr. Shan Sun-Mitchell, PhD assisted in the creation of a statistical method to better analyze experimental groups when using a scoring system. The scores for each trial were summed by animal and by

animal group, and then entered into a non-parametric statistical test in SAS 9.0 (SAS Institute, Inc.)^{34, 35}. Subtracting the score of the contralateral side trials controlled for variability in animal sensitivity. The recommended non-parametric test was the Wilcoxon Rank-Sum Test. An example of the coding with comments can be seen below:

```
data Von Frey;
    input trt $ score;
datalines;
Data entered by group and by score
;
proc sort data = Von Frey;
run;
proc print data = Von Frey;
run;
proc npar1way wilcoxon data = Von Frey;
    class trt; var score;
    Title1 'The Wilcoxon Rank-Sum Test';
    Title2 'Cumulative Pain Analysis (3 Trials)';
run;
```

Results

All animals were reactive to mechanical stimuli on their injured side in a reproducible manner. Figure 2-2 demonstrates a representative withdrawal sequence of the injured appendage following Von Frey application:

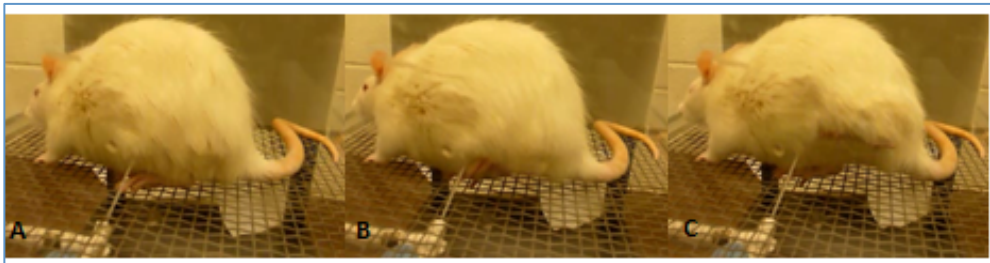


Figure 2-3: Stages of Von Frey stimulation withdrawal. Frame A: Von Frey filament contact, Frame B: withdrawal initiation, Frame C: maximum withdrawal. Withdrawal occurs after filament contact. Total withdrawal time: <0.5 seconds.

The pain score (cumulative pain response of injured side – the cumulative pain response of uninjured side) of each animal was combined and averaged by group. This experiment was repeated for four trials yielding a significant difference between the experimental groups. Approximately 1,360 Von Frey trials were scored. The group with the most mechanical pain was the hollow conduit group, followed by the neuroma group, and then finally the multi-luminal conduit group ($p < 0.05$) (Figure 2-3).

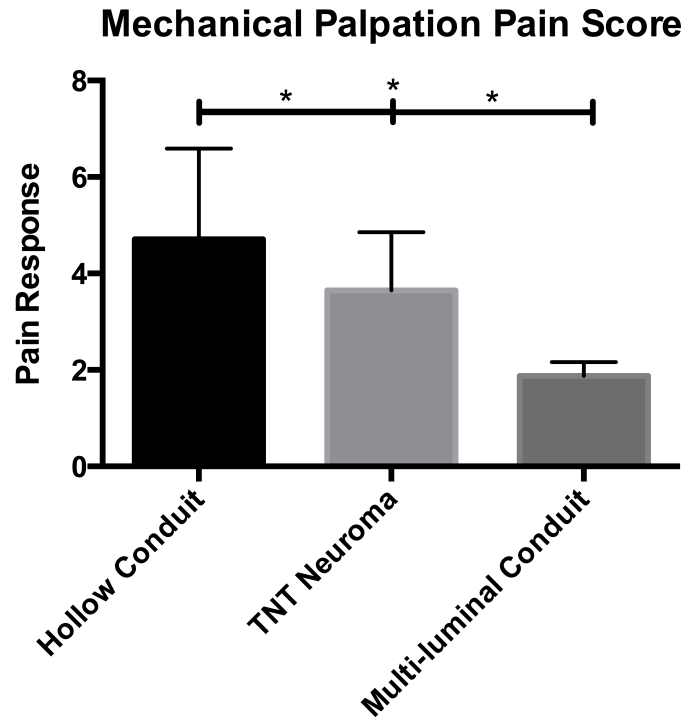


Figure 2-4: Mechanical pain assessment for three experimental groups. Groups are plotted as means with SD, but significance is indicated based on the non-parametric Wilcoxon Rank-Sum testing ($p < 0.05$).

The gross morphology of the explanted conduits was as expected. The TNT neuroma control group had large bulbous neuromas. The hollow conduit group had a small amount of tissue enter the conduit, but the majority of the tissue formed a bulb at the proximal end of the implant. The multi-luminal conduit showed nervous tissue down the parallel micro-channels (Figure 2-4)



Figure 2-5: An explanted multi-luminal gel-gradient conduit. Nervous tissue is confined to tracks within the conduit (yellow arrows).

Discussion

Hollow conduits alone do not provide pain prevention for amputation neuromas. Our results confirm the clinical bias against using hollow conduits for neuroma treatment. Animals had very consistent pain displays that could be elicited by a mechanical palpation. Surprisingly, the amount of elicited pain was higher for animals with hollow conduits than for animals with an unprotected neuroma. It is unclear why the hollow conduit increased the pain score, but it may have to do with confining the neuroma bundle into an even more compact bulb. Whereas the multi-channel conduit allows for the neuroma bulb to disperse into channels, the hollow conduit may have increased the chance for co-activation of pain fibers.

The statistical analysis was designed for this experiment and worked to provide clarity to scaled non-parametric data. Tissue

morphology confirmed our hypothesis that peripheral nervous tissue would grow in segregated tracts.

Conclusion

In conclusion, this work represents a significant improvement in the way amputation neuromas can be treated with surgical implants. We designed, built, and tested a novel design (PCT/US14/16801). We provided a clear answer that multi-luminal conduits provide a benefit in limiting induced-mechanical pain in neuromas.

Chapter 3

Investigations Into Radio-Frequency Induced Neuropathic Pain

Introduction

Neuropathic Pain

Neuropathic pain is characterized by pain that develops following nerve injury^{15, 54-59}. The nerve injury is an initial source of pain, but a number of changes to the nerve following injury lead to neuropathic pain^{15, 60-63}. As was mentioned in Chapter 1, recruited macrophages and reactive Schwann cells produce cytokines that increase inflammation^{15, 61}. This chronic inflammation state causes Schwann cells to proliferate producing more reactive cells^{15, 61, 62}. Sodium (Na), Potassium (K), and Calcium (Ca) channels have different expression levels and excitability from normal nerve tissue^{15, 61}. Na_v1.3 has increased expression, and increased excitability leading to a lower threshold for activation^{15, 60, 61}. Other sodium channels (Na_v1.1, Na_v1.2, Na_v1.6, Na_v1.7, Na_v1.8, Na_v1.9) are associated with neuropathic pain development^{15, 60, 61}. K_v1.1 is up-regulated and has an unusual distribution along the nerve tract in neuromas^{15, 60, 61}. Ion channel expression changes have different effects for motor and sensory fibers – motor fibers are generally less excitable, and sensory neurons are generally more excitable following injury^{15, 60, 61}. As an example, nociceptive fibers become increasingly sensitive to temperature changes

following nerve injury^{61, 63}. When animals were subjected to noxious thermal stimuli the withdrawal threshold was lowered by almost 4 C in injured animals⁶¹⁻⁶³. This increased thermal sensitivity is matched by increased chemo-sensitivity (Bradykinin, adrenalin, etc.)⁶¹⁻⁶³. The induced neural plasticity in the damaged peripheral nerve and subsequent changes in the central nervous system are the key changes that cause neuropathic pain^{15, 54, 57, 59, 61-66}.

Clinical Presentation

During experiments to test the benefit of surgical conduits for treating mechanical neuroma pain, a patient that suffered from amputation neuroma pain met with members of the Regenerative Neurobiology Lab. During his service in the Iraq, this patient was severely injured by an improvised explosive device. Surgeons repaired large sections of his body, but the patient's left arm was detached and unable to be reattached. Unfortunately the patient's amputated arm developed painful neuromas. Surgeons attempted to remove the neuroma bulb to decrease pain levels, but in over 20 operations there was no relief from neuropathic pain. Pain was induced from a number of noxious stimuli: mechanical, thermal, and general stress. Surprisingly, the patient had observed in a systematic manner that his neuromas felt more painful when he travelled close to cell phone towers. The emission spectrum from cell phone towers occupies a

number of frequency ranges, but one of them is 915 megahertz (MHz). This is also the frequency range used to power radio-frequency identification (RFID) devices. The power output from cell phone towers can be measured in a number of units, and reflects the power emanated by all emission spectra. For the purposes of our work, power will be measured in milli-watts per square meter (mW/m^2). With these parameters established and a clear clinical mandate, we set about to investigate if neuroma pain could be elicited by radio-frequency (RF) signals.

Electromagnetic Field (EMF) Effects

There have been a considerable number of studies looking at the effects of electromagnetic fields (EMF) on cells⁶⁷⁻⁷¹. Electromagnetic fields can be static (sometimes referred to as DC fields) or alternating (referred to as AC). This distinction is important as DC fields move ions in one direction with an applied voltage, and AC fields cause repeated vibrations as particles are pulled back and forth by the changing polarity of the field⁷¹. A 915 MHz electromagnetic wave is considered a very high-frequency (Radio Frequency – RF), microwave and generates a very quick alternating field inducing vibrations in ions in solution^{70, 71}. The EMF effect is primarily based on:

1. The type of field (static or alternating)

2. The frequency of the wave if alternating.

3. The power of the field (energy/area)

It has been demonstrated that RF can induce transcriptional, translation, and other cellular activity (e.g. calcium influx), but a clear demonstration of RF induced pain has not been systematically confirmed^{70, 71}.

Pilot Experiments

With the 17 Lewis rats tested in Chapter 2 of this work, we conducted pilot RF experiments. A number of different experimental parameters were tried to optimize methods for larger experimental trials, but briefly: RFID antennas capable of putting out 800 mW/m² power at 915 MHz were used on animals with peripheral nerve damage (TNT surgery axotomy). Animals reacted when the antennas were turned on with characteristic pain behaviors (withdrawal, licking, stretching/shaking). Although this behavior was reproducible, and was gathered in multiple trials over months of recording, we agreed that a repeat experiment just to test the RF phenomenon was in order. New nociceptive assays, new animal models, additional controls, and clear RF testing parameters were optimized with animals before executing a large study. From our pilot experiments, across months of testing, we were confident that RF exposure resulted in neuroma pain.

In Vivo Experiments

Experimental Design

In 2012 a research team in Japan developed a transgenic Wistar rat that expressed the optogenetic protein channelrhodopsin-2 (ChR2) driven by the Thy-1.2 promoter⁷². ChR2 responds to blue light by conforming to a pore that allows sodium ions to flow through⁷³⁻⁷⁶. The Thy-1.2 promoter sequence is associated with mechanoreceptive fibers in the peripheral nervous system⁷². Histological confirmation of ChR2 expression was performed using Venus-4 (a modified yellow fluorescent protein) revealed that ChR2 was largely confined to mechanoreceptive (in nerve endings i.e. Merkel cells and Meissner's corpuscles) and not nociceptive fibers⁷². This meant that the mechanoreceptive fibers in these animals would react to blue light as if they were being touched. These animals were requested and shipped from Japan to begin experimental work. 20 female rats were selected of similar weight and age. All were similarly reactive to blue (473 nm) laser light (20 mW). The animals were divided into the following groups for an initial TNT surgery:

1. Sham surgery (animals were opened, but no nerve damage occurred) (n=4)
2. TNT Neuroma (animals were given a TNT neuroma as was previously described) (n=16)

Blinded researchers tested the animals with the following nociceptive assays (additional details in methods section):

1. Radio-Frequency (RF) – 915 MHz at an approximate power of 700 mW/m²
2. Thermal – skin temperature was raised approximately 4 C by using a heat lamp
3. Von Frey (VF) – a 300 gram filament was used to palpate injured and uninjured areas
4. Optogenetic Laser Von Frey (OLVF) – a 20 mW laser was shined on the injured and uninjured areas in the same manner as the Von Frey testing

Animals were tested once a week for 4 continuous weeks after surgery. A Lidocaine control experiment was performed on the 5th week. These experiments were meant to test if RF stimulus elicited characteristic pain behavior in animals with neuromas. Our hypothesis was that animals without neuromas would show no pain responses, whereas animals with neuromas would have consistent pain responses. The second aspect of this initial testing was to identify the other nociceptive assay (thermal, VF, or OLVF) was most similar to the RF testing.

A second set of surgeries was performed to test one additional hypothesis. We wanted to examine if the bulb of the neuroma acted as a

biological antenna for RF energy. To test this hypothesis, ½ of the TNT neuroma animals had the neuroma bulb removed and the other ½ had a sham surgery. The animals were then immediately retested for 4 weeks.

Finally, a new experimental apparatus was engineered, built, and tested called an RF anxiety chamber. The two-chambered apparatus had a full RF field in one chamber, and 1/7th the field in the other. Animals were tested for location preference – this experiment was designed to test whether neuroma animals and sham animals spent significantly different amounts of time in each chamber.

Materials & Methods

Radio Frequency Environmental Characterization

Field measurements were made directly adjacent to cell phone antenna towers. The TM-196 RF three-axis Field Strength Meter (Tenmars Electronics Co, LTD) was used to record signal strength. Signal strength was measured north, south, east, and west of the tower at various distances. Both the maximum field power and average power were measured (mW/m²).

In addition to cell phone tower antennas, the RFID antenna used for all *in vivo* and *in vitro* testing was fully characterized using the same field strength meter. The antenna was a 915 MHz Andrew RFID-900-SC antenna. The power supply for the antenna was an Alien ALR-9900. The

Alien RFID Gateway v2.20.00 software suite controlled the power supply and antenna.

RF Skin Temperature Testing

Before the first surgery, three rats were randomly selected to undergo a brief experiment with RF exposure. Each was shaved to the skin on the section of skin to be operated on. A black reference point was added with a permanent marker. The animal was allowed to move freely in a clear plastic cage, and the RF antenna was placed overhead. A laser thermometer was used to record skin temperatures every minute for 10 minutes of baseline, 10 minutes of RF stimulus, and 10 minutes of recovery. This was repeated for three complete trials for a total of 270 temperature recordings.

Laser & Optogenetic Animals

20 female transgenic Wistar rats were selected of similar age and weight. Each was tested with a 20 mW 473 nm blue light laser to confirm the mechanoreceptive response. All 20 animals responded to blue light on their feet with a withdrawal and all 20 had minimal responses to blue light on the surgical area above the thigh. Laser power was measured by a Thor light meter (Thor Labs, Inc.).

Surgery

The same TNT neuroma surgery was performed with only a slight modification to the site of neuroma attachment. The nerve stump was attached slightly higher on the muscle (closer to the sciatic notch). This modification was made to avoid palpating the knee repeatedly. The animals were given one week to recover before nociceptive testing began.

During the 5th trial, as a control, Lidocaine was administered by direct injection into the neuroma site (0.1ml of 2% Lidocaine). Animals were tested in the normal manner following this injection, and after the animal was fully alert.

RF Assay

The RF antenna was fixed 10 in. above the animals, which were confined within a clear acrylic tub. Each animal was recorded minute by minute a blinded researcher who was unaware of the experimental group of the animal in question. The observation sequence was for 2 minutes of baseline testing, then 10 minutes of RF stimulation, and then 10 minutes of recovery. The antenna emitted approximately 20 mW/m² when off and 750 mW/m² when on. The animals were scored as follows for all nociceptive assays:

- 0 = No reaction
- 1 = Withdrawal

- 2 = Shaking, stretching, licking, audible squeal

If an animal had multiple pain displays within a minute, the score for that minute was summed. This assay was always performed first to avoid a lingering pain effect from other assays.

Thermal Nociception Assay

Animals were introduced into a clear acrylic box for easy viewing. A 100 W heat lamp was placed over the box with ample room for air exchange, and was 12 inches over the animal. Each animal was recorded minute by minute a blinded researcher who was unaware of the experimental group of the animal in question. The observation sequence was for 2 minutes of baseline testing, then 5 minutes of thermal stimulation, and then 5 minutes of recovery. The animals skin temperature was raised approximately C from the baseline temperature (depended on the animal's location in the heating chamber). The testing duration was shortened to avoid excess stress on the animals.

Von Frey Assay

The Von Frey assay was performed as was described previously. The only exception was that animals were removed from consideration if they had more than three reactions when palpated on the uninjured contralateral side.

OLVF

The animals were individually placed in a clear acrylic box about 5 inches tall. The experiment was performed in the same manner as the Von Frey assay only with a 473 nm blue light laser (20 mW). The experimenters wore O.D.3 glasses (Thor Labs, Inc.) for protection. The laser was directed at the marked surgery site 10 times on the injured and uninjured side. All trials were recorded.

RF Anxiety Chamber

Following the conclusion of the 9 full nociceptive assay trials (8 experimental trials, and one Lidocaine control trial), a series of anxiety chamber experiments were performed. The chamber was constructed using clear acrylic animal housing material and copper electromagnetic shielding mesh. The copper mesh completely surrounded one of the chambers excluding a small opening for a metal tunnel that was built to connect the two chambers. The field power of the RF chamber was 750 mW/m². The field power of the shielded chamber was somewhat variable, but approximately 100 mW/m². An animal was placed individually into the clear RF chamber and after the animal was acclimated to the new environment (30 seconds), the animal's location was recorded for a total of 5 minutes (time in RF chamber + time in shielded chamber totaled 5 minutes). This experiment was repeated for each animal three times.

Results

Radio Frequency Environmental Characterization

The RF power emitted by reached a maximum of 769.20 mW/m² at close range to the cell phone tower (Figure 3-1). There is a significant range of power output based on direction and distance.



Figure 3-1: Cell phone tower used for RF environmental characterization.

To show the variation in output, the maximum power output was compared at various distances from the antenna (Figure 3-2):

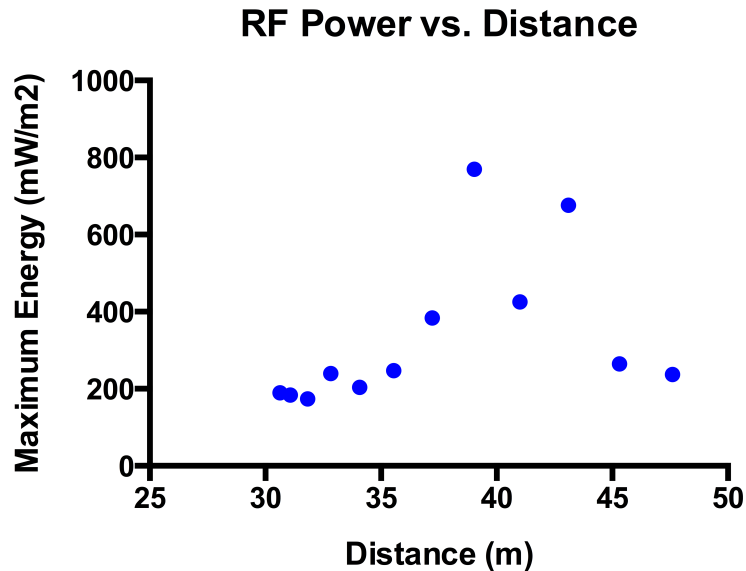


Figure 3-2: RF power output as it relates to distance from the antenna.

RF Skin Temperature Testing

The skin temperature testing indicates that RF stimulus elicited transient, but significant, temperature changes. The mean skin temperature recorded prior to stimulus was 31.28 (SD=1.794). The mean skin temperature increased to 32.97 (SD=3.891) during RF stimulus. The mean skin temperature in the recovery period decreased to 30.64 (SD=1.965). The large standard deviation of the skin temperature during RF stimulus suggests that some readings were skewed during some intervals, and equal standard deviations could not be assumed for statistical analysis. The D’Agostino-Pearson Omnibus Normality test was performed on each recording period. The RF stimulus period was not

normally distributed ($K_2=36.82$, $p<0.0001$; Skewness=1.554; Kurtosis=3.736) whereas the pre-stimulus and post-stimulus recordings had normal distributions.

To further analyze the RF stimulus temperature values, a ROUT outlier method was used with a Q equal to 1%. This analysis was selected to identify as many outliers as possible, rather than an individual outlier. Only the RF ON trial had outliers (3 outliers in 270 readings). These temperature values were all significantly higher than the mean and were removed from analysis. A one-way ANOVA was performed on the three experimental conditions even though one of the groups was non-normally distributed. A highly significant difference was observed ($p<0.0001$), so a multiple comparisons Tukey's test was performed. The baseline temperatures and RF stimulus temperatures were highly significantly different ($p=0.0013$) as were the RF stimulus temperatures to the recovery period temperatures ($p<0.0001$)

Surface Skin Temperature During RF Exposure

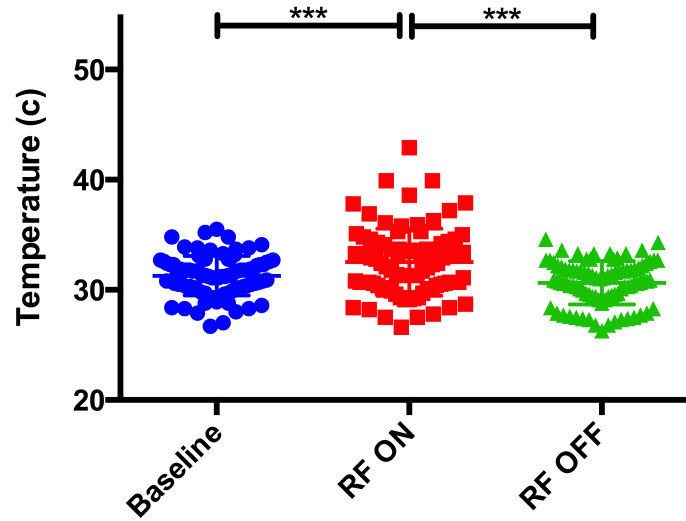


Figure 3-3: Skin temperatures during RF stimulus. Each experimental period is 90 recordings (one-way ANOVA with multiple comparison Tukey's test; $p < 0.0001$).

Another way of presenting the above temperature differences is by a minute-by-minute analysis.

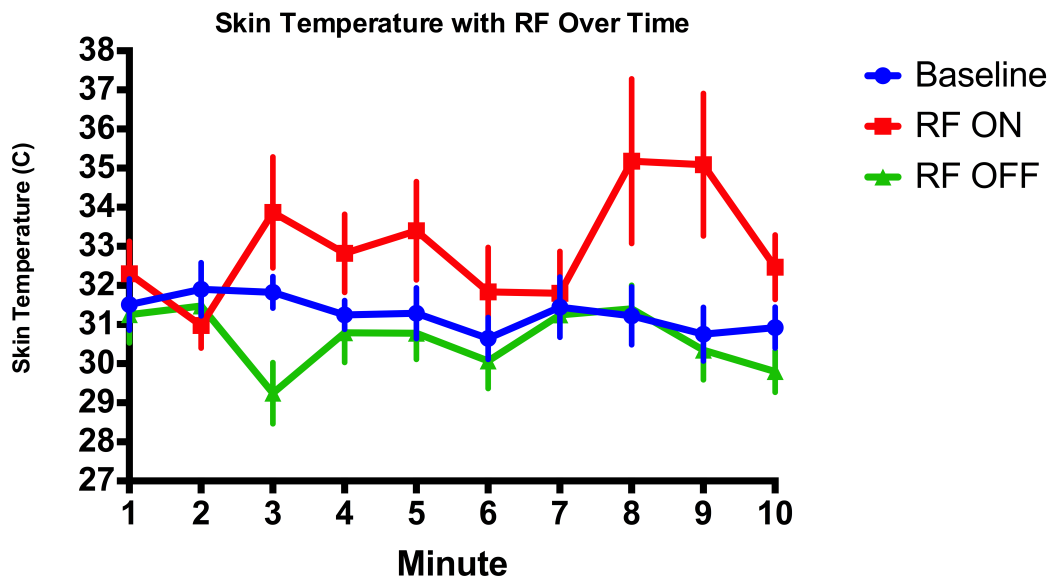


Figure 3-4: Skin temperature values for each minute of baseline, RF-stimulus, and recovery periods. Each point represents the average of 9 values and the standard error of the mean is added for each point.

RF Assay

Neuroma animals were reactive to RF exposure (Figure 3-5).

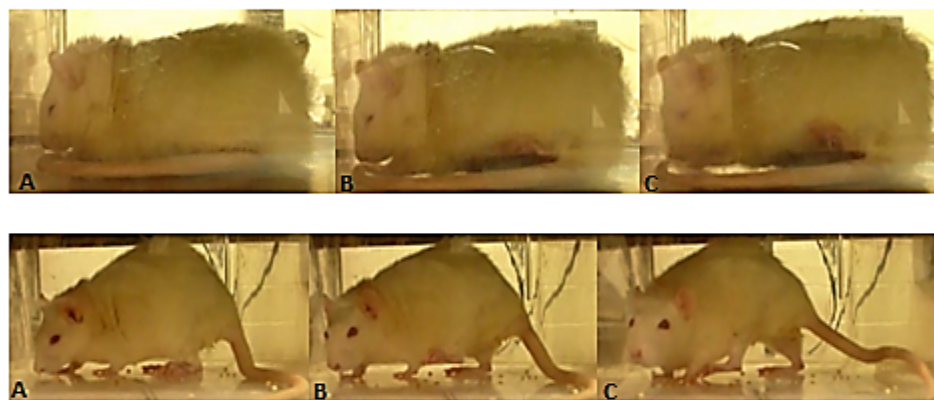




Figure 3-5: Top: Stages of RF stimulation withdrawal. Frame A: relaxed, Frame B: withdrawal initiated, Frame C: withdrawal maximum. Withdrawal occurs less than 10 seconds after initiating RF stimulation, only in limb with neuroma. Total withdrawal time: <math><0.20</math> seconds. Middle: Stages of RF stimulation stretching. Frame A: relaxed state, Frame B: stretch initiation, Frame C: stretching maximum. Stretching occurs while stimulation is on, only in limb with neuroma. Total stretching time: approximately 5 seconds. Bottom: Stages of RF stimulation licking. Frame A: relaxed state, Frame B: licking initiation, Frame C: licking. Licking occurs while stimulation is on, only in limb with neuroma. Total licking time: approximately 15 seconds.

Sham animals showed nearly no reaction to RF stimulus. This indicates that an injured nerve is necessary for reacting to RF stimulus. There was a general increase in number of pain responses for each animal during RF stimulus (pain score) across the 4 weeks of testing Figure 3-6:

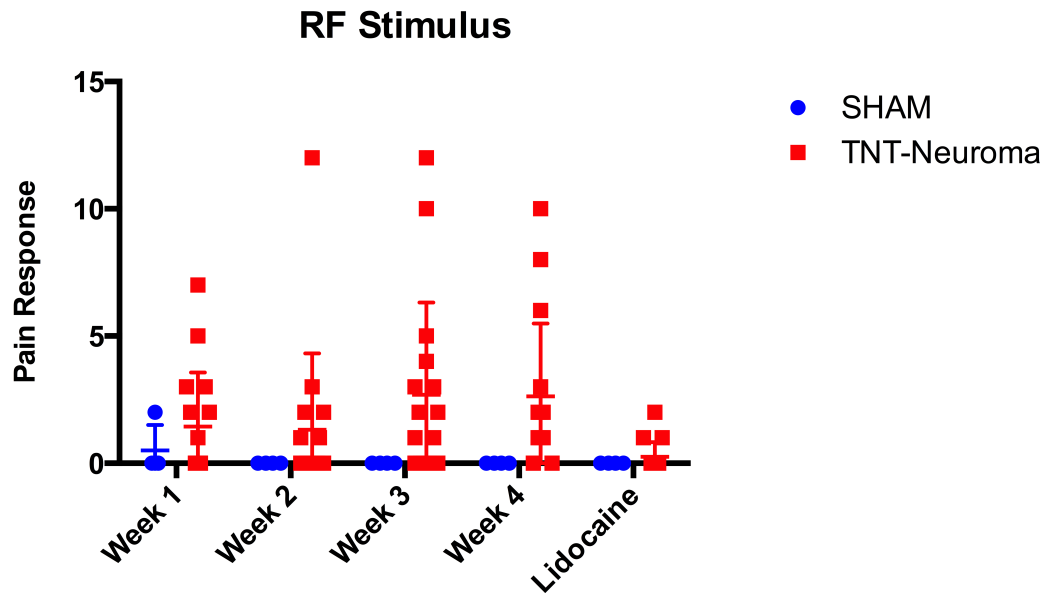


Figure 3-6: RF stimulus pain responses. Each animal is plotted with group means. TNT-Neuroma responses significantly different from sham animal responses ($p < 0.05$).

The pain responses of TNT-Neuroma animals were compared to those of the sham animals by a two-tailed, non-parametric, Mann-Whitney test ($p = 0.0159$). TNT-Neuroma animals have significantly higher responses to RF stimulus compared to the sham animals. Furthermore, the responses of TNT-Neuroma animals were compared when Lidocaine was administered and when Lidocaine was absent. Again, a two-tailed, non-parametric, Mann-Whitney test was performed ($p = 0.0026$) yielding a significant difference between the two experimental groups. This indicates

that Lidocaine is an effective control for RF-induced neuroma pain (Figure 3-7).

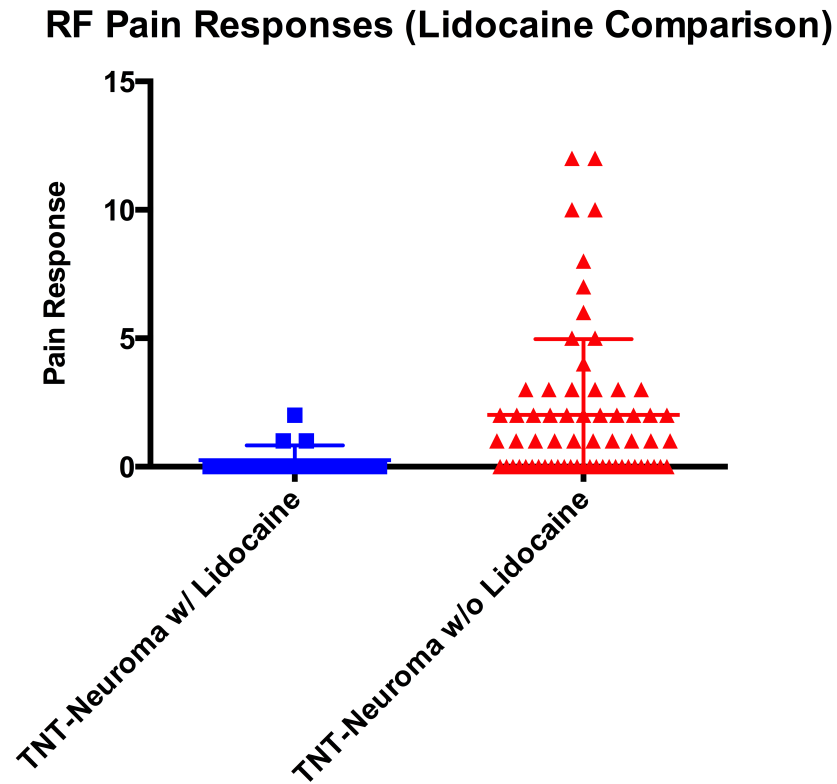


Figure 3-7: A comparison of pain responses of TNT-neuroma animals undergoing RF-stimulus with and without Lidocaine (Mann-Whitney; $p=0.0026$; significant difference).

After the animals underwent a second surgery, 1/2 of the TNT-Neuroma animals had the neuroma bulb disconnected (TNT-BD) and 1/2 had a sham surgery (TNT-SHAM). The original sham animals had a second sham surgery (SHAM-SHAM). No SHAM-SHAM animals showed any indication

of RF-stimulus pain across an additional 4 weeks of testing. The TNT-BD and TNT-SHAM animals showed significantly higher pain responses to RF-stimulus (non-parametric, Kruskal-Wallis test, $p=0.0019$). There was a small increase in pain response over time. Pain responses to RF-stimulus were compared between the TNT-BD and TNT-SHAM groups by the two-tailed, non-parametric, Mann-Whitney test yielding a non-significant difference ($p=0.2$). The results are plotted in Figure 3-8:

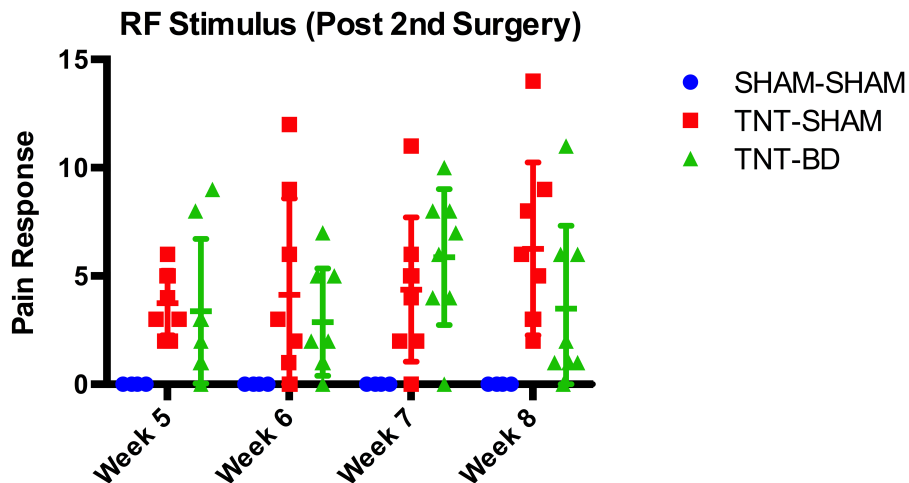


Figure 3-8: RF-stimulus pain responses. Significantly different responses were recorded for animals with and without nerve injury (SHAM-SHAM vs. TNT-SHAM + TNT-BD), but no significant was observed between groups with nerve injury (TNT-SHAM vs. TNT-BD)

A cumulative graph of pain responses (Figure 3-9) shows that pain responses are similar both prior to and post bulb disconnection surgery.

RF Stimulus Pain Responses (All Trials)

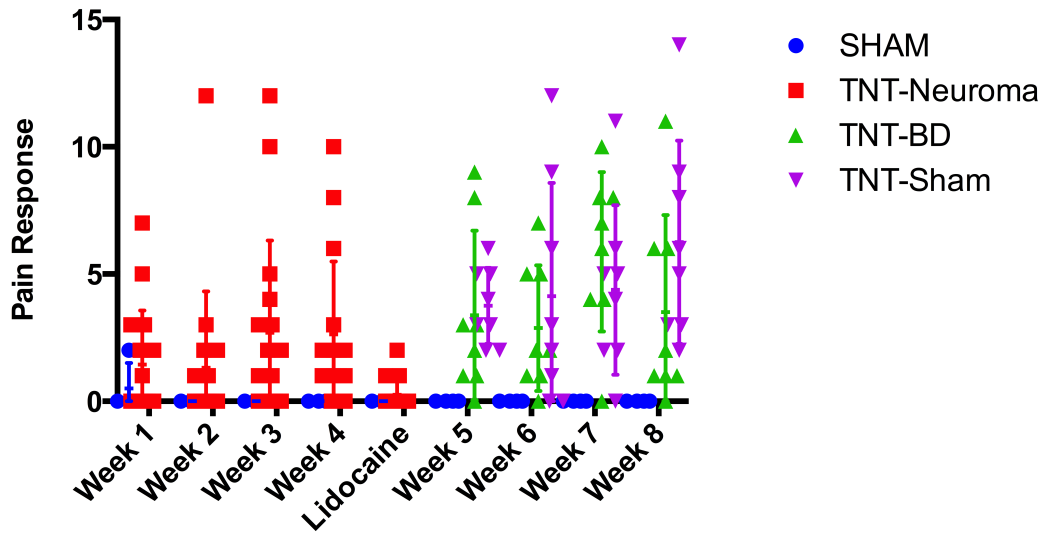


Figure 3-9: All RF-stimulus pain responses from animals across 9 trials.

Thermal Nociception Assay

Animals had a skin temperature rise of approximately 6 C when the heating bulb was on. This however was highly variable. A one-way ANOVA of skin surface temperatures determined that the skin temperature changes significantly from Baseline to heating Bulb-ON to the Recovery period ($p < 0.0001$). The Baseline temperature and Recovery skin temperatures were non-significantly different ($p = 0.7181$) indicating that the testing protocol was administered properly (Figure 3-10):

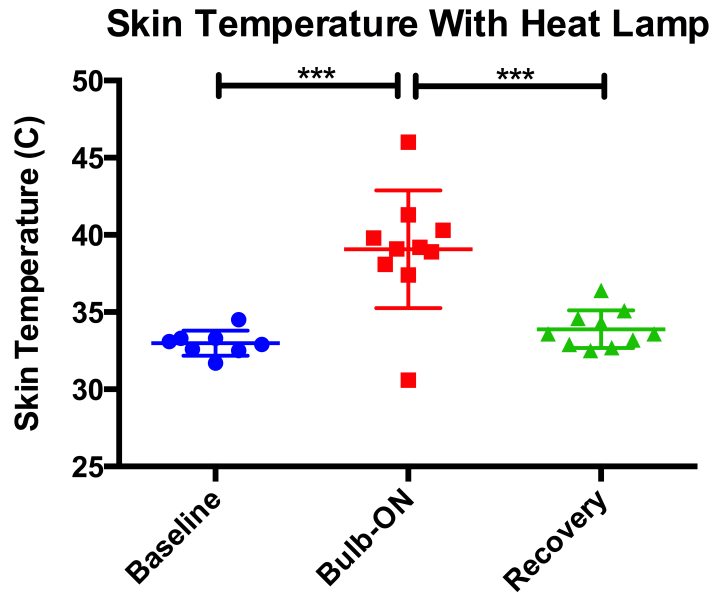


Figure 3-10: The changes in skin temperature when the heating bulb was on or off (one-way ANOVA with multiple comparisons Tukey's test; $p < 0.0001$)

Animals with TNT-Neuromas showed clear pain behavior when stimulated by noxious thermal energy. Sham animals had no responses to noxious thermal stimulation. The response to thermal stimulus for Sham animals and TNT-Neuroma animals was compared by the two-tailed, non-parametric Mann-Whitney test and yielded a significant difference between the groups ($p = 0.0079$) (Figure 3-11).

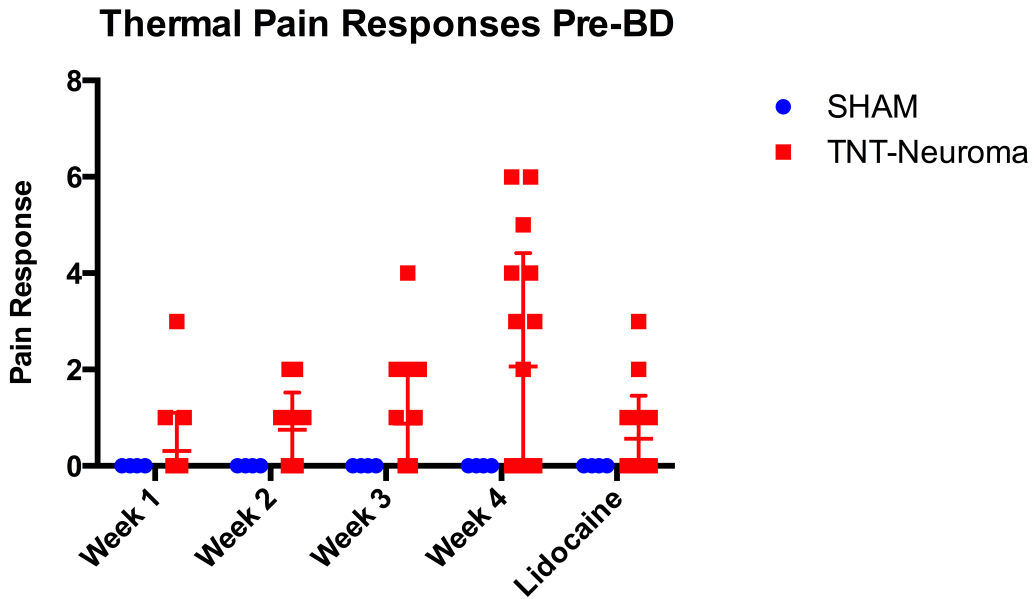


Figure 3-11: Pain responses of Sham and TNT-Neuroma animals were significantly different ($p=0.0079$)

Furthermore, the responses of TNT-Neuroma animals were compared when Lidocaine was administered and when Lidocaine was absent. Again, a two-tailed, non-parametric, Mann-Whitney test was performed ($p=0.4958$) yielding a non-significant difference between the two experimental groups. This indicates that Lidocaine is not an effective control for temperature-induced ($\sim\Delta 6$ C) neuroma pain (Figure 3-12).

Thermal Pain Responses (Lidocaine Comparison)

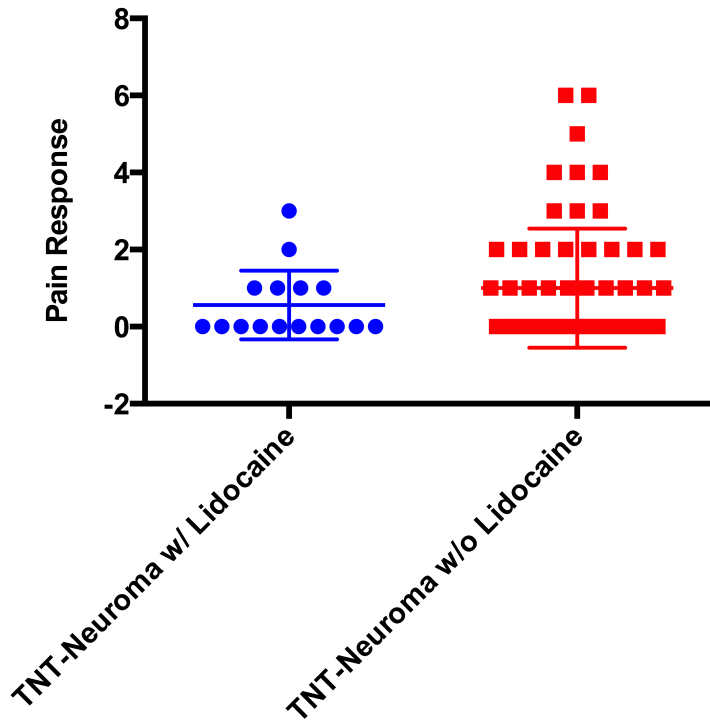


Figure 3-12: A comparison of pain responses of TNT-neuroma animals undergoing thermal-stimulus with and without Lidocaine (Mann-Whitney; $p=0.4958$; non-significant difference).

The animals underwent a second surgery, $\frac{1}{2}$ of the TNT-Neuroma animals had the neuroma bulb disconnected (TNT-BD) and $\frac{1}{2}$ had a sham surgery (TNT-SHAM). The original sham animals had a second sham surgery (SHAM-SHAM). No SHAM-SHAM animals showed any indication of thermal stimulus pain across an additional 4 weeks of testing. The TNT-BD and TNT-SHAM animals showed significantly higher pain responses to

thermal stimulus (non-parametric, Kruskal-Wallis test, $p=0.0116$). There was a small increase in pain response over time. Pain responses to RF-stimulus were compared between the TNT-BD and TNT-SHAM groups by the two-tailed, non-parametric, Mann-Whitney test yielding a non-significant difference ($p=0.826$). The results are plotted in Figure 3-13:

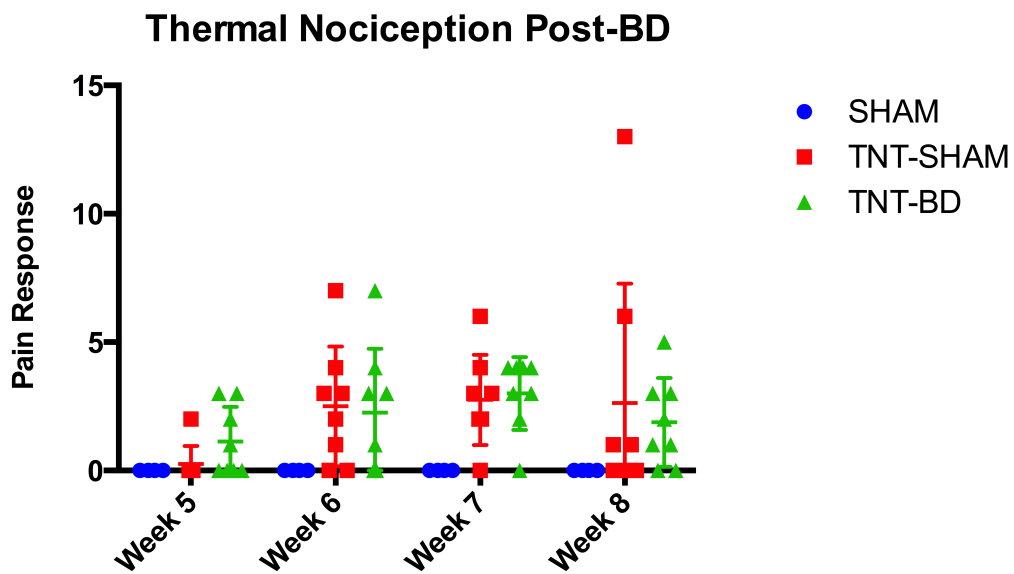


Figure 3-13: Thermal pain responses post bulb disconnection.

Significantly different responses were recorded for animals with and without nerve injury (SHAM-SHAM vs. TNT-SHAM + TNT-BD), but no significant was observed between groups with nerve injury (TNT-SHAM vs. TNT-BD)

A cumulative graph of pain responses (Figure 3-14) shows that pain responses to thermal energy are similar both prior to and post bulb disconnection surgery.

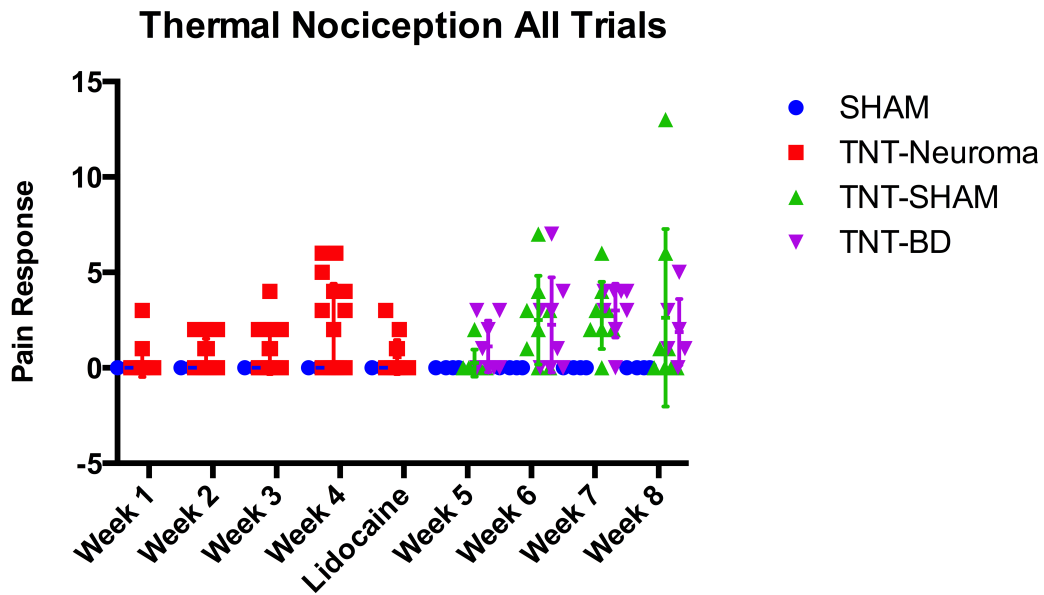


Figure 3-14: All responses to thermal stimulus across 9 trials.

Von Frey Assay

Animals that had TNT-neuromas responded to the Von Frey palpation assay significantly differently from those that received a sham surgery. By the third week of testing sham animals showed no nociceptive responses to mechanical palpation (Figure 3-15):

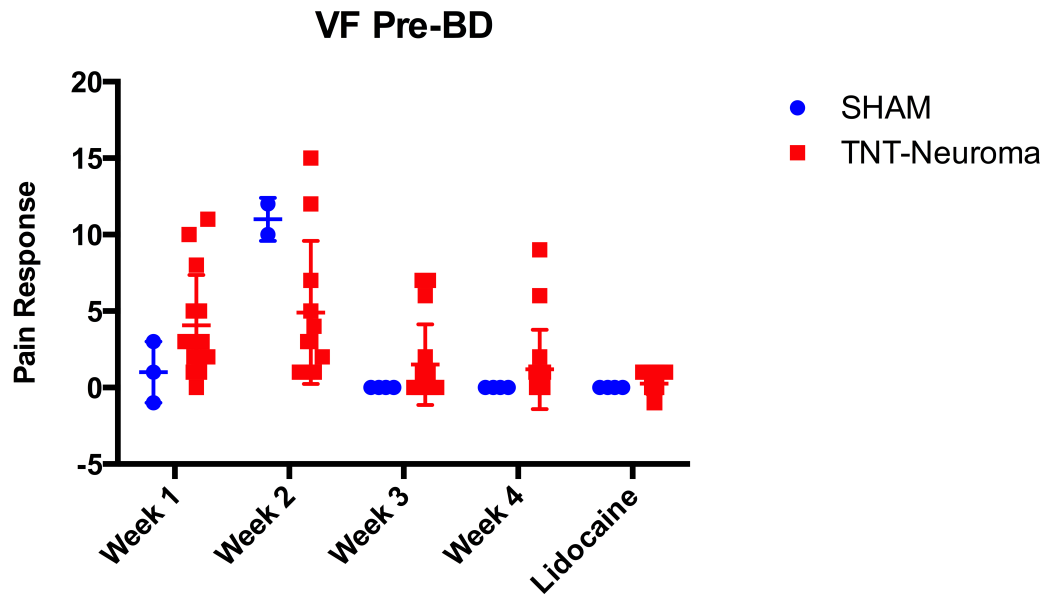


Figure 3-15: Pain responses to mechanical palpation by week for the sham and TNT-neuroma groups.

When the entire dataset is analyzed the groups are non-significantly different (Mann-Whitney; $p=0.243$) due to the high pain responses in Week 2 of the Sham group. When the second week is removed from the statistical analysis the TNT-Neuroma and Sham animals have significant differences in their pain responses (Mann-Whitney; $p=0.0286$). Another way of presenting this analysis is that the pain responses for the first two weeks in sham animals are non-significantly different from TNT-Neuroma animals. Some of the animals in some of the trials were deemed hyper-reactive, and their scores were removed from analysis (10 of 100 recordings were removed).

As was described earlier, the TNT-neuroma animals were split into two groups (Sham Surgery vs. Bulb Disconnection). Animals were retested for 4 additional trials, but many more animals were deemed hyper-reactive (31 of 80). This decision to exclude hyper-reactive animals (those highly reactive to palpation of uninjured areas) decreased the likelihood of observing significantly different behavior between experimental groups. A Kruskal-Wallis test was performed on the three experimental groups, and a significant difference was observed ($p=0.0296$), but upon further analysis using a Dunn's multiple comparisons test, there was no significant difference between any two groups (SHAM-SHAM vs. TNT-SHAM, $p=0.0536$; SHAM-SHAM vs. TNT-BD, $p=0.1452$; TNT-SHAM vs. TNT-BD, $p>0.999$). These results can be seen in Figure 3-17:

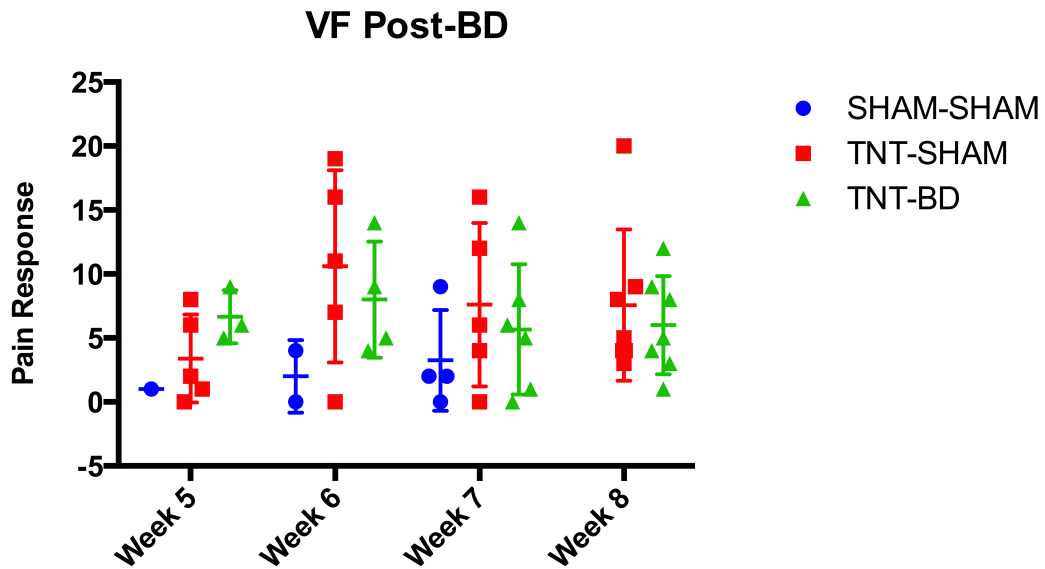


Figure 3-17: The pain responses for Von Frey palpation post bulb disconnection surgery. See above results for statistical analysis.

All trials are plotted in Figure 3-18 indicating that the average pain responses are more variable post bulb connection, and have fewer data points due to hyper-reactive animals.

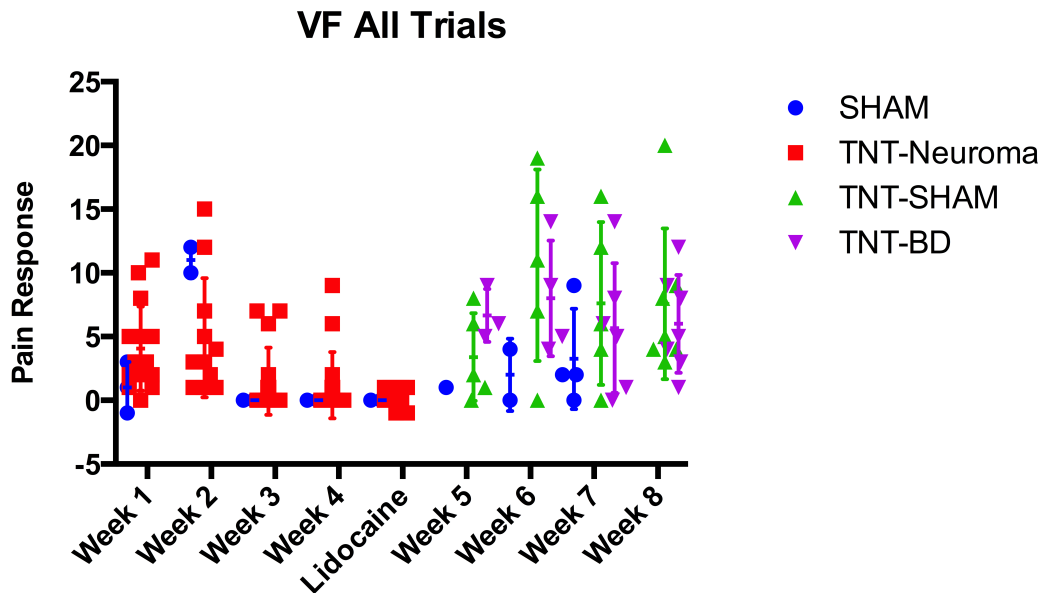


Figure 3-18: All pain responses to mechanical palpation by Von Frey filament across 9 trials (hyper-reactive animals are not plotted)

OLVF

Across all laser stimulations of the neuroma site and the contralateral uninjured site, there were no pain responses recorded. Animals were still responsive when their hind limbs, fore limbs, ears, or nose were bathed in laser light. Some skin twitching was observed above the injury site, but no pain responses.

To test whether or not the skin was blocking transmission of laser light, a TNT-neuroma animal was lightly anaesthetized and the skin was opened to expose a bulb. The animal reacted when light was directed to

the intact CPN, but no reaction was observed when the tibial nerve neuroma was stimulated with laser light.

RF Anxiety Chamber

Animals with a TNT-neuroma were more likely to show a location preference for the shielded chamber of the anxiety chamber apparatus. There was a 57% increase in the preference for the shielded chamber for TNT-neuroma animals (3 trials, 20 animals each trial). This was a consistent observation in three repeated tests. An unpaired, two-tailed t test was performed on the ratio of time spent in the shielded chamber. The preference for the shielded chamber was significantly different ($p=0.0358$) between the sham animals and the TNT-neuroma animals (Figure 3-19).

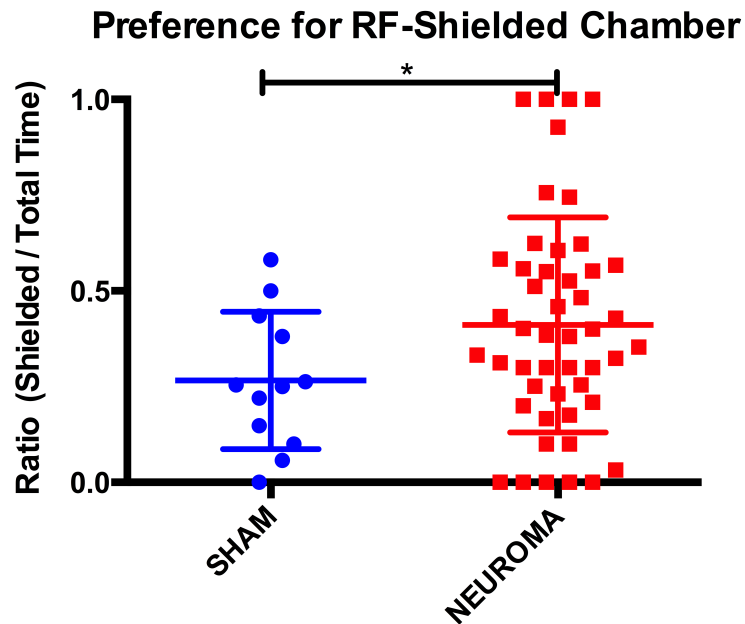


Figure 3-19: TNT-neuroma animals show an enhanced selection preference for the RF-shielded chamber (p=0.0358)

Discussion

The *in vivo* experiments were designed to determine whether or not RF-stimulus could elicit characteristic pain responses in animals with neuromas. It is clear from the preliminary study that TNT-neuroma animals have increased pain when stimulated with RF energy similar to that from a cell phone tower. It is important to note that animals without injured nerves (sham animals) showed extremely few signs of nociception during stimulation. It is reasonable to conclude from the pilot study with 17 Lewis rats and the recent study with 20 Wistar transgenic rats, that RF-stimulus is nociceptive – capable of eliciting neuropathic pain.

The skin temperature changes that accompany RF stimulus are interesting, and may be indicative of stress during RF-stimulus. Although there were a few outlying temperatures during RF-stimulus that were exceptionally high, the means were significantly different, but only by a few degrees (~1.7 C). Small temperature differences on the skin directly above the TNT-neuroma may be sufficient enough to induce a nociceptive response.

In absolute intensity, wound healing response, and response to bulb disconnection, thermal stimulus was more similar to RF-stimulus than to Von Frey or OLVF stimulus. Thermal stimulus was repeatedly elicited and had a generally increasing trend. This newly developed assay was thoroughly benchmarked to elicit a reproducible change in skin temperature. The duration of thermal stimulus was necessarily shorter, but a few degrees higher than the RF-stimulus. This begs the obvious question: would the cumulative pain response of the thermal trials been equal to the pain responses of the RF trial if it had been of equal duration? An analysis of the TNT-neuroma animals' means score for each trial was compared to the RF-stimulus and the thermal stimulus. When the thermal means were doubled (to account for the time difference), there appears to be no significant difference between thermal and RF-stimulus (Wilcoxon matched-pairs signed rank test; $p=0.9102$) (Figure 3-20). Furthermore,

the weekly trends in pain responses are strikingly similar (Figure 3-21). A linear regression of the average pain scores of RF-stimulus and thermal stimulus produces a goodness of fit estimate (R^2) of 0.62. When the 95% confidence interval is superimposed on the regression, very few data points exceed this threshold indicating highly similar responses (Figure 3-22).

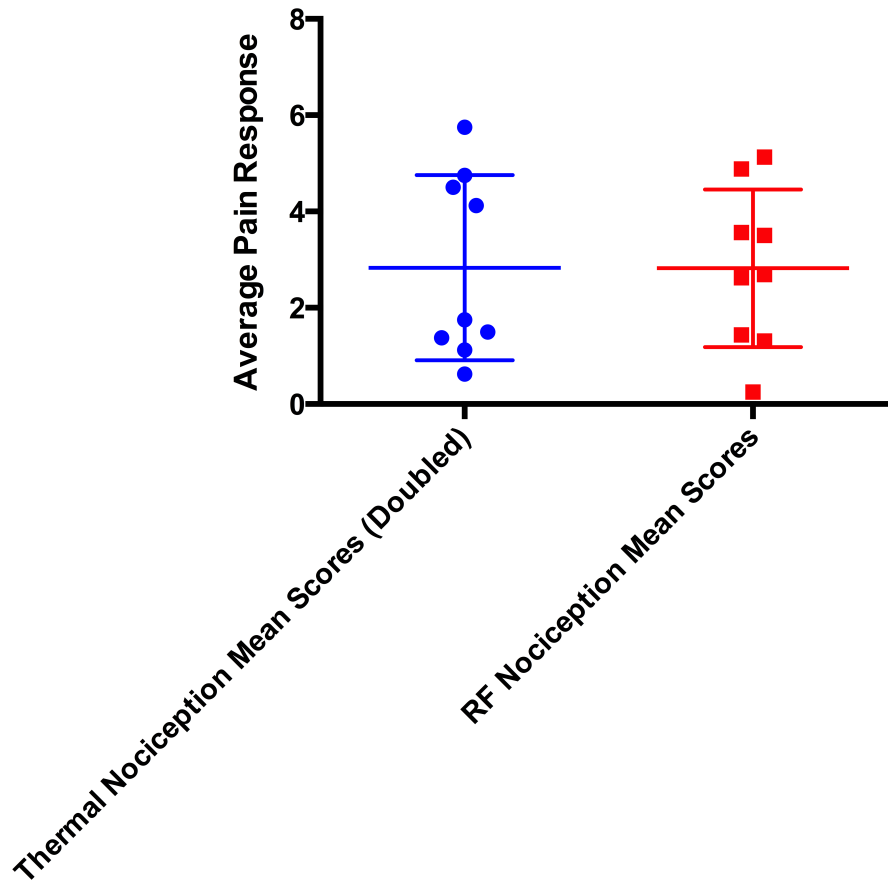


Figure 3-20: Thermal nociception (doubled) and RF nociception mean scores for all animals each recording session (9 trials each assay)

Average Pain Scores (RF & 2xThermal) vs. Trial

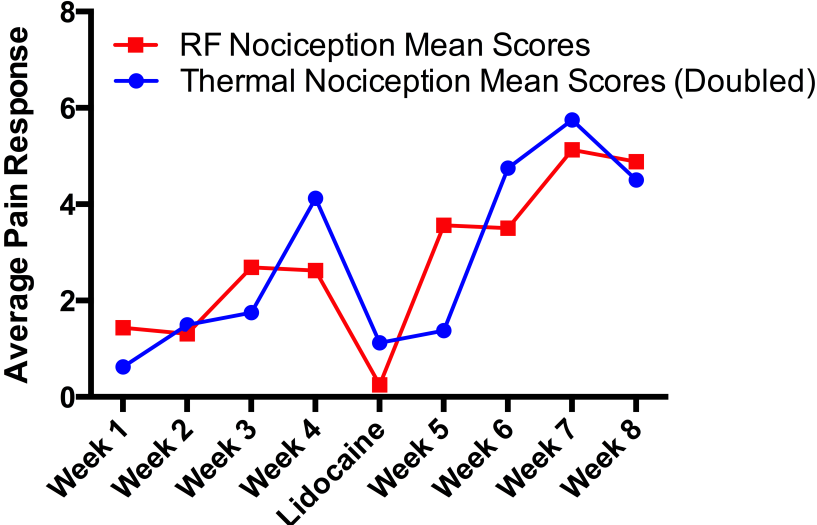


Figure 3-21: Mean RF nociception and thermal nociception (doubled) plotted trial by trial.

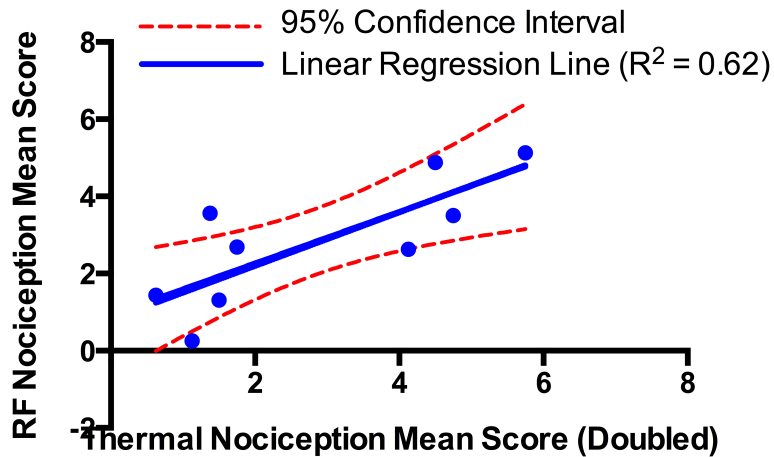


Figure 3-22: Linear regression of thermal nociception (doubled) vs. RF nociception trial means. 95% confidence interval lines calculated and simultaneously plotted.

Von Frey stimulus pain was a confirmation of our earlier work with multi-luminal conduits. In the first two weeks following surgery the sham animals had painful responses to mechanical palpation. By the third week post-surgery this response had abated. It is likely that mechanical pain was due to inflammation of the surgery site, and when inflammation subsided, so did the response to palpation. Only animals with TNT-neuromas had lasting neuropathic pain when mechanically palpated. The general trend in Von Frey pain responses were in a negative direction, and were highly variable following bulb disconnection. This high variability is due to the exclusion of a large number of hyper-reactive animals. It is unclear why the animals were hyper-reactive, but is likely because of the

repeated surgeries, and repeated noxious assays. The animals likely associated any human handling with painful stimulus.

The OLVF assay proved to be ineffective at eliciting a nociceptive response even as the animals were still reactive in the paws, ears, and nose during every trial. Even when the skin was removed and the TNT-neuroma was exposed to direct laser stimulation, the lightly anesthetized animal did not react. There may be vast differences in expression of ChR2 in mature uninjured nerves and injured nerves that could explain this observation. The lack of response could also be explained by a lack of mechanoreceptive fibers within a neuroma bulb. Mature functions of mechanoreceptive fibers are associated with Merkel cells and Meissner's corpuscles, both of which occupy the skin. It is likely that the high concentration of these mechanoreceptive structures in the skin of the paws, ears, and nose allowed for laser palpation, and a lack of ectopic mechanoreceptive structures in the neuroma bulb made laser palpation impossible. Ectopic mechanoreceptive structures in neuroma bulbs have not been reported in the literature and the failure to elicit an optogenetic response from a neuroma may suggest that mechanoreceptive fibers do not play a significant role in neuroma pain.

The Lidocaine control trials for RF, thermal, and VF assays showed an important distinction. While the RF and VF trials had nearly no

responses when Lidocaine was administered, the thermal trial showed more pain responses than would have been expected. This may suggest that neuromas are especially sensitive to thermal noxious stimuli.

The idea that the neuroma bulb acts as an antenna for RF energy does not appear likely. There was no significant difference between animals that had the neuroma bulb removed and those with a TNT-neuroma bulb intact after a sham surgery. The lack of significance may be explained by a small sample size. Only eight animals had a bulb disconnection surgery and eight had a sham surgery. Using a statistical power calculator (www.powerandsamplesize.com) it is unlikely that we would have had a sufficient number of samples for the observed effect size. Based on the recorded mean pain scores between groups: a large (40%) difference in means, a large percentage standard deviation (60%) a high statistical power (0.90), with an assumed low Type I (false positive) error rate (5%), the sample size should have been 48. This sample size could have been achieved with 6 complete trials of the 8 subjects, but may inappropriately assess an experimental condition due to the long delay from the first trial to the last (assuming weekly trials). Ideally, more animals could have been used in a shorter time frame to confirm the existence of an antenna effect, or rule it out.

The anxiety chamber test yielded a few important results. First, that there was a significant difference in behavior between TNT-neuroma animals in location preference. Even though the observers were blinded to the animal group in the RF, thermal, VF, and OLVF trials, there may be some unforeseen bias in the recording. Additionally, those trials are based on scaled data (0, 1, 2) and may lack some sensitivity. These limitations are overcome with the anxiety chamber work, where a large effect size was observed, and a highly significant difference was measured. This suggests that the animals are able to sense the field or at least the discomfort the field causes their neuroma.

With these controlled, blinded, and thorough assays complete, it is reasonable to conclude that RF-stimulus of 915 MHz of approximately 750 mW/m² power can repeatedly induce neuroma pain. This work was initiated to help understand the pain a patient described when travelling near cell phone towers. His hypothesis that RF energy was causing pain in his amputation neuromas is likely true. The most likely mechanism that RF energy causes pain is by transient temperature changes, as evidenced by the skin temperature experiments, and the thermal stimulus nociceptive assay analysis.

Work is already underway to provide a shield to amputation neuromas from RF stimulus (PCT/US14/16801). The material selected

will likely need to significantly inhibit field power, and additionally thermally isolate the neuroma bulb.

In Vitro Experiments

Experimental Design

In concert with the *in vivo* RF experiments, we hoped to understand the effect of RF-stimulus on neuronal cells. The same RFID antenna would be used on cell cultures and various responses (firing rate, number of active cells, and calcium influx) would be measured.

Initially, rat cortical neurons were used on 64-channel multi-electrode arrays (MEA) designed and optimized by the UNT Center for Network Neuroscience (CNNS) lab founded by Dr. Guenter Gross, PhD⁷⁷⁻⁷⁹. These well-characterized MEAs were used in a long series of experiments in three separate trials at UNT. The main parameters explored in these experiments were the firing rate of mature neural networks and the number of active electrodes. We did not assume an increase or decrease in these parameters with RF-stimulus, rather the experiments were two-tailed by design.

In addition to the MEA work, with assistance from the Biophysics and Physiology Group at UTA founded by Dr. Samarendra Mohanty, PhD and the NeuroEngineering Lab founded by Dr. Young-Tae Kim, PhD we performed live-cell fluorescent imaging of Calcium (Ca^{++}) influx during RF-

stimulus. Although literature on applied direct-current (DC) voltage fields suggested that calcium influx would increase, we were unsure if alternating-current (AC) fields would have the same effect^{69, 70, 80}.

This is an investigation into potential field effects of RF-stimulus on electrically active neural cells. It concludes with some modeling to explain the initial observations.

Materials & Methods

MEA Experiments

Extremely thorough protocols are available from the CNNS lab at UNT, or from Gopal et al., 2012⁷⁹. Here, a brief methods overview from Gopal et al., 2012 is presented with key aspects highlighted: In-house fabrication and preparation of 64-electrode MEAs, as well as recording techniques developed by Dr. Gross were used. E-17 mice auditory cortex neurons were used and cultured in the typical manner of CNNS lab. The cultures used in this set of experiments on the average were over 30 days old from the initial culturing date. During recording, pH and temperature of the media was maintained by a stream of 10 ml/minute filtered 10% CO₂ through a gas flow meter (AFC 2600-PRO; Aalborg, Inc.). Osmolarity was maintained at 320 mOsmoles by infusion of sterile water at a 50 ul/hour rate to compensate for evaporation. The housing chamber maintained temperature of the recording MEA at 37 C. Neuronal activity was

monitored by a two-stage, 64-channel amplifier system (Plexon, Inc.). The analog signal was digitized at 40,000 Hz using 64 digital signal processors. The system amplified an initial signal by 10,000. Action potentials were classified by a spike-identification, real-time, template-matching algorithm (Plexon, Inc.). Cumulative network activity was processed by CNNS proprietary software to produce action potential firing rate (action potentials per minute), and the number of active channels (out of 64 channels). MEAs were selected for recoding, by examining the health of the culture under bright-field imaging, and then recoding was initiated. A baseline period was recorded, then a RF-stimulation period, then a recovery period.

Calcium Imaging

Pregnant Lewis rats with day 18 embryos were sacrificed to collect cortical tissue. The uterus was opened to reveal the embryo and then dissection began. The head was separated, and then the unformed skin, skull, and meninges were removed along with the cerebellum, olfactory bulb, and midbrain. The remaining cortical tissue was minced and placed in a tube with ice-cold L-15 medium (Invitrogen, Inc.). 0.025% Trypsin (Sigma, Inc.) was added to digest the intercellular bonds. The solution was placed in a 37 C incubation bath for 20 minutes. After digestion, 0.5 ml of SBTI (1.5% w/v in 1xPBS; Sigma, Inc.) was added to

the solution to inhibit further digestion. A pipette was used to dissociate the tissue, and then the tissue was centrifuged for 5 minutes at 1200 RPM. The supernatant was removed, the pellet was re-suspended in 2 ml of NBM w/ B-27 and penicillin and streptomycin (Sigma, Inc; Invitrogen, Inc.). The media was refreshed every 3 days. Prior to imaging, cell media was refreshed with addition of 2-5 μ M Fura-2 Calcium dye (Life Technologies, Inc.). The solution was incubated for 15 minutes with the cells, and then the media was removed and replaced with low-fluorescence media (BrainBits, LLC). Two imaging systems were used. The Nikon A1R+/A1+ confocal microscope system (Nikon, Inc.) was used for high sampling rate imaging. This high sampling rate allowed for signal averaging to limit background fluorescence. In addition, the Nikon Eclipse Ti was used to image at a lower frame rate, longer exposure, and without a confocal system. Cells were selected for imaging, by looking for healthy cells under bright-field imaging, and then fluorescence was initiated. A baseline period was recorded (typically 2-5 minutes), then a RF-stimulation period (typically 4-6 minutes), then a recovery period (typically 4-6 minutes). Image processing was completed with either the proprietary Nikon software with the assistance of Nikon personnel, or with FIJI (an enhanced version of ImageJ; NIH) to measure fluorescent intensity (either mean or integrated density). Typically, 2 experimental ROIs were added

to healthy cells, and 1 reference ROI was added to a debris free region of the culture. All ROIs were the same size (unless reported otherwise) within each trial.

Radio Frequency

The same RFID antenna and field meter used for all *in vivo* RF experiments was used for *in vitro* trials. The antenna was typically rested on the top of the microscope after focusing and setting up the experiment. The field was measured directly above the culture. The microscope did interfere with the RF power in some trials, but great care was taken to ensure the power at the culture never fell below 550 mW/m².

Field Modeling

To determine effect of AC fields on ions, a model was constructed to examine if a Calcium ion (Ca⁺⁺) would be pulled across a cell membrane (5 nm) by the field. Since the field is alternating the maximum voltage changes polarity with respect to an ion within the period (T) of one wave. To properly calculate the acceleration of the ion, the field dynamics of ½ a period should be modeled, because the second ½ of the period will pull the ion in the exact opposite direction. Impeding the direction of the ion will be fluid drag resistance. This was taken into account. The derivation of the first-order linear non-homogeneous differential equation is below (with all constants or variables used):

Equation 1: Derivation of the first-order linear non-homogeneous differential equation to solve for calcium ion velocity vs. time in water at 37

C.

$$\begin{aligned}
 E &= \bar{E}_0 \sin \omega t \\
 \vec{F} &= qE \\
 \sum F &= m\alpha \\
 F_{drag} &= 6\pi\eta r\vec{v} \\
 m\alpha - q\bar{E}_0 \sin \omega t - 6\pi\eta r\vec{v} \\
 \frac{dv}{dt} &= \frac{q\bar{E}_0 \sin \omega t}{m} - \frac{6\pi\eta r\vec{v}}{m}
 \end{aligned}$$

Variables:

$$\begin{aligned}
 f &= 915 \times 10^6 \text{ Hz} \\
 \omega &= 2\pi(915 \times 10^6) \\
 m &= 40(1.66 \times 10^{-27}) \text{ kg} \\
 r &= 114 \times 10^{-12} \text{ m} \\
 E &= 18 \frac{\text{V}}{\text{m}} \\
 E_0 &= 18\sqrt{2} \\
 \eta &= 0.6532 \text{ (dynamic viscosity @ 40 C)}
 \end{aligned}$$

This equation was solved in MATLAB using the ODE-45 solver function. The code for this equation can be seen below:

```

function dv=ben(t,v);

dv=zeros(1,1);

eta=0.6532;

r=114e-12;

q=2*1.6e-19;

```

```

m=40*1.66e-27;
Eo=18*sqrt(2);
f=915e6;
w=2*pi*f;
dv=-6/m*pi*eta*r*v+q/m*Eo*sin(w*t);
%-6*pi*eta*r*v
End

```

```

% Ben Dissertation

```

```

close all

```

```

eta=0.6532;
r=114e-12;
q=2*1.6e-19;
m=40*1.66e-27;
Eo=18*sqrt(2);
f=915e6;
t1=0;
t2=1/(2*f);
[T,V]=ode23t(@ben,[t1 t2],[0])

```



```
plot(T,V)
xlabel('Time(s)');
ylabel('Velocity(m/s)')
```

This program solves and plots the velocity against time of Ca^{++} for the length of $\frac{1}{2}$ a period of 915 MHz (5.464481×10^{-10} seconds). This calculated time was multiplied by the maximum velocity achieved during one phase of the field to determine the maximum theoretical distance a particle could travel. This was a conservative approach to determine if the field would be able to move the ion across a membrane.

Results

MEA Experiments

Over 9 trials were attempted (approximately 12 hours of 64-channel MEA recordings were analyzed). Whenever the antenna was on, the signal noise generated obscured any cellular activity, so the only parameters that could be observed were spike rate and active channel changes before and after stimulus. In general, cells showed little response after RF-stimulus. As can be seen from Figure 3-23, spike rate and active channels remain very consistent event after 3 hours of RF - stimulus trials.

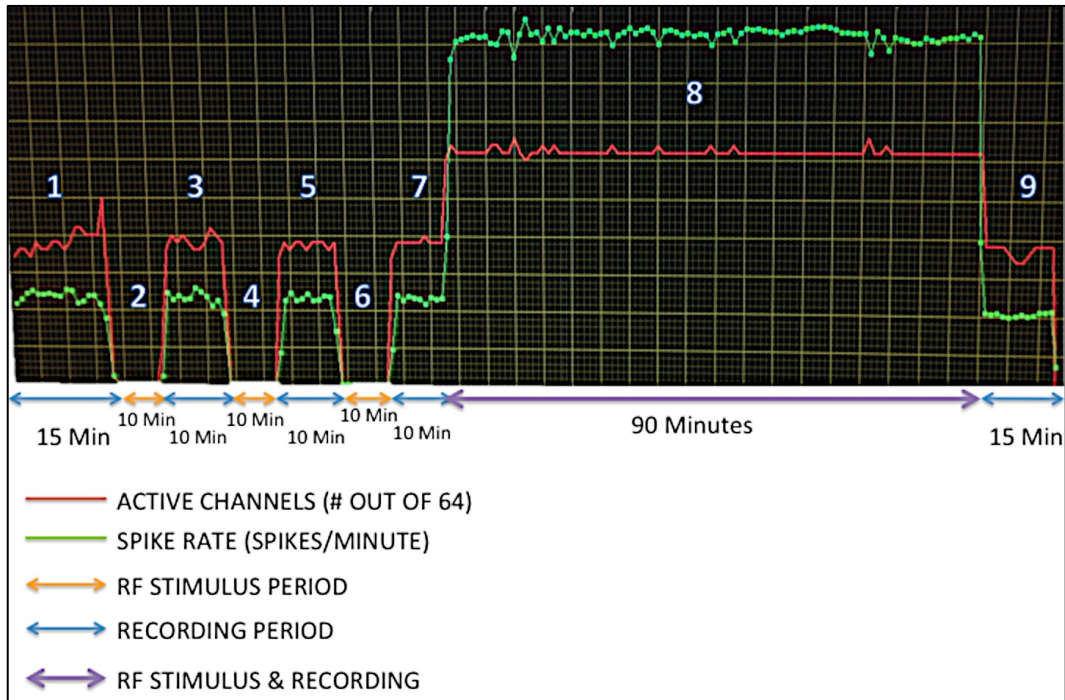


Figure 3-23: Annotated screenshot of MEA activity (firing rate & active channels). Recording sequence is 3 hours.

Additional details for each recording period annotated in Figure 3-23 are below:

1. 15 minutes: this baseline period has some active channel variability (~20 of 64 channels are active), but little spike rate variability (~200 spikes/minute).
2. 10 minutes: the recording equipment was turned off because only noise is recorded when RF-stimulus is on.
3. 10 minutes: this recording period had very similar firing rates and active channels to period 1

4. 10 minutes: a repeat of period 2 (RF-stimulus)
5. 10 minutes: a repeat of period 3, showing nearly identical firing rates and active channels to period 3.
6. 10 minutes: a repeat of period 2 and 4 (RF-stimulus).
7. 10 minutes: a repeat of period 3 and 5. Again, nearly identical firing rates and active channels are observed.
8. 90 minutes of RF-stimulus with the recording equipment recording noise. This extended period of recording was performed to see if RF-stimulus duration was significantly harmful. The recording equipment was left on to test a unrelated aspect of the system.
9. 15 minutes: a repeat of period 1. Only slight decreases in firing rate were observed (<10%). Little difference in active channels was again observed.

Calcium Imaging

Following the MEA experiments, extended trials performed using fluorescent microscopy to examine Ca^{++} influx. 19 trials of approximately 3 hours of recording were performed using standard fluorescent microscopy (approximately 24,000 fluorescent intensity measurements analyzed). Images were taken every 10 seconds (exposure time 500 ms). Images were taken at this rate to limit fluorophore bleaching and cell damage. This also drastically limited the chances of observing significant

calcium influx. Nonetheless, some trials showed clear changes in fluorescent intensity, but a majority did not. Figure 3-24 shows a later trial after fully optimizing the concentration of calcium dye:

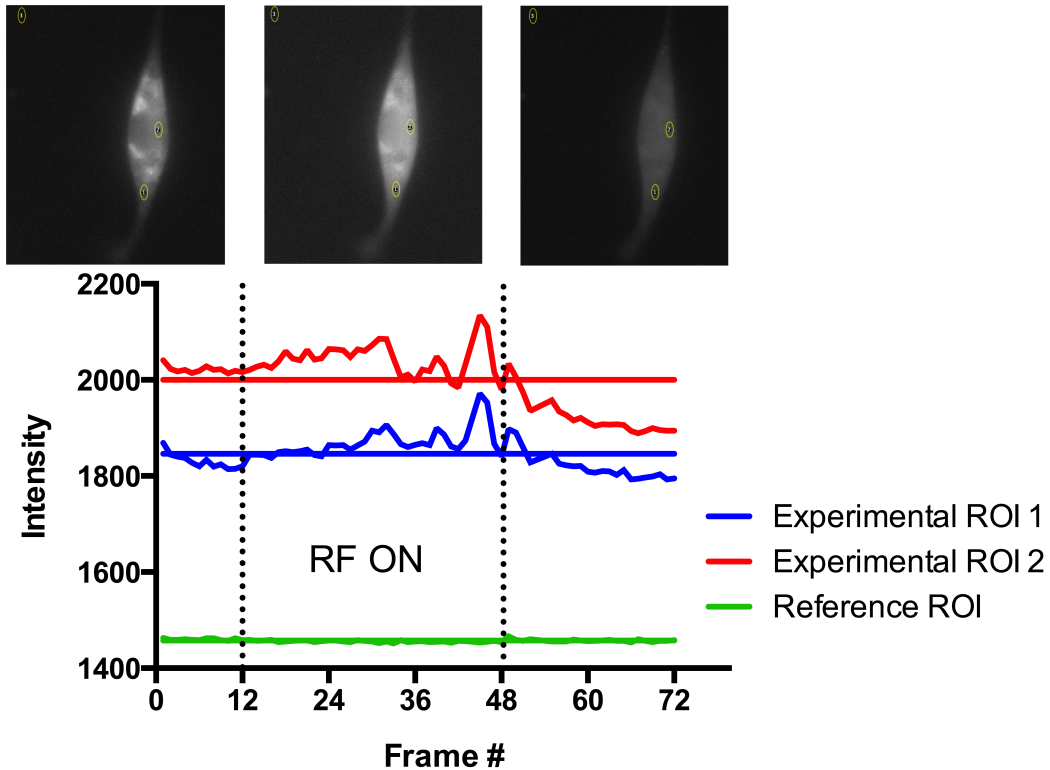


Figure 3-24: Two experimental ROIs are added to a 12-minute recording sequence. 2 minutes of baseline, then 6 minutes of RF-stimulus, then 4 minutes of recovery (Each frame is 10 seconds apart). A horizontal regression line was plotted to analyze the intensity of each recording sequence. Above each recording sequence is a screenshot with the ROIs analyzed (exposure of the image does not reflect or effect ROI intensity measurements).

To analyze the data above, 4 data points where the stage drifted were removed. Each ROI intensity plot was analyzed by horizontal nonlinear regression to identify Runs (extended periods above and below). This analysis was appropriate to conduct because of the nearly horizontal REFERENCE ROI. A baseline variance in intensity of the whole field might obscure the relative intensity changes of the EXPERIMENTAL ROIs (many trials had drifting baseline intensity likely due to stage drift or fluorophore bleaching). The regression analysis allows for the calculation of the residuals of the time series (the differences of each data point from the observable sample mean), and a clearer understanding of how much deviation there was in each data series relative to each other. Figure 3-25 is a plot of the residuals from the nonlinear fit of the same trial.

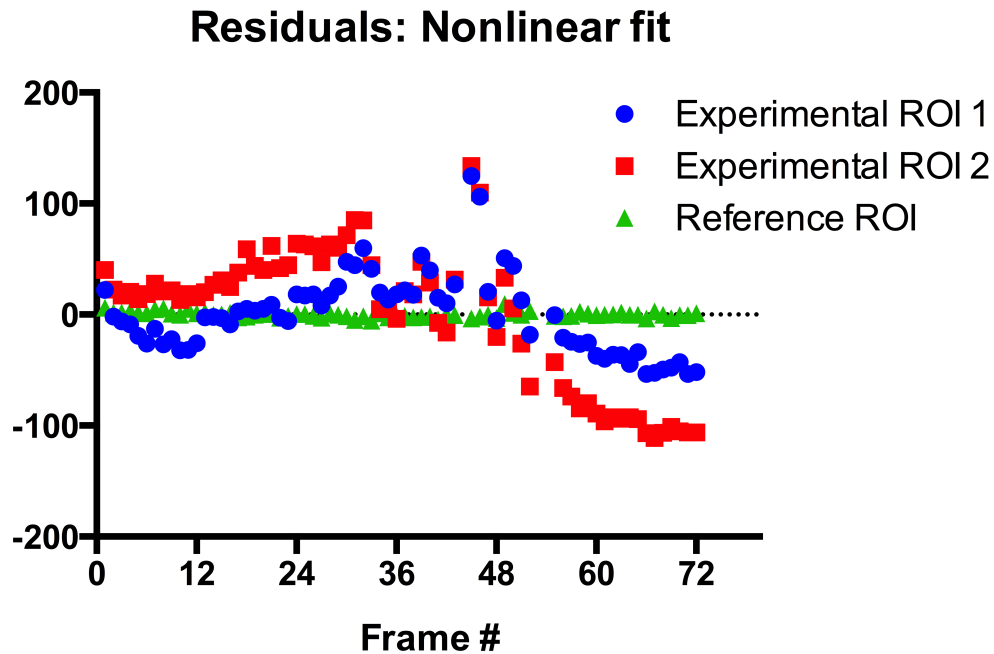


Figure 3-25: A corresponding nonlinear residuals plot of Figure 3-24. The first 12 frames (baseline sequence – RF OFF) have low signal intensity change from the Reference ROI. Frames 13-48 (RF ON) show large residuals above the mean intensity. Frames 49-72 (recovery) show residuals increasing in the negative direction rapidly following RF stimulus. The nonlinear regression RUNS analysis of ROI 1 and ROI 2 for the entire trial can be seen in TABLE 1.

Table 1: The RUNS Test results for ROI1 and ROI 2 from the nonlinear regression residuals.

RUNS TEST		
Points above curve	32	45
Points below curve	37	24
Number of runs	8	8

P value (runs test)	<0.0001	<0.0001
Deviation from Model	Significant	Significant

From the analysis of 10 second interval 500 ms exposure imaging, it was clear that many of the intensity changes that might reflect cell activity were happening on shorter time-scales, and that more advanced image processing might solve this limitation.

The Nikon A1R+/A1+ confocal microscope system was exactly the type of system required for both advanced imaging, but also advanced ROI intensity measurement. The Biophysics and Physiology Lab at UTA was able to get access to this microscope system and a team of Nikon imaging experts. Imaging was done at 30+frames/second by a laser scanning method that traced out the field of view rather than inundating with diffuse fluorescence. This produced a very clear view of cells and intracellular Ca⁺⁺ activity. A number of trials were performed (n=4) with RF-stimulus on rat cortical neurons. The main observation is that RF-stimulus produces transient cellular activity in some neural cells. Careful baseline and experimental ROI measurements revealed that in most instances baseline activity was altered by RF-stimulus. A particularly well-executed trial produced the image analysis seen in Figure 3-26.

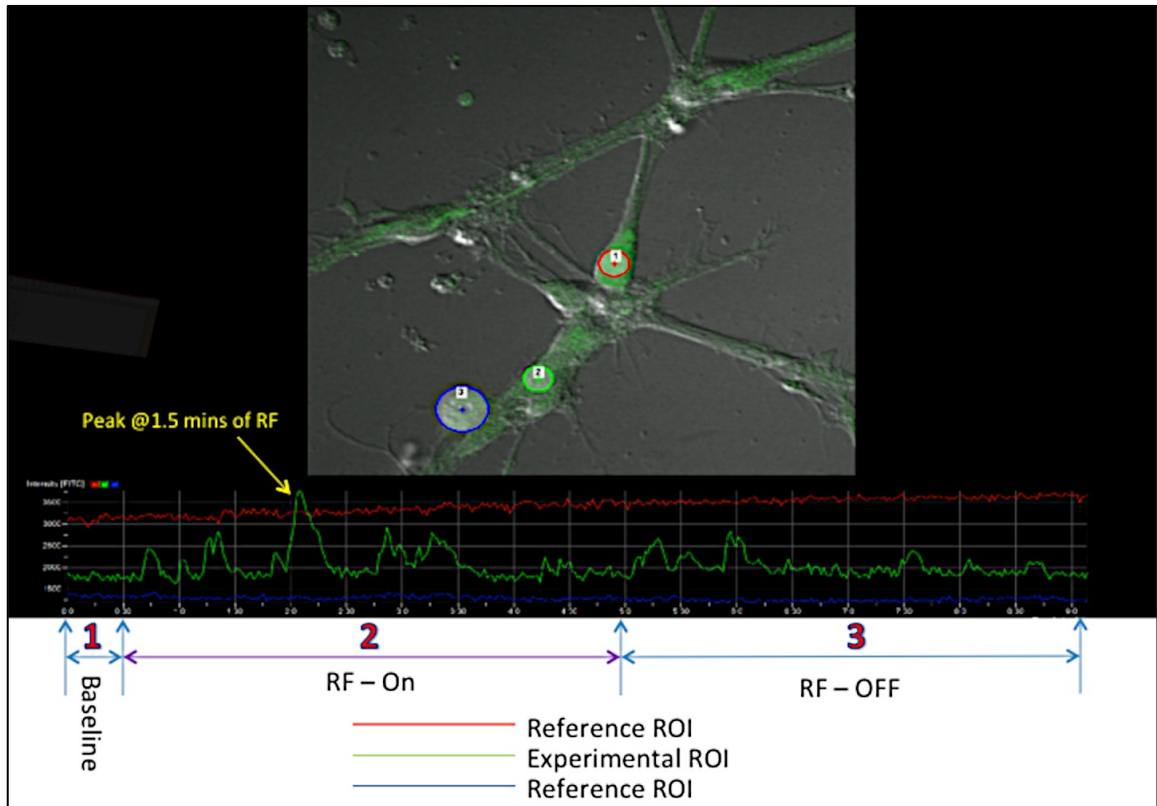


Figure 3-26: Annotated ROI analysis of rat cortical neurons with RF-stimulus using Nikon A1R+/A1+ confocal microscope system (30 seconds of baseline, 4.5 minutes of stimulus, 4 minutes of recovery).

Figure 3-26 shows the ROI analysis of cortical neurons exposed to RF-stimulus, below is a full description of the results:

1. 30 Seconds of Baseline Recording: The RED and BLUE lines are inactive sections of the culture and serve as baselines, whereas GREEN is an active section of the culture. The baseline intensity of the GREEN ROI is approximately 1800 (FITC).

2. 4.5 Minutes of RF-Stimulus: The GREEN ROI begins to have significant changes in intensity within 10 seconds. At 1.5 minutes into stimulus, a peak intensity of approximately 3750 (FITC) is reached. This is an almost 110% increase in signal. However, by minute 3.5 into stimulus the signal has returned to baseline values.
3. 4 Minutes of Recovery: Shortly after RF-stimulus is turned off, there is again a sharp change in signal intensity to a peak of 2750 (FITC). After 1.5 minutes of recovery, the signal has again stabilized around 1800 (FITC).

Field Modeling

The acceleration of Ca^{++} in the field was modeled in MATLAB and the velocity vs. time plot is Figure 3-27.

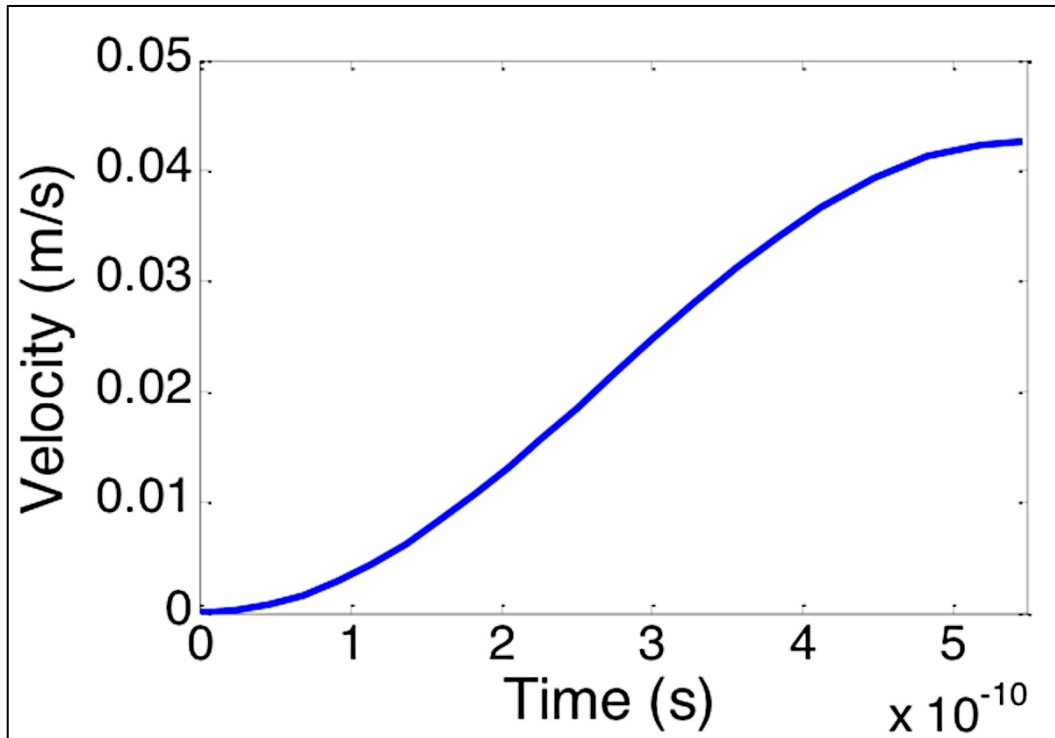


Figure 3-27: The velocity vs. time plot of a Ca⁺⁺ ion in 37 C H₂O in a 915 MHz, 18 V/m field, with a power of 750 mW/m².

The main result is that the maximum speed reached is 0.043 m/s. The period of the sinusoidal wave is the inverse of the frequency. The field switches halfway in the period. This means the total time the field could act on Ca⁺⁺ in one direction is 1/(2f). This time is 5.464481x10⁻¹⁰ seconds. The maximum velocity multiplied by this time gives the maximum distance a particle could travel in one phase of the wave (d=vt; 0.043 m/s * 5.464481x10⁻¹⁰ s = 2.34x10⁻¹¹ m). 2.34x10⁻¹¹ meters is 0.4% of the span of a typical cell membrane (5 nm).

Discussion

The *in vitro* RF-stimulus experiments were designed to investigate well-characterized cellular activities. After seeing strong RF-stimulus responses during *in vivo* experiments, there were a number of hypotheses why this phenomenon was present. It was reasonable to think that the RF waves themselves could cause ion movement and thus a significant flux of ions would lead to action potentials in some neurons. Through the many trials of recording intracellular calcium intensity, it appears that most activity is sub-threshold. There may be significant activity at very short time-scales that were unobserved by our detection timeframe. There is support for this inference from the second set of calcium flux experiments recorded at 30 frames per second and with more advanced background fluorescence management. There was some confusion as to why a calcium ion would not be pulled across a membrane by a high voltage field like the one generated by the RFID antenna used. Other researchers had reported intracellular calcium changes when a field was applied, but in most of these cases the field was fixed – meaning, the polarity did not change over time⁷⁰. The 915 MHz field used in these experiments is reversing polarity approximately every 5×10^{-10} seconds. It took the field and fluid resistance modeling to confirm that the field was not oriented in one direction long enough to pull an ion across a membrane, but this does

not prevent the ions from being vibrated in a confined area. This vibration and a series of other observations lend support to a second explanation for RF-stimulus induced neural activity - transient temperature changes.

The MEA experiments were useful to examine noxious stimuli in an extremely regulated experimental setting. Few systems are as well characterized and controlled (temperature, osmolality, electromagnetic shielding) as the 64-channel MEAs of the CNNS lab at UNT⁷⁹. Years of experiments with mature neural cultures have allowed precise understanding of how noxious chemicals change firing rates, firing patterns, and spike profiles^{78, 79}. We hypothesized that RF-stimulus would have lasting effects on cellular activity *in vitro*, but in recording sessions of up to 1.5 hours of RF-stimulus had negligible effects on firing rate and network activity. One plausible explanation is that most RF-stimulus effects are simply very short in duration, and once the stimulus is stopped the cells return to normal activity. Since the RF-stimulus operation caused tremendous recording system noise, it is possible that cellular activity during RF-stimulus is masked by noise. Another plausible explanation is that the very controlled nature of MEA recording obscured any of the changes that occur during *in vivo* experimentation. Temperature and osmolality were thoroughly controlled in the MEA experiments by cycling media through the MEA dish. It is possible that temperature gradients, ion

gradients, or other RF-stimulus phenomena were eliminated by very controlled experimental conditions.

There are some clear improvements that could be made to the *in vitro* experiments. Live cell imaging of calcium influx appears to be a promising direction. Ideally, a higher sampling rate of the fluorescent intensity would provide a clearer answer if RF-stimulus significantly changes cellular activity in a reproducible way. In the future, this effect should be fully categorized at different RF-stimulus power, frequency, and durations. Once this effect is categorized at each parameter, if the prevailing hypothesis is that transient temperature changes are responsible for the effect, then membrane channels responsible for sensing temperature (TRPV family) could be blocked^{81, 82}. If the effect is fully eliminated, then temperature change is the most likely reason why RF-stimulus produces cellular activity changes.

Although, MEA studies have many advantages to other assays, the difficulty in avoiding signal noise during recording likely rules out the usefulness of MEA experiments in the future. The lack of a clear activity change prior to and after the RF-stimulus was applied indicates that only tests that can measure while the stimulus is applied are useful.

Conclusion

Studies into thermal sensitivity of injured nerves have concluded that nerves are considerably more responsive to noxious thermal stimuli^{61, 63}. In some patients, increased sensitivity to previously non-noxious stimuli is observed following nerve injury⁸³. This is referred to as hyperalgesia⁸³. If the initial stimuli is a brushing or stroking of the skin and it results in a burning pain then the condition is called allodynia⁸³. These are stimulus evoked pain pathways, but there are also spontaneous pain events that characterize post-injury nerve behavior⁵⁸. This distinction between a spontaneous and elicited pain response presented out patient of interest and his physicians an interesting clinical challenge: were the careful observations by the patient of cell phone tower proximity and neuroma pain levels causal or only correlated? This was also the research question. Based on the experiments conducted, it is reasonable to conclude that RF-stimulus pain manifests itself in a similar frequency and intensity to thermal pain. This was shown with correlation analysis from many repeated trials. What is most interesting is that pain can be induced 1-week after a nerve is injured. The neuroma bulb has had little time to develop. The initial response to Von Frey stimulus is likely due to the inflammation at the sore injury site, but why would the damaged nerve react to RF-stimulus so soon? It is likely that ion channel expression has

changed significantly as part of the nerve regeneration process⁶⁰.

Decreased stimulus thresholds provide an evolutionary advantage for a damaged appendage to sense the environment. Fewer intact nerves necessitate that each nerve becomes more sensitive if functionality is to be restored. This response is maladaptive if increased sensitivity results in non-noxious stimuli becoming coded as noxious stimuli. This hypothesis explains why repeated injury to nerves sensitizes them for neuropathic pain. So even though the nerve is recently injured, and the neuroma is small, the damage to the nerve has likely lead to increased sensitivity as part of a maladaptive response during nerve regeneration of some nerve fiber sub-types.

One of the fiber types that our work has likely ruled out is the mechanoreceptive fiber. As was described earlier, the Wistar transgenic rats expressed ChR2 in mechanoreceptive fibers that ended in dermal touch structures. The axotomized nerve with no dermis to innervate may selectively prune the nerve fibers that are not useful. Or, put more simply: without skin, is it likely that mechanoreceptive fibers would mature to their original functionality? This question remains to be answered fully, but in every trial no animal reacted to OLVF in a manner similar to actual Von Frey palpation. And further, when the TNT-neuroma was directly bathed in laser light, the animal did not respond. This finding was surprising, and

may be a worthwhile area of study to investigate ectopic mechanoreceptive structure formation, optogenetic protein nerve distribution prior to and post injury, and mechanoreceptor development.

Fiber subtypes are an area only briefly investigated in this work, but optogenetic and other synthetic biology techniques will be able to introduce selectively activated proteins into cells of interest for the careful control of various neural lineages. Recent publications by colleagues have reported the development of viral vectors that selectively activate or inhibit nociceptive fibers⁸⁴. Additionally, the development of Designer Receptors Exclusively Activated by Designer Drugs (DREADD) technology has eliminated the need for light penetration to elicit cell specific activation or inhibition^{85, 86}. DREADD technology uses synthetic G-protein coupled receptors that are activated by typically inert chemicals. Most experiments that could be designed for optogenetic testing can be designed for DREADD testing. The advantage of optogenetic probing is the enhanced stimulation control, and the advantage of DREADD is the ability to control tissue deep within the body without implantation. These tools may provide years of useful mechanism experiments to fully characterize neuropathic pain.

Yet full characterization is not necessarily needed to help patients today. This interesting case of neuroma pain induced by RF-stimulus

appears to be likely caused by a heating mechanism of the microwave-band radio-frequency wave. Transient temperature changes induced by RF-stimulus are likely the causative agent in this pain pathway. The patient described an environment where he experiences no neuroma pain – deep underwater while SCUBA diving. There are a few reasons why this environment may limit neuroma pain. High pressure from the surrounding fluid and wetsuit would activate A β fibers that would trigger inhibitory interneurons to inhibit signals from nociceptive fibers^{1, 87}. The water would absorb RF waves. Cool water immersion of the entire appendage would lower the temperature of the neuroma slowing conduction velocity and decreasing the chances that the bulb would exceed a noxious threshold. To provide a viable clinical solution for patients, RF-shielding, temperature control, mechanical isolation, and neuroma bulb all likely need to be employed.

This chapter started with a clinical observation and lead to a long series of *in vivo* experiments in 37 rats. Five (RF, thermal, OLVF, VF, and anxiety chamber) nociceptive assays were developed, built, or optimized to characterize this problem, and a likely mechanism emerged from *in vivo* experiments. Subsequent *in vitro* testing and field modeling ruled out one hypothesis for RF-stimulus induced pain, and suggested a way to confirm the transient heat hypothesis by extensive *in vitro* work. Lastly, a reason

to shield neuromas from RF-stimulus was confirmed and has now developed into a patent application. Hopefully, this will allow for the development of surgical products to both impede neuroma development and to shield nerves from noxious stimuli.

Dissertation Summary Statement

Together all data here presented demonstrate the utility of micro-scale fabrication in surgical conduits, the ability to develop and optimize animal behavioral assays to avoid human testing, and the confirmation and suitable explanation for an unusual pain pathway by the available tools in current bioengineering.

Appendix A
International Patent Application
PCT/US14/16905

PCT

REQUEST

The undersigned requests that the present international application be processed according to the Patent Cooperation Treaty.

For receiving Office use only

International Application No.

International Filing Date

Name of receiving Office and "PCT International Application"

Applicant's or agent's file reference
(if desired) (12 characters maximum) 5013205.009PC1

Box No. I TITLE OF INVENTION	
CHEMICAL GRADIENTS	
Box No. II APPLICANT <input type="checkbox"/> This person is also inventor	
Name and address: <i>(Family name followed by given name; for a legal entity, full official designation. The address must include postal code and name of country. The country of the address indicated in this Box is the applicant's State (that is, country) of residence if no State of residence is indicated below.)</i> BOARD OF REGENTS, THE UNIVERSITY OF TEXAS SYSTEM 201 WEST 7TH STREET AUSTIN, TX 78701 US	Telephone No. Facsimile No. Applicant's registration No. with the Office
E-mail authorization: Marking one of the check-boxes below authorizes the receiving Office, the International Searching Authority, the International Bureau and the International Preliminary Examining Authority to use the e-mail address indicated in this Box to send, notifications issued in respect of this international application to that e-mail address if those offices are willing to do so. <input checked="" type="checkbox"/> as advance copies followed by paper notifications; or <input type="checkbox"/> exclusively in electronic form (no paper notifications will be sent). E-mail address: john.zimmer@smithmoorelaw.com	
State <i>(that is, country)</i> of nationality: US	State <i>(that is, country)</i> of residence: US
This person is applicant for the purposes of: <input checked="" type="checkbox"/> all designated States <input type="checkbox"/> the States indicated in the Supplemental Box	
Box No. III FURTHER APPLICANT(S) AND/OR (FURTHER) INVENTOR(S)	
<input checked="" type="checkbox"/> Further applicants and/or (further) inventors are indicated on a continuation sheet.	
Box No. IV AGENT OR COMMON REPRESENTATIVE; OR ADDRESS FOR CORRESPONDENCE	
The person identified below is hereby/has been appointed to act on behalf of the applicant(s) before the competent International Authorities as: <input checked="" type="checkbox"/> agent <input type="checkbox"/> common representative	
Name and address: <i>(Family name followed by given name; for a legal entity, full official designation. The address must include postal code and name of country.)</i> ZIMMER, John P., WIMBISH, J. Clinton, and MCCANN, Philip P. SMITH MOORE LEATHERWOOD LLP 101 N TRYON STREET, SUITE 1300 CHARLOTTE, NC 28246 US	Telephone No. 704-384-2659 Facsimile No. 704-384-2918 Agent's registration No. with the Office 64750, 54545, 30919
E-mail authorization: Marking one of the check-boxes below authorizes the receiving Office, the International Searching Authority, the International Bureau and the International Preliminary Examining Authority to use the e-mail address indicated in this Box to send, notifications issued in respect of this international application to that e-mail address if those offices are willing to do so. <input checked="" type="checkbox"/> as advance copies followed by paper notifications; or <input type="checkbox"/> exclusively in electronic form (no paper notifications will be sent). E-mail address: john.zimmer@smithmoorelaw.com	
<input type="checkbox"/> Address for correspondence: Mark this check-box where no agent or common representative is/has been appointed and the space above is used instead to indicate a special address to which correspondence should be sent.	

Box No. III FURTHER APPLICANT(S) AND/OR (FURTHER) INVENTOR(S)	
<i>If none of the following sub-boxes is used, this sheet should not be included in the request.</i>	
<p>Name and address: <i>(Family name followed by given name; for a legal entity, full official designation. The address must include postal code and name of country. The country of the address indicated in this Box is the applicant's State (that is, country) of residence if no State of residence is indicated below.)</i></p> <p>ROMERO-ORTEGA, Mario I. 1409 Glade Point Drive Coppell, TX 75019 US</p>	<p>This person is:</p> <p><input type="checkbox"/> applicant only</p> <p><input type="checkbox"/> applicant and inventor</p> <p><input checked="" type="checkbox"/> inventor only <i>(If this check-box is marked, do not fill in below.)</i></p> <hr/> <p>Applicant's registration No. with the Office</p>
State <i>(that is, country)</i> of nationality:	State <i>(that is, country)</i> of residence:
<p>This person is applicant for the purposes of: <input type="checkbox"/> all designated States <input type="checkbox"/> the States indicated in the Supplemental Box</p>	
<p>Name and address: <i>(Family name followed by given name; for a legal entity, full official designation. The address must include postal code and name of country. The country of the address indicated in this Box is the applicant's State (that is, country) of residence if no State of residence is indicated below.)</i></p> <p>LOTFI, Parisa 8710 Bevlyn Drive Houston, TX 77025 US</p>	<p>This person is:</p> <p><input type="checkbox"/> applicant only</p> <p><input type="checkbox"/> applicant and inventor</p> <p><input checked="" type="checkbox"/> inventor only <i>(If this check-box is marked, do not fill in below.)</i></p> <hr/> <p>Applicant's registration No. with the Office</p>
State <i>(that is, country)</i> of nationality:	State <i>(that is, country)</i> of residence:
<p>This person is applicant for the purposes of: <input type="checkbox"/> all designated States <input type="checkbox"/> the States indicated in the Supplemental Box</p>	
<p>Name and address: <i>(Family name followed by given name; for a legal entity, full official designation. The address must include postal code and name of country. The country of the address indicated in this Box is the applicant's State (that is, country) of residence if no State of residence is indicated below.)</i></p> <p>JOHNSTON, Benjamin R. 502 Yates Street Arlington, TX 76019 US</p>	<p>This person is:</p> <p><input type="checkbox"/> applicant only</p> <p><input type="checkbox"/> applicant and inventor</p> <p><input checked="" type="checkbox"/> inventor only <i>(If this check-box is marked, do not fill in below.)</i></p> <hr/> <p>Applicant's registration No. with the Office</p>
State <i>(that is, country)</i> of nationality:	State <i>(that is, country)</i> of residence:
<p>This person is applicant for the purposes of: <input type="checkbox"/> all designated States <input type="checkbox"/> the States indicated in the Supplemental Box</p>	
<p>Name and address: <i>(Family name followed by given name; for a legal entity, full official designation. The address must include postal code and name of country. The country of the address indicated in this Box is the applicant's State (that is, country) of residence if no State of residence is indicated below.)</i></p> <p>DASH, Swarupnarayan 1408 Strawberry Lane Apt. 323 Arlington, TX 76011 US</p>	<p>This person is:</p> <p><input type="checkbox"/> applicant only</p> <p><input type="checkbox"/> applicant and inventor</p> <p><input checked="" type="checkbox"/> inventor only <i>(If this check-box is marked, do not fill in below.)</i></p> <hr/> <p>Applicant's registration No. with the Office</p>
State <i>(that is, country)</i> of nationality:	State <i>(that is, country)</i> of residence:
<p>This person is applicant for the purposes of: <input type="checkbox"/> all designated States <input type="checkbox"/> the States indicated in the Supplemental Box</p>	
<p><input checked="" type="checkbox"/> Further applicants and/or (further) inventors are indicated on another continuation sheet.</p>	

Box No. III FURTHER APPLICANT(S) AND/OR (FURTHER) INVENTOR(S)

If none of the following sub-boxes is used, this sheet should not be included in the request.

<p>Name and address: <i>(Family name followed by given name; for a legal entity, full official designation. The address must include postal code and name of country. The country of the address indicated in this Box is the applicant's State (that is, country) of residence if no State of residence is indicated below.)</i></p> <p>RAZAL, Joselito Intelligent Polymer Research Institute University of Wollongong Wollongong NSW 2522 AU</p>	<p>This person is:</p> <p><input type="checkbox"/> applicant only</p> <p><input type="checkbox"/> applicant and inventor</p> <p><input checked="" type="checkbox"/> inventor only <i>(If this check-box is marked, do not fill in below.)</i></p> <hr/> <p>Applicant's registration No. with the Office</p>
--	---

State <i>(that is, country)</i> of nationality:	State <i>(that is, country)</i> of residence:
---	---

This person is applicant for the purposes of: all designated States the States indicated in the Supplemental Box

<p>Name and address: <i>(Family name followed by given name; for a legal entity, full official designation. The address must include postal code and name of country. The country of the address indicated in this Box is the applicant's State (that is, country) of residence if no State of residence is indicated below.)</i></p> <p>WALLACE, Gordon Intelligent Polymer Research Institute University of Wollongong Wollongong NSW 2522 AU</p>	<p>This person is:</p> <p><input type="checkbox"/> applicant only</p> <p><input type="checkbox"/> applicant and inventor</p> <p><input checked="" type="checkbox"/> inventor only <i>(If this check-box is marked, do not fill in below.)</i></p> <hr/> <p>Applicant's registration No. with the Office</p>
--	---

State <i>(that is, country)</i> of nationality:	State <i>(that is, country)</i> of residence:
---	---

This person is applicant for the purposes of: all designated States the States indicated in the Supplemental Box

<p>Name and address: <i>(Family name followed by given name; for a legal entity, full official designation. The address must include postal code and name of country. The country of the address indicated in this Box is the applicant's State (that is, country) of residence if no State of residence is indicated below.)</i></p>	<p>This person is:</p> <p><input type="checkbox"/> applicant only</p> <p><input type="checkbox"/> applicant and inventor</p> <p><input type="checkbox"/> inventor only <i>(If this check-box is marked, do not fill in below.)</i></p> <hr/> <p>Applicant's registration No. with the Office</p>
---	--

State <i>(that is, country)</i> of nationality:	State <i>(that is, country)</i> of residence:
---	---

This person is applicant for the purposes of: all designated States the States indicated in the Supplemental Box

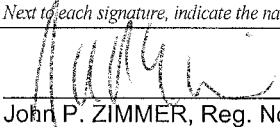
<p>Name and address: <i>(Family name followed by given name; for a legal entity, full official designation. The address must include postal code and name of country. The country of the address indicated in this Box is the applicant's State (that is, country) of residence if no State of residence is indicated below.)</i></p>	<p>This person is:</p> <p><input type="checkbox"/> applicant only</p> <p><input type="checkbox"/> applicant and inventor</p> <p><input type="checkbox"/> inventor only <i>(If this check-box is marked, do not fill in below.)</i></p> <hr/> <p>Applicant's registration No. with the Office</p>
---	--

State <i>(that is, country)</i> of nationality:	State <i>(that is, country)</i> of residence:
---	---

This person is applicant for the purposes of: all designated States the States indicated in the Supplemental Box

Further applicants and/or (further) inventors are indicated on another continuation sheet.

Box No. V DESIGNATIONS				
<p>The filing of this request constitutes under Rule 4.9(a) the designation of all Contracting States bound by the PCT on the international filing date, for the grant of every kind of protection available and, where applicable, for the grant of both regional and national patents.</p> <p>However,</p> <p><input type="checkbox"/> DE Germany is not designated for any kind of national protection</p> <p><input type="checkbox"/> JP Japan is not designated for any kind of national protection</p> <p><input type="checkbox"/> KR Republic of Korea is not designated for any kind of national protection</p> <p><i>(The check-boxes above may only be used to exclude (irrevocably) the designations concerned if, at the time of filing or subsequently under Rule 26bis.1, the international application contains in Box No. VI a priority claim to an earlier national application filed in the particular State concerned, in order to avoid the ceasing of the effect, under the national law, of this earlier national application.)</i></p>				
Box No. VI PRIORITY CLAIM AND DOCUMENT				
The priority of the following earlier application(s) is hereby claimed:				
Filing date of earlier application <i>(day/month/year)</i>	Number of earlier application	Where earlier application is:		
		national application: country or Member of WTO	regional application: regional Office	international application: receiving Office
item (1) 19 FEBRUARY 2013 (19/02/2013)	61/766,366	US		
item (2)				
item (3)				
<input type="checkbox"/> Further priority claims are indicated in the Supplemental Box.				
Furnishing the priority document(s):				
<input checked="" type="checkbox"/> The receiving Office is requested to prepare and transmit to the International Bureau a certified copy of the earlier application(s) (only if the earlier application(s) was filed with the receiving Office which, for the purposes of this international application, is the receiving Office) identified above as:				
<input checked="" type="checkbox"/> all items <input type="checkbox"/> item (1) <input type="checkbox"/> item (2) <input type="checkbox"/> item (3) <input type="checkbox"/> other, see Supplemental Box				
<input type="checkbox"/> The International Bureau is requested to obtain from a digital library a certified copy of the earlier application(s) identified above, using, where applicable, the access code(s) indicated below (if the earlier application(s) is available to it from a digital library):				
<input type="checkbox"/> item (1) access code _____ <input type="checkbox"/> item (2) access code _____ <input type="checkbox"/> item (3) access code _____ <input type="checkbox"/> other, see Supplemental Box				
Restore the right of priority: the receiving Office is requested to restore the right of priority for the earlier application(s) identified above or in the Supplemental Box as item(s) (_____). (See also the Notes to Box No. VI; further information must be provided to support a request to restore the right of priority.)				
Incorporation by reference: where an element of the international application referred to in Article 11(1)(iii)(d) or (e) or a part of the description, claims or drawings referred to in Rule 20.5(a) is not otherwise contained in this international application but is completely contained in an earlier application whose priority is claimed on the date on which one or more elements referred to in Article 11(1)(iii) were first received by the receiving Office, that element or part is, subject to confirmation under Rule 20.6, incorporated by reference in this international application for the purposes of Rule 20.6.				
Box No. VII INTERNATIONAL SEARCHING AUTHORITY				
Choice of International Searching Authority (ISA) (if more than one International Searching Authority is competent to carry out the international search, indicate the Authority chosen; the two-letter code may be used):				
ISA/ EP _____				

Box No. IX CHECK LIST for EFS-Web filings - this sheet is only to be used when filing an international application with RO/US via EFS-Web			
This international application contains the following:	Number of sheets	This international application is accompanied by the following item(s) <i>(mark the applicable check-boxes below and indicate in right column the number of each item):</i>	Number of items
(a) request form PCT/RO/101 (including any declarations and supplemental sheets)	5	1. <input checked="" type="checkbox"/> fee calculation sheet	1
(b) description (excluding any sequence listing part of the description, see (f), below)	35	2. <input type="checkbox"/> original separate power of attorney	
(c) claims	3	3. <input type="checkbox"/> original general power of attorney	
(d) abstract	1	4. <input type="checkbox"/> copy of general power of attorney; reference number:	
(e) drawings (if any)	17	5. <input type="checkbox"/> priority document(s) identified in Box No. VI as item(s)	
(f) sequence listing part of the description in the form of an image file (e.g. PDF)		6. <input type="checkbox"/> Translation of international application into (language):	
Total number of sheets (including the sequence listing part of the description if filed as an image file)	61	7. <input type="checkbox"/> separate indications concerning deposited microorganism or other biological material	
(g) sequence listing part of the description		8. <input type="checkbox"/> <i>(only where item (f) is marked in the left column)</i> copy of the sequence listing in electronic form (Annex C/ST.25 text file) not forming part of the international application but furnished only for the purposes of international search under Rule 13ter.	
<input type="checkbox"/> filed in the form of an Annex C/ST.25 text file		9. <input type="checkbox"/> <i>(only where item (f) is marked in the left column)</i> a statement confirming that "the information recorded in electronic form submitted under Rule 13ter is identical to the sequence listing as contained in the international application" as filed via EFS-Web:	
<input type="checkbox"/> WILL BE filed separately on physical data carrier(s), on the same day and in the form of an Annex C/ST.25 text file		10. <input type="checkbox"/> copy of results of earlier search(es) (Rule 12bis.1(a))	
Indicate type and number of physical data carrier(s)		11. <input type="checkbox"/> other <i>(specify)</i> :	
Figure of the drawings which should accompany the abstract:	2	Language of filing of the international application:	English
Box No. X SIGNATURE OF APPLICANT, AGENT OR COMMON REPRESENTATIVE			
<i>Next to each signature, indicate the name of the person signing and the capacity in which the person signs (if such capacity is not obvious from reading the request).</i>			
 _____ John P. ZIMMER, Reg. No. 64,750		DATE: 18 FEBRUARY 2014	

For receiving Office use only			
1. Date of actual receipt of the purported international application:			
3. Corrected date of actual receipt due to later but timely received papers or drawings completing the purported international application:			
4. Date of timely receipt of the required corrections under PCT Article 11(2):			
5. International Searching Authority (if two or more are competent): ISA /	6. <input type="checkbox"/> Transmittal of search copy delayed until search fee is paid		
		2. Drawings:	<input type="checkbox"/> received:
		<input type="checkbox"/> not received:	

For International Bureau use only
Date of receipt of the record copy by the International Bureau:

This sheet is not part of and does not count as a sheet of the international application.

PCT

FEE CALCULATION SHEET

Annex to the Request

For receiving Office use only

International Application No.

Date stamp of the receiving Office

Applicant's or agent's file reference **5013205.009PC1**

Applicant
BOARD OF REGENTS, THE UNIVERSITY OF TEXAS SYSTEM

CALCULATION OF PRESCRIBED FEES

1. TRANSMITTAL FEE **USD 120** T

2. SEARCH FEE **2545** S

International search to be carried out by EP
(If two or more International Searching Authorities are competent to carry out the international search, indicate the name of the Authority which is chosen to carry out the international search.)

3. INTERNATIONAL FILING FEE
Enter total number of sheets indicated in Box No IX: 61

i1 first 30 sheets **1360** i1

i2 31 x 17 = **527** i2
number of sheets in excess of 30 fee per sheet

Add amounts entered at i1 and i2 and enter total at I **1887** I

(Applicants from certain States are entitled to a reduction of 90% of the international filing fee. Where the applicant is (or all applicants are) so entitled, the total to be entered at I is 10% of the international filing fee.)

4. FEE FOR PRIORITY DOCUMENT (if applicable) P

5. FEE FOR RESTORATION OF THE RIGHT OF PRIORITY (if applicable) RP

6. FEE FOR EARLIER SEARCH DOCUMENTS (if applicable) ES

7. TOTAL FEES PAYABLE **USD 4,552**

Add amounts entered at T, S, I, P, RP and ES, and enter total in the TOTAL box
TOTAL

MODE OF PAYMENT (Not all modes of payment may be available at all receiving Offices)
 authorization to charge deposit or current account (see below) postal money order credit card (details should be furnished separately and not included on this sheet) cash
 check bank transfer revenue stamps other (specify):

AUTHORIZATION TO CHARGE (OR CREDIT) DEPOSIT OR CURRENT ACCOUNT
(This mode of payment may not be available at all receiving Offices)
 Authorization to charge the total fees indicated above.
 (This check-box may be marked only if the conditions for deposit or current accounts of the receiving Office so permit) Authorization to charge any deficiency or credit any overpayment in the total fees indicated above.
 Authorization to charge the fee for priority document.
Receiving Office: RO/ US
Deposit or Current Account No.: 502190
Date: 18 February 2014 (18.02.2014)
Name: John P. ZIMMER
Signature: [Signature]

Electronic Patent Application Fee Transmittal

Application Number:	
Filing Date:	
Title of Invention:	Chemical Gradients
First Named Inventor/Applicant Name:	Board of Regents, The University Of Texas System
Filer:	John P. Zimmer/Tammy Taylor
Attorney Docket Number:	5013205.009PC1

Filed as Small Entity

International Application for filing in the US receiving office Filing Fees

Description	Fee Code	Quantity	Amount	Sub-Total USD(\$)
Basic Filing:				
Transmittal Fee	2601	1	120	120
Intl Filing Fee (1st-30 Pgs.) PCT Easy	1701	1	1360	1360
Suppl. Intl Filing Fee (each page > 30)	1703	31	17	527
International Search (EPO)	1704	1	2545	2545

Pages:

Claims:

Miscellaneous-Filing:

Description	Fee Code	Quantity	Amount	Sub-Total USD(\$)
Patent-Appeals-and-Interference:				
Post-Allowance-and-Post-Issuance:				
Extension-of-Time:				
Miscellaneous:				
			Total in USD (\$)	4552

Electronic Acknowledgement Receipt

EFS ID:	18230954
Application Number:	
International Application Number:	PCT/US14/16905
Confirmation Number:	9792
Title of Invention:	Chemical Gradients
First Named Inventor/Applicant Name:	Board of Regents, The University Of Texas System
Customer Number:	11806
Correspondence Address:	John P. Zimmer Smith Moore Leatherwood LLP 101 N Tryon Street Suite 1300 Charlotte NC 28246 US 704-384-2659 john.zimmer@smithmoorelaw.com
Filer:	John P. Zimmer/Tammy Taylor
Filer Authorized By:	John P. Zimmer
Attorney Docket Number:	5013205.009PC1
Receipt Date:	18-FEB-2014
Filing Date:	
Time Stamp:	17:02:20
Application Type:	International Application for filing in the US receiving office

Submitted with Payment	yes
Payment Type	Deposit Account
Payment was successfully received in RAM	\$4552
RAM confirmation Number	4100
Deposit Account	502190
Authorized User	

File Listing:

Document Number	Document Description	File Name	File Size(Bytes)/ Message Digest	Multi Part /.zip	Page (if ap
1	Specification	PC_Application_Specification.pdf	232086 e3cde48d4741d45ba34e31d962ca7e82c5a07f0a	no	39
Warnings:					
Information:					
2	Drawings-only black and white line drawings	PCFigures.pdf	12028445 6f1b7b04e4e59f5ea88d0ecfd19c4b29cfc94a7	no	17
Warnings:					
Information:					
3	Misc. incoming letter from Applicant - IA	009PC1_Trans.pdf	57726 cbb06cd69f9a9e39f47d00584f97cc79fa4097de	no	1
Warnings:					
Information:					
4	PCT-Transmittal Letter	009PC1_PC_Trans.pdf	237408 8ed29c6bd6619cc1e492ad60df3dd6f6892eb6e5	no	1
Warnings:					
Information:					
5	RO/101 - Request form for new IA - Conventional	009PC1_Request.pdf	969633 18499cad8777bcb631eb04a500da051d604f2636	no	5
Warnings:					
Information:					
6	RO/101 - Annex (fee calculation sheet)	009PC1_Fee.pdf	172099 8a92130268c5e8349d2ae11a7196d415a8130094	no	1
Warnings:					
Information:					
7	Fee Worksheet (SB06)	fee-info.pdf	36231 7d003c5964349c4d91a38dc0156e22317aa	no	2

This Acknowledgement Receipt evidences receipt on the noted date by the USPTO of the indicated documents, characterized by the applicant, and including page counts, where applicable. It serves as evidence of receipt similar to a Post Card, as described in MPEP 503.

New Applications Under 35 U.S.C. 111

If a new application is being filed and the application includes the necessary components for a filing date (see 37 CFR 1.53(b)-(d) and MPEP 506), a Filing Receipt (37 CFR 1.54) will be issued in due course and the date shown on this Acknowledgement Receipt will establish the filing date of the application.

National Stage of an International Application under 35 U.S.C. 371

If a timely submission to enter the national stage of an international application is compliant with the conditions of 35 U.S.C. 371 and other applicable requirements a Form PCT/DO/EO/903 indicating acceptance of the application as a national stage submission under 35 U.S.C. 371 will be issued in addition to the Filing Receipt, in due course.

New International Application Filed with the USPTO as a Receiving Office

If a new international application is being filed and the international application includes the necessary components for an international filing date (see PCT Article 11 and MPEP 1810), a Notification of the International Application Number and of the International Filing Date (Form PCT/RO/105) will be issued in due course, subject to prescriptions concerning national security, and the date shown on this Acknowledgement Receipt will establish the international filing date of the application.

CHEMICAL GRADIENTS

CROSS REFERENCE TO RELATED APPLICATION

[0001] This application claims priority pursuant to 35 U.S.C. § 119(e) to U.S. Provisional Patent Application Ser. No. 61/766,366, filed on February 19, 2013, which is hereby incorporated by reference in its entirety.

STATEMENT REGARDING FEDERALLY SPONSORED RESEARCH

[0002] This invention was made with government support under grant 1R21Ns072955-01A1 awarded by the National Institutes of Health/National Institute of Neurological Disorders and Stroke (NIH/NINDS).

FIELD

[0003] This invention relates to apparatuses and methods for forming chemical gradients and compositions comprising chemical gradients and, in particular, to chemical gradients for drug delivery and other biomedical applications.

BACKGROUND

[0004] During development and after injury, neural cells migrate and elongate their axons towards proper target cells and organs in response to gradients of biomolecules, which guide axonal regeneration (chemotaxis) either by attachment to the cells or to the extracellular matrix (ECM), or by secretion into the extracellular fluid. In some cases, chemotactic soluble molecules are secreted by specific cells, and gradients are formed through diffusion and convection from the site of release. Cellular responses to such gradients can be influenced by the nature of the biomolecules, and physical characteristics of the ECM (which can include collagen, fibronectin, and laminin), such as matrix pore size and stiffness. In the developing peripheral nervous system (PNS), gradients of neurotrophic factors (NTF) such as nerve growth factor (NGF), neurotrophin 3 (NT-3), and brain-derived neurotrophic factor (BDNF), are established by distal target cells and direct axonal elongation and target recognition of motor neurons (VMN) from the ventral spinal cord, as well as sensory neurons in the dorsal root ganglia (DRG). In

the adult PNS, the efferent branch of sensory neurons re-innervates skin and muscle targets spontaneously after injury, but afferent axons are unable to enter the hostile environment of the adult spinal cord, unless enticed by induced NGF expression. Moreover, pathfinding errors made by injured VMN and DGR neurons during regeneration can be dramatically reduced by the expression of the appropriate gene expression that re-establishes NTF gradients.

[0005] Unfortunately, the creation of chemical gradients such as NTF gradients and the use of chemical gradients in nerve repair remain extremely challenging. For example, some prior technologies fail to provide sustained release of desired molecular signals and/or lack ECM support. Other technologies lack the ability to provide non-transient and/or physiologically relevant chemical gradients normally present in vivo. Further, some previous methods for creating a chemical gradient are applicable to only short-term studies in vitro and/or present risks associated with the injection of a viral vector. Therefore, improved apparatuses and methods for providing a chemical gradient are desired.

SUMMARY

[0006] The present disclosure relates to methods, apparatuses and compositions useful in tissue repair through establishing highly tunable chemical gradients such as NTF or NGF gradients designed to direct axonal growth through multiluminal or multichannel hydrogels filled with ECM. To that end, the present disclosure relates to a novel coiled polymeric structure anchored to the walls of hydrogel microchannels to establish highly and predictably regulated gradients of controllable and sustained NTF release that permeates the luminal collagen, which in turn stabilizes gradients of diffusible factors and provides permissive and predictably regulated and controlled/controllable growth substrates for axonal elongation. A mathematical model was determined to describe NTF diffusion in this complex matrix and to determine the luminal NTF concentration over time, using DRG in vitro neural growth assays to provide evidence of chemotactic nerve regeneration along the three-dimensional NGF gradients. This method is thought to prove beneficial for guided tissue repair, among other uses.

[0007] Aspects of the present disclosure are directed to apparatuses, comprising at least one conduit having a first end and a second end and one or more microchannels disposed in the conduit and extending from the first end toward the second end. A fiber is coiled around the exterior of at least one microchannel, wherein the fiber comprises an active agent that is operable to diffuse into the interior of the microchannel. In a further aspect, the conduit comprises catheter tubing such as Micro-Renathane implantation tubing.

[0008] In a still further aspect, the microchannels are disposed within a matrix material disposed in the conduit. Still further, the matrix material can comprise an agarose gel, a polylactic-co-glycolic acid (PLGA), polylactic acid (PLA), polycaprolactone, polyurethane, a polyester, polycarbonate, collagen, polytetrafluoroethylene (PTFE), polymethylmethacrylate (PMMA), an ethylene-vinylacetate copolymer (EVA), a polydimethylsiloxane (PDMS), polyether-polyurethane, a polyethyleneterephthalate (PET), a polysulfone (PS), a polyethyleneoxide (PEO) or polyethylene glycol (PEG), a polyethylene oxide-polypropylene oxide copolymer (PEO-PPO), a polyolefin such as polyethylene (PE) or polypropylene (PP), or a combination of one or more of the foregoing.

[0009] In yet another aspect, the matrix material comprises an agarose gel comprising between about 1.5 weight percent and 2.5 weight percent agarose, based on the total weight of the agarose gel. Still further, a plurality of microchannels is preferably disposed in the conduit, and a plurality of fibers is coiled around the exteriors of a plurality of microchannels.

[0010] In a still further aspect, the plurality of fibers are each coiled around the exterior of a different microchannel, and at least two of the coiled fibers comprise differing active agents, differing amounts of an active agent, and/or differing pitches.

[0011] In yet another aspect, the fiber comprises or is formed from a polymeric material, such as, for example, a polylactic-co-glycolic acid, a polylactic acid, a caprolactone, or a combination thereof. A fiber can also comprise or be formed from other materials. Additionally, in a further aspect, the polymer is biodegradable.

[0012] In a still further variation, the fiber is coiled around the exterior of the microchannel in an isotropic configuration and/or an anisotropic configuration.

[0013] In another aspect, the active agent comprises a drug and/or a growth factor.

[0014] Aspects of the disclosure are further directed to methods of forming a chemical gradient comprising disposing any of the apparatuses described herein in a biological compartment. Further aspects contemplate that the biological compartment comprises a nerve conduit. Preferably, the active agent gradient comprises a drug gradient and/or a growth factor gradient.

[0015] Aspects of the present disclosure are also directed to a composition comprising a coiled polymeric material comprising an active agent operable to diffuse out of the polymeric material when the polymeric material is disposed in a biological compartment. In another aspect, the polymeric material preferably comprises a polylactic-co-glycolic acid, a polylactic acid, a caprolactone, or a combination thereof. In a still further aspect, the polymeric material is biodegradable. In yet another aspect, the active agent comprises a drug and/or growth factor. In a still further aspect, the biological compartment comprises a nerve conduit.

[0016] Further variations of the present disclosure are further directed to a composition, and apparatuses comprising a composition, that comprises a first gel comprising an active agent at a first concentration and a second gel comprising an active agent at a second concentration, wherein the first gel and the second gel are arranged in space to provide a concentration gradient of the active agent.

[0017] In a further aspect, the composition comprises a third gel comprising an active agent at a third concentration, the first gel, second gel, and third gel arranged in space, or oriented, to provide a gradient region comprising a concentration gradient of the active agent. In yet another aspect, the gradient region comprises a linear concentration gradient. Still further, the first, second, and third gels are arranged to provide a plurality of linear concentration gradients, or the first, second, and third gels are arranged or oriented in space to provide a non-gradient region in addition to the gradient region.

[0018] In another variation, the present disclosure is directed to a composition described above, wherein the first gel and/or the second gel comprises an agarose gel, a polylactic-co-glycolic acid, a polylactic acid, a caprolactone, or a combination thereof and the active agent comprises a drug or growth factor.

[0019] Still further, the present disclosure is directed to an apparatus comprising a conduit and any of the aforementioned compositions disposed in the conduit.

[0020] In addition, the present disclosure is directed to a method of forming a chemical or active agent concentration gradient comprising disposing any of the aforementioned apparatuses in a biological compartment, such as, for example a nerve conduit, and wherein the chemical or active agent concentration gradient comprises a drug gradient or a growth factor gradient.

[0021] Still further, the present disclosure is directed to a method for forming a chemical or active agent gradient comprising disposing any of the aforementioned compositions in a biological compartment, such as, for example, a nerve conduit, and wherein the chemical or active agent concentration gradient comprises a drug gradient or a growth factor gradient.

BRIEF DESCRIPTION OF THE DRAWINGS

[0022] FIGS. 1A-B illustrate perspective views of conduits comprising a microchannel.

[0023] FIG. 1C illustrates a perspective view of an apparatus according to one embodiment described herein.

[0024] FIG. 2 illustrates a schematic perspective view of a mixed nerve population directing nerve cells into an apparatus according to one embodiment described herein.

[0025] FIG. 3 illustrates a schematic perspective view of an apparatus according to one embodiment described herein.

[0026] FIGS. 4A-E illustrate photographs of various components of an apparatus according to one embodiment described herein.

[0027] FIG. 5A illustrates a schematic perspective view of an apparatus according to one embodiment described herein.

[0028] FIGS. 5B-D illustrate microscope images of a chemical gradient provided by the apparatus of FIG. 5A.

[0029] FIG. 6 illustrates a graph of the average cell process lengths corresponding to the chemical gradient of FIGS. 5B-D.

- [0030] FIG. 7A illustrates a schematic perspective view of a chemical gradient according to one embodiment described herein.
- [0031] FIGS. 7B-C illustrate perspective views of conduits comprising a plurality of microchannels.
- [0032] FIG. 7D illustrates a perspective view of an apparatus comprising a plurality of microchannels according to one embodiment described herein.
- [0033] FIG. 7E illustrates a perspective view of an apparatus according to one embodiment described herein and the apparatus's corresponding densitometry profile.
- [0034] FIGS. 7F-i-iii illustrate a process of making an apparatus according to embodiment described herein.
- [0035] FIGS. 7G-I are microscope images of a aspect shown in FIG. 7E.
- [0036] FIG. 8A illustrates a series of microscope images of chemical gradients formed according to some embodiments of methods described herein.
- [0037] FIG. 8B illustrates a plot of the chemical gradients of FIG. 8A.
- [0038] FIGS. 9A-C illustrate microscope images of nerve cells disposed in a chemical gradient according to one embodiment described herein.
- [0039] FIGS. 10A-I illustrate microscope images of nerve cells disposed in chemical gradients according to some embodiments described herein.
- [0040] FIG. 10J illustrates a graph corresponding to FIGS. 10A-I.
- [0041] FIG. 10K illustrates a calibration curve corresponding to FIGS. 10A-J.
- [0042] FIG. 11 illustrates a graph of the release profiles of a molecule according to some embodiments of chemical gradients described herein.
- [0043] FIG. 12 illustrates a graph of the release profiles of a molecule according to some embodiments of chemical gradients described herein.
- [0044] FIGS. 13A-D illustrate microscope images of nerve cells disposed in chemical gradients according to some embodiments described herein.
- [0045] FIGS. 13E-F illustrate graphs corresponding to FIGS. 13A-D.
- [0046] FIGS. 14A-B illustrate microscope images of nerve cells disposed in chemical gradients according to some embodiments described herein.
- [0047] FIG. 14C illustrate a graph corresponding to FIGS. 14A-B.

[0048] FIGS. 15A-B illustrate microscope images of nerve cells disposed in chemical gradients according to some embodiments described herein.

[0049] FIGS. 15C-D illustrate graphs corresponding to FIGS. 15A-B.

[0050] FIG. 16 illustrates a graph of turning angle ratio of axonal growth according to one embodiment of a method described herein.

[0051] FIG. 17 illustrates a schematic perspective view of a composition according to one embodiment described herein.

[0052] FIG. 18 illustrates a scanning electron microscope (SEM) image of a composition according to one embodiment described herein.

DETAILED DESCRIPTION

[0053] Aspects described herein can be understood more readily by reference to the following detailed description, examples, and figures. Elements, apparatus, and methods described herein, however, are not limited to the specific embodiments presented in the detailed description, examples, and figures. It should be recognized that disclosed embodiments are merely illustrative of the principles of the present invention. Numerous modifications and adaptations will be readily apparent to those of skill in the art without departing from the spirit and scope of the invention.

[0054] In addition, all ranges disclosed herein are to be understood to encompass any and all sub-ranges subsumed therein. For example, a stated range of “1.0 to 10.0” should be considered to include any and all sub-ranges beginning with a minimum value of 1.0 or more and ending with a maximum value of 10.0 or less, e.g., 1.0 to 5.3, or 4.7 to 10.0, or 3.6 to 7.9.

[0055] All ranges disclosed herein are also to be considered to include the end points of the range, unless expressly stated otherwise. For example, a range of “between 5 and 10” should generally be considered to include the end points 5 and 10.

[0056] Further, when the phrase “up to” is used in connection with an amount or quantity, it is to be understood that the amount is at least a detectable amount or quantity. For example, a material present in an amount “up to” a specified amount can be present from a detectable amount and up to and including the specified amount.

[0057] As described further hereinbelow, the present disclosure relates to methods, apparatuses, and compositions useful for forming chemical gradients, including within a biological environment. Further, such chemical gradients can be used for tissue repair and/or drug delivery. For example, in some cases, tissue repair can be achieved by establishing a highly tunable nerve growth factor (NGF) gradient designed to direct axonal growth through microchannels of an apparatus described herein, such as hydrogel microchannels filled with extracellular matrix (ECM) material.

[0058] Aspects of the present disclosure are, therefore, directed to apparatuses, methods, and compositions that can be used to provide a sustained chemical gradient, including in a biological environment. In one variation, fibers incorporating known amounts of active agents, such as growth factors, are coiled in a predetermined and preselected orientation, preferably about the walls, or outer circumference, of a microchannel in a conduit. In this way, the active ingredient can be controllably provided to a tissue introduced into the microchannel at a predetermined concentration. In some embodiments, the concentration of the active agent delivery can be predictably altered along the length of the microchannel by intentionally altering the fiber pitch or number of coils present in a given area along the length of the microchannel. In this manner, a concentration gradient along the length of the microchannel can be established. For example, when an active agent such as a growth factor (GF) is provided in the coiled fibers, such coiled fibers can be coiled or wrapped around, or inside of, one or more microchannels or lumens to provide one or more defined GF gradients in the microchannels or lumens. Therefore, methods, apparatuses, and compositions are disclosed to create a predetermined, preselected, and predictably controlled chemical gradient. Such a chemical gradient can also be referred to herein as a “programmable” gradient. In some embodiments, the gradient is accomplished by the pitch or number of turns of a fiber described herein.

[0059] An apparatus described herein, in some embodiments, comprises a conduit having a first end and a second end, one or more microchannels disposed in the conduit and extending from the first end toward the second end, and a fiber coiled around the exterior of at least one microchannel, wherein the fiber comprises an active agent that is operable to diffuse into the interior of the microchannel. The conduit of the apparatus

can have any size, shape, and structure and be formed from any material not inconsistent with the objectives of the present invention. In some embodiments, for instance, the conduit is formed from a polymeric material such as a polyurethane, a polyester, a polycarbonate, or a polyolefin such as polyethylene or polypropylene, etc. Moreover, in some cases, the conduit has a substantially tubular or cylindrical shape. Such a tubular or cylindrical conduit, in some embodiments, has an inner diameter between about 100 μm and about 50 mm, between about 100 μm and about 10 mm, between about 1 mm and about 10 mm, between about 1 mm and about 5 mm, or between about 200 μm and about 500 μm . In some cases, the conduit has a diameter greater than about 50 mm or less than about 100 μm . Further, in some cases, a conduit described herein has a length between about 1 mm and about 200 mm, between about 5 mm and about 100 mm, between about 10 mm and about 30 mm, or between about 50 mm and about 150 mm.

[0060] Additionally, a conduit described herein can comprise or be formed from any material not inconsistent with the objectives of the present invention. In some embodiments, for instance, the conduit is formed from a polymeric material such as a polyurethane, a polyester, a polycarbonate, a polycaprolactone, a polylactic acid (PLA), a collagen, a polytetrafluoroethylene (PTFE), a polymethylmethacrylate (PMMA), an ethylene-vinylacetate copolymer (EVA), a polydimethylsiloxane (PDMS), a polyether polyurethane, a polyethyleneterephthalate (PET), a polysulfone (PS), a polyethyleneoxide (PEO) or polyethylene glycol (PEG), a polyethylene oxide-polypropylene oxide copolymer (PEO-PPO), a polyolefin such as polyethylene (PE) or polypropylene (PP), or a combination of one or more of the foregoing. In some instances, the conduit comprises a segment of implantation or catheter tubing, such as Micro-Renathane implantation tubing. Other materials may also be used.

[0061] Similarly, the microchannels of a conduit described herein can have any size and shape not inconsistent with the objectives of the present invention. In some cases, for instance, a substantially tubular or cylindrical microchannel has a diameter between about 100 nm and about 2000 μm , between about 100 nm and about 50 μm , between about 100 nm and about 1 μm , between about 500 nm and about 10 μm , between about 500 nm and about 5 μm , or between about 500 nm and about 1 μm . In some embodiments, the microchannels have an average diameter between about 100 μm and

about 2000 μm , between about 100 μm and about 1000 μm , or between about 300 μm and about 800 μm . In some cases, the microchannels have an average diameter of less than about 100 μm or greater than about 2000 μm . Further, the microchannels can have a length up to about 99%, up to about 95%, up to about 90%, or up to about 80% of the length of the conduit of the apparatus.

[0062] Further, in some embodiments, the microchannels of an apparatus described herein are disposed within a matrix material disposed in the conduit. Any matrix material not inconsistent with the objectives of the present invention may be used. In some cases, for instance, a matrix material comprises a hydrogel, such as, for example, a biodegradable hydrogel. A “biodegradable” material, for reference purposes herein, comprises a material that can decompose within a biological environment, and may provide a non-toxic decomposition product. In some cases, a biodegradable material described herein comprises one or more ester bonds. In some instances, a matrix material of an apparatus described herein comprises an agarose gel. Any agarose gel not inconsistent with the objectives of the present invention may be used. In some cases, for example, the matrix material comprises an agarose gel comprising between about 0.5 and about 5 weight percent agarose, between about 1 and about 4 weight percent agarose, or between about 1.5 and about 2.5 weight percent agarose, based on the total weight of the agarose gel. Additional non-limiting examples of matrix materials suitable for use in some embodiments of apparatuses described herein include polylactic-co-glycolic acid (PLGA), polylactic acid (PLA), polycaprolactone, polyurethane, polyester, polycarbonate, collagen, polytetrafluoroethylene (PTFE), polymethylmethacrylate (PMMA), an ethylene-vinylacetate copolymer (EVA), a polydimethylsiloxane (PDMS), polyether-polyurethane, a polyethyleneterephthalate (PET), a polysulfone (PS), a polyethyleneoxide (PEO) or polyethylene glycol (PEG), a polyethylene oxide-polypropylene oxide copolymer (PEO-PPO), a polyolefin such as polyethylene (PE) or polypropylene (PP), or a combination of one or more of the foregoing. Other matrix materials can also be used alone or in combination.

[0063] Moreover, any fiber not inconsistent with the objectives of the present invention can be coiled around the exterior of a microchannel described herein. A “fiber,” for reference purposes herein, comprises any elongated structure such as, for

example, a strand or filament. A fiber described herein can have any diameter not inconsistent with the objectives of the present invention. In some embodiments, for instance, a fiber described herein has a diameter (prior to being coiled or wrapped in manner described herein) between about 100 nm and about 100 μm , between about 500 nm and about 50 μm , between about 1 μm and about 50 μm , or between about 10 μm and about 50 μm . Additionally, in some embodiments, a coiled fiber comprises coils, loops, or turns having an outer diameter between about 10 μm and about 1000 μm , between about 50 μm and about 500 μm , or between about 100 μm and about 500 μm .

[0064] Referring to the preferred orientation of the fiber relative to the microchannel, it is understood that the fiber, in its preferred coiled state, preferably occupies the region defined by the outer circumference, or is otherwise oriented adjacent to the outer circumference, of the microchannel. In this way, as used herein, the term “exterior of the microchannel” refers to any orientation whereby the coiled fiber is positioned in concert with, or encircles the microchannel.

[0065] Further, in some variations, a fiber of an apparatus described herein comprises or is formed from a polymer such as a biodegradable polymer. In some cases, a fiber comprises or is formed from a poly(glycolide), poly(lactide), poly(glycolide-co-lactide), poly(p-dioxanone), alginate, polylactic-co-glycolic acid, a polylactic acid, a caprolactone, or a combination thereof. In addition, as described further hereinbelow, a fiber of an apparatus described herein can be coiled around the exterior of a microchannel of the apparatus in any manner not inconsistent with the objectives of the present invention. In some cases, for instance, the fiber is coiled around the exterior of the microchannel in an isotropic configuration. An “isotropic” configuration, for reference purposes herein, comprises a configuration having a uniform or substantially uniform pitch. The “pitch” of a fiber, for reference purposes herein, comprises the number of loops or coils of the fiber per length of the microchannel around which the fiber is coiled. A “uniform” pitch, for reference purposes herein, comprises a pitch that does not vary along the length of the microchannel. A “substantially” uniform pitch, for reference purposes herein, comprises a pitch that varies by less than about 10 percent, less than about 5 percent, or less than about 1 percent along the length of the microchannel. Alternatively, it is also possible for a fiber described herein to be coiled around the

exterior of the microchannel in an anisotropic configuration. An “anisotropic” configuration, for reference purposes herein, comprises a non-isotropic configuration, such as a non-isotropic configuration described further hereinbelow. Moreover, in some variations, a fiber described herein does not block or obstruct the microchannel of an apparatus described herein.

[0066] The active agent of a fiber described herein can comprise one or more active agents not inconsistent with the objectives of the present invention. An “active agent” for reference purposes herein, comprises a chemical species that can provide a chemical gradient in a manner described herein. For example, in some cases, an active agent comprises a drug, a peptide, a protein, a growth inhibiting factor, or a growth promoting factor such as a nerve growth factor (NGF). Thus, in some embodiments, the chemical gradient provided by an apparatus described herein comprises a drug concentration gradient or a growth factor concentration gradient. Any drug not inconsistent with the objectives of the present invention may be used. An active agent can also comprise other desired molecular signals or markers. Further, in some embodiments, the active agent is biologically active and/or non-denatured.

[0067] In addition, as described further hereinbelow, some embodiments of apparatuses described herein comprise a plurality of microchannels disposed in the conduit. The microchannels can have the same or differing sizes, shapes, and/or structures. Further, in some cases comprising a plurality of microchannels, a plurality of fibers can be coiled around the exteriors of one or more of the plurality of microchannels. In some instances, the plurality of fibers are each coiled around the exterior of a different microchannel and at least two of the coiled fibers comprise the same or differing active agents, the same or differing amounts of an active agent, and/or the same or differing pitches and/or dimensions.

[0068] In another aspect, compositions are described herein which, in some embodiments, can provide one or more advantages compared to some other compositions. For example, in some embodiments, a composition described herein provides one or more advantages also provided by an apparatus described herein. Moreover, a composition described herein, in some cases, can be used in addition to or instead of an apparatus described herein to form a chemical gradient.

[0069] A composition described herein, in some embodiments, comprises a coiled polymeric material comprising an active agent operable to diffuse out of the polymeric material when the polymeric material is disposed in a biological compartment. The coiled polymeric material, in some cases, can have the same structure as the fiber of an apparatus described herein. For example, in some cases, the coiled polymeric material of a composition described herein is biodegradable. In some embodiments, the polymeric material comprises a polylactic-co-glycolic acid, a polylactic acid, a caprolactone, or a combination thereof. Further, in some cases, the active agent comprises a drug or growth factor. Additionally, the biological compartment of a composition described herein can comprise any biological compartment not inconsistent with the objectives of the present invention. In some cases, for instance, the biological compartment comprises a portion of a living organism. Further, in some embodiments, the biological compartment comprises a nerve conduit. Other biological compartments may also be used, as described further herein.

[0070] In other variations, a composition described herein does not necessarily include a coiled component such as a coiled fiber or polymeric material described herein. In some cases, for instance, a composition described herein comprises a first gradient material or matrix comprising an active agent at a first concentration and a second gradient material or matrix comprising the active agent at a second concentration, wherein the first matrix and the second matrix are arranged in space to provide a concentration gradient of the active agent. The active agent can comprise any active agent described herein, such as a drug or growth factor. Moreover, in some variations, a composition described herein further comprises a third gradient material or matrix comprising the active agent at a third concentration, and the first matrix, second matrix, and third matrix are arranged in space, or oriented, to provide a gradient region comprising a concentration gradient of the active agent. The gradient region, in some cases, can comprise a linear concentration gradient. In addition, in some embodiments, the first, second, and third matrices of a composition described herein are arranged to provide a plurality of concentration gradients, including a plurality of linear concentration gradients. Moreover, in some cases, the first, second, and third matrices can be arranged to provide a non-gradient region in addition to a gradient region described herein. A

gradient material or matrix of a composition described herein can comprise or be formed from any material not inconsistent with the objectives of the present invention. In some cases, for instance, a matrix is a gel that comprises or is formed from a polymeric material, including a biodegradable polymeric material. In some embodiments, a gel comprises a hydrogel. In some instances, a gel comprises or is formed from an agarose gel, a polylactic-co-glycolic acid, a polylactic acid, a caprolactone, or a combination thereof. Other gel or non-gel materials may also be used as matrices to establish the desired gradient(s).

[0071] Further, as described herein, a composition can be disposed in a conduit to provide an apparatus. Thus, in another aspect, apparatuses are described herein, wherein the apparatus comprises a conduit with a composition described herein disposed in the conduit.

[0072] In yet another aspect, methods of forming a chemical gradient are described herein, which, in some variations, may provide one or more advantages compared to some other methods. For example, in some cases, a method described herein can provide a chemical gradient in a modular and/or tunable manner. Additionally, in some instances, a method described herein can provide a chemical gradient exhibiting a sustained, non-transient chemical gradient in vivo. A method of forming a chemical gradient described herein, in some variations, comprises disposing an apparatus and/or a composition described herein in a biological compartment. In some cases, the chemical gradient comprises an active agent concentration gradient, such as a drug gradient or a growth factor gradient. Additionally, in some instances, the biological compartment comprises a nerve conduit. Further, any apparatus and/or composition described herein may be used in a method described herein.

[0073] Some embodiments described herein are further illustrated in the following non-limiting examples.

EXAMPLE 1

Apparatus Comprising a Single Microchannel

[0074] In one variation, an implantable device is fabricated that provides a chemical gradient and enables localized delivery of a specific growth factor within a microchannel

through which axons will grow. For comparative purposes regarding this variation, **FIG. 1A** illustrates a lumen or microchannel 11 within a conduit 10. The microchannel 11 comprises an active agent (not shown) to provide at least a transient region of a desired chemical potential. However, active agent concentration over the microchannel length is difficult to control using the structure of **FIG. 1A**. As an additional comparative example for this variation, **FIG. 1B** shows a microchannel 12 within a conduit 11 comprising embedded microparticles 13. The microparticles 13 are impregnated with an active agent (not shown) such as drug or growth factor and can be biodegradable. The microparticles 13 can degrade or otherwise release the active agent predictably over time in a preselected or controlled, programmable fashion. Therefore, the structure of **FIG. 1B** can provide a concentration of active agent within the microchannel 12 over a period of time. However, this model lacks a concentration gradient. In contrast, **FIG. 1C** shows an embodiment of an apparatus according to the present disclosure. Coiled fiber 16 is impregnated with an active agent and surrounds a microchannel 14. The microchannel 14 is embedded within a hydrogel conduit 10. The positioning of the coils of fibers 16 along the length of microchannel 14 creates a controllable gradient of active agent that is released into the microchannel 14. The concentration, and thus a controllable gradient, can be predictably adjusted by changing the number of helical turns, pitch, or lateral distance between the turns, the dimensions or thickness of the fiber, and/or the length of the channel. Thus, the apparatus of **FIG. 1C** permits long-term active agent delivery by producing a sustained chemical gradient in the microchannel. The chemical gradient is provided through the release of active agents from the coiled fiber and into the microchannel by diffusion over time. The time profile of the release of active agents from the coiled fiber can be controlled based on one or more of: the concentration of the active agent within the fiber, the size and/or chemical composition of the active agent, the chemical composition and/or microstructure of the fiber material, and the chemical composition and/or microstructure any matrix material disposed in the conduit. Further, the number of turns of the fiber around the microchannel, in some embodiments, can be programmed to provide a desired steepness of a chemical gradient. The term “programmed,” for reference purposes herein, is understood to mean any preselected and predetermined orientation of the coils of a fiber that can be controlled and is controllable

to provide a desired result. The “steepness” of a chemical gradient, for reference purposes herein, comprises the slope of a plot of the concentration of a given active agent or other chemical species against the length of the microchannel in a given direction.

EXAMPLE 2

Apparatus Comprising a Plurality of Microchannels

[0075] Apparatuses described herein, in some embodiments, comprise a plurality of microchannels. Such apparatuses can be used to stimulate the growth of axons across a gap. When axons must grow across a gap, there is often a need to separate specific modalities or types of axons into distinct compartments or spatial regions. Such a separation can be useful for the repair of sensory and motor branches and/or for the development of closed-loop peripheral neural interfaces. Moreover, such a separation can be achieved by disposing a plurality of fibers described herein around a plurality of microchannels of a device described herein, wherein the fibers differ in the amount and/or type of growth factor delivered to the different microchannels and/or differ in the steepness of the chemical gradient provided within the different microchannels. In this manner, a specific type of axon from a mixed population of nerves can be enticed into a specific microchannel and thereby eventually guided to the proper target for the specific axon type. Further, this process can be carried out for a plurality of differing axon types in the mixed population.

[0076] **FIG. 2** shows a schematic diagram of the application of several coiled fibers, preferably with differing gradients, in a multi-luminal conduit to guide axons and other cell types with different modality. This allows the guidance of different cell types to the conduit while providing each cell type’s optimal concentration gradient. Modality-specific axonal guidance is one contemplated application of the establishment of the gradient. More specifically, **FIG. 2** is a schematic diagram showing several axons 20 from a mixed nerve population guided into a multiluminal conduit 22 having coiled fibers 24a, 25a, 26a, 27a located in respective microchannels 24b, 25b, 26b, 27b, with each microchannel optionally able to have a different modality. In this variation, each lumen or microchannel is surrounded by a helically wound fiber that contains specific molecular cues (such as neurotrophin or pleiotrophin) known to entice growth of a specific type of

neuron (nerve cells). Release of the molecular cues creates a gradient in the microchannels inside the coiled fibers. The gradient can be controlled by the fiber architecture as described further hereinabove (e.g., by selecting the total number of helical turns, the lateral distance between adjacent turns, and/or the pitch of the turns).

[0077] To confirm the synergistic effects of multiple growth factors, the growth of the sensory neurons sprouted from single neurotrophic or pleiotrophic factors was tested.

This testing determined a base-line of the growth induced by these chemical stimuli.

FIG. 3 is a schematic diagram showing the application of multiple coiled fibers providing differing gradients in a multi-channel conduit to guide axons and other type of cells. As illustrated in **FIG. 3**, conduit 30 includes a first microchannel 32 having two coiled fibers 33, 34 oriented about the length of the microchannel wall. Similarly, a second microchannel 36 has two coiled fibers 37, 38 oriented about the length of the second microchannel wall. This structure permits the guidance of different cell types to different microchannels, where each microchannel can have a desired, preselected, and optimal concentration gradient of a particular active agent corresponding to a desired effect on the different cell types. For example, the differing chemical gradients of the differing microchannels can each be selected to promote growth of differing types of axons. It is to be understood that any number of active agents and any number of fibers may be disposed about a microchannel in any manner to achieve a desired chemical gradient.

EXAMPLE 3

Method of Forming a Chemical Gradient

[0078] An apparatus having the general structure of the apparatus of **FIG. 1C** in Example 1 was used to form a chemical gradient according to one embodiment described herein as follows. First, a poly(DL-lactic-co-glycolic acid) (PLGA) coiled fiber was fabricated. The biodegradable PLGA (85:15) co-polymer (0.84 intrinsic viscosity (i.v.), 135,000 weight average molecular weight (MW)) was fashioned into fibers using a wet-spinning process. Briefly, a solution 20 wt.% PLGA was completely dissolved in dichloromethane (Sigma-Aldrich, St. Louis, MO). This solution was loaded into a glass syringe (gas-tight, Hamilton, Reno, NY) and injected into a 1.5-cm diameter tube filled

with isopropanol to form the fiber. Pre-washed mylar substrates was used as collecting spools. With many spinning parameters possible, the spinning solution injection rate and the fiber collection speed were controlled at 1.8 mL/h and 8.5 m/min, respectively, to achieve 30 μm diameter fibers. In addition, if necessary, polyethylene glycol (PEG) was added to the spinning formulation to preserve the bioactivity of the active agent (such as a growth factor). To form coiled fibers, the fibers were wound around a glass rod (sometimes also called a formation fiber) and dried overnight to allow any remaining dichloromethane to evaporate. Following formation, the fibers were coiled around titanium fibers (diameter = 250 μm) and stored at 4°C prior to use.

[0079] To form fibers comprising an active agent (or a control species), the coiled fibers were disposed in a solution of the active agent overnight. For example, the following solutions were used to form PLGA fibers comprising an active agent (or a control species): (1) nerve growth agent NGF (5 $\mu\text{g}/\text{mL}$, Invitrogen, Carlsbad, CA); (2) control species bovine serum albumin (BSA, 20 mg/mL , Sigma-Aldrich, St. Louis, MO); and (3) fluorescent species cyanine dye-3 (Cy3, 5 $\mu\text{g}/\text{mL}$, Jackson ImmunoResearch Lab, West Grove, PA).

[0080] The Cy3-loaded PLGA coiled fibers were imaged using light microscopy and fluorescent microscopy to demonstrate that the coils provided a chemical gradient and tended to maintain their structures even after removing the fabrication metal. **FIGS. 4A-F** show magnified (microscope) images of the same fiber in the low and high concentrated areas, confirming the significant difference in the number of turns and the fluorescent light emanating from fibers loaded with fluorescent dye (Cy3). **FIG. 4A** shows an image of the wound coil 40 around a fabrication fiber (not shown). **FIG 4B** shows the coiled PLGA fiber 42 that can be placed in a nerve conduit. **FIGS. 4C-F** are higher magnification images of the areas in boxes 44, 46 shown in **FIG. 4B**. The Cy3-PLGA coiled fiber 47 in **FIG. 4D** are imaged from the high density region, where “high density” refers to a relatively high pitch (Box 44). The Cy3-PLGA coiled fibers 48 are imaged from the low density region (Box 46).

[0081] Fabrication of the fibers requires harsh chemical procedures such as application of organic solvents (dichloromethane). To confirm that growth factors (proteins) were preserved throughout the process of the fabrication of the coils, NGF-

loaded coiled fibers were provided in the presence of pheochromocytoma (PC-12) cells. PC-12 cells are a cell line that proliferate and differentiate in the presence of the nerve growth factor (NGF). Cells/ECM suspension were loaded into the cell well of the casting device area using a transparent multiluminal matrix (TMM) device described immediately below further hereinbelow, and were pushed into the lumen by creating a negative pressure. Cells seeded inside the lumen were fixed in 24 hours with 4% paraformaldehyde (PFA) and stained with Oregon Green Phalloidin and TO-PRO 3 Iodide (Invitrogen, Carlsbad, CA) to visualize the as cytoskeletal and nuclear labels, respectively. The PC-12 cells' processes lengths were measured in zero, low, and high concentration areas. To facilitate the penetration of staining dyes, the gels were placed in a cell culture plate while the solution was stirred over night at 40C using a magnetic plate and stir bar.

[0082] Pheochromocytoma cells (PC-12 cells) were loaded in a novel rectangular frame (12.5 mm x 36 mm) used for casting agarose gels. The casting device was made of dental cement and used to guide multiple titanium fibers (0.25 mm x 17 mm; SmallParts, Logansport, IN). Titanium fibers wound with growth factor-containing polymer coils were positioned through perforations at both ends of the device. Under sterile conditions, the casting device was placed over a glass slide in a cell culture dish and a 1.5% ultrapure agarose (Sigma-Aldrich, St. Louis, MO) solution was applied to cover the fibers and allowed to polymerize. PC12 cells (1×10^6 ml) were suspended in growth factor-reduced Matrigel (3.5 mg/mL, BD Biosciences, San Jose, CA). The negative pressure generated during removal of the titanium fibers from the solidified gel, drew the PC12 cells/ECM mix into the lumen of the casted hydrogel microchannels. The growth factor coiled fibers were intact in the lumen and in approximate contact of PC12 cells. The cell cultures were fed with RPMI-1640 medium (Sigma, St. Louis, MO) and kept in the incubator at 37°C and 5% CO₂ for 72 hours.

[0083] For visualization of differentiated PC12 cells in the microchannels, the gels were fixed in 4% paraformaldehyde (PFA) and processed for immunofluorescence. After rinsing the gels with a blocking solution (0.1% Triton-PBS/ 1% normal serum), the samples were incubated with Oregon Green Phalloidin and TO-PRO 3 Iodide (Invitrogen, Carlsbad, CA) as cytoskeletal and nuclear labels, respectively. The

staining was evaluated using a Zeiss confocal microscope (Zeiss Axioplan 2 LSM 510 META). The staining was evaluated and analyzed using regular and fluorescent microscopy and z-stack 3D image reconstruction of the microvascular network in the multi-luminal hydrogels. Quantification of the length of PC-12 cells processes in 3 different coil densities (none, low and high) was achieved using the Axiovision LE software (CarlZeiss, AxioCam, version 4.7.2) and Zeiss LSM Image Browser (version 4.2.0.12).

[0084] All data values were expressed as mean \pm standard error of the mean. The data was analyzed by parametric student-t test or by non-parametric student-t test followed by Mann Whitney post hoc evaluation using the Prism 4 software (GraphPad Software Inc.). Values with $p \leq 0.05$ were considered to be statistically significant.

[0085] **FIGS. 5A-D** demonstrate the bioactivity of the PC-12 cells in NGF-loaded microchannels. **FIG. 5A** is a schematic diagram of the design of the experiment. An NGF-loaded coil fiber 52 was placed in a nerve conduit 50. PC-12 cells were then loaded inside the channel. **FIG. 5B** is a microscope image showing PC-12 cells located distally from the coil (the area in the microchannel corresponding to “Box B” in **FIG. 5A**). These cells did not show any processes 24 hours after being seeded. **FIG. 5C** is a microscope image showing PC-12 cells located in the middle of the coil (the area in the microchannel corresponding to “Box C” in **FIG. 5A**). These cells were differentiated and exhibited some processes in 24 hours. **FIG. 5D** is a microscope image showing PC-12 cells located in the high density area of the channels with the highest number of coil turns (the area in the microchannel corresponding to “Box D” in **FIG. 5A**). After 24 hours cells in this region were differentiated and exhibited long processes. Images of the cells inside the lumen looked spherical and showed no processes in the area where there was no NGF loaded coil. However, cells seeded in the areas with NGF loaded coiled fibers were completely differentiated and had long processes. Interestingly, these processes were longer in the area with higher density of coil. This confirmed that areas with higher numbers of turns will release more NGF and therefore have higher concentration of the growth factor. To quantify the visualized images, the length of all the processes equal to or longer than the cell body was measured. The quantitative analysis of the data showed a significant difference between the lengths of the cell

processes (see **FIG. 6**) in the three “boxed” areas B-D depicted in **FIGs. 5B-D**. P value equal to or less than 0.05 was considered significant. The average length of the processes was significantly higher in proximal ($p < 0.002$; $n = 6$; $71.33 \pm 12.17 \mu\text{m}$) area and middle ($35.66 \pm 12.69 \mu\text{m}$) compared to distal ($1.4 \pm 1.14 \mu\text{m}$).

[0086] **FIG. 6** charts the bioactivity of the PC12 cells in NGF loaded coiled fiber in the microchannel. NGF loaded coil fiber was placed in a nerve conduit. The bioactivity of the PC-12 cells was determined by measuring cells processes in the area without any NGF (“Box B” in **FIG. 5A**), the area with low density of coil turns (“Box C” in **FIG. 5A**) and the area with high density of coil turns (“Box D” in **FIG. 5A**). Cells were imaged 24 hours after seeding and processes length was measured using ImageJ. As shown in **FIG. 6**, PC12 cells loaded distally from the coil (Box B in **FIG. 5A**) did not show any processes 72 hours after being seeded. PC12 cells located in the middle of the coil (Box C in **FIG. 5A**) differentiated and had some processes in 24 hours. After 72 hours, PC12 cells located in the high density area of the channels with the most number of NGF loaded coil turns (Box D in image shown in **FIG. 5A**) were differentiated and had long processes. PC12 cells located in the middle of the coil (Box C in image **FIG. 5A**) differentiated and had some processes in 24 hours. There was a significant difference in the length of the cell processes in the different areas (*) $p < 0.05$ and (**) $p < 0.005$.

EXAMPLE 4

Method of Forming a Chemical Gradient

[0087] Growth factor release from poly-lactic-co-glycolic acid (PLGA) coils was modeled in two configurations (isotropic and anisotropic) of a multi-medium model solved using finite element analysis. The model was implemented in COMSOL Multi physics using a 2.4 GHz Intel® Core™2 Quad processor computer and consisted in rings with a diameter of 250 micrometers and thickness of 1 micrometer distributed inside a cylinder with a diameter of 250 micrometers and a length of 1 centimeter. The first configuration (isotropic) consisted of a uniform distribution of 20 rings. The second configuration (anisotropic) consisted of the arrangement of 3 sections with arrangement of rings at different distances from one another. The sections consisted of sections with 250, 500, and 1000 micrometers. The release profile from the

loaded PLGA coils was modeled using a modified version of Korsmeyer-Peppas equation for the release from a degradable polymer. The initial condition of the coil was taken as a uniform load of 1 microgram. The simulations were run for a period of 28 days.

[0088] In the mathematical model the filling conduit was considered to have the diffusion coefficient of the agarose gel. The diameter of the channels was considered to be 250 μm . The results of the mathematical analysis showed that the isotropic coiled fiber created a homogenous concentration in the channels which was maintained for 28 days. Both ends of the conduit were considered to be open. Therefore, in the proximal and distal end, a decrease in the concentration of the growth factor was observed due to the diffusion flux out of the lumen. However, the change in the concentration of the proximal and distal ends compared to the middle was minimal (less than 15% of the concentration in the middle) and the conduit structure tends to preserve the homogenous concentration. The anisotropic configurations of the coiled fiber created a gradient as early as 5 days and tend to maintain the gradient for long time (at least 28 days). The out flux of the growth factor from the distal and proximal ends did not affect the establishment of the gradient. The steepness of the gradient was maintained substantially the same throughout the study (from day 5 to day 28). The mathematical speculation of the isotropic design of the coiled fiber was noted. The homogeneous distribution of the gradient in the isotropic design will remain for at least 28 days in the microchannels. Images of the predicted concentration distribution in the microchannels using Comsol confirmed the establishment of a sustained gradient at least for 28 days in the anisotropic configuration.

EXAMPLE 5

Method of Forming a Chemical Gradient

Intraluminal NGF-collagen gradient protocol

[0089] A method is described herein that achieves sustained growth factor release through the production of molecular gradients in collagen-filled multiluminal nerve guides, as shown in **FIGs. 7A-G** and **FIGs. 8A-B**. To achieve this, NGF-releasing fibers coiled onto titanium rods were inserted into openings made in a transparent multi-luminal

matrix (TMM) casting device. The TMM consists of a square plastic open frame with holes at opposite ends through which the titanium rods are inserted. 1.5% agarose was subsequently added over the metal rods, effectively embedding the NGF-releasing polymeric coils in agarose.

[0090] Nerve guides (NG) incorporate NTF gradients in the tube wall (**FIG. 7A**) or use NTF-eluting microparticles (**FIG. 7C**). However, current multiluminal NG designs lack NTF release by a gradient. This study uses coiled polymeric fibers anchored to the walls of hydrogel microchannels with luminal collagen to address this limitation (**FIG. 7D**). **FIG. 7E** is a photograph of Cy3 IgG-loaded PLGA fibers coiled onto a metal rod. Fluorescence imaging and densitometry illustrate the resulting gradient. **FIG 7F** is a schematic of the Transparent Multiluminal Matrix (TMM) casting device showing fiber coil deployment. Removal of the metal rod from the TMM after agarose polymerization anchors the coils onto the walls of the microchannels while simultaneously filling the lumen with collagen (**FIG. 7Fi-iii**). In **FIG. 7G**, confocal images show the deployed polymeric coils (red) with the collagen filler (green) in the TMM. Scale bar = 100 um.

[0091] More specifically, as shown in **FIG. 7A**, collagen conduit 70a comprises NGF provided in a gradient. **FIG. 7B** shows a conduit 70b comprising multiluminals or microchannels 72b comprising NGF. **FIG. 7C** shows a conduit 70c comprising multiluminals or microchannels 72c comprising NGF microparticles 74. In this variation, the microchannels 72c each comprise a substantially uniform concentration of NGF. **FIG. 7D** shows a conduit 70d comprising multiluminals or microchannels 72d comprising NGF-loaded coil fiber 76 establishing a gradient.

[0092] According to a TMM method, collagen 77 was then added into the “loading” well of the TMM (**FIG. 7Fi**). Upon removal of the fiber forming metal (titanium) rod 78, the NGF-releasing fiber coil is retained at the walls of the resulting microchannels casted in agarose 79, and the negative pressure created by their removal substantially simultaneously fills the luminal space of such microchannels with collagen 77 (See **FIGs. 9Fii-iii**). This method is designed for the continued release of molecules such as Cy3-IgG, BSA or NGF encapsulated in the polymeric fibers into collagen-filled microchannels over time, providing both permissive and chemotactic nerve growth regulation. **FIG. 7G** is a microphotograph showing the coil 76 with the metal rod

removed. **FIGs. 7H** and **7I** are microphotographs of the coiled fiber 76 with collagen 77 introduced within the circumference of, and to “fill” the coiled fiber 76.

Growth factor releasing from coiled polymeric fibers

[0093] Two fiber sources were used to fabricate 30 μm coiled fibers: poly-lactic-co-glycolic acid (PLGA 85:15; 135KD) and ELUTE™ Biodegradable Polydioxanone. PLGA fibers were fabricated by wet-spinning. Briefly, a 20% PLGA solution was prepared in dichloromethane (DCM; Sigma-Aldrich, St. Louis, MO), dispensed onto a circulating isopropanol coagulation bath using a syringe pump (1.8 mL/hr), collecting the resulting fiber onto a rotating spool (8.5 m/min). Dried PLGA coil fibers were incubated with NGF (10 μg /mL; Invitrogen, Carlsbad, CA), BSA (20 mg/mL; Sigma-Aldrich, St. Louis, MO) or cyanine dye-3 (Cy3; 5 μg /mL; Jackson ImmunoResearch Lab, Inc., West Grove, PA) overnight. Most studies used ELUTE™ Biodegradable Polydioxanone fibers, custom fabricated by TissueGen Inc, Dallas, TX to encapsulate NGF and coil it 80 times over titanium metal rods (0.25 mm x 17 mm; SmallParts, Logansport, IN) either equally (uniform) or differentially spaced at 15, 25, and 40 turns over 3.33 mm longitudinal area (10-100 ng/mL gradient). Fibers were dried at RT and stored at -20°C until used.

[0094] Conductive polymer polypyrrole was loaded with red dye. As shown in **FIG. 8A**, upon electrical simulation, the dye was released over 120 minutes of time from the fiber and established a gradient. **FIG. 8B** shows the quantification of SI and SII areas, confirming the gradient formation.

PC12 cell culture

[0095] Metal rods with coiled PLGA fibers containing either BSA or NGF were deployed in the TMM casting device as described above. Under sterile conditions, the casting device was placed over a glass slide in a cell culture dish and 1.5% ultrapure agarose was used to cover the fibers. After polymerization, Pheochromocytoma cells (PC12; 1×10^6 / mL) suspended in atelomeric chicken collagen (85 % type I, 15 % type II; Millipore) were loaded onto the casted 250 μm OD hydrogel microchannels by the negative pressure generated. The TMM cell cultures were cultured for 72 hrs in RPMI-

1640 medium (Hyclone SH30027.02) supplemented with 10% HS, 5% FBS, and 1% pen/strep and maintained at 37°C and 5% CO₂. At the end of the study, the cell cultures were extensively rinsed with PBS and stained. Separate regular cultures of PC12 cells were cultured in normal dishes at a 1×10^6 plating density and exposed to a 10-100 ng/mL NGF range to determine their biological response (see **FIGs. 9A-C**). Using the PC12 as biosensors, the neurite response to different NGF concentrations was measured. Linear regression was used to define an equation to calculate the luminal concentration of NGF in the TMM microchannels based on the PC12 neurite length. The PC12 cells were shown to respond to variable levels of NGF. As shown in **FIG. 9A-C**, the neurite lengths of differentiated cells increase as the level of NGF concentration increases (as indicated in confocal images). **FIG. 9A** shows a NGF concentration of 10 ng/mL. **FIG 9B** shows a NGF concentration of 20ng/mL. **FIG. 9C** shows a NGF concentration of 50 ng/mL (scale bar = 100µm).

Growth factor diffusion modeling

[0096] Growth factor release from PLGA coils was modeled in both uniform and gradient configurations considering the multi-medium environment (i.e., agarose microchannels with luminal collagen) using finite element analysis. Protein release kinetics were estimated by using fitting release data provided by the manufacturer into a power law equation. The power law equation with geometry ($K = 0.37$), time ($t = 0-28$ d), and release mechanism ($n = 0.25$; $(M_t = M_\infty K^n)$ where M is the amount of drug released and M_∞ is the total amount of drug). Release kinetics from PLGA coils were estimated using the bulk-eroding model considering an initial burst followed by diffusion via interconnected pores. The Carman-Kozeny model was used to estimate molecular diffusion (D) in water, 1.5% agarose, and 0.3% collagen considering molecular concentration (Φ) changes over time (δt) in a fixed volume (Ω). Diffusion flux vectors ($J=D\nabla\Phi$) integrated perpendicular to the surface (S) by the following formula: $\delta\Phi/\delta t \int \nabla\Phi = \sum J \cdot n \nabla S$ released from the polymeric fibers. The model was implemented in Multiphysics Modeling and Engineering Simulation Software (COMSOL 4.0) considering the external tube (T) as a solid cylinder with a 3 mm OD, 1.5 mm ID and 10 mm length, and agarose microchannels. The meshing module used included tetrahedral,

triangular, and hexahedral mesh volume elements for the boundaries with maximum element size of 180-1000 μm , element size, 1.5 growth rates and a curvature resolution of 0.6. The model was validated using published exact solutions, and incorporated release kinetic data obtained in vitro.

DRG explant growth in TMM microchannels

[0097] Neonate (P0-4) DRG cells were isolated from normal mice and placed at one end of the TMM microchannels containing either uniform or gradient NGF-coils. The DRG cultures were cultured in Neurobasal A media (Sigma, St. Louis, MO) and maintained at 37°C and 5% CO₂ for 7 days prior to fixing them in 4% PFA by immersion. Afterwards, the cultures were rinsed and stained.

Immunostaining

TMM gels were extensively rinsed in PBS. The PC12 cells were then reacted with Oregon Green Phalloidin to label cytoskeletal. For immunolabeling of DRG axonal growth, the tissue was incubated in 4% Donkey serum for 1 hour, followed by incubation with a mouse anti- β tubulin III antibody (1:400; Sigma Aldrich) overnight at 4°C. The tissue was then incubated with Cy2-conjugated donkey anti mouse IgG (1:400; Sigma Aldrich) and rinsed. Long-working distance water immersion objectives on a Zeissconfocal microscope (Zeiss Axioplan 2 LSM 510 META) were used to evaluate the cellular staining and axonal growth directly within the hydrogel microchannels.

Image analysis and quantification

[0098] Neurite length in differentiated PC12 cells was evaluated inside the microchannels at low concentration (SI) and high concentration (SII) areas (**FIGs. 10A-K**) corresponding to different numbers of NGF coils. Neurite length was measured from the cell body to the distal end of the neurites. Only cells with neurites longer than the cell diameter are considered for quantification, using Axiovision LE software (CarlZeiss, AxioCam, version 4.7.2), Zeiss LSM Image Browser (version 4.2.0.1). The axonal length of the DRG was quantified at 20X magnification from a z-stack (20 images each at 308 μm slice thickness). Axonal length was measured from the edge of the DRG to the

growth cone terminal using Axiovision LE software (CarlZeiss, AxioCam, version 4.7.2) and Zeiss LSM Image Browser (version 4.2.0.1) for segments with no coils and medium (1-8) or high (9-15) number of coils in that segment. The turning angles of the axons were measured using Image J. Quantification of the turning angle was calculated as a ratio of all the axons present to the number of axons that turned. All experiments were done in duplicate 3-6 times each.

Statistical analysis

[0099] All data values were expressed as mean \pm standard error of the mean. The PC12 data was analyzed by a parametric student t-test followed by Mann Whitney post hoc evaluation. The data obtained from the DRG experiments were evaluated by ANOVA followed by Newman-Keuls Multiple Comparison using the Prism 4 software (GraphPad Software Inc.). Values with $p \leq 0.05$ were considered to be statistically significant.

Results

PC12 Differentiation in a 3D NGF Microgradient

To determine if the polymeric coils can be used to establish biologically active gradients of neural growth factors, the ability of PC12 cells to differentiate in the lumen of the TMM microchannels onto which BSA or NGF-eluting coils were anchored to the hydrogel walls was tested. Three days after seeding, only rounded undifferentiated cells were observed in the BSA controls (see **FIGs. 10A-C**). In contrast, those cultured with NGF-coils showed several degrees of neural differentiation as indicated by neurites elongating from the PC12 cell bodies. Neurite extension was observed to be proportional to the number of coils placed in the channels. Those with low number of coils (segment I; SI) showed a mixed population of round undifferentiated cells and some with neurites (**FIGs. 10D-F**), but those in areas of higher number of coils (segment II; SII) were mostly differentiated cells, with apparently longer neuron-like extensions (**FIGs. 10G-I**). To confirm this observation, the neurite length in differentiated PC12 cells in both areas was estimated, which revealed a significantly larger number of differentiated PC12 cells in the SII region ($87 \pm 14.6 \mu\text{m}$) compared to that in the SI area ($55.76 \pm 12.53 \mu\text{m}$; $p < 0.005$).

Both of these were, in turn, significantly different from that observed in BSA-releasing coils ($9.31 \pm 1.94 \mu\text{m}$; $p < 0.0001$.) See **FIGs. 10J** and **10K**.

[00100] DIC and fluorescent images of PC12 cells cultured in collagen-filled agarose microchannels in which a BSA (**FIGs. 10A-C**; control) or NGF (**FIGs. 10D-I**) releasing fibers were coiled over the wall. The PC12 remain undifferentiated in the CTR group (arrowheads), but extend in those releasing NGF (arrows) and were more abundant in areas under higher number of coils (SII) when compared to areas with lower number of coils (SI). **FIG. 10J** shows the quantification of neurite length of differentiated PC12. **FIG. 10K** shows the calibration curve of neurite length of PC12 cells exposed to variable levels of NGF. The superimposed linear regression shows NGF concentration values corresponding to low (SI) and high (SII) number of fiber coils in the microchannels. * = $p < 0.0001$ compared to CTR; + = $p < 0.005$ compared to SI ($n=6$).

[00101] These observations indicated that the polymeric coils were able to release biologically active NGF into the luminal collagen matrix, forming a gradient at which low (SI) and high (SII) concentrations areas can be established. This notion was supported by quantification of protein release from the SI and SII regions of coils eluting ELISA BSA-releasing coils placed in the TMM agarose microchannels over 24 hrs, confirming a differential concentration of 50% less in the SI area compared to that in SII (See **FIG. 11**). The concentration of biologically active NGF in the SI and SII microchannel areas in situ was then directly evaluated by using PC12 as biosensors, as it is known that their differentiation is linearly proportional to the NGF concentration. The neurite length of PC12 exposed to a NGF 10-100 ng/mL concentration range was determined. It was further determined that these cells extended from 5 to 120 μm in length, linearly correlating to the NGF concentration ($R=0.96$; see **FIG. 10K**). A linear regression equation estimated from the PC12 growth calibration curve was then used to determine the intraluminal NGF ($\text{NGF} = [(\text{PC12 neurite length} + 1.91) / (17.06)]$). Using this formula it was determined that the growth observed at low (SI) and moderate (SII) coiling regions of the TMM microchannels corresponded to 40 and 83 ng/mL of NGF; respectively, which is in close agreement with the observed differences with protein release. Quantification of BSA release from the TMM microchannels shows 40% of

encapsulated BSA was released from segment II, compared to 20% release in SI after 24 hours.

Modeling of Protein Microgradient Diffusion

[00102] Next, a computer model was designed to predict the kinetics of NGF diffusion on the luminal collagen filler of the TMM microchannels. A computer simulation model in COMSOL was implemented that incorporated the diffusion coefficient values of proteins of similar size to NGF from the polymer fiber to the microchannel lumen, both in agarose and in collagen, over a 10 mm longitudinal distance according to the actual physical dimensions of the TMM gel. It was estimated that the NGF concentration in the microchannel volume (0.7 μ l) over 1, 5 and 7 days, and compared those with uniform (U) and gradient (G) coil distribution patterns on their wall surfaces. As protein diffusion coefficient through luminal 0.1% collagen (7.6-12 m^2/sec) is faster than that through the 1.5% agarose microchannel structure (2.31-14 m^2/sec), diffusion occurs primarily through the collagen axis. According to the model, at 7 days, polymeric fibers in the U coil configuration form an even concentration along the microchannel at approximately 7 ng/mL, that dilutes out close to the proximal and distal openings. In contrast, the G coil configuration results in a linear gradient ranging from 0.02-12.42 ng/mL towards the end with a higher number of coils and also dilutes out near the ends. In addition to the expected concentration differences, the model predicted changes over time that appear significant between the two configurations. The U configuration remains stable over time with increasingly larger dilution zone at the end of the channels.

[00103] However, G deployment of the coils results in extension of the gradient from the higher to the lower concentration over time. Despite the dilution effect at the end of the microchannel, the steepness of the gradient in the G configuration does not seem to change significantly during the simulation period, providing a 0.02-12 ng/mL gradient at average 30 degree steepness (see **FIG. 12**).

[00104] The uniform distribution of the coils results in even diffusion of NGF across the microchannel over 1-7 days with some dilution at the ends. The differential deployment of coiled fibers results in a 10-100 ng/mL NGF concentration gradient with a steep angle of 22 degrees, which increases and expands over time to cover most of the

volume of the microchannel. As shown in **FIG. 12**, this difference is accentuated when the uniform and gradient concentrations are compared along the longitudinal axis.

[00105] Together, the results confirmed that greater numbers of coiled fibers on the walls of the agarose microchannels were able to establish linear molecular gradients of biologically active growth factors in the luminal collagen matrix that can then be used to chemotactically guide axonal growth.

Nerve Growth is Enhanced and Directed by 3D Gradient Growth Factor Delivery

[00106] After confirming that the polymeric coils decorating the wall of the hydrogel microchannels can produce a sustaining growth factor gradient, the effect of NGF-eluting coils on nerve regeneration in vitro was tested by evaluating the number of axon fibers that extended from neonatal DRG placed at one end of the TMM gel (**FIGs. 13A-F**). Gels with no coils (**FIG. 13B**) were compared to those with uniform 7 turns and 14 turns of NGF encapsulated coil. The extent of axonal growth was qualitatively better in the gels with NGF coils in comparison to the negative controls, although the increase in the number of axons did not reach statistical difference. However, quantification of the axonal length increased significantly ($p < 0.005$; $n = 4$) in the denser NGF coil group ($1321 \pm 51.71 \mu\text{m}$; 9-15 coil turns) compared to both the no growth factor ($651.2 \pm 40.40 \mu\text{m}$) and the low density coil groups ($808.18 \pm 55.57 \mu\text{m}$; < 8 turns; **FIGs. 13E-F**). To confirm the beneficial effect of NGF gradients on sensory neuron regeneration, a separate group of DRGs was exposed to either uniform or gradient conditions in which the NGF concentration was maintained constant at 18 ng/mL.

[00107] **FIG. 13A**, shows differential intensity contrast (DIC) images of the TMM gel showing one casted microchannel filled with collagen and after placing a DRG explant at one end of the lumen. The PDO fiber coil is anchored into the agarose and onto the walls of the microchannel, filled with air for visualization. Confocal images of the DRGs axonal growth immunolabeled for β -tubulin visualization (green) is shown for TMM gels with: no coils (see **FIG. 13B**); less than 9 turns of the NGF loaded fibers (see **FIG. 13C**); and 9-15 turns of the NGF eluting coils (see **FIG. 13D**). Quantification is shown for both: the Number of axons (see **FIG. 13E**); and the axonal length of DRG (see **FIG. 13F**). The axonal length was measured using Zeiss LSM Image Browser (version

4.2.0.12). There was a significant difference in the length of the cell processes in the different areas (* <0.001).

[00108] To confirm the beneficial effect of NGF gradients on sensory neuron regeneration, a separate group of DRGs were exposed to either uniform (U) or gradient (G) conditions in which the NGF concentration was maintained at 18 ng/mL. Compared to the uniform concentration group (U) (**FIG. 14A**), those with coils arranged to establish a gradient (G) showed a more robust axonal regeneration (**FIG. 14B**). Quantification of the axonal length confirmed that a significant growth advantage ($p < 0.05$) of neurons growing through cylindrical, collagen filled pathways supplemented with gradient NGF (1694 ± 100.1 ; $n = 3$), compared to those containing uniform growth factor concentration (1045 ± 81.33 , $n = 5$; see **FIG. 14C**). Direct comparison of the axonal length observed in microchannels of DRG stained for β -tubulin (green) under uniform or gradient NGF conditions, while maintaining the same concentration, showed a significant increase in the axonal length of neurons growing towards an increasing NGF concentration. * $p < 0.001$, $n = 3-5$. Scale bar = 100 μm .

Robust Axonal Chemotaxis towards NGF Gradients

[00109] In addition to the growth-promoting effect of gradient NGF in DRG axonal elongation, it was noted that neurite elongation in the uniform groups was directed towards the coils on the walls of the microchannels. Indeed, axons in those groups were observed to follow upward and downward trajectories as they grew through the collagen (**FIG. 15A**). In sharp contrast, groups in which the NGF gradient was established towards the distal end, showed a robust linear growth, with axons ignoring the coils as they elongate (**FIG. 15B**). Quantification of the growth angle supported this notion as those in the uniform groups showed a broad directional growth ranging from $+60^\circ$ to -60° (**FIG. 15C**). Conversely, those presented with a gradient of NGF showed more directed growth angles, ranging from $+30^\circ$ to -30° (**FIG. 15D**).

[00110] β -tubulin labeled DRG axons were cultured and allowed to grow through a uniform distribution of the coils. The axonal growth was oriented toward the NGF loaded coils. See **FIGs. 15 A and C**. However, as shown in **FIGs. 15B and 15D** through a gradient distribution, the axonal growth tends to grow in the middle of the channel.

[00111] The turning angle ratio of the axonal growth shows sharp, acute angles. Quantification of the turning angle was determined as a ratio of all the axon present to the number of the axon that turned. There was a significant difference in the turning ratio when uniform and gradient distribution were compared (* $p < 0.005$). To further confirm this observation, the turning angle ratio was measured and determined that the number of axons that made sharp turns were significantly larger in the uniform group compared to those growing towards the NGF gradient (0.5368 ± 0.06321 , $n = 4$; 0.1909 ± 0.03772 , $n = 3$; $p < 0.005$) respectively. **FIG. 16** shows the comparative observed turning angle ratio of DRGs exposed to either uniform (U) or gradient (G) NGF conditions. Together, this data shows that a strong chemotactic growth environment can be achieved through the release of growth factors into luminal collagen using a gradient of coiled polymeric fibers.

[00112] Further, target cells secrete growth factors forming molecular gradients that serve as chemotactic guidance cues for developing and adult injured neurons during axonal elongation and target recognition. During active path finding, axons sense gradients of attractive and repulsive molecules, which they use to orient their growth.

[00113] According to the present disclosure, and as stated above, a reproducible in vivo method was devised for anchoring protein loaded fibers, preferably polymeric fibers, into the wall of multiluminal hydrogel conduits, such as, for example, nerve conduits. The apparatuses, methods and compositions disclosed herein provide an intraluminal gradient without any obstruction to the regenerating axons. In addition, the present designs are highly tunable by varying the number of coil turns in each area to provide the proper gradient steepness.

[00114] Cells in living body migrate, differentiate and proliferate in response to diverse gradients of stimuli. The gradient can be physical or chemical in nature. Physical gradients include, for example, a gradual change in physical properties, such as surface topology, stiffness, and material porosity. For instance, in bone the pore size decreases from outside to inside. This phenomenon allows the mechanical properties to change as well as the gradient feature to allow cell migration and differentiation. Chemical gradients, especially those gradients of biological molecules, are also very important in all cell processes. For instance, cell migration not only depends on the absolute concentration, but also on the slope of the gradient. It has also been noted that the speed

of the migrated cells was much faster when gradient and uniform surface are compared. Factors such as bFGF have been immobilized in a gradient orientation on a hydrogel to investigate the effect of this gradient on aortic smooth muscle cells. It is known that these cells align and migrate in the direction of the increasing gradient. Theoretical analysis has been used to predict the migration speed of cells over uniform and gradient substrate. Such models predict the relationship between speed and gradient to be biphasic dependent.

[00115] According to one variation, presently disclosed models allow the evaluation of the system performance and gives insight into the mechanism affecting dosage and release of the gradient. Despite all efforts to re-establish the gradient, most of these current technologies pertain to planer surface, ignoring that the three dimensional matrices are more closely mimicking the situation in vivo. Variations of the present disclosure provide methods to establish the gradient in 3D and can incorporate multiple gradient cues, and can be predictably, selectively, and controllably tuned based on the cell type.

[00116] According to the present disclosure, a bioactive concentration gradient of NGF has been established. The gradient of NGF can be controlled by varying the number of turns of the coiled fiber over a selected area. More specifically, PC12 responded to the concentration of NGF by extending neurites in a manner similar to that seen in soluble NGF. In addition, DRG growth and orientation were also influenced by the presence of the gradients. The gradient methodology described herein allows the encapsulation of any protein to target the cell of interest. The present disclosure contemplates the use of the disclosed apparatuses, methods and compositions with regard to either long gap repair in peripheral nervous system or axonal guidance in the injured spinal cord.

[00117] The repeatable and programmable gradient-formation methods disclosed herein have the capacity to deliver consistently more biological active agents to a desired site, such as, for example, into a nerve regeneration site for the purpose of guiding axonal growth. The gradient concentration can be controlled by the number of turns (i.e., pitch) of the bio-fiber, either conducting or non-conducting, containing the active agent. The methods, apparatuses, and compositions disclosed herein can also be incorporated into

implantable apparatus for releasing biological active agents in a time-controlled or quality-controlled manner through diffusion or electrical stimulation.

[00118] Therefore, the controlled gradient of the active agents (e.g. chemicals or biological substances, etc.) disclosed herein, can be applied in enticing and guiding nerve regeneration such as, for example, artificial cochlear electrodes, in which the controlled delivery of substances such as brain-derived growth factor (BDNF) can be beneficial to attract neurons to the electrode and to preserve cell viability. Drug delivery of agents, where the concentration gradient is critical for biological effect, can also be carried out. This method is replicable and established gradients can be predictably achieved.

[00119] More specifically, in some variations, a plurality or sequences of gradient materials or matrices, such as, for example, gels, etc. are stacked or otherwise arranged to provide a gradient. The gradient materials comprise different concentrations of a therapeutic agent and thus can provide a therapeutic gradient. The gradient materials can have any combination of therapeutic or other properties (such as physical properties) not inconsistent with the objectives of the present invention and can be used to model and/or recreate a variety of natural environments, including biological environments. In addition, any number of gels can be used. **FIG. 17** shows a conduit 1700 comprising three gradient material sections 1702, 1704 and 1706, each having differing concentrations of a therapeutic agent, and arranged to form a gradient. However, it is also possible to use other numbers of gradient materials, such as, for example, two, four, five, or six gradient materials. In some cases, more than six gradient materials can be used. As shown in **FIG. 17**, gradient material section 1702 has the highest concentration; section 1704 is less concentrated; and section 1706 is least concentrated.

[00120] In addition, methods of forming a gradient using a soft, biocompatible component are also contemplated. These methods can be modified in various manners to achieve various objectives. In addition, as described herein, encapsulation of various factors can be achieved by the inclusion of various microparticle carriers to form a gradient. Contemplated variations include microparticles that are incorporated/suspended into a gel (e.g. a hydrogel, etc.) to provide a therapeutic gradient. **FIG. 18** illustrates a scanning electron microscope (SEM) image of a composition

according to one variation, where microparticles 1802 are shown suspended in a carrier matrix 1802, such as, for example, a gel such as a hydrogel.

[00121] Moreover, in some variations, a plurality of gradient materials or matrices, such as, for example, gels comprising active agents, such as, for example, therapeutic agents with each material preferably comprising a varying concentration of one active agent, multiple active agents, or varying concentrations of multiple active agents, can be arranged in an orientation to provide a preselected, predetermined and predictable gradient region and, if desired, a non-gradient region.

[00122] Various embodiments of the present invention have been described in fulfillment of the various objectives of the invention. It should be recognized that these embodiments are merely illustrative of the principles of the present invention. Numerous modifications and adaptations thereof will be readily apparent to those skilled in the art without departing from the spirit and scope of the invention.

CLAIMS

That which is claimed is:

1. An apparatus comprising:
a conduit having a first end and a second end;
one or more microchannels disposed in the conduit and extending from the first end toward the second end; and
a fiber coiled around the exterior of at least one microchannel,
wherein the fiber comprises an active agent that is operable to diffuse into the interior of the microchannel.
2. The apparatus of claim 1, wherein the conduit comprises implantation tubing.
3. The apparatus of claim 1, wherein the microchannels are disposed within a matrix material disposed in the conduit.
4. The apparatus of claim 3, wherein the matrix material comprises an agarose gel, a polylactic-co-glycolic acid, a polylactic acid, a caprolactone, or a combination thereof.
5. The apparatus of claim 3, wherein the matrix material comprises an agarose gel comprising between 1.5 percent and 2.5 percent agarose.
6. The apparatus of claim 1, wherein a plurality of microchannels are disposed in the conduit.
7. The apparatus of claim 6, wherein a plurality of fibers are coiled around the exteriors of a plurality of microchannels.
8. The apparatus of claim 7, wherein the plurality of fibers are each coiled around the exterior of a different microchannel.

9. The apparatus of claim 8, wherein at least two of the coiled fibers comprise differing active agents, differing amounts of an active agent, and/or differing pitches.
10. The apparatus of claim 1, wherein the fiber comprises a biodegradable polymer.
11. The apparatus of claim 1, wherein the fiber is formed from poly(glycolide), poly(lactide), poly(glycolide-co-lactide), poly(dioxanone), caprolactone, alginate, or a combination thereof.
12. The apparatus of claim 3, wherein the matrix material comprises an agarose gel and the fiber comprises a coil formed from poly(glycolide), poly(lactide), poly(glycolide-co-lactide), poly(p-dioxanone), caprolactone, alginate, or a combination thereof.
13. The apparatus of claim 1, wherein the fiber is coiled around the exterior of the microchannel in an isotropic configuration.
14. The apparatus of claim 1, wherein the fiber is coiled around the exterior of the microchannel in an anisotropic configuration.
15. The apparatus of claim 1, wherein the active agent comprises a drug, a peptide, a protein, growth inhibiting factor, or growth promoting factor.
16. A composition comprising:
a coiled polymeric material comprising an active agent operable to diffuse out of the polymeric material when the polymeric material is disposed in a biological compartment.
17. The composition of claim 16, wherein the biological compartment comprises a nerve conduit.

18. A method of forming a chemical gradient comprising:
 - disposing an apparatus in a biological compartment, the apparatus comprising:
 - a conduit having a first end and a second end;
 - one or more microchannels disposed in the conduit and extending from the first end toward the second end; and
 - a fiber coiled around the exterior of at least one microchannel,
 - wherein the fiber comprises an active agent that is operable to diffuse into the interior of the microchannel.

19. The method of claim 18, wherein the biological compartment comprises a nerve conduit.

20. The method of claim 18, wherein the chemical gradient comprises a drug gradient or a growth factor gradient.

ABSTRACT

In one aspect, apparatuses for providing chemical gradients are described herein. In some embodiments, an apparatus described herein comprises a conduit having a first end and a second end, one or more microchannels disposed in the conduit and extending from the first end toward the second end, and a fiber coiled around the exterior of at least one microchannel, wherein the fiber comprises an active agent that is operable to diffuse into the interior of the microchannel.

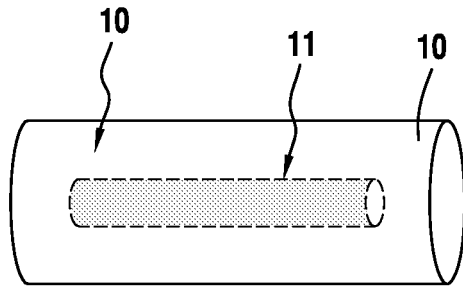


FIG. 1A

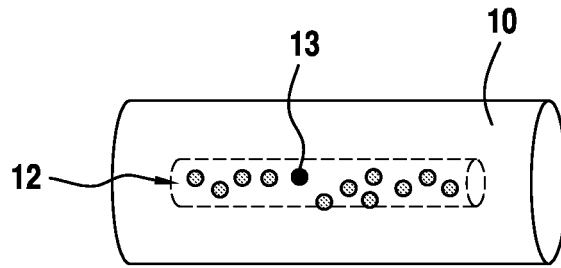


FIG. 1B

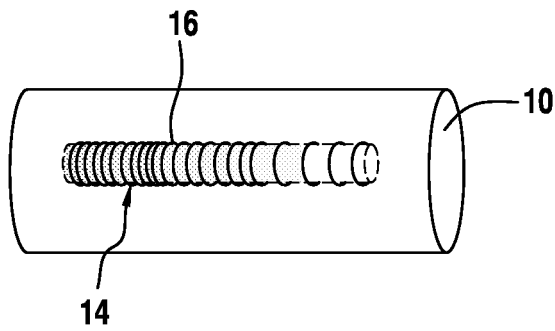


FIG. 1C

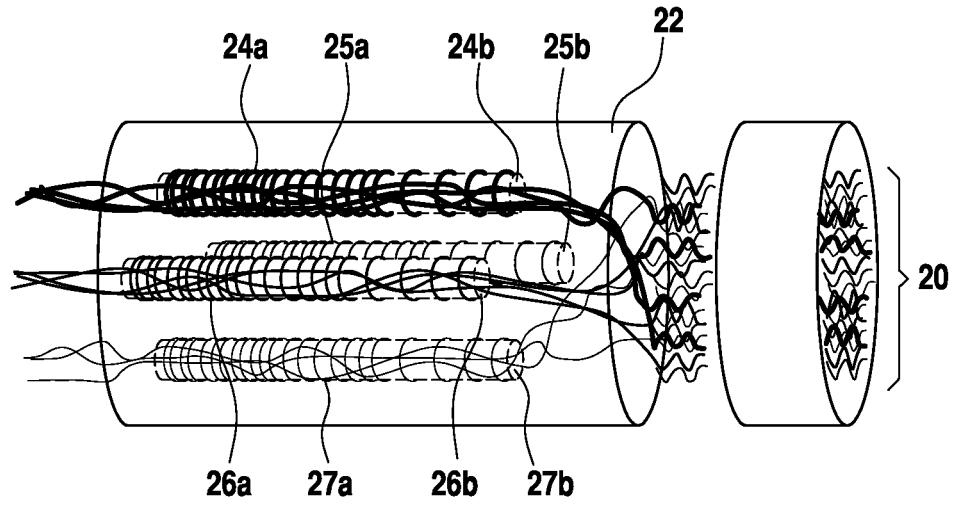


FIG. 2

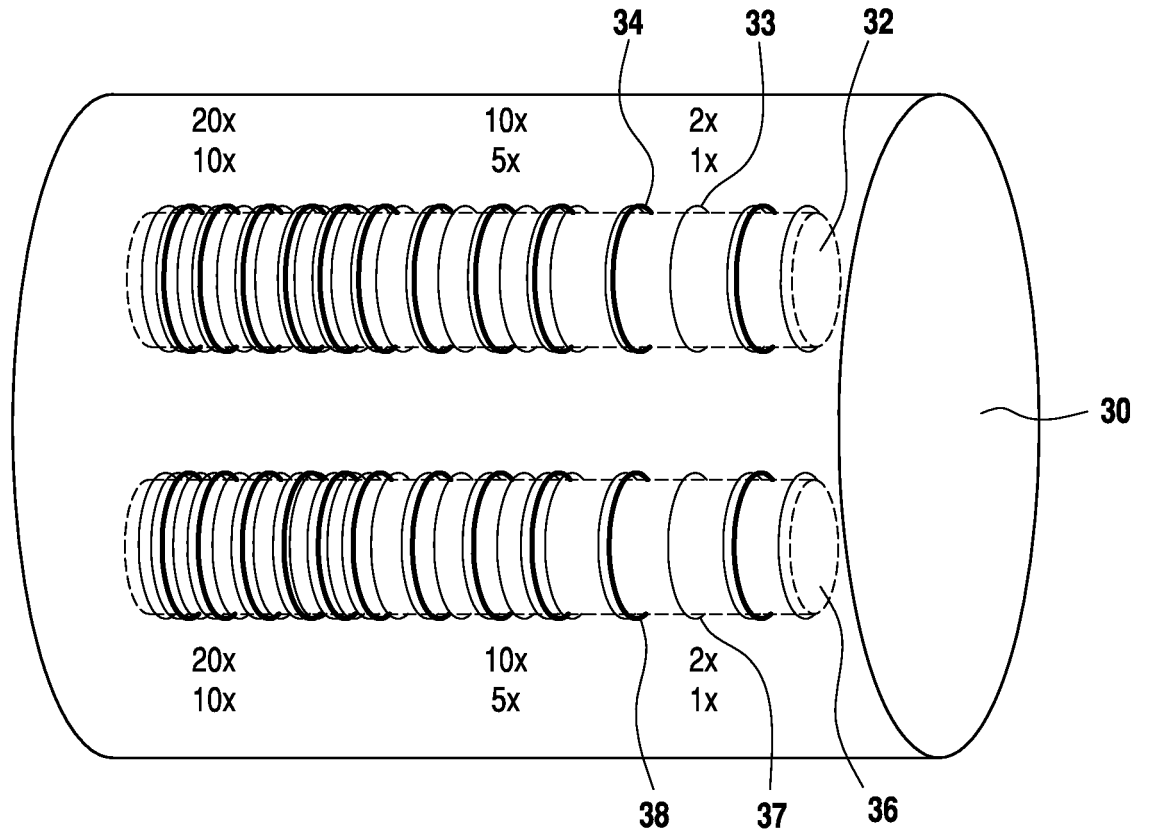


FIG. 3

3/17

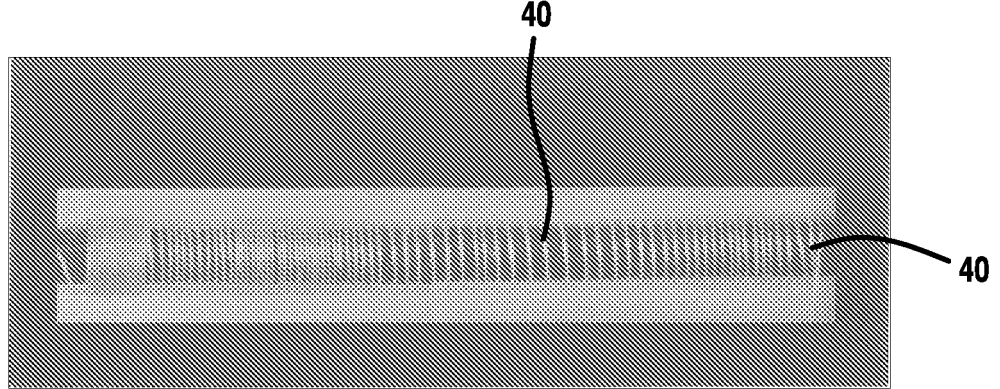


FIG. 4A

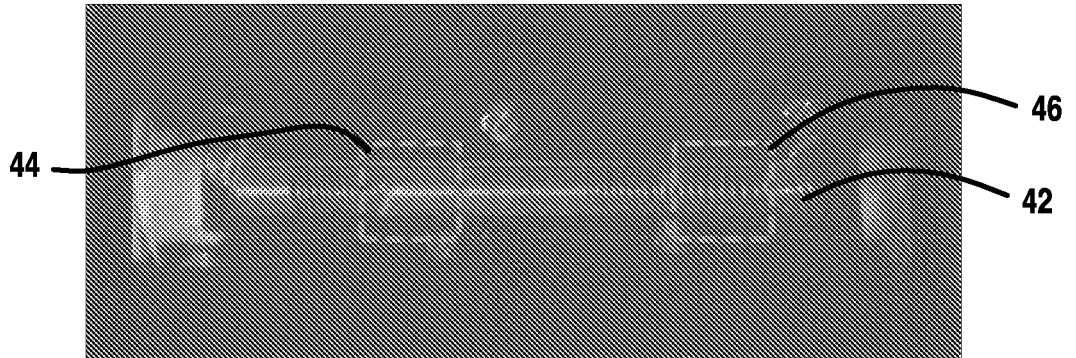


FIG. 4B

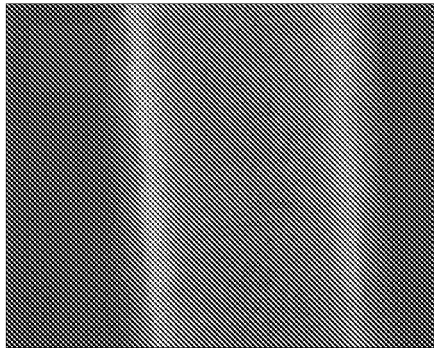


FIG. 4C

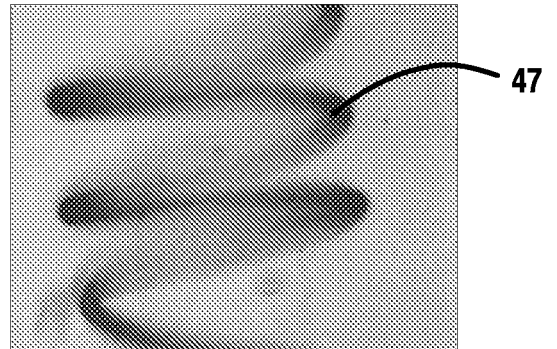
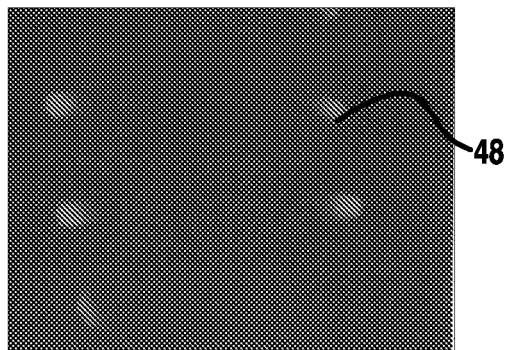
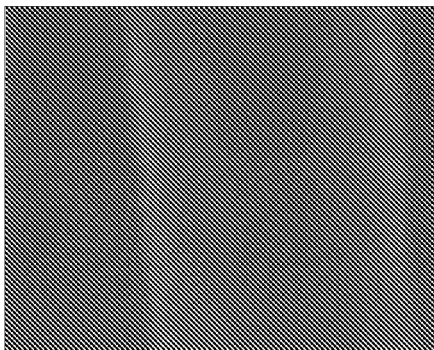


FIG. 4D



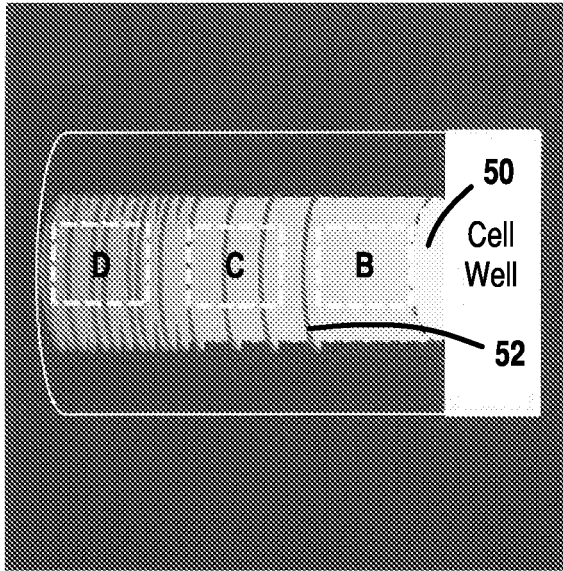


FIG. 5A

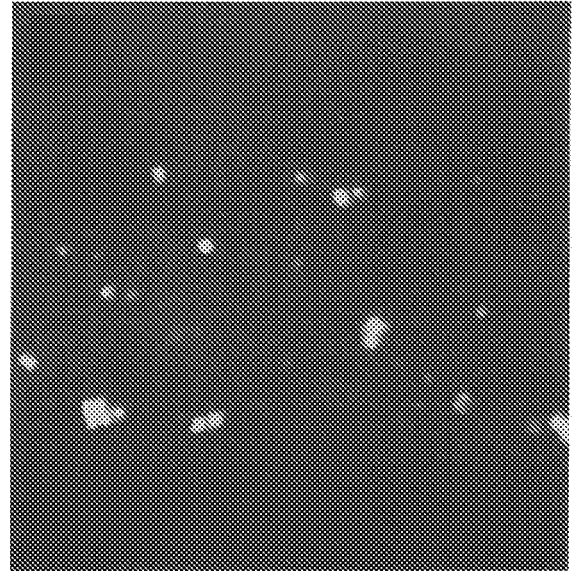


FIG. 5B

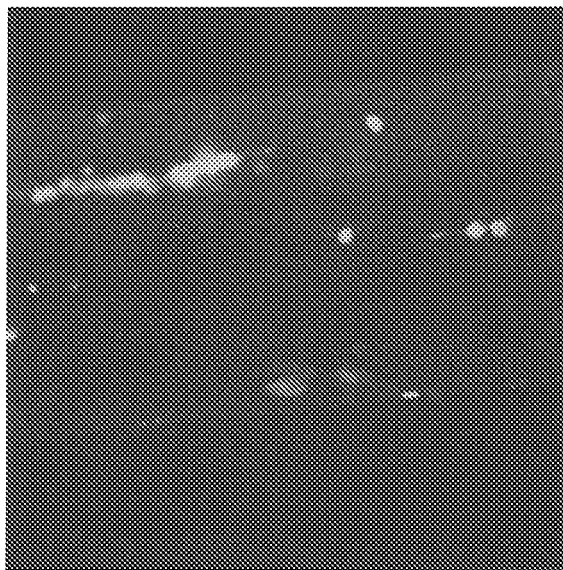


FIG. 5C

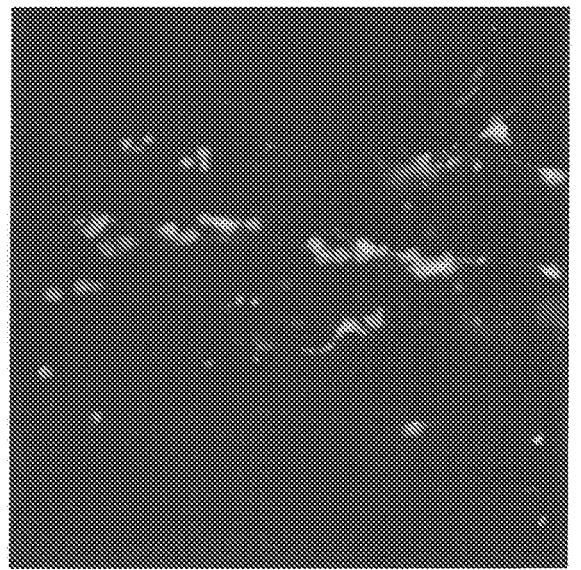


FIG. 5D

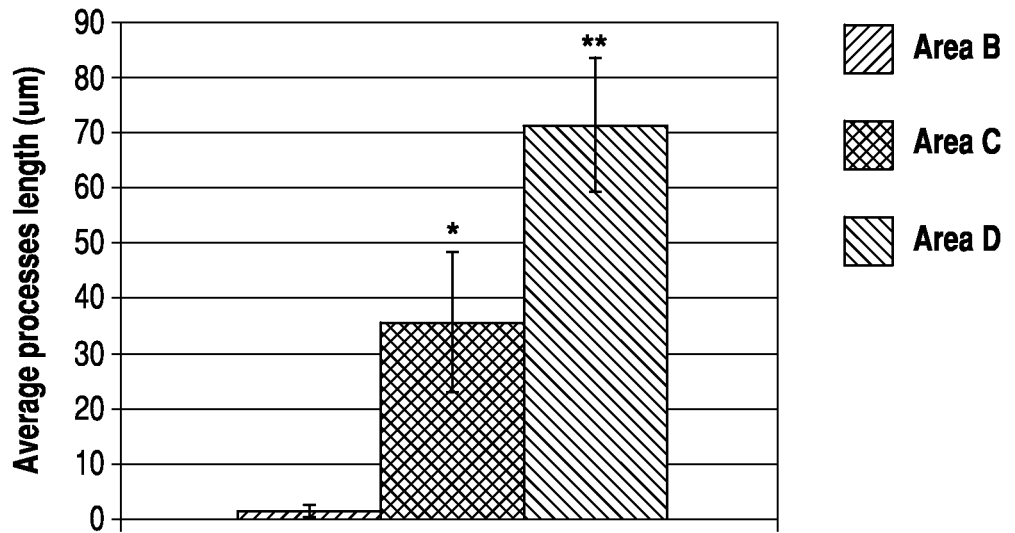
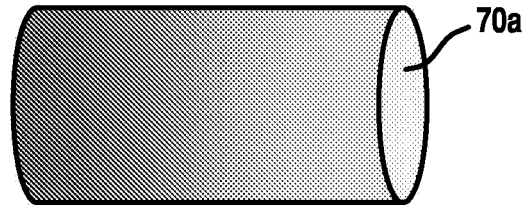


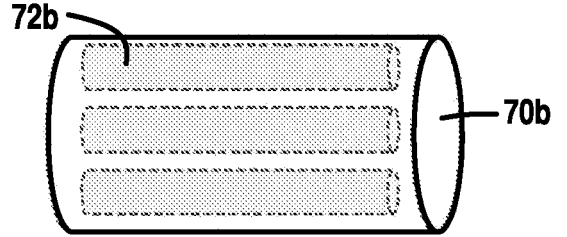
FIG. 6

6/17



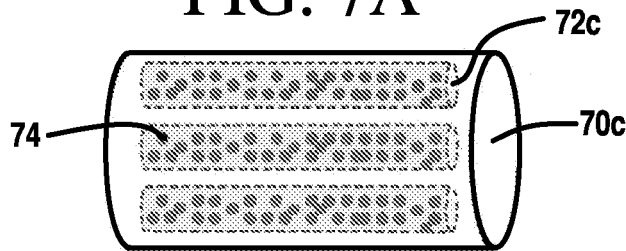
Simple NG w/ Gradient

FIG. 7A



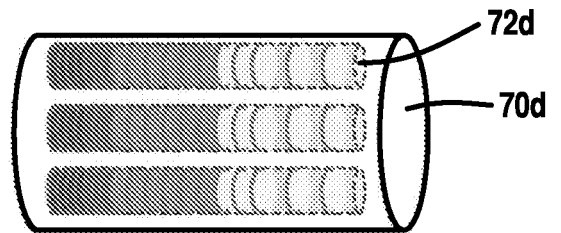
Multiluminal NG

FIG. 7B



Multiluminal NG w/Uniform NTF

FIG. 7C



Multiluminal NG w/ Gradient

FIG. 7D

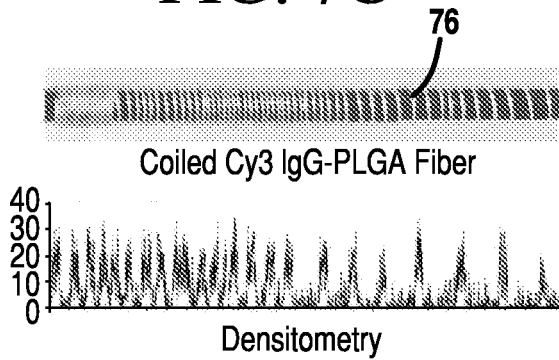
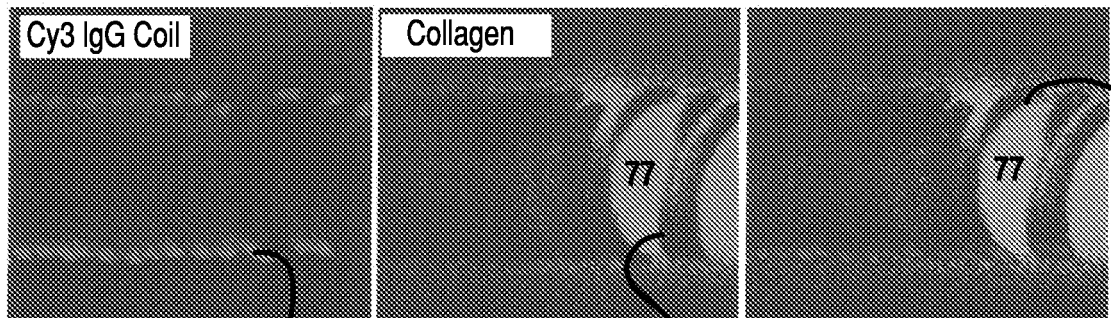
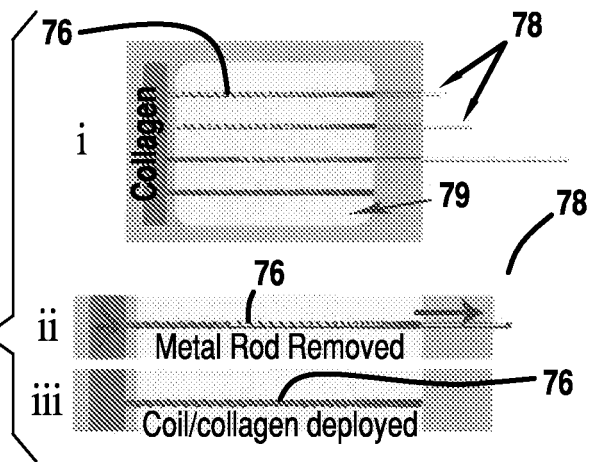
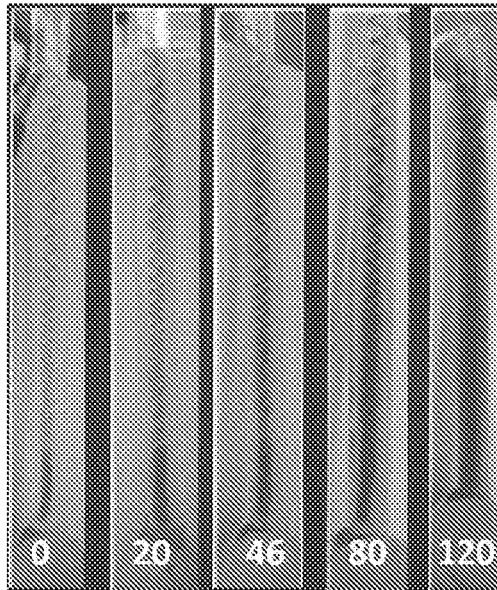


FIG. 7E

FIG. 7F





Time (min)

FIG. 8A

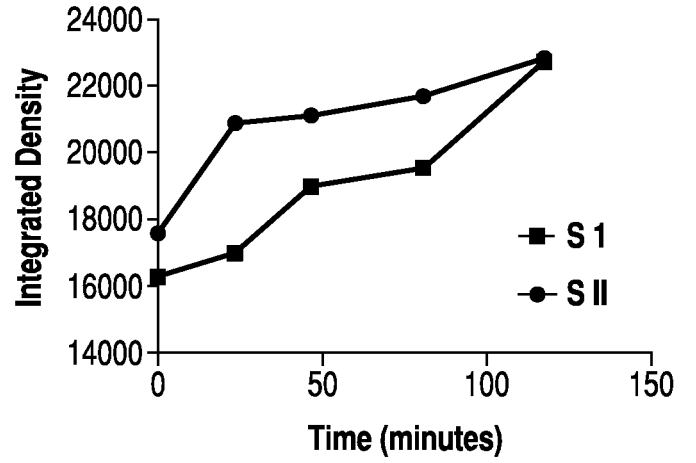


FIG. 8B

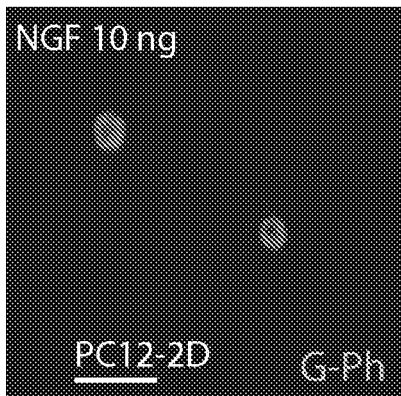


FIG. 9A

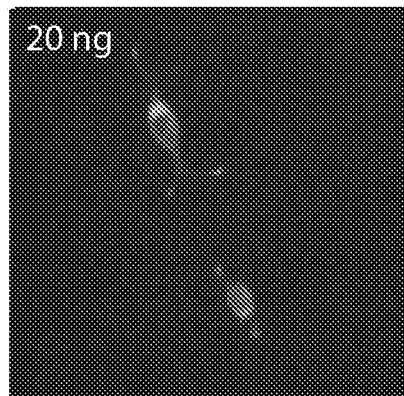


FIG. 9B



FIG. 9C

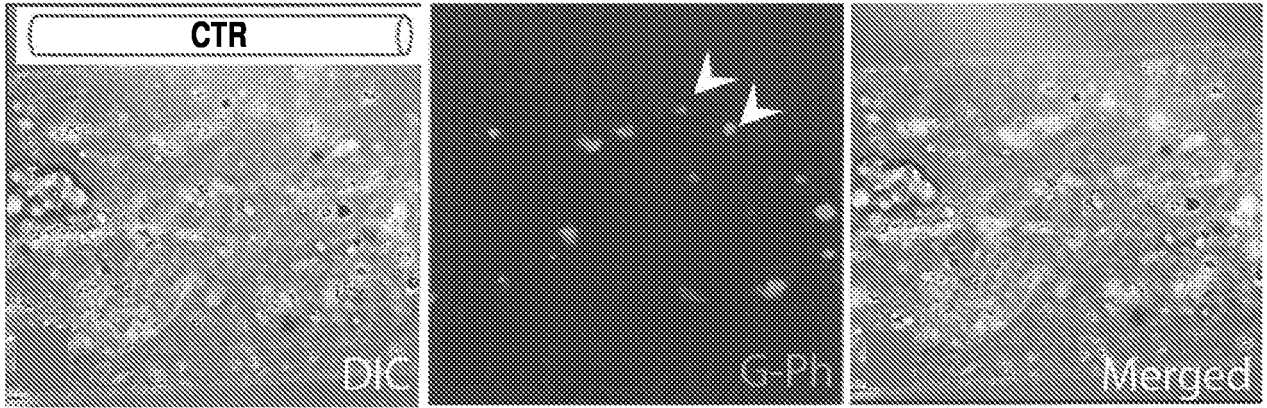


FIG. 10A

FIG. 10B

FIG. 10C

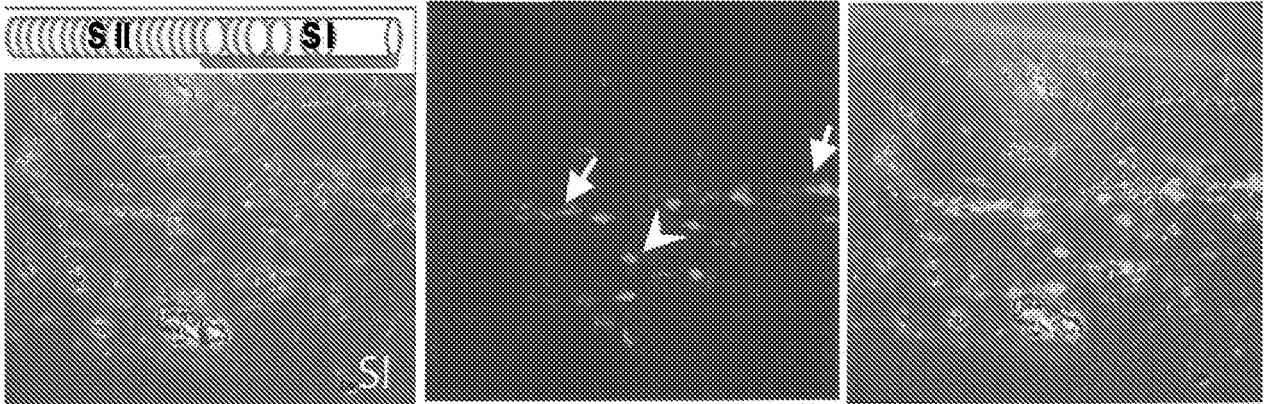
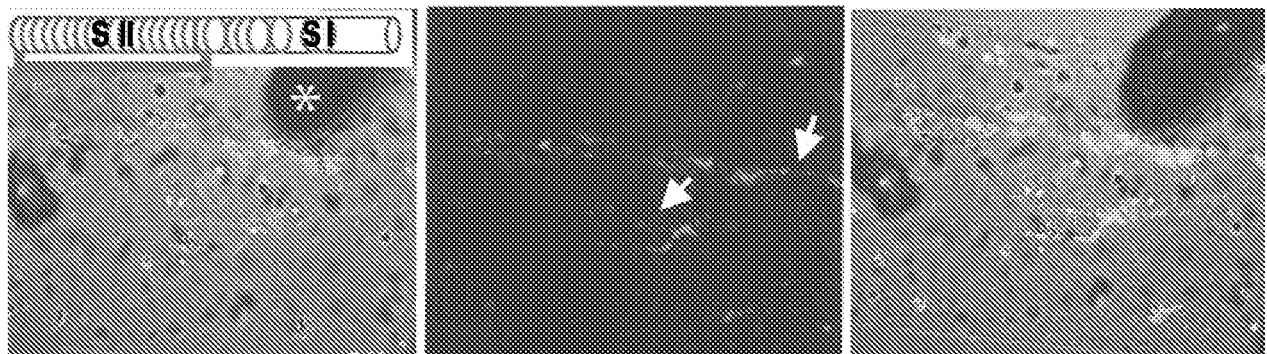


FIG. 10D

FIG. 10E

FIG. 10F



9/17

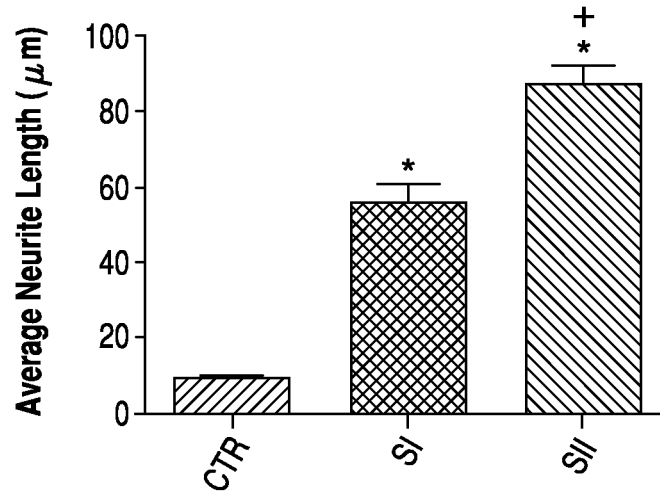


FIG. 10J

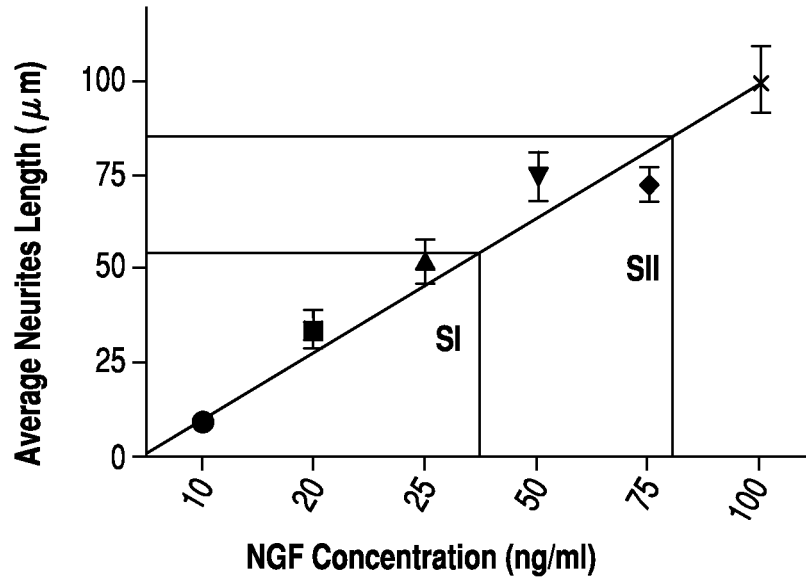


FIG. 10K

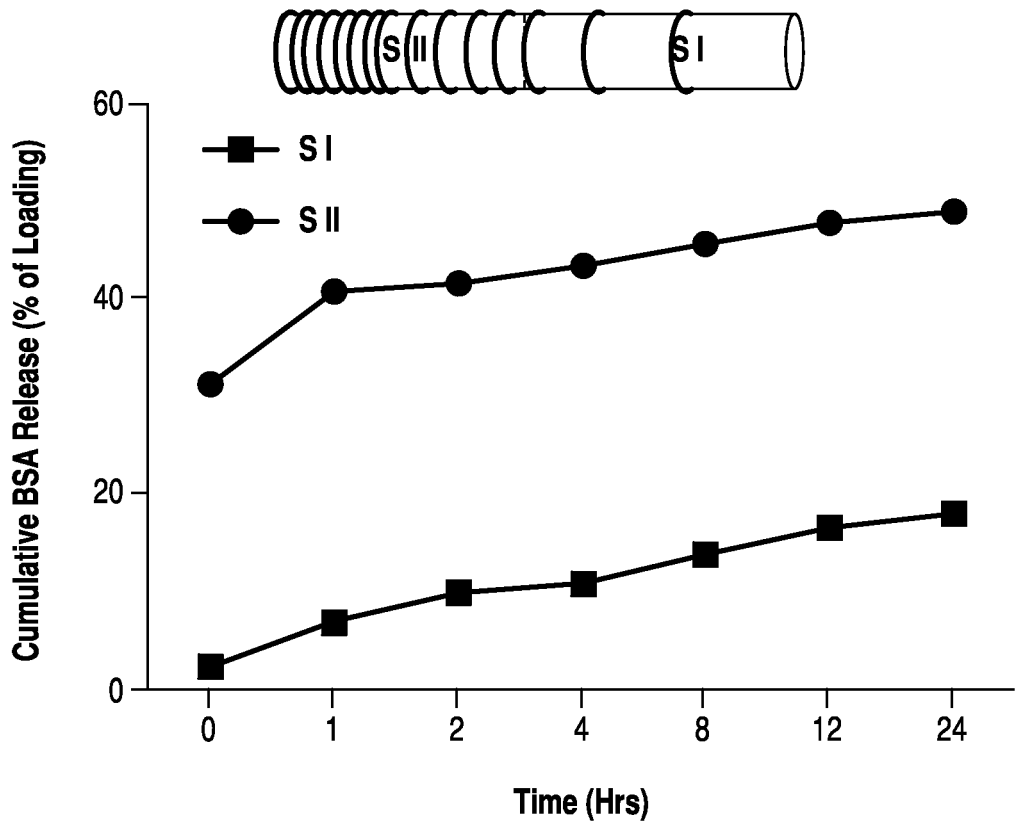


FIG. 11

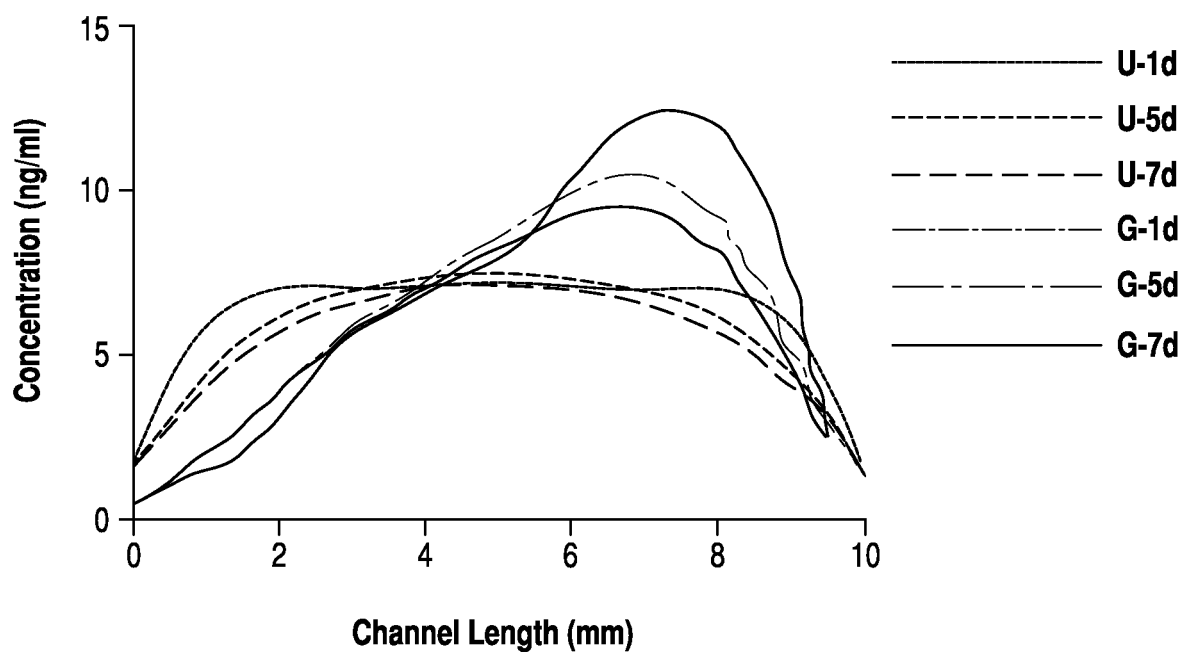


FIG. 12

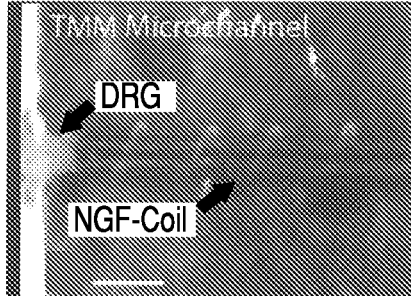


FIG. 13A

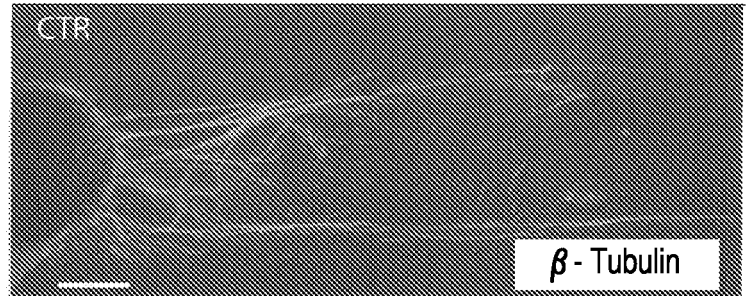


FIG. 13B

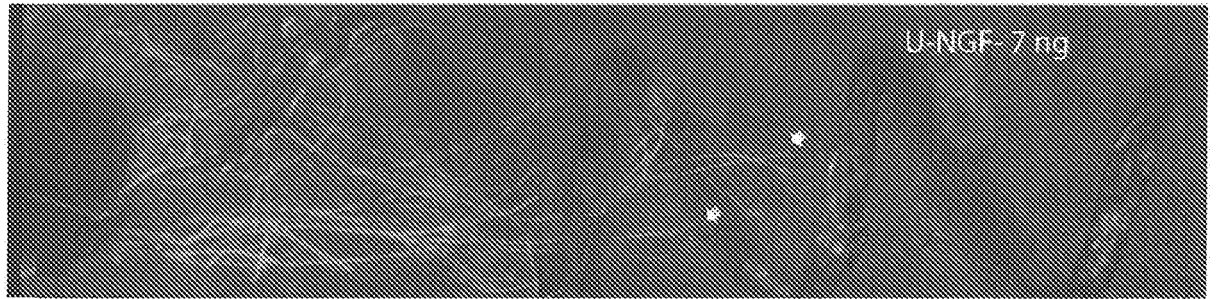
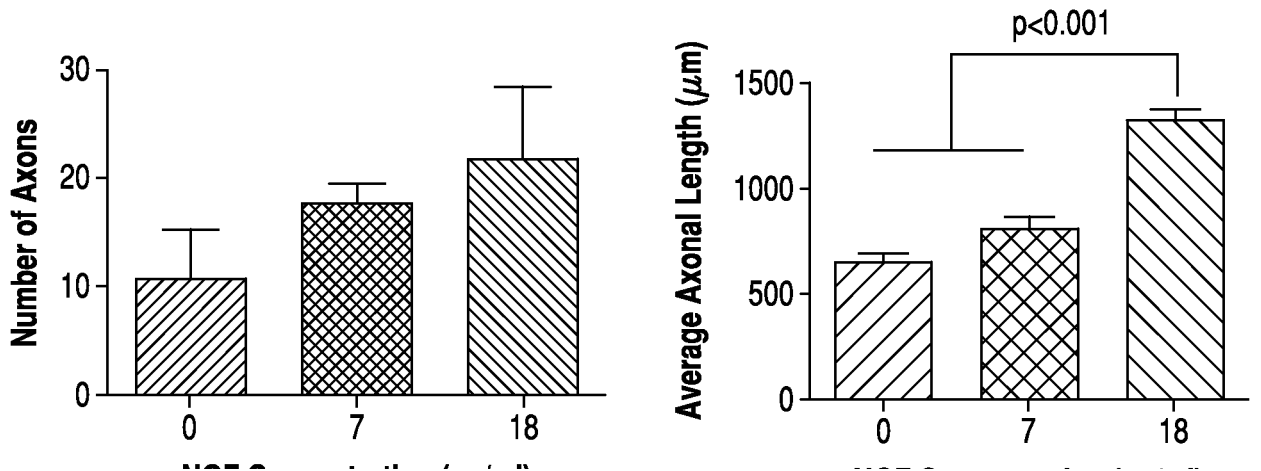


FIG. 13C



FIG. 13D



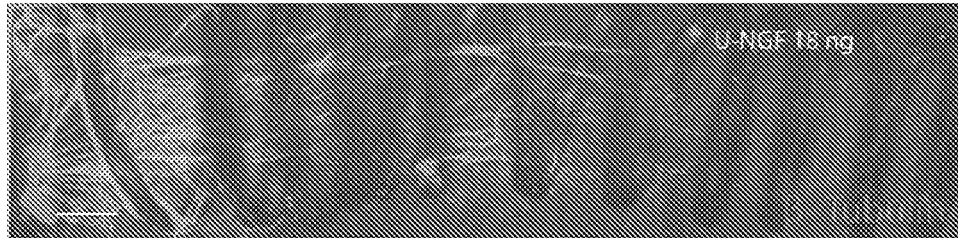


FIG. 14A

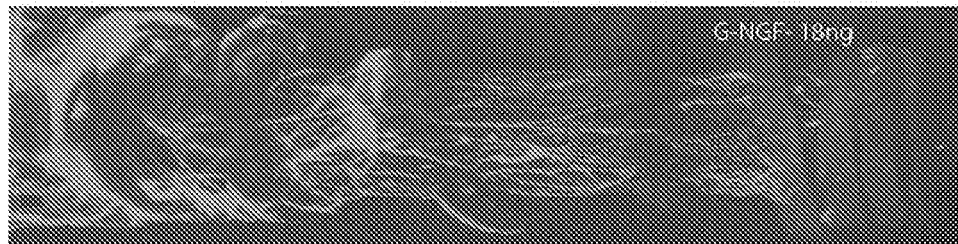


FIG. 14B

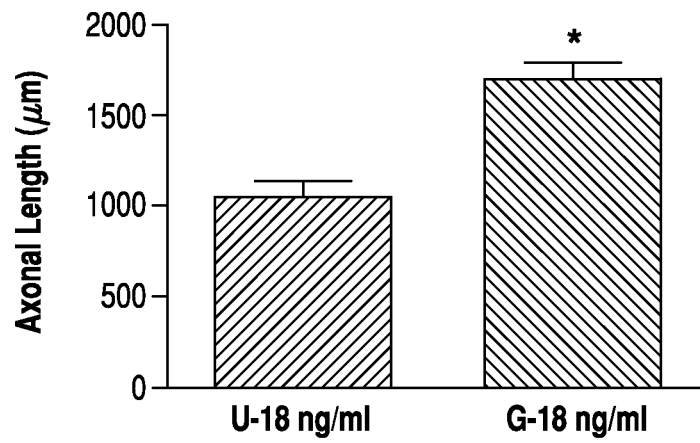


FIG. 14C

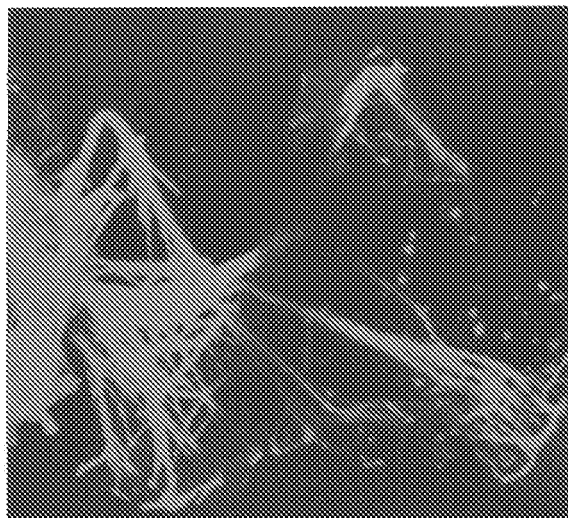


FIG. 15A

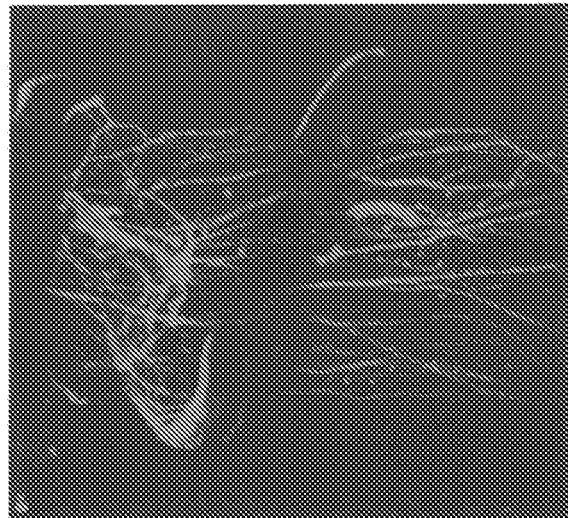


FIG. 15B

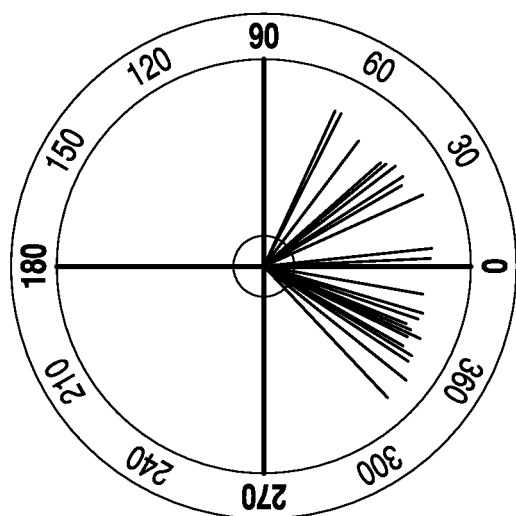


FIG. 15C

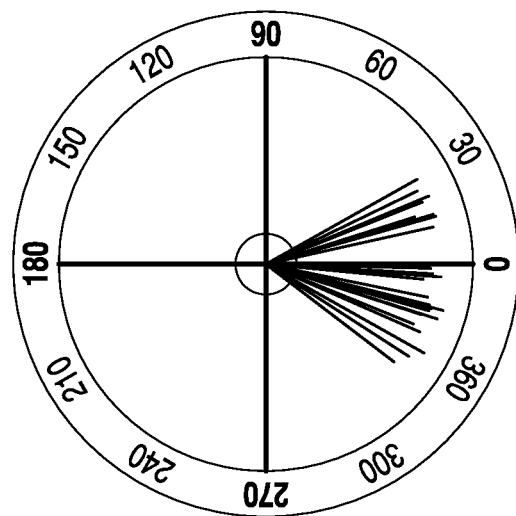


FIG. 15D

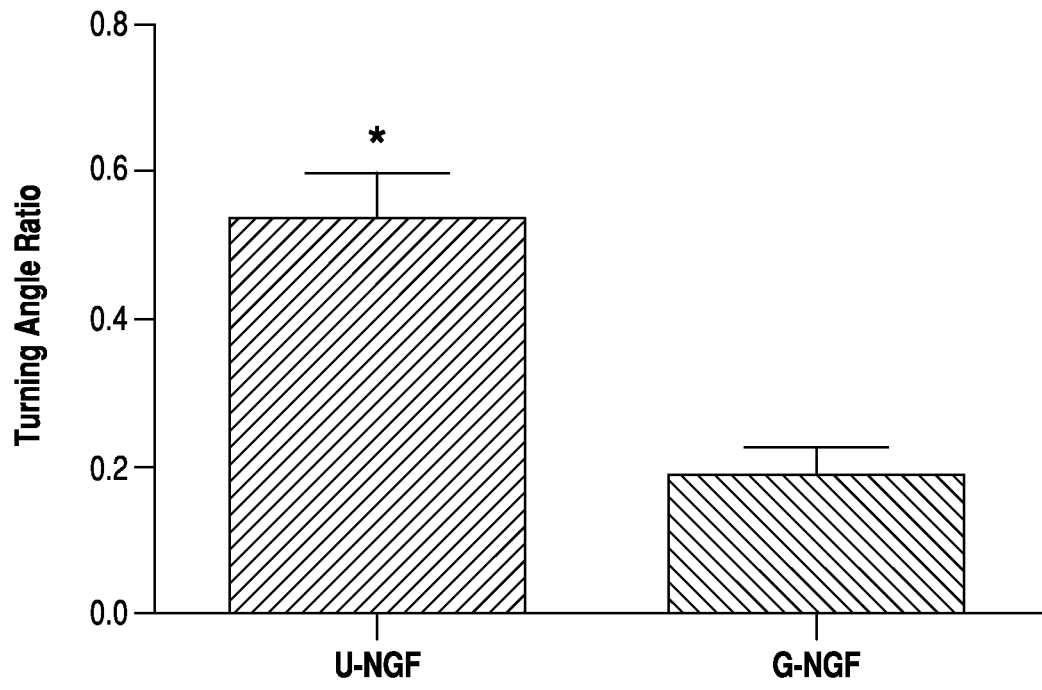


FIG. 16

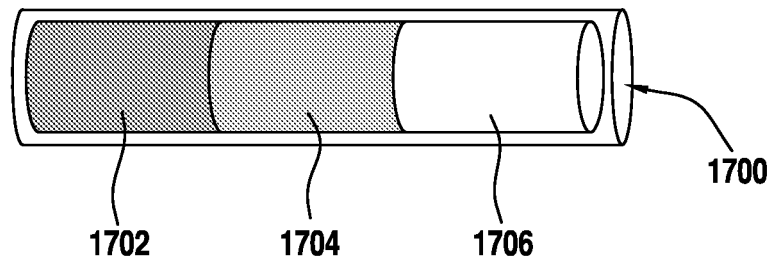


FIG. 17

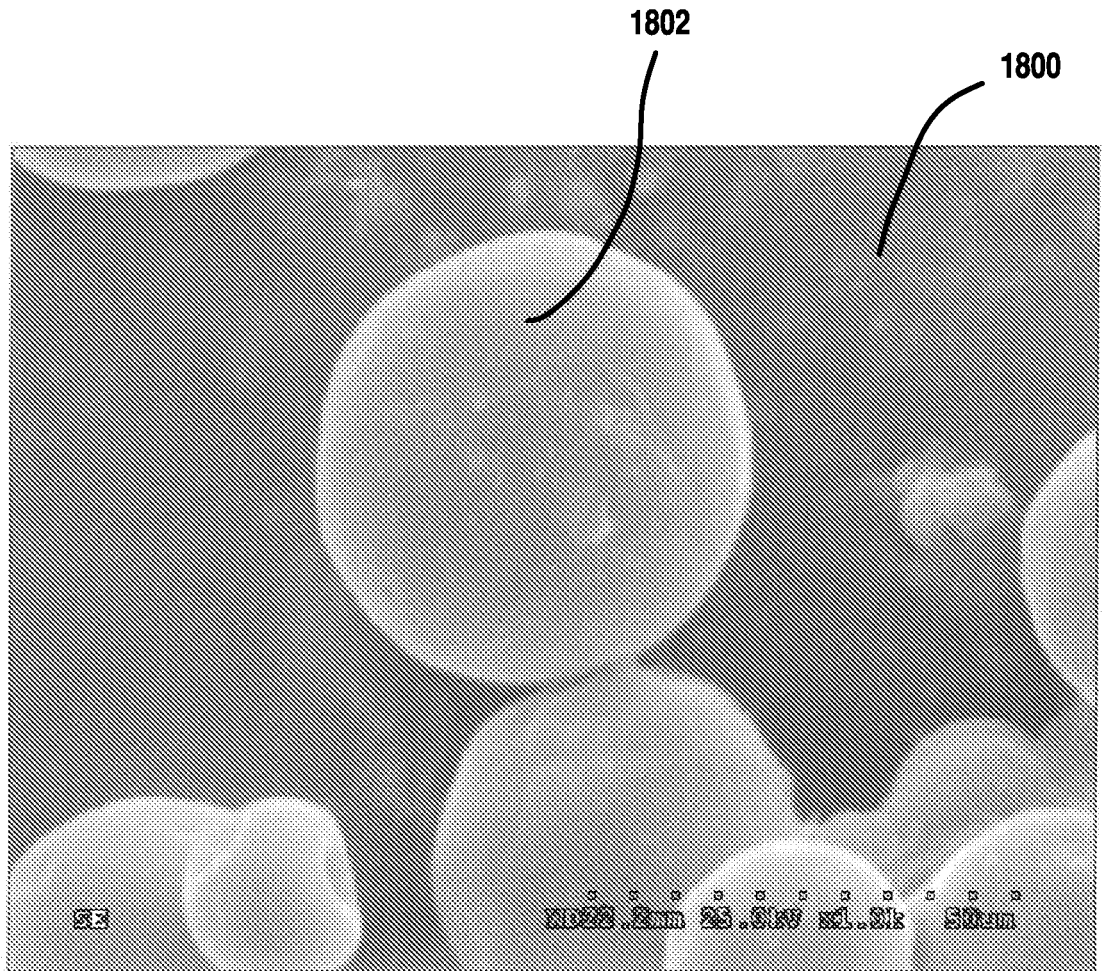


FIG. 18

**IN THE UNITED STATES PATENT AND TRADEMARK OFFICE
UNITED STATES RECEIVING OFFICE**

FILED ELECTRONICALLY VIA EFS-WEB

Mail Stop PCT
Commissioner for Patents
P.O. Box 1450
Alexandria, VA 22313-1450

CERTIFICATE OF TRANSMISSION

Date of Deposit : 18 February 2014

Type of Document(s) : Transmittal Letter to the United States Receiving Office - 1 page
PCT Request and Fee Calculation Sheet - 6 pages
Required Fees in the amount of \$4552
Specification, claims and abstract – 39 pages
Drawings – 17 pages

International Application No. : Unassigned

Filing Date : 18 February 2014

I hereby certify that the documents identified above in connection with Our File No. 5013205.009PC1 are being filed electronically via EFS-Web on the date indicated above and is addressed to: Mail Stop PCT, Commissioner for Patents, P.O. Box 1450, Alexandria, VA 22313-1450.

Electronically Filed by: /tammy taylor/
Tammy Taylor

TRANSMITTAL LETTER TO THE UNITED STATES RECEIVING OFFICE

Express Mail mailing number:	Date of deposit: 18.02.2014
File reference no.: 5013205.009PC1	International application no. (if known):
Customer Number ¹ : 11806	Earliest priority date claimed (Day/Month/Year): 19.02.2013
Title of the invention: CHEMICAL GRADIENTS	

¹ Customer Number will allow access to the application in Private PAIR but cannot be used to establish or change the correspondence address.

This is a new International Application

SCREENING DISCLOSURE INFORMATION:

In order to assist in screening the accompanying international application for purposes of determining whether a license for foreign transmittal should and could be granted and for other purposes, the following information is supplied. (check as boxes as apply):

The invention disclosed was **not** made in the United States of America.

There is no prior U.S. application relating to this invention.

The following prior U.S. application(s) contain subject matter which is related to the invention disclosed in the attached international application. (NOTE: priority to these applications may or may not be claimed on the Request (form PCT/RO/101) and this listing does not constitute a claim for priority.)

application no.	61/766,366	filed on	19 February 2013
application no.		filed on	

The present international application contains additional subject matter not found in the prior U.S. application(s) identified above. The additional subject matter is found on pages 1-39 and **DOES NOT ALTER** **MIGHT BE CONSIDERED TO ALTER** the general nature of the invention in a manner which would require the U.S. application to have been made available for inspection by the appropriate defense agencies under 35 U.S.C. 181 and 37 C.F.R. 5.15.

Itemized list of contents

Sheets of Request form:	5	Check no.:
Sheets of description (excluding sequence listing):	35	Return receipt postcard:
Sheets of claims:	3	Power of attorney:
Sheets of abstract:	1	Certified copy of priority document (specify):
Sheets of drawings:	17	Other (specify):
Sheets of sequence listing:		
Sequence listing diskette/CD:		

The person signing this form is:	<input type="checkbox"/> Applicant	Name of person signing <p style="text-align: center; font-size: 1.2em;">John P. Zimmer</p> Signature
	<input checked="" type="checkbox"/> Attorney/Agent (Reg. No.) 64,750	
	<input type="checkbox"/> Common Representative	

This collection of information is required by 37 CFR 1.10 and 1.412. The information is required to obtain or retain a benefit by the public, which is to file (and by the USPTO to process) an application. Confidentiality is governed by 35 U.S.C. 122 and 37 CFR 1.11 and 1.14. This collection is estimated to take 15 minutes to complete, including gathering information, preparing, and submitting the completed form to the USPTO. Time will vary depending upon the individual case. Any comments on the amount of time you require to complete this form and/or suggestions for reducing this burden, should be sent to the Chief Information Officer, U.S. Patent and Trademark Office, U.S. Department of Commerce, P.O. Box 1450, Alexandria, VA 22313-1450. DO NOT SEND FEES OR COMPLETED FORMS TO THIS ADDRESS.
SEND TO: Mail Stop PCT, Commissioner for Patents, P.O. Box 1450, Alexandria, VA 22313-1450.

Appendix B
International Patent Application
PCT/US14/16801

DEVICES AND METHODS FOR THE PREVENTION AND TREATMENT OF NEUROMAS

CROSS REFERENCE TO RELATED APPLICATION

[0001] This application claims priority pursuant to 35 U.S.C. § 119(e) to U.S. Provisional Patent Application Ser. No. 61/766,368, filed on February 19, 2013, which is hereby incorporated by reference in its entirety.

FIELD

[0002] This invention relates to devices and methods for the prevention and treatment of neuromas and, in particular, to devices and methods that inhibit erratic nerve growth.

BACKGROUND

[0003] The number of amputees in the world has risen significantly in recent years, with war injuries and dysvascular diseases such as diabetes accounting for approximately 90% of all amputee cases. There are currently about 1.7 million amputees living in the United States alone, and approximately 135,000 new amputee patients are discharged annually from hospitals. Further, it has been estimated that there will be a 20% increase in the number of new amputee cases per year by 2050.

[0004] Unfortunately, due to persistent pain in limb remnants, about 25% of amputees are not able to commence rehabilitation, much less resume ordinary daily activities. The cause of such pain can be a neuroma. One recent study reported that 78% of amputees experienced mild to severe pain as a consequence of neuroma formation over the 25-year study period, of which 63% described the pain as constant aching pain. The pain is also frequently described as sharp, shooting, or electrical-like phantom sensations that persist for years after surgical amputation. In addition, patients experience tenderness

to palpation of the skin overlying the neuroma, spontaneous burning pain, allodynia, and hyperalgesia.

[0005] Neuromas are benign tumors that arise from neural tissue and are composed of abnormally sprouting axons, Schwann cells, and connective tissue. Even though neuromas can appear following various types of injuries, some of the most common and challenging to treat are derived from amputation surgeries in which neural tissue is sectioned by retraction axotomy. The lack of organ-target acquisition by the resulting nerve stump results in a subsequent cascade of biological events that culminate in the formation of a neural nodule.

[0006] To treat patients with painful neuromas, doctors have relied on multiple treatment modalities. However, many existing treatment modalities have a high recurrence rate, address the problem only after it has established itself in the patient, and/or are not definitive. A high neuroma recurrence rate can lead to repeated surgical resections. Further, the prevention of neuroma formation by some prior methods has also proven unsatisfactory, sometimes requiring multiple procedures. Therefore, there exists a need for improved devices and methods for the prevention and treatment of neuromas.

SUMMARY

[0007] In one aspect, nerve growth inhibition devices are described herein which, in some embodiments, can provide one or more advantages compared to some prior devices. For example, in some embodiments, a device described herein can be used to prevent painful neuroma formation, including from the first surgery. For example, devices described herein, in some cases, can be used for post-amputation surgery in which it is known that patients will otherwise likely develop a neuroma. It is also possible to use devices described herein at the time of the initial surgery in new amputee cases as well as in those who have already presented with pain of the nerve stump. Devices described herein, in some embodiments, can treat and/or prevent neuromas by hindering

neuroma formation in the peripheral nervous system. In some cases, a device described herein can effectively block the natural progression of abnormal nerve sprouting that would otherwise translate into the formation of a painful neuroma. Further, devices described herein, in some instances, can also provide analgesia. For example, in some embodiments, a device described herein can provide at least partial analgesia by physically protecting an injured nerve from surrounding tissue and/or direct pressure, such as continually moving surrounding muscle tissue. Additionally, in some cases, a device described herein can provide at least partial analgesia by protecting an injured nerve from environmental electromagnetic radiation such as radio frequency (RF) radiation.

[0008] A nerve growth inhibition device described herein, in some embodiments, comprises a tube having a proximal end and a distal end. A matrix material is disposed in the tube, and the matrix material comprises one or more microchannels or lumens. The proximal end of the tube comprises an opening operable to receive nerve tissue, the distal end of the tube is sealed, and the microchannels of the matrix material extend from the proximal end of the tube toward the distal end of the tube. Further, in some cases, the tube is sealed with a capping material disposed in the distal end of the tube. The capping material, in some instances, blocks or substantially blocks the distal end of the one or more microchannels.

[0009] In addition, in some embodiments, the matrix material of the device, alone or in combination with the capping material, exhibits a compositional gradient from the proximal end of the tube toward the distal end of the tube. In some cases, the compositional gradient of the matrix material and/or capping material provides a nerve growth region and a nerve growth inhibition region within the tube. The use of such a device, in some instances, can induce nerve axons to enter the tube and grow toward the distal end of the tube (within the nerve growth region), followed by inhibition or total cessation of nerve growth

within the tube (once the nerves reach the nerve growth inhibition region), thereby sequestering the nerve endings within the tube and preventing neuroma formation. In some embodiments, a matrix material, alone or in combination with a capping material, has a binary chemical composition comprising a nerve growth region and a nerve growth inhibition region. Alternatively, in other cases, a matrix material has a chemical composition that varies continuously or in a step-wise manner as a function of distance from the proximal end of the tube.

[0010] Moreover, in some embodiments, a device described herein further comprises a fluid, such as a saline solution, disposed in one or more microchannels of the device. Additionally, in some instances, one or more microparticles are disposed in the fluid, the microparticles comprising one or more nerve growth inhibition factors. The use of such microparticles, in some cases, can permit the time-delayed release of nerve growth inhibition factors into the microchannels of a device described herein. Further, in some embodiments, the microchannels of a device described herein are free or substantially free of an extracellular matrix (ECM) material, such as collagen, disposed within the microchannels.

[0011] In addition, a device described herein, in some cases, further comprises an electromagnetic radiation (EMR) shielding layer substantially surrounding the exterior circumference of the tube of the device. Such a shielding layer can be formed from an electrically conductive metal. A device described herein can also further comprise an encapsulation layer substantially surrounding the exterior of the EMR shielding layer. Such an encapsulation layer can be formed from an insulating material.

[0012] In another aspect, methods of treating and/or preventing a neuroma are described herein. In some cases, treating and/or preventing a neuroma comprises inhibiting nerve growth and/or providing analgesia in a biological compartment. In some embodiments, such a method described herein

comprises disposing a device described herein in a biological compartment comprising nerve tissue. In some cases, the biological compartment comprises a stump of a severed or transected nerve. Further, in some embodiments, the device is disposed over the nerve stump.

[0013] These and other embodiments are described in more detail in the detailed description which follows.

BRIEF DESCRIPTION OF THE FIGURES

[0014] **FIG. 1** illustrates a sectional, side view of a device according to one embodiment described herein.

[0015] **FIG. 2** illustrates a sectional view of the device of **FIG. 1** taken along lines 2--2.

[0016] **FIG. 3** illustrates a perspective view of a device according to one embodiment described herein.

[0017] **FIG. 4** illustrates a cutaway perspective view of the device of **FIG. 3**.

[0018] **FIG. 5** illustrates a graph of some results of a method of inhibiting nerve growth according to one embodiment described herein.

[0019] **FIG. 6** illustrates a sectional view of a device used to inhibit nerve growth according to one embodiment described herein.

DETAILED DESCRIPTION

[0020] Embodiments described herein can be understood more readily by reference to the following detailed description, examples, and figures.

Elements, apparatus, and methods described herein, however, are not limited to the specific embodiments presented in the detailed description, examples, and figures. It should be recognized that these embodiments are merely illustrative of the principles of the present invention. Numerous modifications and adaptations will be readily apparent to those of skill in the art without departing from the spirit and scope of the invention.

[0021] In addition, all ranges disclosed herein are to be understood to encompass any and all subranges subsumed therein. For example, a stated range of “1.0 to 10.0” should be considered to include any and all subranges beginning with a minimum value of 1.0 or more and ending with a maximum value of 10.0 or less, e.g., 1.0 to 5.3, or 4.7 to 10.0, or 3.6 to 7.9.

[0022] All ranges disclosed herein are also to be considered to include the end points of the range, unless expressly stated otherwise. For example, a range of “between 5 and 10” should generally be considered to include the end points 5 and 10.

[0023] Further, when the phrase “up to” is used in connection with an amount or quantity, it is to be understood that the amount is at least a detectable amount or quantity. For example, a material present in an amount “up to” a specified amount can be present from a detectable amount and up to and including the specified amount.

I. Nerve Growth Inhibition Devices

[0024] In one aspect, nerve growth inhibition devices are described herein. In some embodiments, a nerve growth inhibition device comprises a tube having a proximal end and a distal end; and a matrix material disposed in the tube and comprising or defining one or more microchannels, wherein the proximal end of the tube comprises an opening operable to receive nerve tissue, the distal end of the tube is sealed, and the microchannels of the matrix material extend from the proximal end of the tube toward the distal end of the tube. In addition, in some cases, a device described herein further comprises a fluid, such as a saline solution, disposed in one or more microchannels of the device. Additionally, in some instances, one or more microparticles are disposed in the fluid, the microparticles comprising one or more nerve growth inhibition factors. Moreover, in some embodiments, a device described herein further comprises an electromagnetic radiation (EMR) shielding layer

substantially surrounding the exterior circumference of the tube. A device described herein can also comprise an encapsulation layer substantially surrounding the exterior circumference of the EMR shielding layer.

[0025] Turning now to specific components of devices, devices described herein comprise a tube having a proximal end and a distal end, wherein the proximal end of the tube comprises an opening operable to receive nerve tissue and the distal end of the tube is sealed. The tube and the opening of the tube can have any size, shape, and structure not inconsistent with the objectives of the present invention. In some embodiments, for instance, the tube has a substantially cylindrical shape. Further, in some cases, a tube described herein has an inner diameter between about 100 μm and about 50 mm, between about 1 mm and about 10 mm, or between about 1 mm and about 5 mm. In some cases, the tube has a diameter greater than about 50 mm or less than about 100 μm . The opening of a tube described herein, in some embodiments, can have the same inner diameter as the tube. Alternatively, in other instances, the opening can have a smaller size than the inner diameter of the tube. Further, in some cases, a tube described herein has a length between about 1 mm and about 200 mm, between about 5 mm and about 100 mm, between about 10 mm and about 30 mm, or between about 50 mm and about 150 mm.

[0026] Additionally, a tube described herein can comprise or be formed from any material not inconsistent with the objectives of the present invention. In some embodiments, for instance, the tube is formed from a polymeric material such as a polyurethane, a polyester, a polycarbonate, a polycaprolactone, a polylactic acid (PLA), a collagen, a polytetrafluoroethylene (PTFE), a polymethylmethacrylate (PMMA), an ethylene-vinylacetate copolymer (EVA), a polydimethylsiloxane (PDMS), a polyether polyurethane, a polyethyleneterephthalate (PET), a polysulfone (PS), a polyethyleneoxide (PEO) or polyethylene glycol (PEG), a polyethylene oxide-polypropylene oxide copolymer (PEO-PPO), a polyolefin such as polyethylene (PE) or polypropylene

(PP), or a combination of one or more of the foregoing. In some instances, the tube comprises a segment of implantation or catheter tubing, such as Micro-Renathane implantation tubing. Other materials may also be used.

[0027] Further, in some cases, a tube described herein has a flat or curved surface on the sealed end of the tube, such that the tube is sealed by a wall formed from the same material that forms the remainder of the tube. The wall, in some cases, can be a flat or curved wall that is continuous with the remainder of the tube. In such an embodiment, the sealed end or wall of the tube can block or substantially block the distal end of the microchannels of the device, such that the microchannels of the device terminate at the sealed end of the tube. In other cases, the tube is sealed with a capping material disposed in the distal end of the tube. In this instance, the capping material can block or substantially block the distal end of the one or more microchannels.

“Substantially” blocking the microchannels, for reference purposes herein, comprises blocking the microchannels sufficiently to prevent nerve tissue disposed in the microchannels from exiting the microchannels on the distal end. Therefore, the tube of a device described herein can be used to “cap” or otherwise isolate nerve endings and/or other nerve tissue.

[0028] Any capping material not inconsistent with the objectives of the present invention may be used. In some cases, for instance, a capping material comprises a gel, an adhesive, or a combination thereof. For example, in some instances, a capping material comprises agarose gel, a cyanoacrylate, or a combination thereof. Other gels and adhesives may also be used. Further, in some embodiments, a capping material comprises a plurality of capping layers. In some embodiments, for instance, a capping material comprises at least two layers or at least three layers. Moreover, the plurality of layers can comprise one or more gels, one or more adhesives, or a combination thereof. In some embodiments, a capping material comprises a first capping layer comprising an

agarose gel and a second capping layer comprising a cyanoacrylate. Other configurations are also possible.

[0029] A capping material or a capping layer of a capping material described herein can have any thickness not inconsistent with the objectives of the present invention. For example, in some cases, a capping material forms a wall having a thickness between about 1 μm and about 100 μm , between about 10 μm and about 10 mm , between about 10 μm and about 1 mm , between about 50 μm and about 10 mm , between about 100 μm and about 10 mm , or between about 100 μm and about 1 mm . Other thicknesses are also possible. Moreover, the thickness of a capping material or capping layer described herein, in some cases, can be selected based on the composition of the capping material or capping layer used and/or a desired ability of the capping material or capping layer to prevent nerve growth through the capping material or capping layer.

[0030] Devices described herein also comprise a matrix material disposed in the tube of the device, the matrix material comprising one microchannel or a plurality of microchannels. The matrix material of a device described herein can comprise any number of microchannels not inconsistent with the objectives of the present invention. In some cases, for example, a matrix material comprises between 1 and 10 microchannels or between 1 and 5 microchannels. In addition, the microchannels can have any size not inconsistent with the objectives of the present invention. In some embodiments, for instance, the microchannels have an average diameter between about 100 μm and about 2000 μm , between about 100 μm and about 1000 μm , or between about 300 μm and about 800 μm . In some cases, the microchannels have an average diameter of less than about 100 μm or greater than about 2000 μm . Further, the microchannels can have a length up to about 99%, up to about 95%, up to about 90%, or up to about 80% of the length of the tube of the device. Moreover, the size and/or number of microchannels in a device described

herein, in some cases, can be selected based on the size of a nerve to be treated by the device, wherein a larger nerve may require a larger number and/or a larger size of microchannels for effective treatment. For example, in some cases, a device for the treatment of a nerve having a diameter of about 1.5 mm may comprise three microchannels having a diameter of about 600 μm each.

[0031] In addition, the matrix material of a device described herein can comprise or be formed from any material not inconsistent with the objectives of the present invention. In some cases, for instance, a matrix material comprises or is formed from a polymeric material. In some embodiments, a matrix material comprises or is formed from a hydrogel, such as, for example, a biodegradable hydrogel. A “biodegradable” material, for reference purposes herein, comprises a material that can decompose within a biological environment, and may provide a non-toxic decomposition product. In some embodiments, a biodegradable material described herein comprises one or more ester bonds. A matrix material described herein can also comprise or be formed from a non-biodegradable material, including a non-biodegradable polymeric material. In some instances, a matrix material described herein comprises an agarose gel. Any agarose gel not inconsistent with the objectives of the present invention may be used. In some cases, for example, a matrix material comprises an agarose gel comprising at least about 3 weight percent agarose, at least about 4 weight percent agarose, or at least about 5 weight percent agarose, based on the total weight of the agarose gel. In some embodiments, a matrix material comprises an agarose gel comprising between about 3 weight percent and about 10 weight percent agarose, between about 3 weight percent and about 8 weight percent agarose, or between about 3 weight percent and about 4 weight percent agarose, based on the total weight of the agarose gel. In other cases, a matrix material comprises an agarose gel comprising less than about 3 weight percent or less than about 2 weight percent

agarose, based on the total weight of the agarose gel. In some instances, a matrix material comprises an agarose gel comprising between about 1 weight percent and about 2.5 weight percent agarose, based on the total weight of the agarose gel. Additional non-limiting examples of matrix materials suitable for use in some embodiments of devices described herein include polylactic-co-glycolic acid (PLGA), polylactic acid (PLA), polycaprolactone, polyurethane, polyester, polycarbonate, collagen, polytetrafluoroethylene (PTFE), polymethylmethacrylate (PMMA), an ethylene-vinylacetate copolymer (EVA), a polydimethylsiloxane (PDMS), polyether-polyurethane, a polyethyleneterephthalate (PET), a polysulfone (PS), a polyethyleneoxide (PEO) or polyethylene glycol (PEG), a polyethylene oxide-polypropylene oxide copolymer (PEO-PPO), a polyolefin such as polyethylene (PE) or polypropylene (PP), or a combination of one or more of the foregoing. Other matrix materials can also be used, alone or in combination.

[0032] Moreover, in some embodiments, the matrix material of a device described herein exhibits a compositional gradient from the proximal end of the tube toward the distal end of the tube. In some cases, the compositional gradient of the matrix material provides a nerve growth region and a nerve growth inhibition region within the tube, wherein the chemical composition of the nerve growth region differs from the chemical composition of the nerve growth inhibition region. A “nerve growth region” for reference purposes herein, comprises a spatial region in which nerve growth is promoted or at least not inhibited. A “nerve growth inhibition region,” for reference purposes herein, comprises a spatial region in which nerve growth is inhibited. The promotion or inhibition of nerve growth in a nerve growth or nerve growth inhibition region described herein, in some instances, can be caused by the chemical composition of the region. Moreover, in some cases, the nerve growth region of a tube described herein is located closer to the proximal end of the tube than the nerve growth inhibition region is. Thus, in some embodiments, the use of a

matrix material having a varying composition between the proximal end and the distal end of the tube of a device described herein can induce nerve axons to enter the tube and grow toward the distal end of the tube (within the nerve growth region), followed by inhibition or total cessation of nerve growth within the tube (once the nerves reach the nerve growth inhibition region), thereby sequestering the nerve endings within the tube and preventing neuroma formation.

[0033] Further, it is to be understood that the boundary between a nerve growth region and a nerve growth inhibition region of a device described herein can be a sharp boundary or a gradual boundary. For example, in some cases, a matrix material described herein, alone or in combination with a capping material described herein, has an essentially binary chemical composition, such that the compositional gradient forms sharply divided nerve growth and nerve growth inhibition regions within the tube. Alternatively, in other embodiments, the compositional gradient of the matrix material comprises a regularly changing gradient or a gradient having the form of a step function, wherein the chemical composition of the matrix material varies continuously or in a step-wise manner, respectively, as a function of distance from the proximal end of the tube.

[0034] For example, in some cases, a compositional gradient of a matrix material is provided by varying the weight percent of agarose in an agarose gel matrix material, where the weight percent of agarose is varied as a function of the distance from the proximal end of the tube. In some such embodiments, the weight percent of agarose increases as a function of distance from the proximal end of the tube. Moreover, the boundary between the nerve growth region and the nerve growth inhibition region of the matrix material in such an embodiment can be formed by the transition from a weight percent of agarose below about 3 weight percent or below about 2 weight percent (the nerve growth region) to a weight percent of agarose above about 3 weight percent or above about 2.5

weight percent (the nerve growth inhibition region). Other configurations of a compositionally graded matrix material are also possible.

[0035] Devices described herein, in some embodiments, further comprise a fluid disposed in one or more microchannels of the device. Any fluid not inconsistent with the objectives of the present invention may be used. In some cases, the fluid comprises a saline solution such as a sterile solution of sodium chloride in water. Non-limiting examples of saline solutions suitable for use in some embodiments described herein include normal saline (about 0.90% w/v NaCl) and hypertonic saline (about 3-7% w/v NaCl). Other saline solutions may also be used.

[0036] In addition, in some cases, one or more microparticles are disposed in the fluid of a device described herein. Moreover, the microparticles can comprise one or more nerve growth inhibition factors disposed within the interior and/or on the exterior surface of the microparticles. Any nerve growth inhibition factor not inconsistent with the objectives of the present invention may be used. In some embodiments, for example, a nerve growth inhibition factor comprises an axon regeneration inhibitor (ARI). Non-limiting examples of ARIs suitable for use in some embodiments described herein include chondroitin sulphate proteoglycans (CSPGs), myelin-associated glycoprotein (MAG), reticulon-4 (also known as Neurite outgrowth inhibitor or Nogo), and oligodendrocyte-myelin glycoprotein (OMgp). A nerve growth inhibition factor can be present in a microparticle described herein in any amount not inconsistent with the objectives of the present invention. In some embodiments, for instance, a nerve growth inhibition factor is present in a microparticle in an amount between about 0.0001 and about 1 weight percent, based on the total weight of the microparticle.

[0037] Further, a microparticle can have any size and shape and be formed from any material not inconsistent with the objectives of the present invention. In some embodiments, for example, a microparticle is a spherical or

substantially spherical microparticle having a diameter between about 10 μm and about 1000 μm or between about 50 μm and about 500 μm . Microparticles having other sizes and shapes may also be used. In addition, in some cases, a microparticle is formed from a polymeric material, including any polymeric material described hereinabove for a tube or matrix material. Alternatively, in other instances, a microparticle is formed from an inorganic material such as silicon dioxide and/or titanium dioxide. Other materials may also be used.

[0038] The use of microparticles described herein, in some embodiments, can permit the time-delayed release of nerve growth inhibition factors into the microchannels of a device described herein. In this manner, a device described herein can facilitate nerve growth into and within the device at early time points following implantation of the device for the prevention and/or treatment of a neuroma, but inhibit or completely stop nerve growth within the device at later time points. Thus, in some embodiments comprising microparticles described herein, the matrix material of the device may or may not exhibit a compositional gradient described herein.

[0039] Additionally, in some cases, the microchannels of a device described herein are free or substantially free of an extracellular matrix material (ECM), such as collagen, disposed within the microchannels. A device that is “substantially” free of an ECM, for reference purposes herein, comprises a device that includes less than about 10 weight percent, less than about 5 weight percent, less than about 3 weight percent, less than about 1 weight percent, less than about 0.5 weight percent, or less than about 0.1 weight percent ECM disposed in the microchannels, based on the total weight of the contents of the microchannels.

[0040] Devices described herein, in some embodiments, further comprise an electromagnetic radiation (EMR) shielding layer. The EMR shielding layer can surround or substantially surrounding the exterior circumference of the tube of the device. For example, in some cases, the shielding layer surrounds at least

about 70%, at least about 80%, at least about 90%, at least about 95%, or at least about 99% of the circumferential surface area of exterior of the tube. Moreover, in some embodiments, the shielding layer is disposed directly on the exterior surface of the tube. In other cases, one or more additional layers such as one or more adhesive layers are disposed between the tube and the shielding layer.

[0041] Further, the shielding layer of a device described herein, in some embodiments, can absorb and/or reflect incident EMR that would otherwise impinge on nerve tissue disposed within the device. In some cases, the shielding layer absorbs and/or reflects at least about 60%, at least about 70%, at least about 80%, at least about 90%, at least about 95%, or at least about 99% of incident radiation having a radio frequency (RF), such as a frequency between about 3 kHz and about 300 GHz, between about 3 kHz and about 30 kHz, between about 30 kHz and about 300 kHz, between about 300 kHz and about 3 MHz, between about 3 MHz and about 30 MHz, between about 30 MHz and about 300 MHz, between about 300 MHz and about 3 GHz, or between about 300 MHz and about 1000 MHz. In other instances, the shielding layer absorbs and/or reflects between about 60% and about 100%, between about 75% and about 99%, between about 80% and about 99%, between about 80% and about 95%, between about 85% and about 99%, or between about 90% and about 99.9% of incident EMR having a frequency described hereinabove.

[0042] The shielding layer of a device described herein can comprise or be formed from any material not inconsistent with the objectives of the present invention. For example, in some cases, a shielding layer comprises or is formed from an electrically conductive metal, including an elemental metal, metal alloy, or combination of metals. Any electrically conductive metal not inconsistent with the objectives of the present invention may be used. In some instances, a shielding layer comprises or is formed from one or more of cobalt, silver, copper, gold, aluminum, molybdenum, zinc, lithium, tungsten, brass,

carbon, nickel, iron, palladium, platinum, tin, bronze, carbon steel, lead, titanium, and stainless steel. In other embodiments, a shielding layer comprises or is formed from an electrically conductive polymeric material. Any electrically conductive polymeric material not inconsistent with the objectives of the present invention may be used. In some cases, for instance, an electrically conductive polymeric materials comprises or is formed from a polypyrrole (PPY), a polyaniline (PANI), a polythiophene (PT), a poly(3,4-ethylenedioxythiophene) (PEDOT), a poly(p-phenylene sulfide) (PPS), a polyacetylene (PAC), a poly(p-phenylene vinylene) (PPV), or a combination of two or more of the foregoing.

[0043] Additionally, a shielding layer of a device described herein can have any thickness not inconsistent with the objectives of the present invention. In some embodiments, for instance, a shielding layer has a thickness between about 500 nm and about 1 mm, between about 500 nm and about 500 μm , between about 1 μm and about 500 μm , between about 1 μm and about 100 μm , between about 10 μm and about 500 μm , between about 10 μm and about 100 μm , between about 100 μm and about 1 mm, or between about 100 μm and about 500 μm . In some cases, a shielding layer has a thickness of less than about 500 nm or more than about 1 mm. Moreover, the thickness of a shielding layer described herein, in some cases, can be selected based on a desired absorptivity and/or reflectivity of the shielding layer.

[0044] The use of an EMR shielding layer described herein, in some embodiments, can reduce the amount of pain registered by a nerve disposed in a device described herein. In particular, the use of an EMR shielding layer can reduce the amount of pain induced by incident or environmental EMR.

[0045] A device described herein, in some cases, further comprises an encapsulation layer substantially surrounding the exterior circumference of an EMR shielding layer. Such an encapsulation layer can be formed from any material and have any thickness not inconsistent with the objectives of the

present invention. In some embodiments, for instance, an encapsulation layer is formed from an electrically insulating layer such as a rubber or plastic. Other materials may also be used. Further, in some cases, an encapsulation layer described herein has a thickness between about 10 μm and about 10 mm. Other thicknesses may also be used.

[0046] Various components of devices have been described herein. It is to be understood that a device according to the present invention can comprise any combination of components and features not inconsistent with the objectives of the present invention. For example, in some cases, a device described herein comprises any tube described herein in combination with any matrix material described herein and any EMR shielding layer described herein.

[0047] Further, a device described herein can be made in any manner not inconsistent with the objectives of the present invention. In some instances, for example, a casting and/or negative extrusion process is used to form a tube or matrix material comprising one or more microchannels or lumens. In other embodiments, a device described herein is formed by 3D printing.

II. Methods of Preventing and Treating Neuromas

[0048] In another aspect, methods of preventing and treating neuromas are described herein. In some cases, preventing and/or treating a neuroma comprises inhibiting nerve growth and/or providing analgesia. In some embodiments, such a method comprises disposing a device described herein in a biological compartment comprising nerve tissue. Any device described hereinabove in Section I may be used. Further, the biological compartment can comprise any biological compartment not inconsistent with the objectives of the present invention. In some instances, the biological compartment comprises, consists, or consists essentially of nerve tissue, including nerve endings. In some cases, the biological compartment comprises a stump of a severed nerve, and the device is disposed on, over, or near the nerve stump. Additionally, in

some cases, disposing a device described herein in a biological compartment described herein comprises surgically placing the device in the desired location.

[0049] Some embodiments described herein are further illustrated in the following non-limiting examples.

EXAMPLE 1

Device for Inhibiting Nerve Growth

[0050] A device for inhibiting nerve growth according to one embodiment described herein was prepared as follows. Specifically, a transparent multi-luminal (or multi-channel) matrix (TMM) casting device was used. Such a device is described in United States Patent Application Publication 2008/0300691, which is hereby incorporated by reference in its entirety. The TMM casting device consists of a square plastic open frame that accommodates an external polyurethane (or similar material) catheter tube with holes at opposite ends through which metal rods can be inserted. To form a device, the precursor of a desired matrix material described herein (such as an agarose gel) was added over the metal rods (such as titanium rods) disposed in the tube, followed by polymerization of the precursor to provide the matrix material. In this manner, the metal rods were effectively embedded in the matrix material. The metal rods were then removed from the frame to provide a matrix material comprising microchannels corresponding to the areas vacated by the metal rods. This matrix material could then be disposed within a tube described herein, including a tube sealed at the distal end.

[0051] Alternatively, a tube open on both ends could be disposed in the TMM frame prior to placement of the metal rods and the matrix material precursor within the tube. The fabrication procedure could then be completed as described above. It was also possible to provide a saline solution within the microchannels by disposing the saline solution in a loading well of the TMM prior to removal of the metal rods. The loading well was disposed such that the

contents of the loading well were proximate the metal rods. Rapid removal of the metal rods resulted in a negative pressure within the microchannels, which was able to “pull” or “suck” the saline solution into the microchannels. Next, a separately formed capping material was prepared and disposed in the distal end of the tube to seal the distal end. In some cases, the capping material was disposed in the distal end of the tube after the tube was disposed over and sutured to a severed nerve. In such cases, an adhesive capping material could be polymerized in situ with saline.

[0052] A device formed in this manner is depicted schematically in **FIG. 1** and **FIG. 2**. **FIG. 1** illustrates a sectional view of the device from the side. **FIG. 2** illustrates a sectional view of the device taken along lines 2--2. As illustrated in **FIGS. 1** and **2**, the nerve growth inhibition device (100) comprises a polyurethane tube (110) having a proximal end (111) and a distal end (112). A matrix material (120) is disposed in the tube (110) and comprises a plurality of microchannels (130). The proximal end (111) of the tube (110) comprises an opening (113) operable to receive nerve tissue (not shown). The distal end (112) of the tube (110) is sealed, and the microchannels (130) of the matrix material (120) extend from the proximal end (111) toward the distal end (112) of the tube (110). In the embodiment of **FIG. 1**, the tube (110) is sealed with a capping material (140) disposed in the distal end (112) of the tube (110) and the capping material (140) blocks or substantially blocks the distal end (112) of the one or more microchannels (130). The capping material (140) comprises a first capping layer (141) comprising 3 wt. % agarose gel and a second capping layer (142) formed from a cyanoacrylate adhesive. The first capping layer (141) can also be considered to form a nerve growth inhibition region (122) within the device (100), in contrast to a nerve growth region (121) provided by the matrix material (120), which could be formed, for example, from 1.5 wt.% agarose gel.

[0053] Further, as illustrated in **FIG. 1**, the device 100 is in fluid communication with a saline loading well (210) of a TMM casting device. The loading well (210) is in fluid communication with the microchannels through a tube insertion node (220).

EXAMPLE 2

Device for Inhibiting Nerve Growth

[0054] A device for inhibiting nerve growth according to one embodiment described herein is prepared as follows. The manufacturing process is carried out in a class 10,000 cleanroom environment. The process consists of semi-automated and manual steps. Semi-automated processes are performed using a manufacturing cell developed with a 3-axis gantry type positioning system having a payload capacity of 4 kg on the z-axis and a precision of 20 μm . The system includes the following process tools: a pick and place gripper; a dip coating gripper; and two precision dispensing syringes. The manufacturing cell contains multiple stations that include heating and cooling areas, a dip coating station, tools to create channels, and various fixtures to hold the device. Positioning is accomplished via precision touch sensors and encoders. Dispensing of the matrix material is performed by precision Engineered Fluid Dispensing (EFD) systems using heated syringes. The manufacturing cell is controlled by custom software written in Labview. Devices having different sizes of microchannels and/or tubes can be formed by altering the tooling of the manufacturing cell.

[0055] To manufacture a device comprising a tube formed from polyurethane, a sacrificial mandrill is used, the mandrill having a diameter that corresponds to the desired inner diameter of the polyurethane tube. The mandrill undergoes several dip coating and drying cycles in a polyurethane or polyurethane precursor solution. After the desired thickness of polyurethane is achieved on the mandrill, the dip-coated mandrill is removed to create the polyurethane

tube. Next, an EMR shielding layer material is disposed on the outer surface of the polyurethane tube. The device is then vapor-sterilized. Finally, a TMM casting device similar to that described in Example 1 above is used to provide a matrix material comprising microchannels within the coated polyurethane tube. The TMM casting device can be pulled manually or by the robot pick and place gripper to form the microchannels.

[0056] The resulting device is depicted schematically in **FIG. 3** and **FIG. 4**. **FIG. 3** illustrates a perspective view of the device. **FIG. 4** illustrates a cutaway perspective view of the device. As illustrated in **FIG. 4**, the nerve growth inhibition device (100) comprises a tube (110) having a proximal end (111) and a distal end (112). A matrix material (120) comprising agarose gel is disposed in the tube (110) and comprises a plurality of microchannels (130). Further, the matrix material (120) has a binary chemical composition comprising a nerve growth region (121) and a nerve growth inhibition region (122). The nerve growth region (121) is provided by a matrix material composition comprising 1.5 wt.% agarose, and the nerve growth inhibition region (122) is provided by a matrix material composition comprising 3 wt.% agarose. The binary chemical composition of the matrix material (120) is provide by serially disposing the differing agarose gels within the tube (110). The proximal end (111) of the tube (110) comprises an opening (113) operable to receive nerve tissue (not shown). The distal end (112) of the tube (110) is sealed, and the microchannels (130) of the matrix material (120) extend from the proximal end (111) toward the distal end (112) of the tube (110). In the embodiment of **FIG. 4**, the tube (110) includes a sealed end comprising a wall (114) formed from the same material as the remainder of the tube (110). The wall (114) blocks or substantially blocks the distal end (112) of the one or more microchannels (130). An EMR shielding layer (150) is disposed on the exterior circumference of the tube (110). Further, an encapsulation layer (160) is disposed around the shielding layer (150). The EMR shielding layer (150) is formed by wrapping the EMR

shielding material around the tube (110). The encapsulation layer (160) is formed by dip-coating with additional polyurethane.

EXAMPLE 3

Method of Inhibiting Nerve Growth

[0057] A method of inhibiting nerve growth according to one embodiment described herein was carried out as follows. Specifically, a device having the structure described in Example 1 was used to inhibit nerve growth or regeneration in rats (the “experimental” device). For comparison, a device similar to the device of Example 1 was used as a control (the “control” device). However, the tube of the control device was not sealed at the distal end. Instead, both ends of the tube of the control device included openings.

[0058] Both devices (control and experimental) were disposed over an acutely severed proximal nerve stump in living test animals and directed toward a distal nerve stump of the animals. Specifically, twenty adult Long Evans rats were used to test the regeneration inhibition method. Seven animals were treated with the control device and observed after 60 days (n = 3) or 210 days (n = 4). Thirteen animals were treated with the experimental device and observed after 60 days (n = 5) or 210 days (n = 8). Observation was carried out by photographing the implantation sites and by gross morphology of the harvested devices following the stated time period. The relative distance of tissue penetration through the length of the tubes of the devices was determined. The amount of tissue area per tube was also determined. For quantification purposes, recovered regenerated nerves were divided into proximal and distal segments and embedded in paraffin for transverse sectioning. In addition, sections at 6 mm penetration, the critical regeneration distance observed in the experimental group, were further analyzed by (a) staining with hematoxylin and eosin (H&E), a common histological stain for

visualizing cellular morphology, and (b) antibodies against neurofilament protein (NFP), a marker specific for neuronal axons.

[0059] Nerve growth and vascularization was observed in both the experimental and control groups after 210 days. Specifically, organized tissue regrowth consisting of axons, Schwann cells, and fibroblasts was observed within the microchannels of the tubes of each of the implants in both the control and experimental groups. Flat cells resembling a perineurium were organized around the outer layer of regenerating tissue, while NFP-positive axons were observed more centrally within the conduits. However, quantitative analysis of the regenerated nerve area indicated that nerve growth was statistically lower in the group treated with the experimental device. The number of regenerated axons in the experimental group was up to 50% less than in the control group. Moreover, the penetration of the regenerated nerves within the microchannels of the experimental device was limited to only the first 7 mm of the tube. In contrast, nerve cables reconnected to the distal nerve stump in each instance in the control group. Some results are illustrated in **FIG. 5**.

[0060] In addition, the growth of nerves within the experimental device is illustrated schematically in **FIG. 6**. As illustrated in **FIG. 6**, a nerve growth inhibition device (100) is disposed over a nerve stump (300). Specifically, the nerve stump is inserted into the tube (110) of the device (100) to a nerve insertion point (310) corresponding to the proximal end (131) of the microchannels (130). Regenerated nerve axons (320) initially are guided within the microchannels (130) toward the distal end (112) of the tube (110). Within a nerve growth region (121) of the device (100), the regenerated nerve axons (320) are viable. However, within a nerve growth inhibition region (122) of the device (100), growth of the nerve axons (320) is retarded and ultimately ceases.

EXAMPLE 4

Method of Providing Analgesia

[0061] A method of providing analgesia according to one embodiment described herein was carried out as follows. First, a device having a structure corresponding to Example 1 was used to reduce mechanically-induced pain caused by neuromas. Specifically, 17 adult Lewis rats were subjected to surgery according to the tibial neuroma transposition (TNT) model described in Dorsi et al., “The tibial neuroma transposition (TNT) model of neuroma pain and hyperalgesia,” *Pain*, 134(3), 320-334 (2008). Briefly, the posterior tibial nerve of an anesthetized animal was exposed from approximately 8 mm proximal to the calcaneal branch to 1 mm distal to the plantar nerve bifurcation. The transected tibial nerve was then redirected to approximately 8-10 mm superior to the lateral malleolus in the hind limb in which the tibial nerve will be ligated and to the lateral side of the ankle. This transposition and superficial placement of the tibial nerve permitted routine screening for abnormal sensation at this site. Therefore, this model created a neuroma that was accessible for mechanical testing and allowed evaluation of pain perception in a way that resembles clinical evaluation of the Hoffman-Tinel sign in amputees (i.e., neuroma tenderness).

[0062] Mechanical testing was carried out using a von Frey test derived from a clinical procedure to assess allodynia, particularly in patients with neuropathic pain. The von Frey test is considered reliable to ascertain mechanoreceptive pain in rats. The von Frey filaments were plastic hairs, 5 cm long and having various diameters, fixed on applicators. For testing, each animal was placed separately in a clear chamber with a wire-mesh floor and allowed to acclimate before testing. Each animal was then probed with a 300 g von Frey filament at the neuroma position. For comparison, the uninjured side was also palpated.

[0063] The animals were randomly assigned to three groups (each having n = 4): (1) neuroma positive control, (2) treatment with a hollow non-biodegradable polyurethane tube, and (3) treatment with a device according to Example 1. Two months following the TNT surgery, all animals in groups (1)

and (2) developed a vigorous paw withdrawal in response to von Frey stimulation at the ligature, which persisted for all three months over which these animals were observed. In sharp contrast, rats implanted with the nerve growth inhibition device of Example 1 showed a significant reduction in mechanically-induced pain.

[0064] Additionally, when the neuromas were dissected at the end of the study (after 8 months), conventional neuromas had formed in all control TNT animals. Those implanted with hollow polyurethane tubes showed no nerve growth into the nerve conduit, but clear neuromas formed at the proximal site. In contrast, the animals of group (3) showed no neuroma formation. Instead, nerve fiber growth into the device microchannels was observed. The regenerated fascicles extended inside the tube and then stopped at the middle of the tube's length. The binary composition of the matrix material hydrogel of the device promoted initial nerve growth into the microchannels (in regions comprising 1.5 wt.% agarose) but halted further growth when the nerves reached a higher density gel (3 wt.% agarose). The cyanoacrylate capping material added an extra level of safety, since it could prevent the escape of any nerve fibers that extended beyond the higher density gel. Thus, the regenerated nerves were essentially trapped inside the device.

[0065] Various embodiments of the present invention have been described in fulfillment of the various objectives of the invention. It should be recognized that these embodiments are merely illustrative of the principles of the present invention. Numerous modifications and adaptations thereof will be readily apparent to those skilled in the art without departing from the spirit and scope of the invention.

CLAIMS

That which is claimed is:

1. A nerve growth inhibition device comprising:
a tube having a proximal end and a distal end; and
a matrix material disposed in the tube and comprising one or more microchannels,
wherein the proximal end of the tube comprises an opening operable to receive nerve tissue, the distal end of the tube is sealed, and the microchannels of the matrix material extend from the proximal end of the tube toward the distal end of the tube.
2. The device of claim 1, wherein the tube is sealed with a capping material disposed in the distal end of the tube and the capping material blocks or substantially blocks the distal end of the one or more microchannels.
3. The device of claim 2, wherein the capping material comprises a gel, an adhesive, or a combination thereof.
4. The device of claim 2, wherein the capping material comprises agarose gel, a cyanoacrylate, or a combination thereof.
5. The device of claim 2, wherein the capping material comprises a plurality of capping layers.
6. The device of claim 5, wherein a first capping layer comprises agarose gel and a second capping layer comprises a cyanoacrylate.

7. The device of claim 1, wherein the matrix material comprises a plurality of microchannels.
8. The device of claim 1, wherein the matrix material comprises an agarose gel, a polylactic-co-glycolic acid, a polylactic acid, a caprolactone, or a combination thereof.
9. The device of claim 1, wherein the matrix material comprises an agarose gel.
10. The device of claim 1, wherein a fluid is disposed in the one or more microchannels.
11. The device of claim 10, wherein the fluid comprises a saline solution.
12. The device of claim 1, wherein the microchannels are free or substantially free of an extracellular matrix material disposed within the microchannels.
13. The device of claim 12, wherein the extracellular matrix material comprises collagen.
14. A method of inhibiting nerve growth comprising:
 - disposing a device in a biological compartment comprising nerve tissue, the device comprising
 - a tube having a proximal end and a distal end; and
 - a matrix material disposed in the tube and comprising one or more microchannels,

wherein the proximal end of the tube comprises an opening operable to receive the nerve tissue, the distal end of the tube is sealed, and the microchannels of the matrix material extend from the proximal end of the tube toward the distal end of the tube.

15. The method of claim 14, wherein the biological compartment comprises a stump of a severed nerve.

16. The method of claim 15, wherein the device is disposed over the nerve stump.

17. A method of providing analgesia comprising:
disposing a device in a biological compartment comprising nerve tissue,
the device comprising
a tube having a proximal end and a distal end; and
a matrix material disposed in the tube and comprising one or more
microchannels,

wherein the proximal end of the tube comprises an opening operable to receive the nerve tissue, the distal end of the tube is sealed, and the microchannels of the matrix material extend from the proximal end of the tube toward the distal end of the tube.

18. The method of claim 17, wherein the biological compartment comprises a stump of a severed nerve.

19. The method of claim 18, wherein the device is disposed over the nerve stump.

ABSTRACT

In one aspect, nerve growth inhibition devices are described herein. In some embodiments, a nerve growth inhibition device described herein comprises a tube having a proximal end and a distal end. A matrix material is disposed in the tube, and the matrix material comprises one or more microchannels. The proximal end of the tube comprises an opening operable to receive nerve tissue, the distal end of the tube is sealed, and the microchannels of the matrix material extend from the proximal end of the tube toward the distal end of the tube.

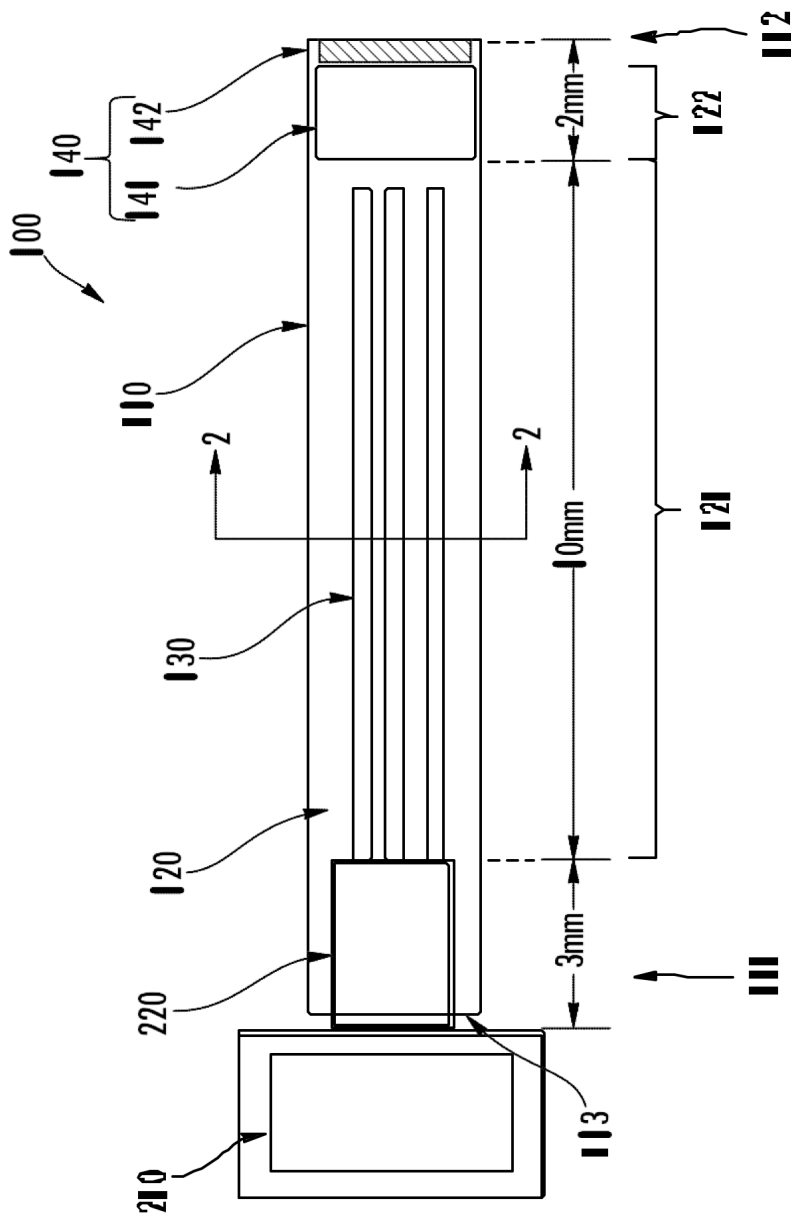


FIG. 7

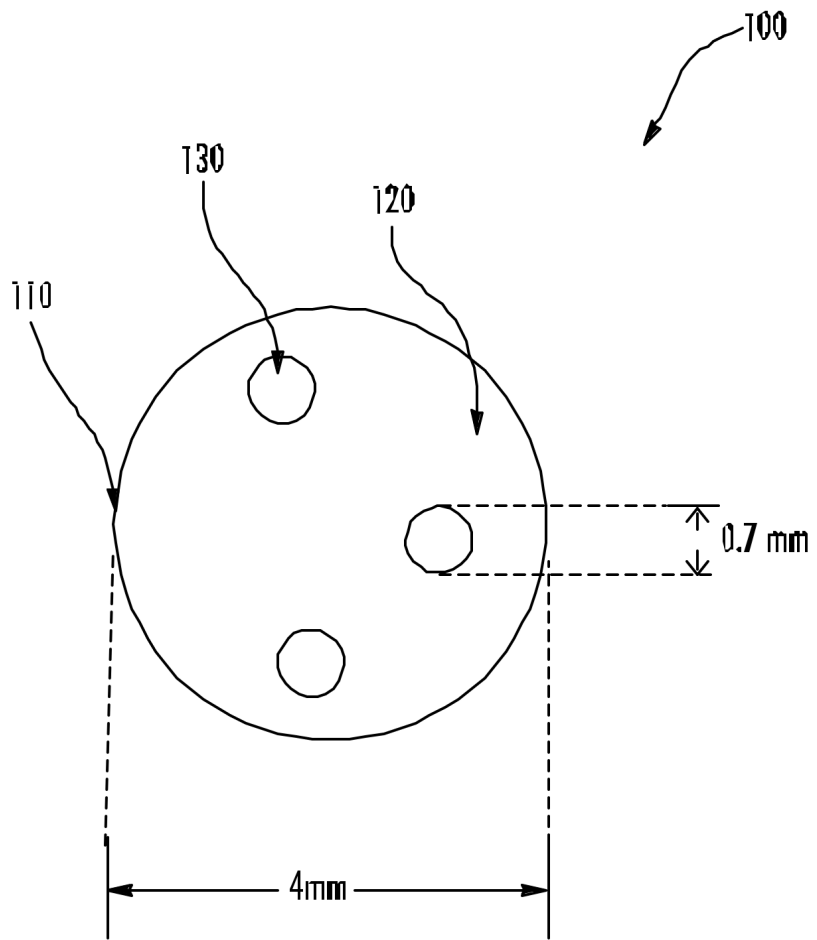


FIG. 2

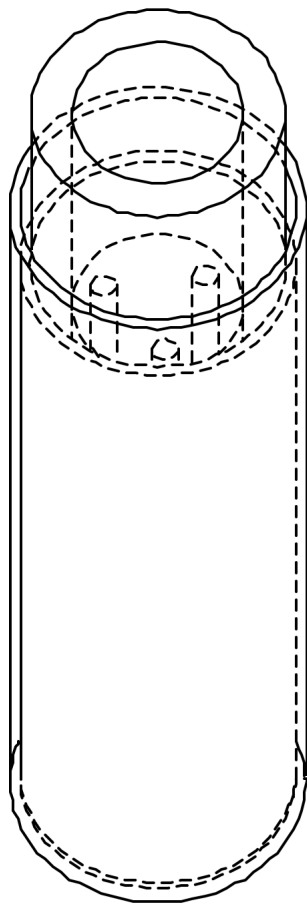


FIG. 3

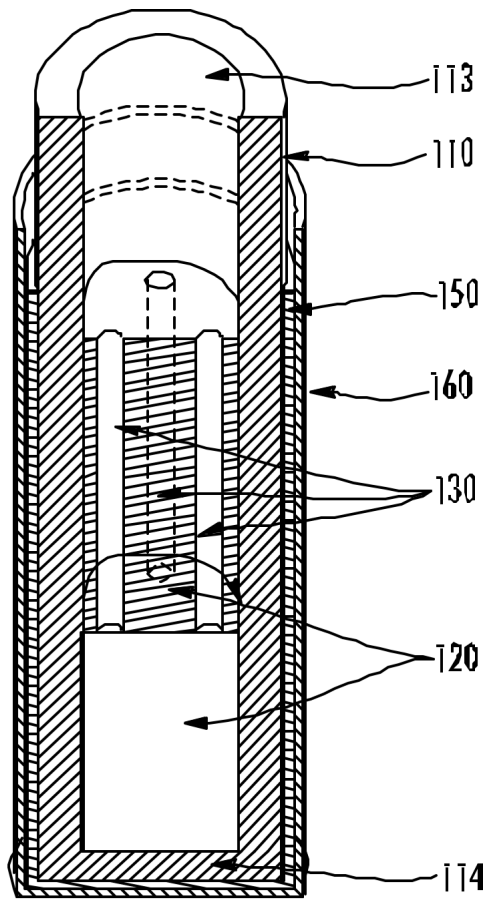


FIG. 4

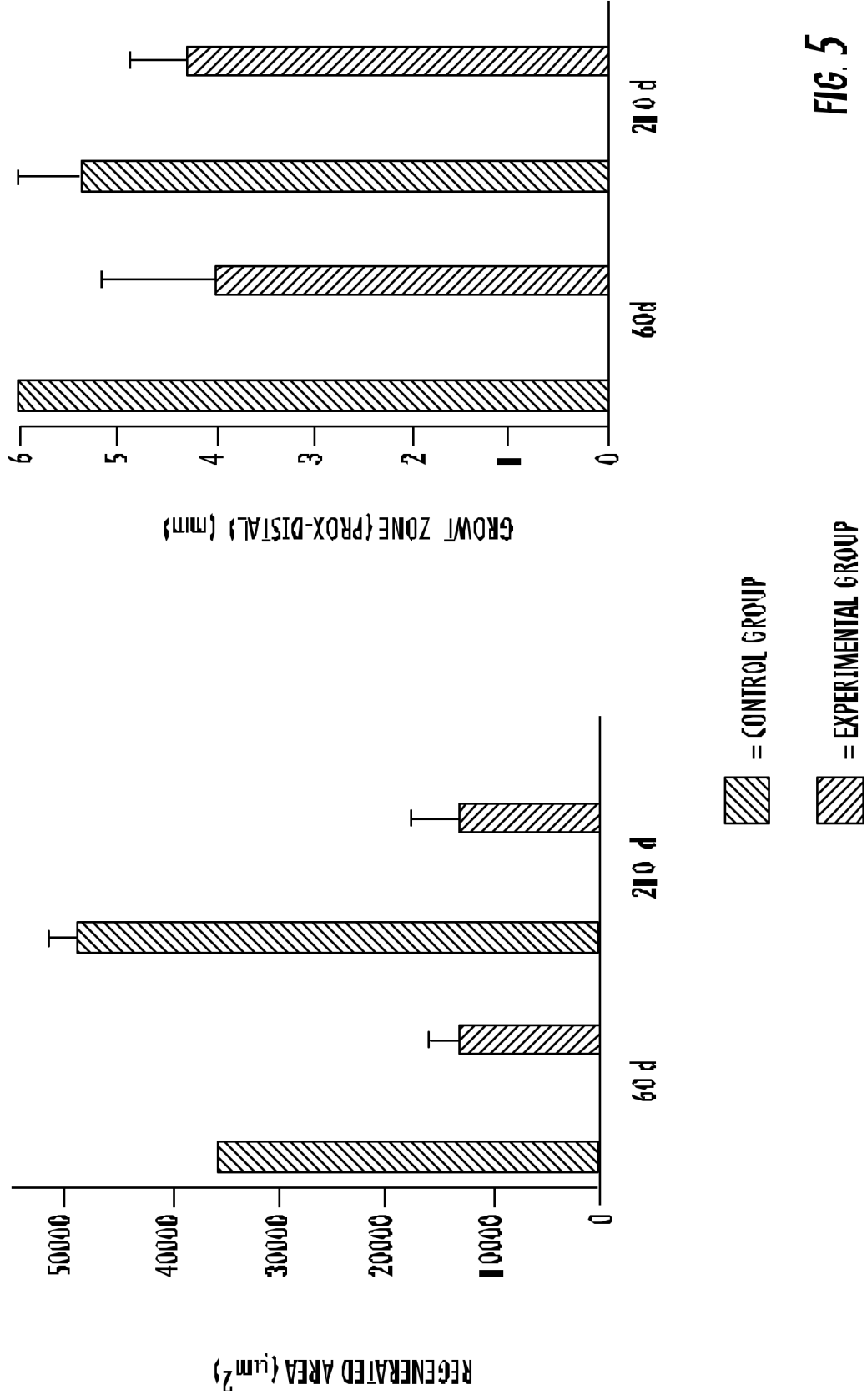


FIG. 5

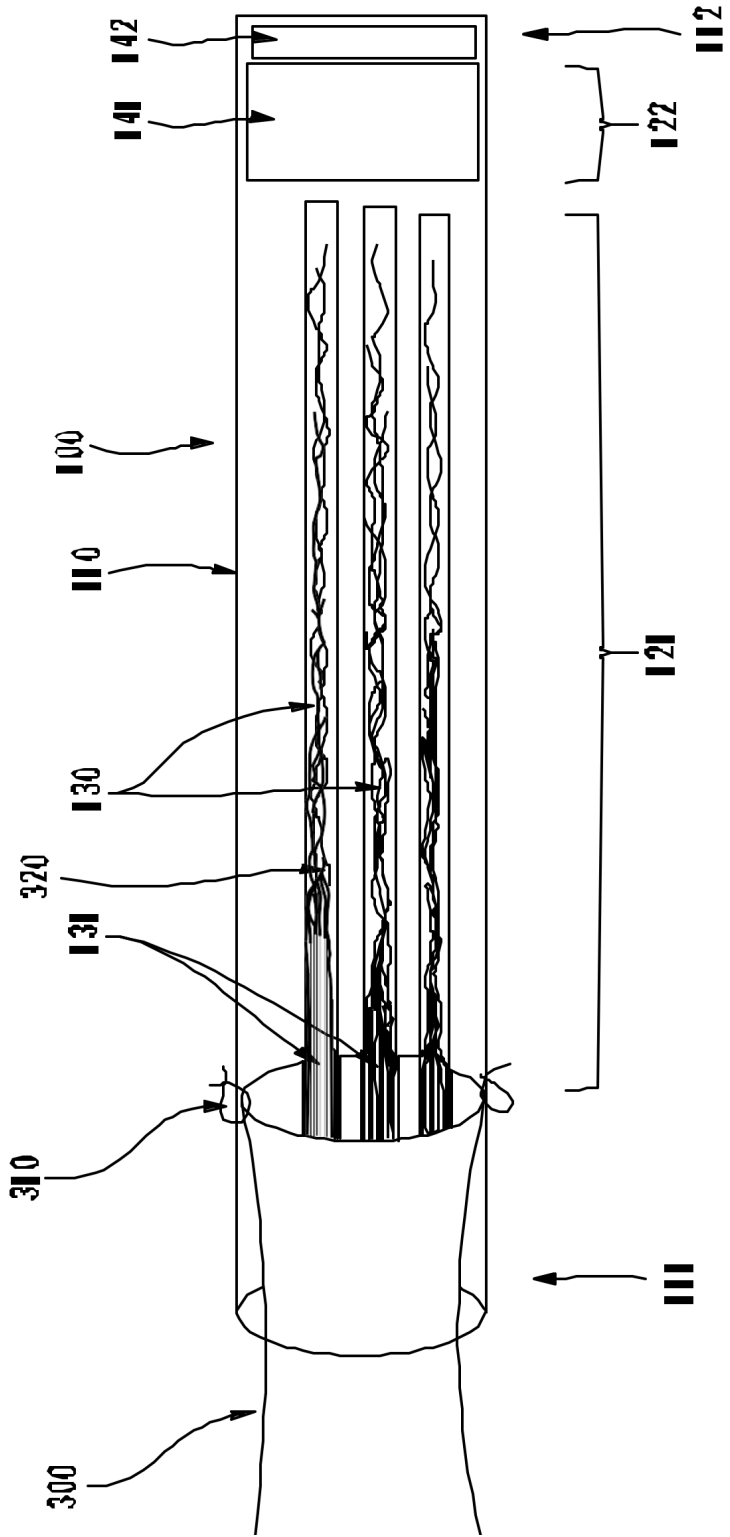


FIG. 6

References

1. Johnson, B., Ober, W., Garrison, C. & Silverthorn, A. in *Human Physiology: An Integrated Approach* (Pearson Benjamin Cummings, San Francisco, 2009).
2. Lundborg, G. in *Nerve Injury and Repair - Regeneration, Reconstruction, and Cortical Remodeling (Second Edition)* 256 (Churchill Livingstone, 2005).
3. Brushart, T. M. in *Nerve Repair* 480 (Oxford University Press, USA, 2011).
4. Brushart, T. M. *et al.* Schwann cell phenotype is regulated by axon modality and central–peripheral location, and persists in vitro. *Exp. Neurol.* **247**, 272-281 (2013).
5. Allt, G. & Lawrenson, J. G. The blood–nerve barrier: enzymes, transporters and receptors—a comparison with the blood–brain barrier. *Brain Res. Bull.* **52**, 1-12 (2000).
6. Savastano, L. E. *et al.* Sciatic nerve injury: A simple and subtle model for investigating many aspects of nervous system damage and recovery. *J. Neurosci. Methods* **227**, 166-180 (2014).
7. Sunderland, S. **A classification of peripheral nerve injuries producing loss of function** *Brain* **74**, 491-516 (1951).
8. Seddon, H. J. A classification of nerve injuries. *Br Med J* **2**, 237-239 (1942).
9. Belkas, J. S., Shoichet, M. S. & Midha, R. Axonal guidance channels in peripheral nerve regeneration. *Operative Techniques in Orthopaedics* **14**, 190-198 (2004).
10. Daly, W., Yao, L., Zeugolis, D., Windebank, A. & Pandit, A. A biomaterials approach to peripheral nerve regeneration: bridging the peripheral nerve gap and enhancing functional recovery. *Journal of The Royal Society Interface* **9**, 202-221 (2012).

11. Deal, D. N., Griffin, J. W. & Hogan, M. V. Nerve Conduits for Nerve Repair or Reconstruction. *Journal of the American Academy of Orthopaedic Surgeons* **20**, 63-68 (2012).
12. Johnson, E. O. & Soucacos, P. N. Nerve repair: Experimental and clinical evaluation of biodegradable artificial nerve guides. *Injury* **39**, 30-36 (2008).
13. Hess, J. R. *et al.* Use of Cold-Preserved Allografts Seeded with Autologous Schwann Cells in the Treatment of a Long-Gap Peripheral Nerve Injury. *Plast. Reconstr. Surg.* **119** (2007).
14. Whitlock, E. L. *et al.* Processed allografts and type I collagen conduits for repair of peripheral nerve gaps. *Muscle Nerve* **39**, 787-799 (2009).
15. Navarro, X., Vivó, M. & Valero-Cabré, A. Neural plasticity after peripheral nerve injury and regeneration. *Prog. Neurobiol.* **82**, 163-201 (2007).
16. Cheepudomwit, T., Güzelsu, E., Zhou, C., Griffin, J. W. & Höke, A. Comparison of cytokine expression profile during Wallerian degeneration of myelinated and unmyelinated peripheral axons. *Neurosci. Lett.* **430**, 230-235 (2008).
17. Ramer, M. S., French, G. D. & Bisby, M. A. Wallerian degeneration is required for both neuropathic pain and sympathetic sprouting into the DRG. *Pain* **72**, 71-78 (1997).
18. Wu, C. *et al.* Arp2/3 Is Critical for Lamellipodia and Response to Extracellular Matrix Cues but Is Dispensable for Chemotaxis. *Cell* **148**, 973-987.
19. Lowery, L. A. & Vactor, D. V. The trip of the tip: understanding the growth cone machinery. *Nature Reviews Molecular Cell Biology* **10**, 332-343 (2009).
20. Gordon, T. The role of neurotrophic factors in nerve regeneration. *Neurosurgical Focus* **26**, E3 (2009).

21. Madduri, S. & Gander, B. Growth factor delivery systems and repair strategies for damaged peripheral nerves. *J. Controlled Release* **161**, 274-282 (2012).
22. Blondet, B., Carpentier, G., Lafdil, F. & Courty, J. Pleiotrophin Cellular Localization in Nerve Regeneration after Peripheral Nerve Injury. *Journal of Histochemistry & Cytochemistry* **53**, 971-977 (2005).
23. Chung, H. W. *et al.* Pleiotrophin (PTN) and midkine (MK) mRNA expression in eutopic and ectopic endometrium in advanced stage endometriosis. *Molecular Human Reproduction* **8**, 350-355 (2002).
24. Mi, R., Chen, W. & Höke, A. Pleiotrophin is a neurotrophic factor for spinal motor neurons. *Proceedings of the National Academy of Sciences* **104**, 4664-4669 (2007).
25. Kehoe, S., Zhang, X. F. & Boyd, D. FDA approved guidance conduits and wraps for peripheral nerve injury: A review of materials and efficacy. *Injury*.
26. Giusti, G. *et al.* Return of Motor Function after Segmental Nerve Loss in a Rat Model: A Comparison of Autogenous Nerve Graft, Collagen Conduit and Processed Nerve Allograft (Axogen): Level 1 Evidence. *J. Hand Surg.* **34**, 27-28 (2009).
27. Brooks, D. N. *et al.* Processed nerve allografts for peripheral nerve reconstruction: A multicenter study of utilization and outcomes in sensory, mixed, and motor nerve reconstructions. *Microsurgery* **32**, 1-14 (2012).
28. Sedaghati, T., Jell, G. & Seifalian, A. M. in *Regenerative Medicine Applications in Organ Transplantation* (eds Orlando, G., Lerut, J., Soker, S. & Stratta, R. J.) 799-810 (Academic Press, Boston, 2014).
29. Angius, D. *et al.* A systematic review of animal models used to study nerve regeneration in tissue-engineered scaffolds. *Biomaterials* **33**, 8034-8039 (2012).
30. Tansey, K., Seifert, J., Botterman, B., Delgado, M. & Romero, M. Peripheral Nerve Repair Through Multi-Luminal Biosynthetic Implants. *Ann. Biomed. Eng.* **39**, 1815-1828 (2011).

31. Lee, K., Silva, E. A. & Mooney, D. J. Growth factor delivery-based tissue engineering: general approaches and a review of recent developments. *Journal of The Royal Society Interface* **8**, 153-170 (2011).
32. Nelson, K. *et al.* Technique Paper for Wet-Spinning Poly(L-lactic acid) and Poly(DL-lactide-co-glycolide) Monofilament Fibers. *Tissue Engineering* **9 (6)**, 1323 - 1330 (2004).
33. http://www.promega.com/products/biochemicals-and-labware/biochemical-buffers-and-reagents/agarose_low-melting-point_analytical-grade/?activeTab=0.
34. Walker, G. & Shostak, J. in *Common Statistical Methods for Clinical Research with SAS® Examples, Third Edition* (SAS Institute Inc., Cary, NC, USA, 2010).
35. Bland, J. *et al.* in *Statistics Guide for Research Grant Applicants* (ed Department of Public Health Sciences St. George's Hospital Medical School London) 67 (Department of Public Health Sciences St. George's Hospital Medical School London, SERO - Research and Knowledge Management Directorate, London, England, 2012).
36. Prasad, P. 5 cm GAP INJURY REPAIR: GROWTH FACTOR SUPPORT AND FUNCTIONAL ANALYSIS IN A RABBIT COMMON PERONEAL NERVE MODEL (Master's Thesis). *N/A N/A, N/A* (2012).
37. Granholm, A. *et al.* Glial Cell Line-Derived Neurotrophic Factor Is Essential for Postnatal Survival of Midbrain Dopamine Neurons. *Journal of Neuroscience* **20(9)**, 3182 - 3190 (2000).
39. Weber, R. A., Proctor, W. H., Warner, M. R. & Verheyden, C. N. Autotomy and the sciatic functional index. *Microsurgery* **14**, 323-327 (1993).
40. De Koning, P., Brakkee, J. H. & Gispen, W. H. Methods for producing a reproducible crush in the sciatic and tibial nerve of the rat and rapid and precise testing of return of sensory function: Beneficial effects of melanocortins. *J. Neurol. Sci.* **74**, 237-246 (1986).
41. Deumens, R., Jaken, R. J., Marcus, M. A. & Joosten, E. A. The CatWalk gait analysis in assessment of both dynamic and static gait

- changes after adult rat sciatic nerve resection. *J. Neurosci. Methods* **164**, 120-130 (2007).
42. Nelson, A. W. The painful neuroma: The regenerating axon versus the epineural sheath. *J. Surg. Res.* **23**, 215-221 (1977).
43. Blumberg, H. & Jänig, W. Discharge pattern of afferent fibers from a neuroma. *Pain* **20**, 335-353 (1984).
44. Guse, D. M. & Moran, S. L. Outcomes of the Surgical Treatment of Peripheral Neuromas of the Hand and Forearm: A 25-Year Comparative Outcome Study. *Ann. Plast. Surg.* (2012).
45. Pacciani, E., Randisi, F., Orazi, C., Valle, M. & Martinoli, C. in (eds Martino, F., Defilippi, C. & Caudana, R.) 83-95 (Springer Milan, 2011).
46. Sinis, N. *et al.* in *How to Improve the Results of Peripheral Nerve Surgery* (eds Millesi, H. & Schmidhammer, R.) 61-64 (Springer Vienna, 2007).
47. Tyner, T. R. *et al.* Effects of collagen nerve guide on neuroma formation and neuropathic pain in a rat model. *The American Journal of Surgery* **193**, e1-e6 (2007).
48. van der Avoort, D., Hovius, S., Selles, R., van Neck, J. & Coert, J. The incidence of symptomatic neuroma in amputation and neurorrhaphy patients. *Journal of Plastic, Reconstructive & Aesthetic Surgery* **66**, 1330-1334 (2013).
49. Ziegler-Graham, K., MacKenzie, E. J., Ephraim, P. L., Travison, T. G. & Brookmeyer, R. Estimating the Prevalence of Limb Loss in the United States: 2005 to 2050. *Archives of Physical Medicine and Rehabilitation* **89(3)**, 422 - 429 (2008).
50. Owings, M. & Kozak, L. J. National Center for Health S. Ambulatory and Inpatient Procedures in the United States. *U. S. Dept. of Health and Human Services, Centers for Disease Control and Prevention, National Center for Health Statistics N/A* (1998).
51. Dorsi, M. J. *et al.* The tibial neuroma transposition (TNT) model of neuroma pain and hyperalgesia. *Pain* **134**, 320-334 (2008).

52. Meyer, R. A., Raja, S. N., Campbell, J. N., Mackinnon, S. E. & Dellon, A. L. Neural activity originating from a neuroma in the baboon. *Brain Res.* **325**, 255-260 (1985).
53. Midenberg, M. & Kirschenbaum, S. Utilization of Silastic nerve caps for the treatment of amputation neuromas. *J. Foot Surg.* **25**, 489-494 (1985).
54. Baron, R. Mechanisms of Disease: neuropathic pain—a clinical perspective. *Nature Clinical Practice Neurology* **2**, 95-106 (2006).
55. Dorsi, M. J. *et al.* The tibial neuroma transposition (TNT) model of neuroma pain and hyperalgesia. *Pain* **134**, 320-334 (2008).
56. Possidente, C. J. & Tandan, R. A survey of treatment practices in diabetic peripheral neuropathy. *Primary Care Diabetes* **3**, 253-257 (2009).
57. Steven P Cohen & Jianren Mao. Neuropathic pain: mechanisms and their clinical implications. *BMJ* **348** (2014).
58. Thomas R., T. Challenges with current treatment of neuropathic pain. *European Journal of Pain Supplements* **4**, 161-165 (2010).
59. Woolf, C. J. & Mannion, R. J. Neuropathic pain: aetiology, symptoms, mechanisms, and management. *The lancet* **353**, 1959-1964 (1999).
60. Waxman, S. G. & Zamponi, G. W. Regulating excitability of peripheral afferents: emerging ion channel targets. *Nature Neuroscience* **17**, 153 - 163 (2014).
61. Zimmermann, M. Pathobiology of neuropathic pain. *Eur. J. Pharmacol.* **429**, 23-37 (2001).
62. Zimmermann, M. & Herdegen, T. in *Progress in Brain Research* 233-259 (Elsevier).
63. Zimmermann, M. in *Clinical Neurophysiology in Peripheral Neuropathies* (ed P.J. Delwaide, A. G.) 41-56, 1985).
64. Coderre, T. J., Vaccarino, A. L. & Melzack, R. Central nervous system plasticity in the tonic pain response to subcutaneous formalin injection. *Brain Res.* **535**, 155-158 (1990).

65. Romero, M. I. *et al.* Extensive Sprouting of Sensory Afferents and Hyperalgesia Induced by Conditional Expression of Nerve Growth Factor in the Adult Spinal Cord. *The Journal of Neuroscience* **20**, 4435-4445 (2000).
66. Stein, C. *et al.* Peripheral mechanisms of pain and analgesia. *Brain Res. Rev.* **60**, 90-113 (2009).
67. Bernardi, P., Cavagnaro, M., Pisa, S. & Piuze, E. Specific Absorption Rate and Temperature Elevation in a Subject Exposed in the Far-Field of Radio-Frequency Sources Operating in the 10–900-MHz Range. *IEEE TRANSACTIONS ON BIOMEDICAL ENGINEERING* **50**, 295 - 304 (2003).
68. Hirata, A., Ushio, G. & Shiozawa, T. Calculation of Temperature Rises in the Human Eye Exposed to EM Waves in the ISM Frequency Bands. *IEICE Transactions on Communications* **E83-B(3)**, 541-548 (2000).
69. Hardell, L. & Sage, C. Biological effects from electromagnetic field exposure and public exposure standards. *Biomedicine & Pharmacotherapy* **62**, 104-109 (2008).
70. Funk, R. H. W., Monsees, T. & Özkucur, N. Electromagnetic effects – From cell biology to medicine. *Prog. Histochem. Cytochem.* **43**, 177-264 (2009).
71. Blank, M. & Goodman, R. Electromagnetic fields stress living cells. *Pathophysiology* **16**, 71-78 (2009).
72. Ji, Z. *et al.* Light-evoked Somatosensory Perception of Transgenic Rats That Express Channelrhodopsin-2 in Dorsal Root Ganglion Cells. *PLoS ONE* **7**, e32699 (2012).
73. Bamann, C., Nagel, G. & Bamberg, E. Microbial rhodopsins in the spotlight. *Curr. Opin. Neurobiol.* **20**, 610-616 (2010).
74. Boyden, E. **A history of optogenetics: the development of tools for controlling brain circuits with light.** *F1000 Biol Rep.* **3**, 11 (2011).
75. Yizhar, O., Fenno, L., Davidson, T., Mogri, M. & Deisseroth, K. Optogenetics in Neural Systems. *Neuron* **71**, 9-34 (2011).

76. Zhang, F. *et al.* Optogenetic interrogation of neural circuits: technology for probing mammalian brain structures. *Nat. Protocols* **5**, 439-456 (2010).
77. Gross, G. W., Wen, W. Y. & Lin, J. W. Transparent indium-tin oxide electrode patterns for extracellular, multisite recording in neuronal cultures. *J. Neurosci. Methods* **15**, 243-252 (1985).
78. Gross, G. W. Multielectrode arrays. *Scholarpedia* **6(3)**, 5749 (2011).
79. Gopal, K. V. *et al.* d-Methionine protects against cisplatin-induced neurotoxicity in cortical networks. *Neurotoxicol. Teratol.* **34**, 495-504 (2012).
80. Blank, M. & Goodman, R. Electromagnetic fields stress living cells. *Pathophysiology* **16**, 71-78 (2009).
81. Gunthorpe, M. J., Benham, C. D., Randall, A. & Davis, J. B. The diversity in the vanilloid (TRPV) receptor family of ion channels. *Trends Pharmacol. Sci.* **23**, 183-191 (2002).
82. Szallasi, A., Cortright, D., Blum, C. & Eid, S. The vanilloid receptor TRPV1: 10 years from channel cloning to antagonist proof-of-concept. *Nat Rev Drug Discov* **6**, 357 - 372 (2007).
83. Sandkühler, J. Models and Mechanisms of Hyperalgesia and Allodynia. *Physiological Reviews* **89**, 707 - 758 (2009).
84. Iyer, S. *et al.* Virally mediated optogenetic excitation and inhibition of pain in freely moving nontransgenic mice. *Nature Biotechnology* **32**, 274 - 278 (2014).
85. Rogan, S. C. & Roth, B. L. Remote Control of Neuronal Signaling. *Pharmacological Reviews* **63**, 291-315 (2011).
86. Wess, J., Nakajima, K. & Jain, S. Novel designer receptors to probe GPCR signaling and physiology. *Trends Pharmacol. Sci.* **34**, 385-392 (2013).
87. Mendell, L. M. Constructing and deconstructing the gate theory of pain. *PAIN®* **155**, 210-216 (2014).

Biographical Information

Benjamin Roche Johnston graduated with honors in biology from Hamilton College in Clinton, New York. He worked in Boston, Massachusetts as a teacher and researcher before returning to graduate school at UT Arlington and UT Southwestern Medical Center. He will be attending the Warren Alpert Medical School of Brown University in Providence, Rhode Island as part of the MD class of 2018.